

Dipartimento di / Department of
Material Science

Dottorato di Ricerca in / PhD program Science Ciclo / Cycle XXIX

Curriculum in Chemistry

**Synthesis and investigations of multifunctional organic
molecules and materials for applications in the field of
renewable energy**

Cognome / Surname Manfredi Nome / Name Norberto

Matricola / Registration number 598430

Tutor: Prof. A. Abbotto

Coordinatore / Coordinator: Prof. M. L. Frezzotti

ANNO ACCADEMICO / ACADEMIC YEAR 2015-2016

Università degli studi Milano Bicocca

Scuola di Dottorato in Scienze

Doctorate in Chemistry



**Synthesis and investigations of
multifunctional organic molecules and
materials for applications in the field of
renewable energy**

Ph.D. thesis of:

Norberto Manfredi

Supervisor:

Prof. Alessandro Abbotto

Dean of the Doctorate:

Prof. Maria Luce Frezzotti

February 2017

XXIX Cycle

TABLE OF CONTENTS

List of Publications.....	6
Abstract.....	7
Chapter 1	15
Introduction	15
The energy issue.....	15
Photovoltaic	21
Working principles.....	29
Artificial photosynthesis and photocatalysis	33
Working principles.....	37
References	43
Chapter 2	54
Dye sensitized solar cells.....	54
Aim of this section.....	54
Benzodithiophene based organic dyes for DSSC	57
Synthesis, DFT calculation and electrochemical properties	58
Optical properties.....	64
Photovoltaic properties.....	68
Thiophene-base phenothiazine branched dye for dye-sensitized solar cells	77
Synthesis.....	79
Optical and electrochemical characterization.....	82
Electrochemical characterization	85
Photovoltaic investigation	88
Hydrophilic phenothiazine dyes for dye-sensitized solar cells using an	
water based electrolyte solution	94
Synthesis.....	96
Optical and electrochemical properties.....	98
Water affinity and photovoltaic properties.....	100
C-Doped-titania paste for Dye-Sensitized Solar Cells	104
Synthesis and characterization of the C-doped TiO ₂ paste.....	106
Photovoltaic characterization	109
Experimental section	117
General information.....	117
Electrochemical characterization	117
Dye loading	118

General procedure for the preparation of the TiO ₂ pastes	118
DSSCs fabrication procedure.....	119
DSSCs characterization.....	120
Synthetic procedures	121
References	133
Chapter 3	146
Perovskite solar cells	146
Aim of this work.....	146
Multijunction perovskite base hybrid solar cells.....	149
Device fabrication	151
Mesoporous architecture	156
Planar architecture.....	161
Optimized geometry	164
Multijunction tandem device	167
New heteroaromatic hydrazone-based hole transporting material for	
perovskite solar cells.....	171
Design and synthesis	174
Optical and electrochemical properties	175
Photovoltaic investigation	180
Experimental section	186
General information.....	186
Electrochemical characterization	187
Device fabrication	187
Device characterization.....	189
OFET Fabrication	189
Synthesis.....	190
References	194
Chapter 4	204
Aim of this section.....	204
Thiophene-based phenothiazines for long-term irradiation photocatalytic H₂	
production	208
Hydrogen production using dye-sensitized Pt/TiO ₂	212
Dye degradation study and intrinsic photocatalytic activity	218
Enhanced photocatalytic hydrogen production in a glucose derivative of a	
phenothiazine dye: water affinity and self-organization	224
H ₂ production in hydrophilic phenothiazine based dyes	227
H ₂ production in glucose functionalized phenothiazine based dyes in presence of	
templating agent	236

Enhanced photocatalytic hydrogen generation using carbazole-based sensitizers.....	241
Design and synthesis.....	241
Optical and electrochemical characterization.....	244
Photocatalytic hydrogen production.....	247
New organic p-type dyes as photocathode sensitizers for photoelectrochemical hydrogen production.....	252
Design and synthesis.....	254
Optical and electrochemical characterization.....	258
Photoelectrochemical hydrogen production.....	265
Experimental section.....	273
General information.....	273
Electrochemical and photoelectrochemical characterization.....	273
Preparation of Pt/TiO ₂ nanopowder.....	274
Characterization of Pt/TiO ₂ nanopowder.....	274
Adsorption of dyes on Pt/TiO ₂	275
Hydrogen production through water splitting.....	275
Degradation measurements of dye-sensitized Pt/TiO ₂	276
Preparation of NiO photocathodes.....	276
NiO films sensitization.....	277
Synthetic procedures.....	277
References.....	285
Chapter 5.....	298
Conclusions.....	298

List of Publications

(1) **Manfredi, N.**; Cecconi, B.; Abboto, A. "Multi-Branched Multi-Anchoring Metal-Free Dyes for Dye-Sensitized Solar Cells". *Eur. J. Org. Chem.* **2014**, 7069-7086, doi:10.1002/ejoc.201402422.

(2) Baldoli, C.; Bertuolo, S.; Licandro, E.; Viglianti, L.; Mussini, P.; Marotta, G.; Salvatori, P.; De Angelis, F.; Manca, P.; **Manfredi, N.**; Abboto, A. "Benzodithiophene based organic dyes for DSSC: Effect of alkyl chain substitution on dye efficiency". *Dyes Pigm.* **2015**, *121*, 351-362, doi:10.1016/j.dyepig.2015.04.028.

(3) Cecconi, B.; **Manfredi, N.**; Ruffo, R.; Montini, T.; Romero-Ocana, I.; Fornasiero, P.; Abboto, A. "Tuning Thiophene-Based Phenothiazines for Stable Photocatalytic Hydrogen Production". *ChemSusChem* **2015**, *8*, 4216-4228, doi:10.1002/cssc.201501040.

(4) Cecconi, B.; **Manfredi, N.**; Montini, T.; Fornasiero, P.; Abboto, A. "Dye-Sensitized Solar Hydrogen Production: The Emerging Role of Metal-Free Organic Sensitizers". *Eur. J. Org. Chem.* **2016**, *2016*, 5194-5215, doi:10.1002/ejoc.201600653.

(5) **Manfredi, N.**; Cecconi, B.; Calabrese, V.; Minotti, A.; Peri, F.; Ruffo, R.; Monai, M.; Romero-Ocana, I.; Montini, T.; Fornasiero, P.; Abboto, A. "Dye-sensitized photocatalytic hydrogen production: distinct activity in a glucose derivative of a phenothiazine dye". *Chem. Commun.* **2016**, *52*, 6977-6980, doi:10.1039/c6cc00390g.

(6) Manfredi, N.; Monai, M.; Montini, T.; Matteo Salamone, M.; Ruffo, R.; Fornasiero, P.; Abboto, A. "Enhanced photocatalytic hydrogen generation using carbazole-based sensitizers". **2016**, *Submitted*

Abstract

In order to growth in a sustainable manner, human society needs to access renewable and eco-friendly energy sources and progressively abandon fossil fuels as energy sources, limiting their use as carbon sources for industrial intermediates. In this scenario, scientists all over across the world have focused their efforts in studying and discovering new materials to better transform solar radiation to electricity in photovoltaic devices. However, electricity accounts for only a minor portion of total energy needs, being more than 60% of the present world energy consumption constituted by fuels for transportation and synthesis of chemical intermediates. In particular, in the field of transportation important recent technological progresses have been made for electrical-powered vehicles but still not sufficient to replace present fossil fuel combustion engines. The first priority is, therefore, to develop new methods to produce sustainable energy and green fuels so as to reduce or remove the use of fossil fuels. At the moment, the best alternatives to fossil fuels to produce energy seem to be photovoltaic and hydrogen.

The most accessible way to produce clean energy from the sun is photovoltaics (PV). In the past four decades, a large numbers of different technologies to transform sunlight into electricity have been exploited starting from silicon solar cells to the multi-junction solar cells to improve the efficiency of the process. In the last years, due to the considerable increase of air pollution and the emission of greenhouse gases, the scientific community started to focus its attention on the possibility to produce “green” fuels using sunlight. Fuels such as hydrogen, with zero carbon footprints, is commonly produced via steam reforming with a considerable carbon dioxide emission. Current main R&D with high TRL and MRL is devoted to electrolyzers with very fast response aiming at grid balance. Photochemical and photoelectrochemical water splitting are currently cutting edge topics but with lower TRL and MRL.

In this research project different renewable energy technologies, from organic photovoltaic to artificial photosynthesis, have been investigated. A number of new materials have been studied in order to optimise their capabilities to produce energy in the cheapest and most efficient manner.

The first part of this research project has been devoted to the study of new materials, within different collaboration projects with other universities and research institutes, for hybrid organic-inorganic PV, namely dye-sensitized solar cells (DSSCs). This technology uses an organic dye as a photosensitizer to harvest light and transfer electrons to an inorganic semiconductor, typically titanium dioxide. The circuit is completed using a counter electrode and an electrolyte solution to regenerate the dye. Graetzel and O'Regan, have presented the first example of DSSCs in 1991. Since then, an uncountable number of variations have been proposed to improve the efficiency of the device.

The first series of materials tested in a DSSCs device was a carbon doped titanium dioxide nanoparticles (C-TiO₂-Np) produced at the university of Padova (Prof. G. Brusatin). These new materials have been tested in different configuration, either in double or single layer architecture, with or without a commercial scattering TiO₂ paste in order to study the photovoltaic response. This investigation, and the comparison with different standard commercial reference, led to interesting properties. In fact, the prepared titanium dioxide showed comparable or even better photovoltaic performance compared to the commercial reference. Moreover, an investigation over the dye-loading on the semiconductor showed that the performances of the device prepared using the doped titanium dioxide have been achieved using half of the amount of dyes compared to the amount bounded on the commercial standards.

Secondly, a series of push-pull triarylamine organic dyes containing the benzo[1,2-b:4,5-b']dithiophene unit as a spacer and bearing alkyl chains in different positions of the molecule obtained in a collaboration with University of Milano have been studied. The new dyes were used as sensitizers in liquid DSSC. The best PCE was recorded for

the dye bearing two 3,7-dimethyloctyl groups on the benzodithiophene core (dye **1**), (6.6% at 0.5 sun, 8.4% without mask on top of the cell), the molecule with the simplest donor core, to be compared with a value of 8.1% for N719-based devices under the same fabrication conditions. Therefore the photovoltaic performance of this sensitizer was only ~20% less than the benchmark dye N719. The best LHE profile, in agreement with optical properties, and the APCE values, greater than 80%, suggested that the efficiency of **1** originates from high light harvesting and charge formation and collection efficiency. Photovoltaic performances were dramatically dependent on the choice of the solvent used for the dye-sensitizing bath. The results were correlated, through extensive optical studies in different solvents and acid/base additives, with protonation equilibrium of COOH/COO⁻ group of dyes. These data clearly show that when an unsuitable, though very common, solvent as EtOH is used for dye solutions, misleading PCEs even close to 0% may be obtained, although in the presence of performing sensitizers, as ascertained when proper conditions are alternatively selected, thus showing the strategic importance of selecting appropriate solvents for DSSC fabrication conditions.

Concerning PV, we have also focused our attention to the more recent perovskite based technologies. This type of device uses a hybrid organic-inorganic perovskite acting as active material and can be used either as sensitizer, in combination with a semiconductor as charge carrier, or as active semiconducting material. This interesting property allows us to use it in different devices configurations. Even though there is a huge literature about perovskite solar cells (PSCs), the fabrication of the device is still under active investigation to improve the reproducibility and the stability of the final device.

We have dedicated our efforts to develop a procedure in order to produce a stable device capable of been coupled with more conventional technologies, such as silicon or copper indium gallium (di)selenide (CIGS), as bottom cell to realize a cheap and easy-to-process hybrid high efficiency multi-junction solar cell. Two different architectures have been studied, the mesoporous and the planar. Both configurations

uses a blocking layer made of compact titanium oxide (cmp-TiO₂), a hole transport material (HTM) and a metallic back contact. The difference lies in the active layer: in the mesoporous configuration the perovskite is adsorbed on a mesoporous layer of TiO₂, in the planar is directly deposited onto the cmp-TiO₂ layer. Different materials and deposition methods of the cmp-TiO₂ layer have been investigated and the reproducibility tested. The use of the different TiO₂ precursors have been tested resulting that the best choice was Titanium diisopropoxide bis(acetylacetonate) deposited via spray pyrolysis. Then, the active layers, perovskite and HTM, have been deposited using spin coating technique varying the deposition parameters, and the obtained devices studied with a silver back contact. Achieved a proper reproducible efficiency using planar cell, the so obtained devices have been studied replacing the silver back contact with a semi-transparent layer made of silver nanowires (NWs) in order to grant a proper illumination to the bottom cell of the multi-junction. Using this configuration, we have obtained a working prototype of a four terminal multi-junction solar cell with a good efficiency.

Furthermore, we have designed and investigated a series of hydrazone-based HTM to be used instead of the conventional Spiro-OMeTAD molecule in PSCs. Different electron-rich π spacers and substituents characterize the series to finely tune the position of electronic levels in order to be properly coupled with the perovskite. These new materials have been designed to easy to synthesise and to be transferred to mass production. Cheap precursors and short synthetic pathways have been chosen. The HTM candidates have been characterised optically and electrochemically showing good optical properties and reversible oxidation behaviour. In collaboration with the group of Prof. Stingelin at Imperial College, London, the mechanical and charge transport properties have been investigated with poor result. The conductivity measurements performed preparing organic field effect transistor (OFETs) shows that the new hydrazone-based HTM act as insulating materials instead of semiconductors. This fact is confirmed by the very low efficiency obtained in PSCs devices.

The second part of this research project has been dedicated to the study of organic sensitizer prepared in our research group both in DSSC and dye sensitized photo-production of hydrogen. In terms of hydrogen photo-production, two different technologies have been investigated: dye-sensitized photocatalytic hydrogen production and dye-sensitized photoelectrochemical cells (PECs). In the case of the photocatalysis, organic sensitizers are bounded to the surface of a Pt/TiO₂ photocatalysts. Upon photo-excitation, an electron of the dyes is promoted to the LUMO level and transferred to the photocatalyst that is capable of reduce water to hydrogen in the presence of a sacrificial donor to regenerate the neutrality of the dyes. In the PECs, the dyes are bounded on the surface of NiO-nanoparticles deposited on a transparent conductive oxide (TCO). Upon photo-excitation, an electron of the dyes is promoted to the LUMO level and transferred to the photocatalyst that is capable of reduce water to hydrogen. In this case the catalysts is an organometallic complex that can be either bounded or not to the dyes. The NiO that is capable to accept a hole grants the neutrality of the dyes. The holes are transferred to a counter electrode, usually platinum net, placed in a separated part of the device in which water is oxidized to oxygen and the resulting proton are transferred, through a proton exchange membrane, to the active part where the reduction happens.

We have designed and investigated a series of phenothiazine (PTZ)-based donor-acceptor dyes for dye-sensitized photocatalytic H₂ production from water and dye-sensitized solar cells (DSSC). The series is characterized by having different thiophene-based π spacers, from the simple thiophene ring to the alkoxy-substituted thiophene derivatives. The introduction of the thiophene-based π spacers afforded significantly enhanced optical properties both in terms of longer wavelength absorption and molar absorptivities, with up to a four-fold increase compared to the reference dye PTZ1. Pt/TiO₂ photocatalysts sensitized by dyes PTZ1–6 showed a remarkable H₂ productivity from triethanolamine (TEOA) aqueous solution at pH 7.0 under irradiation with visible light for long irradiation times (20 h). The preferred longer irradiation times are in contrast with previously reported experimental

conditions, which typically use much shorter irradiation periods (2–5 h). Although the photocatalyst sensitized by the dye PTZ1 without the thiophene spacers demonstrated the highest initial H₂ production rate, it undergoes a progressive deactivation with irradiation time, behaviour commonly reported, but so far not clearly rationalized, for this class of dyes. Such characteristic is critical for practical long-term applications. On the contrary, photocatalysts sensitized with the new substituted PTZ2–6 dyes revealed improved stability after longer irradiation times and enhanced performances after an initial activation period. An unprecedented degradation study revealed for the first time that the anomalous photocatalytic activity of the catalyst sensitized by the reference dye PTZ1 is the clear consequence of the strong degradation of the dye with irradiation times. Notably, the new dye PTZ5 is a promising candidate for efficient dye-sensitized photocatalytic H₂ production, with stable H₂ production rate and an overall productivity comparable to that of the reference compound PTZ1. The degradation investigation has evidenced that this finding is the direct consequence of the remarkable stability of PTZ5 under irradiation, though the intrinsic photocatalytic efficiency was lower than that of the reference dye.

A thiophene-based donor–acceptor phenothiazine dye has been functionalized with a peripheral glucose unit (PTZ-GLU) to boost its affinity to water and enhance dye-sensitized photogeneration of hydrogen. The insertion of the glucose unit yielded a higher affinity towards the aqueous medium compared to the commonly used hydrophilic TEG functionality, while maintaining the high activity recorded for the alkyl derivative. By comparing contact angle measurements, photocatalytic data, and by considering the structural peculiar features of the side substituents, we have concluded that the distinct behaviour of PTZ-GLU is associated to the unique rigid, bulky, hydrophilic geometry of the glucose ring, where lower degrees of freedom and extra-wettability, favouring the interaction with reactants in aqueous solution and suppressing intermolecular quenching, cooperate in producing the final findings. The general and scalable synthetic approach and the large variety of sugar derivatives will

allow the access to a library of photosensitizers with finely tuned properties and potential to improve the efficiency of the production of solar fuels.

Furthermore, PTZ-GLU has been tested in presence of D-glucuronic acid as co-adsorbent to study the self-assembly effect induced by the glucose moiety in comparison with the chenodeoxycolic acid (CDCA). A series of experiments have been done exploiting various loading of dye and co-adsorbent on Pt/TiO₂ photocatalysts. While there is a detrimental effect in presence of CDCA, the addition of D-glucuronic acid lead to a remarkable enhancement of the hydrogen evolution with PTZ-GLU. The hydrophobic analogous PTZ2, in the same conditions, shows a reduced activity. This phenomenon can be ascribed to a supramolecular organization induced by hydrogen bonding between the sugar functionalities. Indeed, reducing concentration of the dye with a consequent reduction of catalysts surface coverage, the coordination effects becomes less significant as well as the enhancement of hydrogen production.

Another way to improve the hydrogen production can lies in a different molecular design. In order to investigate the effect of molecular structure on the efficiency in hydrogen generation, a series of dyes containing different electron rich donor moieties have been synthesised and studied in comparison with the previous PTZ dye. The new dyes have been designed to reduce or even eliminate the presence of sulphur in the molecular structure. To do so, the phenothiazine has been replaced with phenoxazine (POZ) first, and then carbazole (CBZ). Moreover, the substitution of sulphur took place also in the π spacers, using furan as alternative to thiophene. In the case of POZ dyes, the molecular 3D structure was analogous to that of PTZ sensitizers, due to the "butterfly" shape of the donor group. Otherwise, the CBZ structure results planar with a better conjugation through the donor group. The effects of these structural variations on the properties of the dyes are unexpected and astonishing. While the optical properties of POZ dyes are better than those of the respective analogues CBZ, the former do not show photocatalytic activity while the

latter show an activity 10 times greater than that of the reference PTZ systems. These types of values are to be placed among the best ever reported in the literature.

Chapter 1

Introduction

*“We came all this way to explore the Moon,
and the most important thing is that we discovered the Earth”*

William Anders, Apollo 8 astronaut, 1968

The energy issue

The twentieth century, without any doubt, was characterized by the most important technological development recorded in the history of mankind. This incredible progress has been made possible by a massive exploitation of natural resources to produce energy. This unprecedented development has led to a dramatic change in the population's lifestyle. In fact, if on one hand this development has led to an improvement in the living conditions of a large part of the current 7.4 billion inhabitants of the planet,¹ it has also brought a number of new problems related to the retrieval and consumption of natural resources the production of energy. Since the dawn of civilization, mankind has been able to obtain their energy from sources that were almost immediate transformations of solar radiation (flowing water and wind) or that took relatively short periods of time to become available (wood). What made the twentieth century so prosperous, in terms of progress and development, was the massive use of energy sources such as fossil fuels and nuclear fuels.² This increase in energy production has allowed us to keep the costs thereof

low enough to make it accessible to large numbers of people and available for the most diverse applications. To date, approximately 85% of the energy produced in the world, is produced using these sources; the main contribution is given by the exploitation of fossil fuels like natural gas, oil and coal.³ This energy surplus has allowed us to improve the quality of life and allowed the technological development that has brought us, for the first time in human history, to explore a planet that was not the planet earth. Space exploration has also changed the way we look at the planet on which we live. Figure 1.1 shows the famous photograph taken during the flight of the spaceship Apollo 8 astronaut William Anders, who captures in a historic shot, the rise of the Earth from lunar orbit. This picture became, in the years to follow, the symbol of many environmental movements because it represents the beauty and fragility of the planet that hosts us. Of the thousands of images of our planet obtained in the years of space exploration, there is another that will come straight into history. The image, shown in Figure 1.2, represents the whole of humanity. Astronaut Michael Collins took this image during the famous mission that brought the astronauts of Apollo 11, Neil Armstrong and Buzz Aldrin to put their first steps on the moon. In fact, in this picture are portraits, in addition to the two astronauts returning from the moon's surface, even all the inhabitants of the earth alive and lived except Michael Collins himself who took this shot. These so iconic photos, together with all that in those years we were discovering and learning on energy and environment, have expanded our knowledge about the effects of our presence on the planet. In fact, all of these impressive results were not obtained without consequences. This so intensive use of fossil fuels, though extremely affordable, also brought a series of negative effects on the environment that we must face.⁴ The first inevitable consequence that soon we will have to face is that by using these fuels current rate, they will end very soon we will have to find new energy sources to replace them.



Figure 1. 1: Earthrise: a photograph of the Earth taken by astronaut William Anders on December 24, 1968, during the Apollo 8 mission while in orbit around the Moon. This picture is one of the Life ' s 100 Photographs that Changed the World. Credit: NASA.

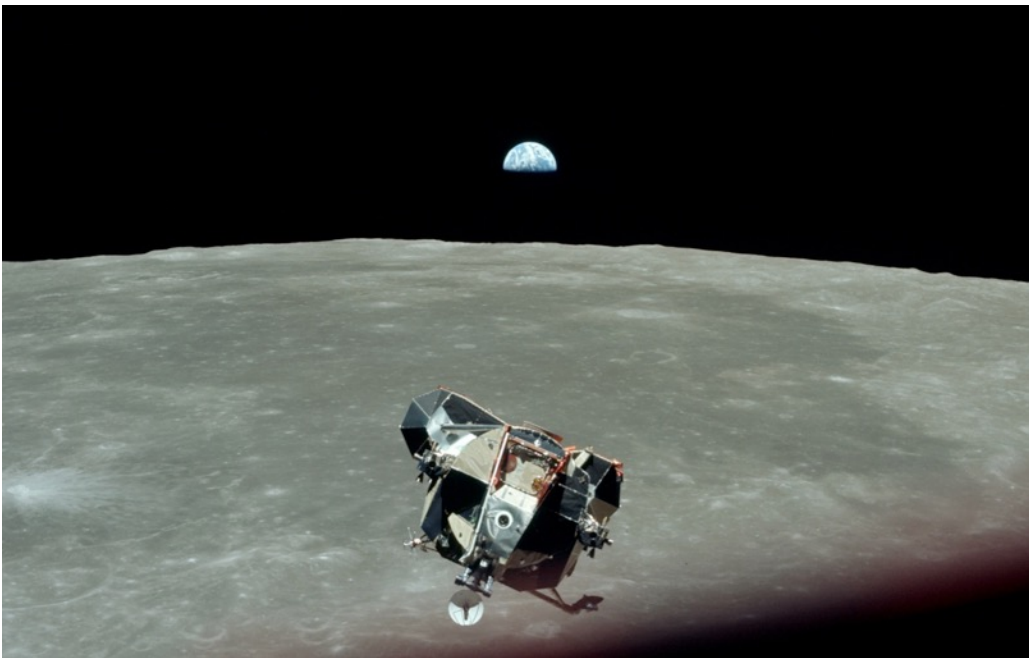


Figure 1. 2: Michael Collins took this picture around at 21:25 GMT on July 21, 1969: shooting, one of a long close series, was used to monitor the approach to the orbiting of the LM module, return from the lunar surface, carrying Armstrong and Aldrin. In this image are captured all the inhabitants of the earth, lived or alive, but the astronaut himself. Credit: NASA

In the last 140 years, a little more than 1 trillion barrels of oil have been consumed and currently the world's growing needs for energy amounts to almost 1100 barrels of oil, 110000 cubic meters of natural gas, and 122 tons of coal per second.⁵ Furthermore, we must consider the impact that the use of such fuels has on people's health and the environment in which we live. Among all the parameters taken into account, one of the most significant is the increase of the level of CO₂ in the atmosphere. It is important to note that over the past 35 years, this value has increased from 340 ppm in 1981 to 400 ppm, the value recorded in August 2016.⁶ This increase is strongly related to the intensive use of fossil fuels. Last but not least is the economic and social impact that the exploitation of these resources.

It is beyond question that the human presences, and the ongoing search for energy sources, have an impact on the planet and the ecosystem in which we live. Ecologists and climatologists stress out that dominant patterns of production and consumption are causing environmental devastation and a massive extinction of species, as well as an anthropogenic climate change.^{7,8} A similar argument can be made considering the environmental impact derivative from the exploitation of fossil fuels and the production of waste. In 2002, P.J. Crutzen postulated that since the Industrial Revolution, we have entered a new epoch that can be called Anthropocene, in which the Earth has endured changes sufficient to leave a global stratigraphic signature distinct from the Earth has undergone changes sufficient to leave a global stratigraphic signature primarily related to human activity, different from those of previous geological eras.⁹ Furthermore, as reported by the United Nations Intergovernmental Panel on Climate Change (IPCC),⁸ the massive exploitation of fossil fuels and the consequent increase in production of CO₂, will lead to an increase of greenhouse effect responsible of many related environmental issues. In fact, an increase in greenhouse effect can impact on the level and pH of oceans as well as on the melting of permafrost and polar ice caps. It will also impact on the water and food availability and led to massive negative effect on the humanity.

Another important consideration that must be made is related to the production and use of energy itself. In fact, the energy or better the energy issue is not only a scientific problem but is primarily a socio-economic problem. What we will notice is that there is a wide disparity related the use of energy. In fact, an American consumes an average of two times the energy it consumes a European, 17 times an Indian and 240 Ethiopian.¹⁰ This kind of inequality is reflected in all aspects of the life of these peoples: culture, health, education and life expectancy. In developed countries where access to energy is widespread and warranted, both life expectancy and cultural level are considerably higher than in countries where there is poor access to energy.¹ If things do not change, sooner or later, this inequality will lead to a considerable risk of war between rich and poor countries. The boost of “illegal” immigration in affluent countries that lie at the boundary between the North and the South of the world (*i.e.*, United States, Italy, Spain) is indeed a forewarning of what will happen in the international scene. In this scenario, the major world economic powers have signed, in recent years, a number of important treaties in order to remedy this complicated situation. The Tokyo Protocol before, and the Treaty of Paris in 2015 are trying to reduce the impact of human activities on climate change, by committing member nations to a massive reduction in greenhouse gasses emissions to be made in the next decades.¹¹

In order to achieve these objectives, it will be necessary an action that goes from the reduced use of fossil fuels, the carbon dioxide capture, up to the study and development of new technologies for the production of energy from renewable sources. Once again, nature comes to our aid, and shows us the ways to solve this complex task. In fact, nature is powering us since the very beginning of the human species on this planet. Nature provides us all we need using sunlight and basic elements to synthesize biomasses that, during millennia, have been transformed in fossil fuels. This suggests us to use the energy coming from our star to resolve our energy issue. Sunlight is abundant and is almost equally diffused all over the entire globe. Furthermore we receive from the sun almost 90 PW on the earth’s surface,

that is orders of magnitude greater than the rate of energy consumption of our society (17.2 TW in 2014) and it will last or more than 4 billion years.² In Figure 1.3,¹² is possible to see a pictorial of the amount of energy produce using different renewable and not-renewable sources compared to the energy given to us by the sun. It is straightforward that, if we will be able to efficiently transform just a small amount of that energy, we shall overcome any future energy issue.

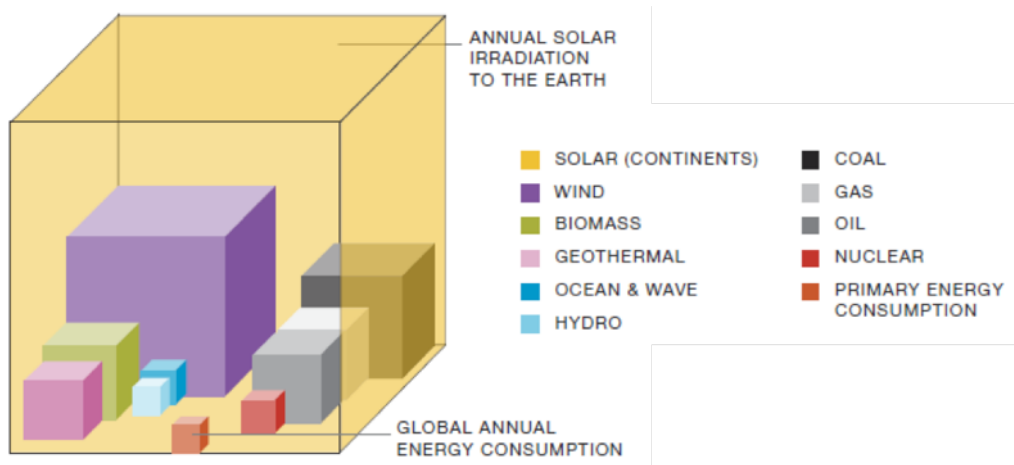


Figure 1. 3: Available energy sources compared to the global annual energy consumption.

The main problem in the conversion of solar energy into electricity or fuel is that the processes involved in this transformation are threshold-based implying a consequent limit on the conversion efficiency. Secondly, the solar energy is discontinuous and subject to intensity fluctuations due to diurnal cycles and atmospheric conditions. Therefore, in the case of solar energy conversion into electricity, we also have to face the problem of the storage. Up to now, the two main strategies for storing the excess of electricity have been the use of battery¹³ and the production of solar fuels through the use of electrolyzers. A good alternative strategy to store solar energy could be the direct conversion into chemical energy in the same way the nature does with the natural photosynthesis.¹⁴

Photovoltaic

Among all renewable energy resources, solar energy is definitely the one present in greater quantity and more uniformly distributed over the entire planet. The Earth is invested in every moment by an electromagnetic radiation with a power of about 1.7×10^5 TW and, just outside the earth's atmosphere, with a power density 1367 W m^{-2} (AM0). Considering reflection and absorption by the atmosphere, on the Earth's surface, the solar spectrum has an average power density of about 1000 W m^{-2} (AM1.5).¹⁵ This variation can be explained considering what happens along the way that photons move through the atmosphere. Solar radiation has a spectrum unperturbed that does not differ much from that of a black body at $T \approx 6000 \text{ K}$, the passage through the atmosphere, where there are mainly O_2 , H_2O , CO_2 , O_3 and particulate, reduces the radiation because of the aforementioned considerations and removals and it is clear that the greater the portion of atmosphere will be crossed, the greater the attenuation. This optical path through the atmosphere (L) is defined by the well known air mass coefficient "AM".

$$AM = \frac{L}{L_0} = \frac{1}{\cos(\vartheta_z)}$$

where L_0 is the normal path to the Earth's surface and ϑ_z it is the zenith angle in degrees. Note that the AM1.5 value is mostly used for the calibration and the measurement of the standard photovoltaic cells.

Every square meter of the Earth's surface receives an average variable annual amount of energy, mainly depending on the latitude, between 1 and 2 MWh that, even taking into account the current efficiency of photovoltaic devices, potentially could provide coverage for much of the global energy needs.

The photovoltaic effect was observed for the first time in 1839 by French physicist Edmond Becquerel while devoting himself to studies of electrolytic cells. The first solar cell was built in 1883 by the American inventor Charles Fritts and

consisted of a junction formed from selenium and gold with an efficiency of only 1%. The first devices with significant efficiencies saw the light in the second half of the last century, based on the development of semiconductor studies. In particular, scientists D. Chapin, Fuller and C. G. Person of Bell Laboratories in 1954 put in place the first silicon photovoltaic cell with an efficiency of about 6%.¹⁶ From that first device, studies have focused on the development of ever more efficient cells. This development has made it possible to achieve high conversion efficiencies dramatically reducing the cost of production. Current technologies are divided into three generations that take into account of the different degrees of technological advancement and their availability in terms of costs and materials. The first two generations includes semiconductor devices: in particular, the first generation includes the monocrystalline or polycrystalline silicon cells which are those studied for longer and that are the most commercially widespread. The second generation regards the thin-film devices that have lower efficiency than silicon but a lower cost. To date have been unable to find much space in the photovoltaic market but, at the research level, they are still a topic of great interest. Finally, shall be deemed third-generation, all the emerging technologies still in the basic research stage such as organic cells (OPV), the dye-sensitized cells (DSSCs), perovskite solar cells (PSC), and quantum dot and some types of multi-junction cells. The third generation promises to take the best from the past so as to reach a cost/efficiency ratio, which makes photovoltaic a major player among the different energy sources used for meeting the global need.

We decided to focus our interest on third-generation cells as DSSCs and PSC. We also want to exploit them in a multi-junction system with commercial silicon-based solar cells to achieve high efficiency and low cost systems.

The first DSSCs sensitized dyes in the form of organometallic ruthenium complexes with bi-pyridines bi-carboxylated to activate the titanium oxide comes from the early 80s¹⁷ and their development continued in the second half of the 80s using ruthenium complexes with three bi-pyridines bi-carbossilate.¹⁸ Famous the

publication in Nature magazine of 1991 where Brian O'Regan and Michael Graetzel presented for the first time a photovoltaic device base on the titanium dioxide functionalized with tri-nuclear Ruthenium based complexes using as bi-pyridines bi-carboxylated ligand.¹⁹ Since then, various complexes of ruthenium have been tested and, in 1993 Graetzel reported as sensitizers a series of mononuclear ruthenium complexes, of which the best performing was N3, where Ruthenium shows two thiocyanate ligands and two bi-pyridines substituted in position 4, 4' with carboxylic acid units.²⁰ The carboxyl groups allow the anchoring of the titanium dioxide and are conjugate to the pyridine groups. In the ground state electron density it is concentrated on the metal center, but in the excited state resulting in the absorption of electromagnetic radiation, such density is concentrated on carboxylate groups linked to TiO₂. The thiocyanate groups are electron-donors which increase the absorption coefficient of the complex. Nazeeruddin and coworkers have tested different forms of protonated N3: N712 has four carboxylate groups with tetra-butyl ammonium salt, N719 has two carboxylate groups and two carboxylic acids.^{21,22} The carboxylic acids allow a better anchorage of titanium oxide and higher current, but carboxylates increase the voltage of the cells. The cells up to now carried more performing with ruthenium complexes make use of N719 dye and the redox couple I⁻/I₃⁻ as the electrolyte (12% efficiency). It is now normal practice for each new tested dye, to use N719 as reference. Changes on the molecular structure allowed synthesizing many other photo-sensitizers. For example it was synthesized the Z907, in which a bi-pyridine bi-carboxylate substituent is replaced by a nonyl-4,4'-bipyridine.²³ The presence of alkyl hydrophobic chains makes the molecular structure most stable. The cell constructed making use of hexa-decyl-phosphonic acid as co-absorbent, showed efficiency around 7%, which is also maintained when subjected to thermal stress. The structure of the two references dye, N719 and Z907, is shown in Figure 1. 4.

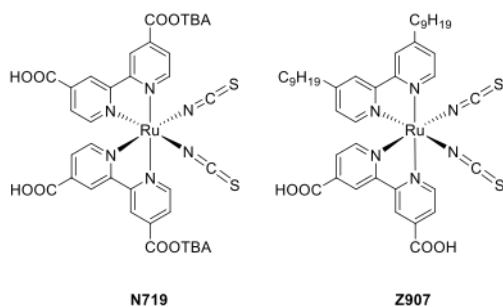


Figure 1. 4: Structure of the two references dye, N719 and Z907, presented by Nazeeruddin in 1999 and Wang in 2003.

With the aim of improving the optical properties of such complexes, in the following years, many new ruthenium-based complexes have been synthesized, in which one of the two bi-pyridine ligands has been replaced with more conjugated systems. All these derivatives have showed improved optical properties, but lower efficiencies than those obtained with the reference dyes.²⁴⁻²⁹

Also metal free organic dyes have been deeply investigated. These new dyes with a dipolar donor-acceptor molecular structures such as D- π -A, in which the acceptor is also linked to the anchoring group that is generally a unit vinyl-cyano-acetic. As donor groups, different electro-rich donor moieties have been investigated and different π -spacers have been bonded on each. As for the latter, generally the most efficient are those thiophenic or poly-thiophenic. Between the different investigated donors groups, the most performing were found to be coumarin, indolines, tetrahydroquinoline, carbazoles, dialchilaniline, and especially trifenilamine. Further structural modifications, followed by an optimization of the devices have allowed obtaining results comparable with those of the organometallic reference dyes.³⁰⁻³⁵ The literature on these compounds is very extensive (Figure 1. 5), since it is simple from the synthetic point of view to obtain a great variety of molecules. In particular, using as spacers 3-hexyl-thiophen unit, were obtained 8.5% efficiency.³⁶ The best efficiencies with organic dyes using triphenylamine as donor group have been obtained with alkoxy-triphenylamine linked to spacers thieno-thiophene. In particular, the C217 in which a tri-

phenylamine is conjugated to a EDOT and a thieno-thiophene, has allowed a record efficiency of 9.8%.³⁷

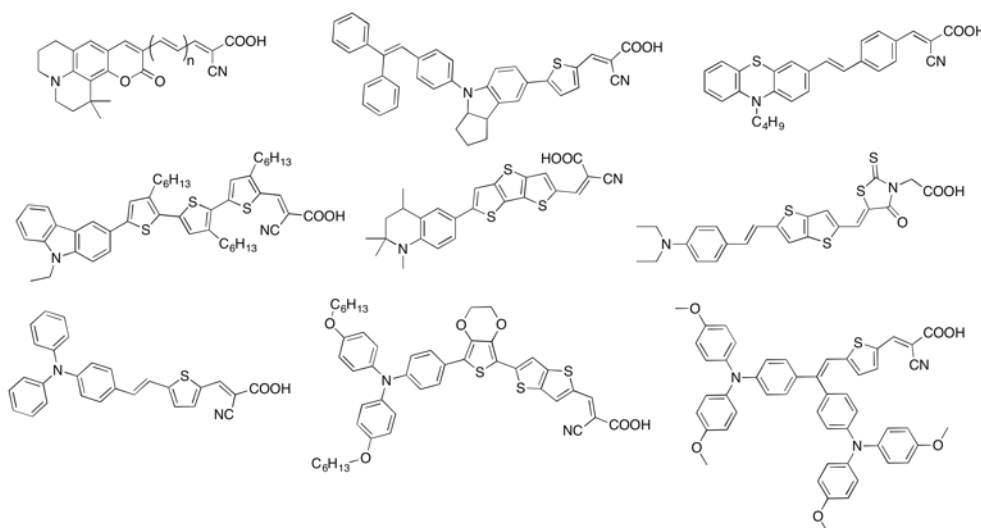


Figure 1. 5: Examples of linear organic dyes.

More recently, Abbotto and co-workers have published a major work on a new class of multibranching triphenylamine based derivatives.³⁸ These derivatives present a structure of the type $D-(\pi-A)_2$, where a single triphenylamine donor is connected to two conjugated π -spacers and, as a result, two anchor groups. This configuration allows to obtain a longer time stability compared to the corresponding linear system. Another important development of this class of compounds was subsequently proposed by synthesizing a system in which the two branches exhibited different structures connected to a more complex donor centre with the objective of improving the optical properties.^{39,40} The validity of this approach (Figure 1. 6) has been demonstrated by many other works published in the following years.⁴¹

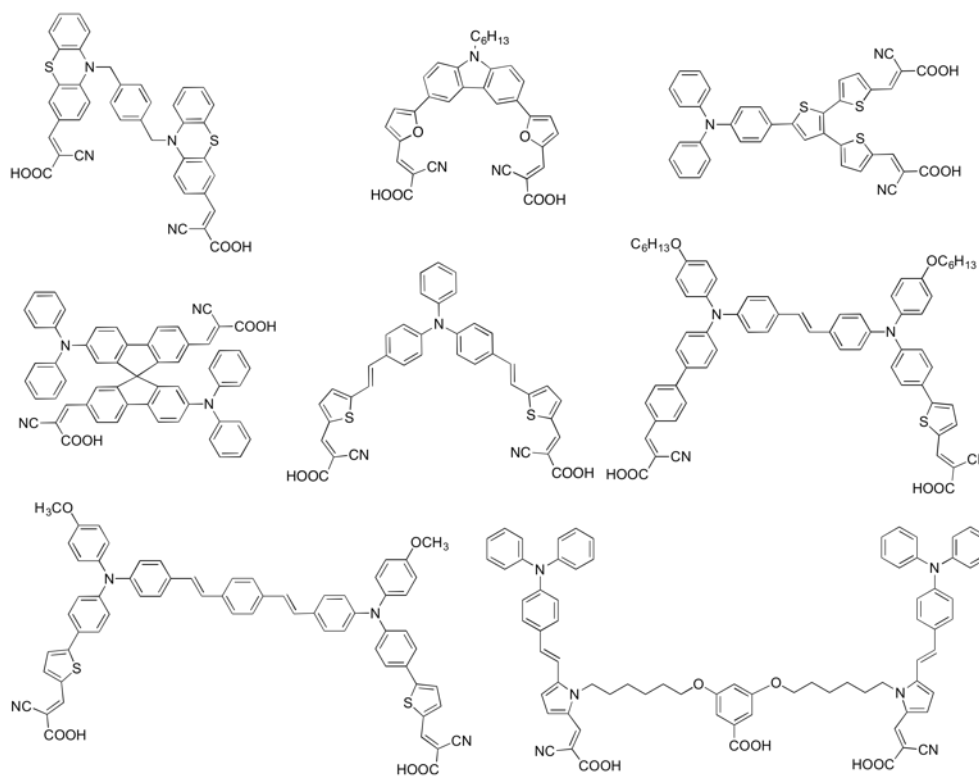


Figure 1. 6: Examples of multibranching organic dyes.

After such a strong development of sensitizers, the focus has shifted to the development of the device to make it more commercially attractive. Indeed, a further weak point of traditional DSSC technology on which it is important to pay attention, it is the presence of a liquid electrolyte containing iodine. Up to now, such an electrolyte is the best redox mediator in order to obtain high efficiencies. There have been some attempts to replace iodine with more efficient redox systems such as the redox couple $\text{Co}^{2+}/\text{Co}^{3+}$ with which, using a zinc porphyrin YD2-o-C8, Yella and coworkers have reached and exceeded the previous record efficiency bringing the value 12.7%.⁴² This outstanding result, however, was not enough to push the marketing of this type of devices, because, once again made with sensitizers with a complex synthesis and in the presence of a liquid electrolyte particularly toxic due to the presence of cobalt salts. In order to make these devices attractive to the market, it was necessary to develop solid state systems, thus eliminating the risk related to the presence of electrolytes containing solvents and

toxic or corrosive components.^{43,44} In this scenario, the best devices are those made using the molecular organic hole transport material (HTM) called 2,2',7,7'-tetrakis (*N,N*-dimethoxyphenylamino)-9,9'-spirobifluorene (spiro-MeOTAD) (Figure 1. 7) which it has allowed Graetzel and co-workers, in 2011, to reach a certified efficiency of 6.08%.⁴⁵ Despite the many efforts made in research, the most widely used HTM remains the spiro-MeOTAD which, however, has the problem of being easily oxidized to air and to be very expensive; a complicated synthesis and very few commercial sources make the product difficult to find. The growing interest in solid-state devices has prompted researchers to further investigate on more efficient systems and in 2012 were presented for the first time a ssDSSC cells (solid state dye sensitized solar cell) that used the traditional configuration with the spiro-MeOTAD as a hole conductor and a hybrid perovskite with structure $\text{CH}_3\text{NH}_3\text{PbI}_3$ sensitizer with an efficiency of 10.9%, the highest ever recorded for systems of this type.⁴⁶

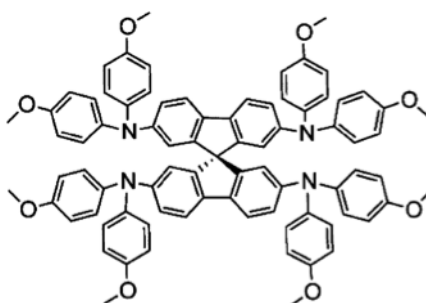


Figure 1. 7: Benchmark hole transport material, Spiro-MeOTAD.

The perovskites are those materials with the general structure ABX_3 , (Figure 1. 8), typical of calcium titanate. They have been studied for their various physical properties such as antiferromagnetism, piezoelectricity, thermoelectricity and especially for superconductivity.⁴⁷

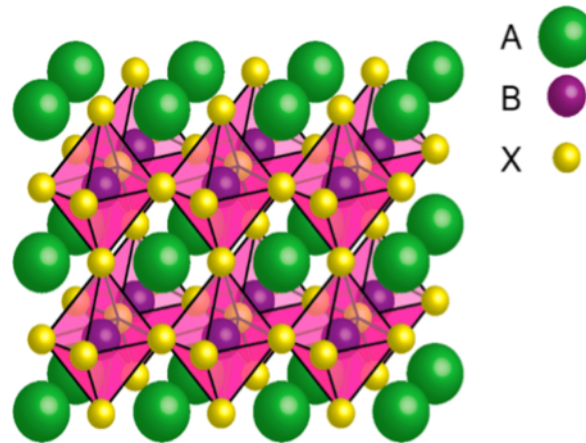


Figure 1. 8: Typical structure of a perovskite material.

From this first work to date it has been a few years, nevertheless the advances that there has been are sensational and briefly has seen unprecedented growth in efficiency up to 20.2%.⁴⁸ The working principles and properties of this technology are a highly debated topic and many questions are still waiting for an answer.⁴⁹⁻⁵⁴ As reported by Delgado and co-workers in a recent paper, one of the reasons why the efficiency of these solar cells is so superior to that achieved by the DSSCs lies in the fact that, unlike the latter, the nature of the photovoltaic conversion is not of excitonic.⁵⁵ In fact, it can be observed an almost instantaneous generation of free charges subsequently to absorption of electromagnetic radiation by the perovskite, which avoids loss of energy due to migration and dissociation of excitons.

The interest in perovskite solar cells (PSC) is not only due to the astonishing fast development observed so far, but also because they could be used for renovating an already mature and established technology such as that of the semiconductor solar cells. Silicon, for example, is the undisputed leader among the photovoltaic devices but a further acceleration of this market could result from improved its cost/efficiency ratio, which can be achieved, as proposed by H.J. Snaith, coupling them with an emerging technology such as PSC.

In the last few years a numbers of study have reported the integration of perovskite solar cell with silicon and theoretically also with different thin film technologies.⁵⁶⁻⁶¹

WORKING PRINCIPLES

A DSSC is a multi-component device comprising: a) a dye-sensitizer S; b) a n-type semiconductor metal oxide (typically TiO₂); c) a p-type semiconductor or a redox electrolyte (typically a redox couple); d) a transparent working anode and a counter electrode (based on fluorine-doped tin oxide, FTO). Under light irradiation the sensitizer S passes to its excited state S* from which an electron is injected into the conduction band (CB) of TiO₂, leaving the dye in its oxidized state S⁺. The collected electrons at the photoanode are then transferred through the external load to the counter electrode where, *via* Pt catalysis, sensitizer regeneration takes place (S⁺ → S). If a p-type semiconductor is used in place of the electrolyte (solid state devices), dye-regeneration occurs *via* hole transfer from S⁺ to the HOMO of the hole transporter. A DSSC is a very efficient device where, formally, one photon is converted to one electron without permanent modification of any component. In addition to the main processes, a number of undesired pathways and losses are present including recombination of injected electrons from TiO₂ to either S⁺ or the oxidized form of the electrolyte, incomplete light harvesting, and inefficient electron transfer from S*. The main source of loss-in potential of a DSC is the high overpotential needed to regenerate the dye, which strongly limits the maximum attainable photovoltage.⁶²

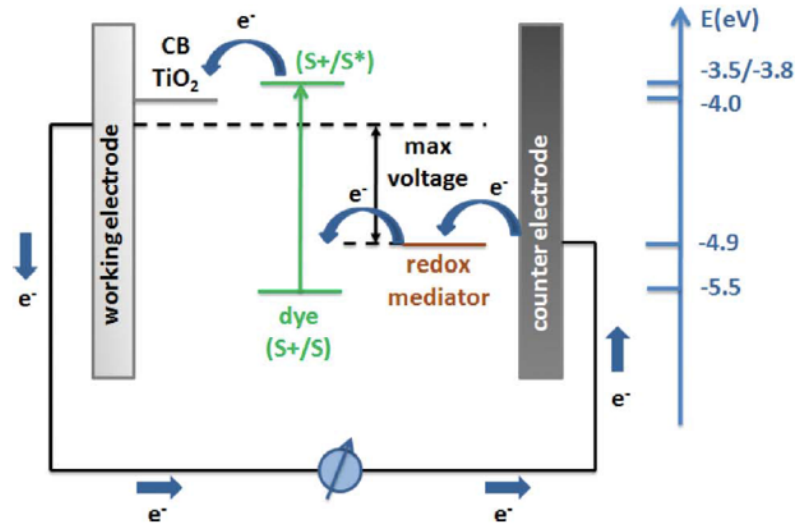


Figure 1. 9: Scheme of a dye-sensitized solar cell (dye energy levels refer to N719).

The performance of a DSSCs, or in general of a PV cell, is determined by measuring the overall power conversion efficiency (sometimes referred to as PCE) from the ratio of maximum output power density (P_{out} , in $W m^{-2}$) and the input light irradiance (P_{in} , in the same units) as shown below. Under standard reporting conditions the light intensity P_{in} is $1000 W m^{-2}$, the sun spectrum is AM 1.5 G,¹⁵ and the sample temperature is $25 ^\circ C$.^{63,64}

$$\eta = PCE = \frac{P_{out}}{P_{in}} \quad (Eq. 1)$$

According to the Shockley-Queisser model the maximum theoretical efficiency for a single junction device under non-concentrated sunlight is $\sim 30\%$.⁶⁵ The maximum power point P_{out} of a cell is given by the following equation where J_{mp} and V_{mp} represent the current density and voltage at the maximum power point.

$$P_{out} = V_{mp} J_{mp} \quad (Eq. 2)$$

By defining the fill factor ff as the ratio (values between 0 and 1) of P_{out} and the product of the maximum attainable voltage (open circuit conditions) V_{oc} (in V) and

current density (short circuit conditions) J_{sc} (in mA cm^{-2}), the efficiency relationship can be rewritten as follow, which is used to determine the cell performance.

$$ff = \frac{P_{out}}{V_{oc}J_{sc}} \quad (\text{Eq. 3})$$

$$\eta = \frac{V_{oc}J_{sc}ff}{P_{in}} \quad (\text{Eq. 4})$$

The J_{sc} , V_{oc} and ff values are measured by plotting the current density as the bias voltage is varied while irradiating the PV cell by means of a calibrated solar simulator. A typical diode current/voltage characteristic is shown in Figure 1. 10. DSC researchers usually report J and V as positive values, but other J/V curve notations are used as well.

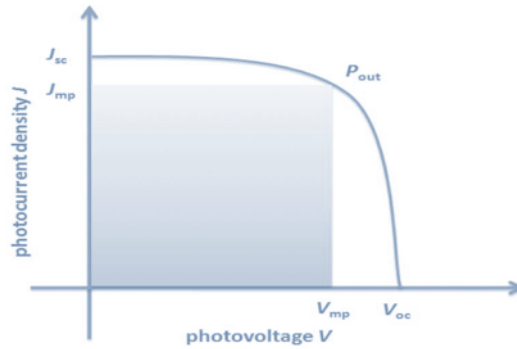


Figure 1. 10: Current–voltage characteristics of a DSSCs device under light irradiation.

An additional PV parameter, which is routinely employed to determine the quality of a PV device, is the external quantum efficiency (EQE), usually referred to as the incident photon-to-current conversion efficiency (IPCE) by the DSSCs community. $IPCE(\lambda)$ is defined as the number of collected electrons under short circuit conditions per number of incident photons at a given excitation wavelength λ and gives the ability of a cell to generate current as a function of the wavelength of the incident monochromatic light. IPCE is calculated by measuring the short-circuit photocurrent as a function of the monochromatic photon flux.

$$IPCE(\lambda) = \frac{J_{sc}(\lambda)/e}{P_{in}(\lambda)/h\nu} = \frac{hc}{\lambda e} \times \frac{J_{sc}(\lambda)}{P_{in}(\lambda)} = \frac{1240}{\lambda} \times \frac{J_{sc}(\lambda)}{P_{in}(\lambda)} \quad (\text{Eq. 5})$$

IPCE is determined by the sensitizer light harvesting efficiency at λ (LHE), the quantum yield for electron injection from S^* to the semiconductor oxide (Φ_{inj}), and the charge collection efficiency (η_{coll}), the product of the latter two parameters giving the absorbed photon-to-current efficiency (APCE) or internal quantum efficiency.

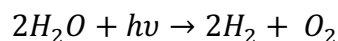
$$IPCE(\lambda) = APCE(\lambda) \times LHE(\lambda) \quad (\text{Eq. 6})$$

The integral of IPCE with the AM 1.5 G spectrum gives the photocurrent, which should match that measured under the solar simulator. Therefore higher IPCE and broader spectra correspond to higher J_{sc} .

Artificial photosynthesis and photocatalysis

Human society needs to access renewable and eco-friendly fuels and progressively abandon fossil fuels as energy sources, limiting their use as carbon sources for industrial intermediates. In this scenario, scientists all over across the world have focused their efforts in studying and discovery new materials to better transform solar radiation to electricity in photovoltaic devices.⁶⁶⁻⁶⁸ However, electricity accounts for only a minor portion of total energy needs, being more than 60% of the present world energy consumption constituted by fuels for transportation and synthesis of chemical intermediates.⁶⁹ In particular, in the field of transportation important recent technological progresses have been made for electrical-powered vehicles but still not sufficient to replace present fossil fuel combustion engines.⁷⁰ The first priority is therefore to develop new methods to produce green fuels so as to reduce or eliminate the use of fossil fuels. At the moment, the best alternative to fossil fuels appears to be hydrogen. In fact, hydrogen appears to be the ideal solution since it has no carbon footprint when it is burnt and can be obtained from an inexhaustible and sustainable energy source as water.⁷¹ Nature gives a hint through the natural photosynthetic process that is, very schematically, the dye-sensitized solar-induced splitting of water to yield oxygen and “reduction equivalents” of hydrogen, which are then exploited to reduce carbon dioxide and generate chemical fuels as carbohydrates. Similarly, scientists can mimic this process and fabricate an artificial photosynthetic process to produce solar fuels starting from water and sun.⁷²

Water is abundant and inexpensive and can be conveniently split into molecular hydrogen and molecular oxygen according to the following reaction:



Hydrogen, as energy carrier, is currently produced by electrolysis of water or from natural gas. It is evident, though, that in this case the original energy sources

inevitably remain fossil fuels and nuclear energy, which is neither ecologically nor economically acceptable. Production of hydrogen by solar-energy induced water splitting offers an obvious way to capture solar energy and thus provide “greener” energy for the future. Not only is H_2 a fuel itself, able to produce electricity in fuel cells, but it can also be processed to produce conventional fuels (via Fischer-Tropsch reactions) and is an essential material for the organic chemical industry, in medicine, and for producing ammonia based fertilizers by the Haber-Bosch process.

From the first attempts to hydrogen production made in 1972 by Fujishima and Honda,⁷³ many decades are passed and improvements have been made in the field of artificial photosynthesis. To be able to talk about artificial photosynthesis we must first identify the basic components of this photosynthetic system. First of all, we need an antenna system capable of absorbing the solar radiation and promote the formation of the charge. Hence, another system is needed that allows us to separate and conduct the charges to the catalytic centres where there will be the formation of hydrogen and oxygen as in nature.⁷⁴ Several types of devices has been proposed in the last years to separately photoproduce hydrogen and oxygen using both organic and inorganic material⁷⁵ The most investigated topics are about the catalytic centres in both water oxidation and reduction. In any cases, the semireactions have been considered separately due to their complexity. The easiest approach to photocatalytic water splitting involves the use of inorganic (Cu_2O , TiO_2 , Fe_2O_3 , WO_3 , $BiVO_4$) semiconductors as light harvester and catalytic centres.^{76,77} The weak point in this strategy is that the required high-energy radiation to activate the process lies in the UV region (*i.e.* TiO_2) and the energy levels of the semiconductors do not allow both oxidation and reduction on the same materials (*i.e.* Cu_2O , Fe_2O_3). To construct a complete system for the overall water-splitting process, the two matching narrow band gap materials, the oxygen evolving complex (OEC) an the hydrogen evolution reaction (HER) catalyst, must be wired

in a tandem configuration akin to PSII and PSI in the Z-scheme of the natural photosynthesis. The aforementioned alternatives are depicted in Figure 1. 11

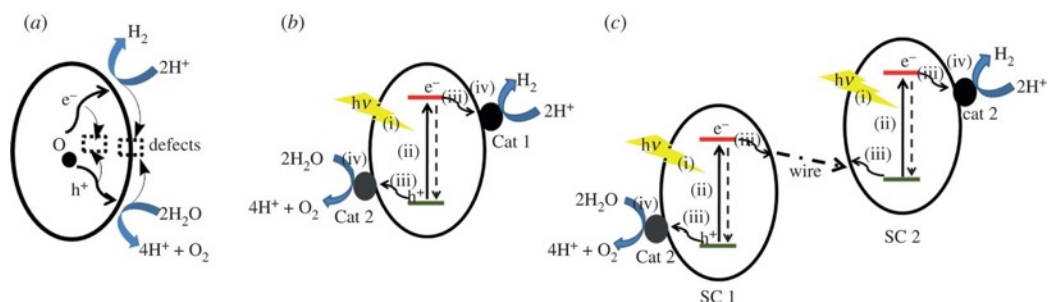


Figure 1. 11: Schematic of how semiconducting materials can be used as photocatalysts for water oxidation and hydrogen generation. Large band gap semiconductors can be used without (a) or with electrocatalysts Cat1 and Cat2 (b). Two narrow band gap semiconductors could be wired in a Z-scheme tandem configuration (c). Reprinted with permission from ref [78]

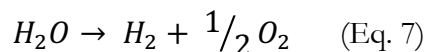
Moreover, it is important to better tune the optical properties of these materials to improve the light harvesting efficiency and so the light to fuel efficiency (LFE). A possible alternative way to solve the spectral problem lies in the use of organic or organometallic PS to change the absorption spectrum of the material.⁷⁹ The most common PS are ruthenium-based complexes,⁸⁰⁻⁸³ even though more recently it has been reported the use of metal porphyrins or metal phthalocyanines,⁸⁴⁻⁸⁶ and organic dyes.^{41,87-94} Over recent years, a large number of complexes of Ru, Ir and Co both have been proposed as PS and catalytic centres for water oxidation. Regarding the WOC catalysts, the first example recently reported is a Ru complex called "blue dimer".⁹⁵ This complex has opened the way to a whole series of possible new catalysts, some of which with efficiencies comparable to PSII.⁹⁶ Given the high costs related to the presence of ruthenium, new examples of catalysts such as Mn and Ca clusters with similar structures to the cluster contained in the PSII were developed.⁹⁷ In other cases it has been proposed the use of Co based polyoxometalates ligands.⁹⁸ However, one of the most promising WOC are those proposed by D. Nocera et al., a self-healing cobalt-oxide-phosphate based catalyst (CoPi) capable of operating at neutral pH.⁹⁹

However, these catalysts suffer from the fact that they are in the form of nanoparticles deposited on the semiconductor and poorly stand removal effects during operational conditions. This problem can be solved covalently linking the catalyst to the PS and/or the semiconductor. Some examples are reported in the literature.^{100,101} Concerning hydrogen evolution reaction (HER) the most used catalyst in so far Pt, in form of nanoparticles deposited onto the semiconductor surface or as a wire/net as passive cathode in a PEC cell.⁷³ A similar efficiency can be achieved using hydrogenases decorated electrodes as HER.¹⁰² However, owing to the large geometric size of hydrogenases, the level of loading onto the semiconductor surface is low, thus limiting the efficiency of this approach. Cobaloxime, a bio-inspired equivalent of hydrogenases, was also successfully integrated with an organic dye-sensitized-NiO or a Ru-dye-sensitized TiO₂ electrode via either non-covalent,¹⁰³ or covalent grafting.¹⁰⁴ Alternatively, they have been used oxides and sulfides of non-noble metals such as Ni, W, Mo, Cu. Lastly, the catalyst formed from the metal alloy used NiMoZn from Nocera and collaborators in the implementation of the first prototype of artificial leaf has been reported.¹⁰⁵

As mentioned before, the processes involved in the artificial photosynthesis are complexes and involve many different steps. In this study, we decided to focus our attention on the reaction of photoreduction of water to produce H₂ either via photocatalysis or photoelectrochemistry.

WORKING PRINCIPLES

The standard potential ΔE° of water splitting or water electrolysis to H_2 and O_2 (Equation) is 1.23 V at any pH (Equation 7).



From the reaction stoichiometry, the volume of produced hydrogen is twice that of oxygen. In energetic terms, water splitting requires a free energy $\Delta G^\circ = -nF \Delta E^\circ$ (where F is the Faraday constant, $96485.3365 \text{ C mol}^{-1}$). For the splitting of 1 mol of H_2O to 1 mol of H_2 and 0.5 mol of O_2 , n is equal to 2 electrons and $\Delta G^\circ = -2 \times 96485 \text{ C mol}^{-1} \times -1.23 \text{ J C}^{-1} = 237 \text{ kJ mol}^{-1} H_2O$ or $\Delta G^\circ = 2.46 \text{ eV mol}^{-1} H_2O$ (with $1 \text{ eV} = 96.48 \text{ kJ mol}^{-1}$). Accordingly, for each electron involved in the redox reaction, the free energy is 1.23 eV. Water splitting is a multi-electronic (2 electrons per each molecule of hydrogen and 4 electrons per each molecule of oxygen evolved), multi-atomic thermodynamic energy demanding, and kinetically hampered process with a high activation barrier (Figure 1. 12). Thermodynamic losses and overpotentials associated to the reaction kinetics increase the voltage required for water splitting to higher values, up to 1.8 - 2.0 V, the typical voltage at which commercial electrolyzers operate.⁷⁷

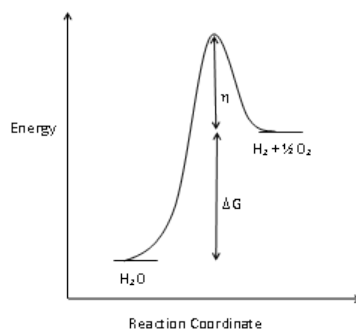


Figure 1. 12: Energetic path of water splitting process

As mentioned before, many various alternatives are available to overcome this energetic demand. We focus our effort in studying the so-called, dye-sensitized photocatalysis in presence of a sacrificial electron donor (SED) to produce hydrogen, whereas SED plays the role of hole scavengers, in place of water in the water splitting half-reaction which is omitted. This option recently attracted the interest of many research groups since it is the common strategy adopted by other more mature solar technologies, such as dye-sensitized solar cells (DSSC).^{30,106} The schematic of the process is depicted in Figure 1. 13.

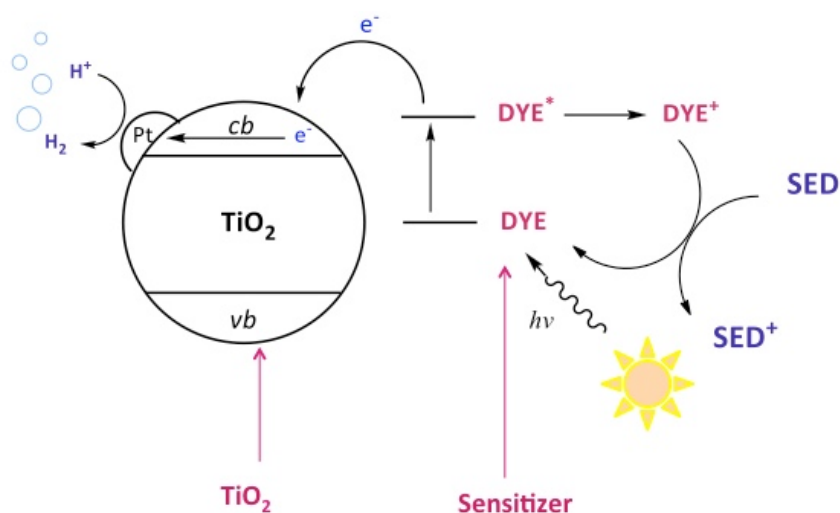
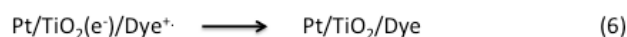
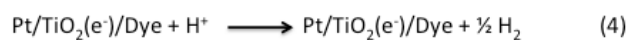
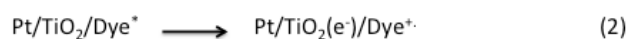


Figure 1. 13: Hydrogen production in the presence of sacrificial agent.

In this half-reaction, the working mechanism reminds the DSSC process presented in the previous paragraph. Following light harvesting, dye excitation, and injection of the photoelectrons in the CB of the semiconductor oxide, electrons are transferred to the TiO_2 CB and reach the active reaction center (reduction catalyst) to generate H_2 (chemical energy instead of electrical energy) in the photocatalytic system.

In a typical photocatalytic system for the dye-sensitized reduction of water to hydrogen using Pt/ TiO_2 as a catalyst, the involved steps are as follow:



Dye is responsible for light harvesting and goes to an excited state upon the absorption of a photon (1) followed by electron injection into the CB of TiO₂, resulting in charge separation (2). To have an efficient process and high durability of the dye, fast regeneration from the SED agent must take place (3) recovering the dye starting redox state. Electrons are trapped on Pt(0) particles adsorbed on the TiO₂ surface and reduce water (H⁺) to molecular hydrogen (4). A few detrimental paths can be present in the process, with two main steps responsible for loss in activity: relaxation of the dye to its ground state before electron injection to the CB of the semiconductor (5) and hole-electron recombination between TiO₂ and dye stimulated by slow H₂ generation and/or dye regeneration (6).

In order to properly describe the different sensitizers and their main properties in the production of hydrogen, we first introduce the most used and important parameters for performance evaluation.

The photoreactor containing the dye sensitized photocatalyst, is then evacuated from oxygen and irradiated with a Xenon lamp or a solar simulator provided with a UV filter at ~ 400 – 410 nm in order to cut off the UV portion of the irradiation and avoid direct TiO₂ excitation of electrons to the CB of the semiconductor. The produced hydrogen gas is finally quantitatively determined by using a gas chromatograph equipped with a thermal conductivity detector (TCD).

The amount of hydrogen evolved is recorded vs time and elaborated to give comparable entities (Figure 1. 14a). The amount should typically increase with

irradiation time unless dye deactivation takes place. Typical amounts are of the order of μmol , more rarely mmol . In order to check dye stability in terms of ability to withstand the production of H_2 , gas evolution rates, reported as $\mu\text{mol h}^{-1}$, are also important (Figure 1. 14b). In some cases, particularly for practical purposes, it is convenient to normalize the amount of evolved gas or the evolution rate to the weight of the catalytic powder (e.g. $\mu\text{mol h}^{-1} \text{g}^{-1}$). In this case comparison is meaningful only when catalysts with similar loadings of dye (that is, active sites) are considered.

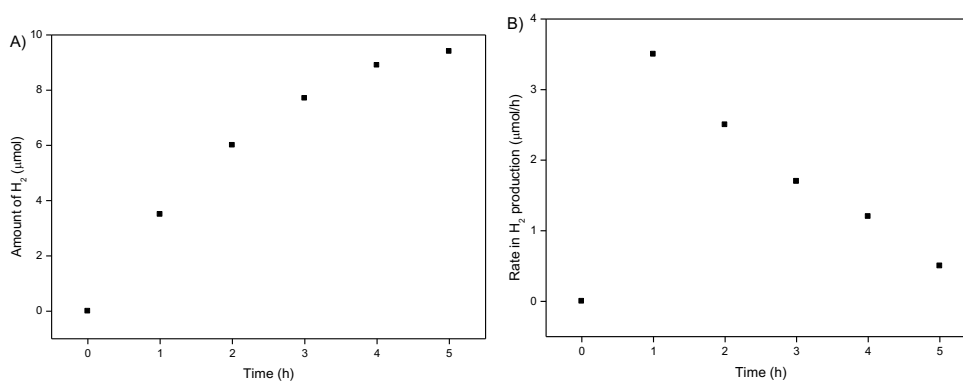


Figure 1. 14: Elaboration of experimental data of a) amount of produced hydrogen vs irradiation time, and a) rate of hydrogen production vs irradiation time.

The first parameter to evaluate the ability of a photocatalytic system, in general, and in particular of a photocatalytic system to efficiently produce hydrogen is the Turnover Number (TON). In the reduction reaction from water to hydrogen, TON is the number of reacted electrons to hydrogen (which corresponds to the complete catalytic cycle), per active catalyst site, before the catalyst becomes inactive. Accordingly, the ideal catalyst would have an infinite TON. Indeed, in a catalytic process the equivalent molar amount of evolved hydrogen should always exceed that of the active photocatalyst. TON is described by Equation 8.

$$TON = \frac{\text{number of reacted electrons}}{\text{number of active sites}} \quad (\text{Eq.8})$$

where the reacted electrons are those actually involved in the reduction from H₂O or H⁺ to H₂. Since the number of active sites is difficult to directly determine, the alternative Equation 9 may be used.

$$TON = \frac{\text{number of reacted electrons}}{\text{number of atoms in the catalyst}} \quad (\text{Eq. 9})$$

In the specific case of dye-sensitized photocatalytic evolution of hydrogen, the catalytic active sites may be taken equal to the number of molecules of sensitizer and, considering that the number of reacted electrons is equal to (2 x molecules of produced H₂), the simplified expression Equation 10, where molecules have been replaced by moles, is used in practical experiments.

$$TON = \frac{2 \times \text{moles of produced hydrogen}}{\text{moles of dye on the nanoparticles}} \quad (\text{Eq. 10})$$

Since the moles of evolved hydrogen are clearly dependent on how long the reaction is followed over time, TON is dependent on the irradiation period. Therefore each TON value should be always referred to the time scale (e.g. TON(20 h)). For this reason, the Turnover Frequency (TOF), that is rate per active site, can be also used. TON and TOF are also dependent on all the specific conditions of the catalytic reaction, in particular temperature, intensity of the light irradiation and presence of wavelength filters.

An alternative way to describe the conversion efficiency is the Light-to-Fuel Efficiency (LFE), as defined in Equation 11, where $\Delta H_{H_2}^0$ is the enthalpy associated with H₂ combustion (285.8 x 10³ J mol⁻¹):

$$LFE = \frac{F_{H_2} \times \Delta H_{H_2}^0}{S \times A_{irr}} \quad (\text{Eq. 11})$$

LFE give an indication of the efficiency in conversion of solar energy into chemical energy stored in the form of H₂ and derive from photoelectrochemical studies,

being calculated through the voltage, current, and the faradaic efficiency for hydrogen evolution.¹⁰⁷

It must be underlined that LFE is dependent on the experimental conditions and the irradiation time. Therefore, comparison of LFE between different studies must carefully check the adopted experimental conditions.

References

- (1) Population Reference Bureau **2016**. "2016 World Population Datasheet," <http://www.prb.org/>.
- (2) Armaroli, N.; Balzani, V.: In *Energy for a Sustainable World*; Wiley-VCH Verlag GmbH & Co. KGaA, 2010.
- (3) International Energy Agency. **2016**. "Key World Energy Statistics." <http://www.iea.org/>.
- (4) Kruger, P.: In *Alternative Energy Resources: the Quest for Sustainable Energy*; John Wiley & Sons, Inc.: Hoboken, NJ, 2006.
- (5) British Petroleum. **2016**. "BP Statistical Review of World Energy." <http://www.bp.com/>.
- (6) Ed Dlugokencky and Pieter Tans, NOAA/ESRL (<http://www.esrl.noaa.gov/gmd/ccgg/trends/>)
- (7) Wilson , E. O.: In *The Creation. An Appeal to Save Life on Earth*; W. W. Norton & Company: New York, 2006.
- (8) UN Intergovernmental Panel on Climate Change. **2007**. "IPCC Fourth Assessment Report: Climate Change 2007." <http://www.ipcc.ch/>.
- (9) Crutzen, P. J. "Geology of mankind". *Nature* **2002**, *415*, 23, doi:10.1038/415023a.
- (10) EIA , <http://www.eia.doe.gov/>
- (11) UN Framework Convention on Climate Changes. **2016**. <http://newsroom.unfccc.int/>.
- (12) <http://www.solarpowereurope.org/home/>
- (13) Letcher, T. M.: In *Storing Energy*; Elsevier: Oxford, 2016.
- (14) Barber, J. "Photosynthetic energy conversion: natural and artificial". *Chem Soc Rev* **2009**, *38*, 185-196, doi:10.1039/b802262n.

(15) NREL, American Society for Testing. **2010**. "Terrestrial Reference Spectra for Photovoltaic Performance Evaluation (ASTM G-173-03)." <http://rredc.nrel.gov/solar/spectra/am1.5/>.

(16) Chapin, D. M.; Fuller, C. S.; Pearson, G. L. "A New Silicon p-n Junction Photocell for Converting Solar Radiation into Electrical Power". *J. Appl. Phys.* **1954**, *25*, 676, doi:10.1063/1.1721711.

(17) Desilvestro, J.; Gratzel, M.; Kavan, L.; Moser, J.; Augustynski, J. "Highly Efficient Sensitization of Titanium-Dioxide". *J. Am. Chem. Soc.* **1985**, *107*, 2988-2990, doi:DOI 10.1021/ja00296a035.

(18) Vlachopoulos, N.; Liska, P.; Augustynski, J.; Gratzel, M. "Very Efficient Visible-Light Energy Harvesting and Conversion by Spectral Sensitization of High Surface-Area Polycrystalline Titanium-Dioxide Films". *J. Am. Chem. Soc.* **1988**, *110*, 1216-1220, doi:DOI 10.1021/ja00212a033.

(19) O'Regan, B.; Gratzel, M. "A low-cost, high-efficiency solar cell based on dye-sensitized colloidal TiO₂ films". *Nature* **1991**, *353*, 737-740.

(20) Nazeeruddin, M. K.; Kay, A.; Rodicio, I.; Humphry-Baker, R.; Mueller, E.; Liska, P.; Vlachopoulos, N.; Graetzel, M. "Conversion of light to electricity by cis-X₂bis(2,2'-bipyridyl-4,4'-dicarboxylate)ruthenium(II) charge-transfer sensitizers (X = Cl-, Br-, I-, CN-, and SCN-) on nanocrystalline titanium dioxide electrodes". *J. Am. Chem. Soc.* **1993**, *115*, 6382-6390, doi:10.1021/ja00067a063.

(21) Nazeeruddin, M. K.; Zakeeruddin, S. M.; Humphry-Baker, R.; Jirousek, M.; Liska, P.; Vlachopoulos, N.; Shklover, V.; Fischer, C. H.; Gratzel, M. "Acid-base equilibria of (2,2'-bipyridyl-4,4'-dicarboxylic acid)ruthenium(II) complexes and the effect of protonation on charge-transfer sensitization of nanocrystalline titania". *Inorg. Chem.* **1999**, *38*, 6298-6305, doi:DOI 10.1021/ic990916a.

(22) Nazeeruddin, M. K.; Humphry-Baker, R.; Liska, P.; Gratzel, M. "Investigation of sensitizer adsorption and the influence of protons on current and voltage of a dye-sensitized nanocrystalline TiO₂ solar cell". *J. Phys. Chem. B* **2003**, *107*, 8981-8987, doi:10.1021/jp022656f.

(23) Wang, P.; Zakeeruddin, S. M.; Moser, J. E.; Nazeeruddin, M. K.; Sekiguchi, T.; Gratzel, M. "A stable quasi-solid-state dye-sensitized solar cell with an amphiphilic ruthenium sensitizer and polymer gel electrolyte". *Nat Mater* **2003**, *2*, 402-407.

(24) Abbotto, A.; Barolo, C.; Bellotto, L.; De Angelis, F.; Gratzel, M.; Manfredi, N.; Marinzi, C.; Fantacci, S.; Yum, J. H.; Nazeeruddin, M. K. "Electron-rich

heteroaromatic conjugated bipyridine based ruthenium sensitizer for efficient dye-sensitized solar cells". *Chem. Commun.* **2008**, 5318-5320, doi:10.1039/b811378e.

(25) Abbotto, A.; Sauvage, F.; Barolo, C.; De Angelis, F.; Fantacci, S.; Graetzel, M.; Manfredi, N.; Marinzi, C.; Nazeeruddin, M. K. "Panchromatic ruthenium sensitizer based on electron-rich heteroarylvinylene pi-conjugated quaterpyridine for dye-sensitized solar cells". *Dalton Transactions* **2011**, 40, 234-242, doi:10.1039/c0dt01190h.

(26) Chen, C. Y.; Wu, S. J.; Wu, C. G.; Chen, J. G.; Ho, K. C. "A ruthenium complex with superhigh light-harvesting capacity for dye-sensitized solar cells". *Angew Chem Int Ed Engl* **2006**, 45, 5822-5825, doi:10.1002/anie.200601463.

(27) Coluccini, C.; Manfredi, N.; Calderon, E. H.; Salamone, M. M.; Ruffo, R.; Roberto, D.; Lobello, M. G.; De Angelis, F.; Abbotto, A. "Photophysical and Electrochemical Properties of Thiophene-Based 2-Arylpyridines". *Eur. J. Org. Chem.* **2011**, 5587-5598, doi:10.1002/ejoc.201100651.

(28) Sauvage, F.; Decoppet, J. D.; Zhang, M.; Zakeeruddin, S. M.; Comte, P.; Nazeeruddin, M.; Wang, P.; Gratzel, M. "Effect of sensitizer adsorption temperature on the performance of dye-sensitized solar cells". *J Am Chem Soc* **2011**, 133, 9304-9310, doi:10.1021/ja110541t.

(29) Shi, D.; Pootrakulchote, N.; Li, R. Z.; Guo, J.; Wang, Y.; Zakeeruddin, S. M.; Gratzel, M.; Wang, P. "New Efficiency Records for Stable Dye-Sensitized Solar Cells with Low-Volatility and Ionic Liquid Electrolytes". *J. Phys. Chem. C* **2008**, 112, 17046-17050, doi:10.1021/jp808018h.

(30) Hagfeldt, A.; Boschloo, G.; Sun, L.; Kloo, L.; Pettersson, H. "Dye-sensitized solar cells". *Chem Rev* **2010**, 110, 6595-6663, doi:10.1021/cr900356p.

(31) Hao, Y.; Yang, X.; Cong, J.; Tian, H.; Hagfeldt, A.; Sun, L. "Efficient near infrared D-pi-A sensitizers with lateral anchoring group for dye-sensitized solar cells". *Chem. Commun.* **2009**, 4031-4033, doi:10.1039/b908396k.

(32) Mishra, A.; Fischer, M. K.; Bauerle, P. "Metal-free organic dyes for dye-sensitized solar cells: from structure: property relationships to design rules". *Angew Chem Int Ed Engl* **2009**, 48, 2474-2499, doi:10.1002/anie.200804709.

(33) Wang, Z. S.; Cui, Y.; Dan-Oh, Y.; Kasada, C.; Shinpo, A.; Hara, K. "Thiophene-functionalized coumarin dye for efficient dye-sensitized solar cells: Electron lifetime improved by coadsorption of deoxycholic acid". *J. Phys. Chem. C* **2007**, 111, 7224-7230, doi:10.1021/jp067872t.

- (34) Wang, Z. S.; Koumura, N.; Cui, Y.; Takahashi, M.; Sekiguchi, H.; Mori, A.; Kubo, T.; Furube, A.; Hara, K. "Hexylthiophene-functionalized carbazole dyes for efficient molecular photovoltaics: Tuning of solar-cell performance by structural modification". *Chem. Mater.* **2008**, *20*, 3993-4003, doi:10.1021/cm8003276.
- (35) Hagberg, D. P.; Yum, J. H.; Lee, H.; De Angelis, F.; Marinado, T.; Karlsson, K. M.; Humphry-Baker, R.; Sun, L.; Hagfeldt, A.; Gratzel, M.; Nazeeruddin, M. K. "Molecular engineering of organic sensitizers for dye-sensitized solar cell applications". *J Am Chem Soc* **2008**, *130*, 6259-6266, doi:10.1021/ja800066y.
- (36) Choi, H.; Baik, C.; Kang, S. O.; Ko, J.; Kang, M. S.; Nazeeruddin, M. K.; Gratzel, M. "Highly efficient and thermally stable organic sensitizers for solvent-free dye-sensitized solar cells". *Angew Chem Int Ed Engl* **2008**, *47*, 327-330, doi:10.1002/anie.200703852.
- (37) Zhang, G.; Bala, H.; Cheng, Y.; Shi, D.; Lv, X.; Yu, Q.; Wang, P. "High efficiency and stable dye-sensitized solar cells with an organic chromophore featuring a binary pi-conjugated spacer". *Chem. Commun.* **2009**, 2198-2200, doi:10.1039/b822325d.
- (38) Abboto, A.; Manfredi, N.; Marinzi, C.; De Angelis, F.; Mosconi, E.; Yum, J. H.; Zhang, X. X.; Nazeeruddin, M. K.; Gratzel, M. "Di-branched di-anchoring organic dyes for dye-sensitized solar cells". *Energy Environ. Sci.* **2009**, *2*, 1094-1101, doi:10.1039/b910654e.
- (39) Abboto, A.; Leandri, V.; Manfredi, N.; De Angelis, F.; Pastore, M.; Yum, J. H.; Nazeeruddin, M. K.; Gratzel, M. "Bis-Donor-Bis-Acceptor Tribranched Organic Sensitizers for Dye-Sensitized Solar Cells". *Eur. J. Org. Chem.* **2011**, 6195-6205, doi:10.1002/Ejoc.201100821.
- (40) Leandri, V.; Ruffo, R.; Trifiletti, V.; Abboto, A. "Asymmetric Tribranched Dyes: An Intramolecular Cosensitization Approach for Dye-Sensitized Solar Cells". *Eur. J. Org. Chem.* **2013**, *2013*, 6793-6801, doi:10.1002/ejoc.201300962.
- (41) Manfredi, N.; Cecconi, B.; Abboto, A. "Multi-Branched Multi-Anchoring Metal-Free Dyes for Dye-Sensitized Solar Cells". *Eur. J. Org. Chem.* **2014**, 7069-7086, doi:10.1002/ejoc.201402422.
- (42) Yella, A.; Lee, H.-W.; Tsao, H. N.; Yi, C.; Chandiran, A. K.; Nazeeruddin, M. K.; Diau, E. W.-G.; Yeh, C.-Y.; Zakeeruddin, S. M.; Grätzel, M. "Porphyrin-Sensitized Solar Cells with Cobalt (II/III)-Based Redox Electrolyte Exceed 12 Percent Efficiency". *Science* **2011**, *334*, 629-634, doi:10.1126/science.1209688.

- (43) Wu, J.; Lan, Z.; Lin, J.; Huang, M.; Huang, Y.; Fan, L.; Luo, G. "Electrolytes in dye-sensitized solar cells". *Chem Rev* **2015**, *115*, 2136-2173, doi:10.1021/cr400675m.
- (44) Yun, S. N.; Freitas, J. N.; Nogueira, A. F.; Wang, Y. M.; Ahmad, S.; Wang, Z. S. "Dye-sensitized solar cells employing polymers". *Prog. Polym. Sci.* **2016**, *59*, 1-40, doi:10.1016/j.progpolymsci.2015.10.004.
- (45) Cai, N.; Moon, S.-J.; Cevey-Ha, L.; Moehl, T.; Humphry-Baker, R.; Wang, P.; Zakeeruddin, S. M.; Grätzel, M. "An Organic D- π -A Dye for Record Efficiency Solid-State Sensitized Heterojunction Solar Cells". *Nano Lett.* **2011**, *11*, 1452-1456, doi:10.1021/nl104034e.
- (46) Lee, M. M.; Teuscher, J.; Miyasaka, T.; Murakami, T. N.; Snaith, H. J. "Efficient Hybrid Solar Cells Based on Meso-Superstructured Organometal Halide Perovskites". *Science* **2012**, *338*, 643-647, doi:10.1126/science.1228604.
- (47) Bednorz, J. G.; Müller, K. A. "Possible highTc superconductivity in the Ba-La-Cu-O system". *ZPhyB* **1986**, *64*, 189-193, doi:10.1007/BF01303701.
- (48) Yang, W. S.; Noh, J. H.; Jeon, N. J.; Kim, Y. C.; Ryu, S.; Seo, J.; Seok, S. I. "SOLAR CELLS. High-performance photovoltaic perovskite layers fabricated through intramolecular exchange". *Science* **2015**, *348*, 1234-1237, doi:10.1126/science.aaa9272.
- (49) Aristidou, N.; Sanchez-Molina, I.; Chotchuangchutchaval, T.; Brown, M.; Martinez, L.; Rath, T.; Haque, S. A. "The Role of Oxygen in the Degradation of Methylammonium Lead Trihalide Perovskite Photoactive Layers". *Angew Chem Int Ed Engl* **2015**, *54*, 8208-8212, doi:10.1002/anie.201503153.
- (50) Christians, J. A.; Manser, J. S.; Kamat, P. V. "Best Practices in Perovskite Solar Cell Efficiency Measurements. Avoiding the Error of Making Bad Cells Look Good". *J. Phys. Chem. Lett.* **2015**, *6*, 852-857, doi:10.1021/acs.jpcllett.5b00289.
- (51) Fabregat-Santiago, F.; Bisquert, J.; Cevey, L.; Chen, P.; Wang, M.; Zakeeruddin, S. M.; Grätzel, M. "Electron Transport and Recombination in Solid-State Dye Solar Cell with Spiro-OMeTAD as Hole Conductor". *J. Am. Chem. Soc.* **2009**, *131*, 558-562, doi:10.1021/ja805850q.
- (52) Gratzel, M. "The light and shade of perovskite solar cells". *Nature Materials* **2014**, *13*, 838-842.

- (53) Berhe, T. A.; Su, W.-N.; Chen, C.-H.; Pan, C.-J.; Cheng, J.-H.; Chen, H.-M.; Tsai, M.-C.; Chen, L.-Y.; Dubale, A. A.; Hwang, B.-J. "Organometal halide perovskite solar cells: degradation and stability". *Energy Environ. Sci.* **2016**, doi:10.1039/C5EE02733K.
- (54) Trifiletti, V.; Manfredi, N.; Listorti, A.; Altamura, D.; Giannini, C.; Colella, S.; Gigli, G.; Rizzo, A. "Engineering TiO₂/Perovskite Planar Heterojunction for Hysteresis-Less Solar Cells". *Advanced Materials Interfaces* **2016**, 1600493-n/a, doi:10.1002/admi.201600493.
- (55) Collavini, S.; Völker, S. F.; Delgado, J. L. "Understanding the Outstanding Power Conversion Efficiency of Perovskite-Based Solar Cells". *Angew. Chem. Int. Ed.* **2015**, *54*, 9757-9759, doi:10.1002/anie.201505321.
- (56) Jiang, F.; Liu, T.; Luo, B.; Tong, J.; Qin, F.; Xiong, S.; Li, Z.; Zhou, Y. "A two-terminal perovskite/perovskite tandem solar cell". *J. Mater. Chem. A* **2016**, doi:10.1039/C5TA08744A.
- (57) Bailie, C. D.; Christoforo, M. G.; Mailoa, J. P.; Bowring, A. R.; Unger, E. L.; Nguyen, W. H.; Burschka, J.; Pellet, N.; Lee, J. Z.; Gratzel, M.; Noufi, R.; Buonassisi, T.; Salleo, A.; McGehee, M. D. "Semi-transparent perovskite solar cells for tandems with silicon and CIGS". *Energy Environ. Sci.* **2015**, *8*, 956-963, doi:10.1039/C4EE03322A.
- (58) Bailie, C. D.; McGehee, M. D. "High-efficiency tandem perovskite solar cells". *MRS Bull.* **2015**, *40*, 681-686, doi:doi:10.1557/mrs.2015.167.
- (59) Mailoa, J. P.; Bailie, C. D.; Johlin, E. C.; Hoke, E. T.; Akey, A. J.; Nguyen, W. H.; McGehee, M. D.; Buonassisi, T. "A 2-terminal perovskite/silicon multijunction solar cell enabled by a silicon tunnel junction". *Appl Phys Lett* **2015**, *106*, 121105, doi:doi:<http://dx.doi.org/10.1063/1.4914179>.
- (60) Albrecht, S.; Saliba, M.; Correa Baena, J. P.; Lang, F.; Kegelmann, L.; Mews, M.; Steier, L.; Abate, A.; Rappich, J.; Korte, L.; Schlattmann, R.; Nazeeruddin, M. K.; Hagfeldt, A.; Gratzel, M.; Rech, B. "Monolithic perovskite/silicon-heterojunction tandem solar cells processed at low temperature". *Energy Environ. Sci.* **2016**, *9*, 81-88, doi:10.1039/C5EE02965A.
- (61) Werner, J.; Weng, C.-H.; Walter, A.; Fesquet, L.; Seif, J. P.; De Wolf, S.; Niesen, B.; Ballif, C. "Efficient Monolithic Perovskite/Silicon Tandem Solar Cell with Cell Area >1 cm²". *J. Phys. Chem. Lett.* **2016**, *7*, 161-166, doi:10.1021/acs.jpcl.5b02686.
- (62) Snaith, H. J. "Estimating the Maximum Attainable Efficiency in Dye-Sensitized Solar Cells". *Advanced Functional Materials* **2010**, *20*, 13-19, doi:10.1002/adfm.200901476.

- (63) Green, M. A.; Emery, K.; Hishikawa, Y.; Warta, W. "Solar cell efficiency tables (version 36)". *Prog. Photovolt: Res. Appl.* **2010**, *18*, 346-352, doi:10.1002/pip.1021.
- (64) Brabec, C.; Dyakonov, V.; Parisi, J.; Sariciftci, N. S.: *Organic Photovoltaics*; Springer-Verlag, Berlin, 2003.
- (65) Shockley, W.; Queisser, H. J. "Detailed Balance Limit of Efficiency of p-n Junction Solar Cells". *J. Appl. Phys.* **1961**, *32*, 510, doi:10.1063/1.1736034.
- (66) Green, M. A.; Emery, K.; Hishikawa, Y.; Warta, W.; Dunlop, E. D. "Solar cell efficiency tables (Version 45)". *Prog Photovoltaics* **2015**, *23*, 1-9, doi:10.1002/pip.2573.
- (67) Donne, A. L.; Scaccabarozzi, A.; Tombolato, S.; Binetti, S.; Acciarri, M.; Abbotto, A. "Solar Photovoltaics: A Review". *Reviews in Advanced Sciences and Engineering* **2013**, *2*, 170-178, doi:10.1166/rase.2013.1030.
- (68) Yan, J. F.; Saunders, B. R. "Third-generation solar cells: a review and comparison of polymer: fullerene, hybrid polymer and perovskite solar cells". *Rsc Adv* **2014**, *4*, 43286-43314, doi:10.1039/c4ra07064j.
- (69) International Energy Agency, Key World Energy Statistics, 2015, <http://www.iea.gov/>
- (70) Armaroli, N.; Balzani, V. "Towards an electricity-powered world". *Energy Environ. Sci.* **2011**, *4*, 3193-3222, doi:10.1039/c1ee01249e.
- (71) Armaroli, N.; Balzani, V. "The hydrogen issue". *ChemSusChem* **2011**, *4*, 21-36, doi:10.1002/cssc.201000182.
- (72) Balzani, V.; Credi, A.; Venturi, M. "Photochemical conversion of solar energy". *ChemSusChem* **2008**, *1*, 26-58, doi:10.1002/cssc.200700087.
- (73) Fujishima, A.; Honda, K. "Electrochemical Photolysis of Water at a Semiconductor Electrode". *Nature* **1972**, *238*, 37-38, doi:10.1038/238037a0.
- (74) Zhou, X. L.; Tyson, D. S.; Castellano, F. N. "First generation light-harvesting dendrimers with a [Ru(bpy)(3)](2+) core and aryl ether ligands functionalized with coumarin 450". *Angew Chem Int Edit* **2000**, *39*, 4301-+, doi:Doi 10.1002/1521-3773(20001201)39:23<4301::Aid-Anie4301>3.0.Co;2-9.
- (75) Barber, J.; Tran, P. D. "From natural to artificial photosynthesis". *J R Soc Interface* **2013**, *10*, 20120984, doi:10.1098/rsif.2012.0984.

- (76) Chen, X.; Shen, S.; Guo, L.; Mao, S. S. "Semiconductor-based photocatalytic hydrogen generation". *Chem Rev* **2010**, *110*, 6503-6570, doi:10.1021/cr1001645.
- (77) Kudo, A.; Miseki, Y. "Heterogeneous photocatalyst materials for water splitting". *Chem Soc Rev* **2009**, *38*, 253-278, doi:10.1039/b800489g.
- (78) Barber, J.; Tran, P. D. "From natural to artificial photosynthesis". *J. R. Soc. Interface* **2013**, *10*, doi:10.1098/rsif.2012.0984.
- (79) Zhang, X. H.; Peng, T. Y.; Song, S. S. "Recent advances in dye-sensitized semiconductor systems for photocatalytic hydrogen production". *J. Mater. Chem. A* **2016**, *4*, 2365-2402, doi:10.1039/c5ta08939e.
- (80) Borgarello, E.; Kiwi, J.; Pelizzetti, E.; Visca, M.; Gratzel, M. "Photochemical Cleavage of Water by Photocatalysis". *Nature* **1981**, *289*, 158-160, doi:DOI 10.1038/289158a0.
- (81) Maeda, K.; Sahara, G.; Eguchi, M.; Ishitani, O. "Hybrids of a Ruthenium(II) Polypyridyl Complex and a Metal Oxide Nanosheet for Dye-Sensitized Hydrogen Evolution with Visible Light: Effects of the Energy Structure on Photocatalytic Activity". *Acc Catal* **2015**, *5*, 1700-1707, doi:10.1021/acscatal.5b00040.
- (82) Saupe, G. B.; Mallouk, T. E.; Kim, W.; Schmehl, R. H. "Visible light photolysis of hydrogen iodide using sensitized layered metal oxide semiconductors: The role of surface chemical modification in controlling back electron transfer reactions". *J. Phys. Chem. B* **1997**, *101*, 2508-2513, doi:DOI 10.1021/jp9625319.
- (83) Vinodgopal, K.; Hua, X.; Dahlgren, R. L.; Lappin, A. G.; Patterson, L. K.; Kamat, P. V. "Photochemistry of Ru(Bpy)₂(Dcbpy)₂⁺ on Al₂O₃ and TiO₂ Surfaces - an Insight into the Mechanism of Photosensitization". *J. Phys. Chem.* **1995**, *99*, 10883-10889, doi:DOI 10.1021/j100027a032.
- (84) Kim, W.; Tachikawa, T.; Majima, T.; Li, C.; Kim, H.-J.; Choi, W. "Tin-porphyrin sensitized TiO₂ for the production of H₂ under visible light". *Energy Environ. Sci.* **2010**, *3*, 1789, doi:10.1039/c0ee00205d.
- (85) Martin-Gomis, L.; Fernandez-Lazaro, F.; Sastre-Santos, A. "Advances in phthalocyanine-sensitized solar cells (PcSSCs)". *J. Mater. Chem. A* **2014**, *2*, 15672-15682, doi:10.1039/c4ta01894j.
- (86) Urbani, M.; Gratzel, M.; Nazeeruddin, M. K.; Torres, T. "Meso-substituted porphyrins for dye-sensitized solar cells". *Chem Rev* **2014**, *114*, 12330-12396, doi:10.1021/cr5001964.

- (87) Watanabe, M.; Hagiwara, H.; Iribe, A.; Ogata, Y.; Shiomi, K.; Staykov, A.; Ida, S.; Tanaka, K.; Ishihara, T. "Spacer effects in metal-free organic dyes for visible-light-driven dye-sensitized photocatalytic hydrogen production". *J. Mater. Chem. A* **2014**, *2*, 12952-12961, doi:10.1039/c4ta02720e.
- (88) Tiwari, A.; Mondal, I.; Pal, U. "Visible light induced hydrogen production over thiophenothiazine-based dye sensitized TiO₂ photocatalyst in neutral water". *RSC Adv.* **2015**, *5*, 31415-31421, doi:10.1039/c5ra03039k.
- (89) Cecconi, B.; Manfredi, N.; Montini, T.; Fornasiero, P.; Abbotto, A. "Dye-Sensitized Solar Hydrogen Production: The Emerging Role of Metal-Free Organic Sensitizers". *Eur. J. Org. Chem.* **2016**, *2016*, 5194-5215, doi:10.1002/ejoc.201600653.
- (90) Cecconi, B.; Manfredi, N.; Ruffo, R.; Montini, T.; Romero-Ocana, I.; Fornasiero, P.; Abbotto, A. "Tuning Thiophene-Based Phenothiazines for Stable Photocatalytic Hydrogen Production". *ChemSusChem* **2015**, *8*, 4216-4228, doi:10.1002/cssc.201501040.
- (91) Manfredi, N.; Cecconi, B.; Calabrese, V.; Minotti, A.; Peri, F.; Ruffo, R.; Monai, M.; Romero-Ocana, I.; Montini, T.; Fornasiero, P.; Abbotto, A. "Dye-sensitized photocatalytic hydrogen production: distinct activity in a glucose derivative of a phenothiazine dye". *Chem. Commun.* **2016**, *52*, 6977-6980, doi:10.1039/c6cc00390g.
- (92) Lee, S. H.; Park, Y.; Wee, K. R.; Son, H. J.; Cho, D. W.; Pac, C.; Choi, W.; Kang, S. O. "Significance of hydrophilic characters of organic dyes in visible-light hydrogen generation based on TiO₂". *Org Lett* **2010**, *12*, 460-463, doi:10.1021/ol9026182.
- (93) Chen, S.; Li, Y.; Wang, C. "Visible-light-driven photocatalytic H₂ evolution from aqueous suspensions of perylene diimide dye-sensitized Pt/TiO₂ catalysts". *RSC Adv.* **2015**, *5*, 15880-15885, doi:10.1039/c4ra16245e.
- (94) Abe, R.; Shinmei, K.; Hara, K.; Ohtani, B. "Robust dye-sensitized overall water splitting system with two-step photoexcitation of coumarin dyes and metal oxide semiconductors". *Chem. Commun.* **2009**, 3577-3579, doi:10.1039/b905935k.
- (95) Gersten, S. W.; Samuels, G. J.; Meyer, T. J. "Catalytic-Oxidation of Water by an Oxo-Bridged Ruthenium Dimer". *J. Am. Chem. Soc.* **1982**, *104*, 4029-4030, doi:DOI 10.1021/ja00378a053.
- (96) Duan, L. L.; Bozoglian, F.; Mandal, S.; Stewart, B.; Privalov, T.; Llobet, A.; Sun, L. C. "A molecular ruthenium catalyst with water-oxidation activity comparable to that of photosystem II". *Nature Chemistry* **2012**, *4*, 418-423, doi:10.1038/Nchem.1301.

- (97) Mukherjee, S.; Stull, J. A.; Yano, J.; Stamatatos, T. C.; Pringouri, K.; Stich, T. A.; Abboud, K. A.; Britt, R. D.; Yachandra, V. K.; Christou, G. "Synthetic model of the asymmetric [Mn₃CaO₄] cubane core of the oxygen-evolving complex of photosystem II". *Proc Natl Acad Sci U S A* **2012**, *109*, 2257-2262, doi:10.1073/pnas.1115290109.
- (98) Yin, Q.; Tan, J. M.; Besson, C.; Geletii, Y. V.; Musaev, D. G.; Kuznetsov, A. E.; Luo, Z.; Hardcastle, K. I.; Hill, C. L. "A fast soluble carbon-free molecular water oxidation catalyst based on abundant metals". *Science* **2010**, *328*, 342-345, doi:10.1126/science.1185372.
- (99) Kanan, M. W.; Nocera, D. G. "In situ formation of an oxygen-evolving catalyst in neutral water containing phosphate and Co²⁺". *Science* **2008**, *321*, 1072-1075, doi:10.1126/science.1162018.
- (100) Moore, G. F.; Blakemore, J. D.; Milot, R. L.; Hull, J. F.; Song, H. E.; Cai, L.; Schmuttenmaer, C. A.; Crabtree, R. H.; Brudvig, G. W. "A visible light water-splitting cell with a photoanode formed by codeposition of a high-potential porphyrin and an iridium water-oxidation catalyst". *Energy Environ. Sci.* **2011**, *4*, 2389-2392, doi:10.1039/c1ee01037a.
- (101) Li, G.; Sproviero, E. M.; McNamara, W. R.; Snoeberger, R. C., 3rd; Crabtree, R. H.; Brudvig, G. W.; Batista, V. S. "Reversible visible-light photooxidation of an oxomanganese water-oxidation catalyst covalently anchored to TiO₂ nanoparticles". *J Phys Chem B* **2010**, *114*, 14214-14222, doi:10.1021/jp908925z.
- (102) Hambourger, M.; Gervaldo, M.; Svedruzic, D.; King, P. W.; Gust, D.; Ghirardi, M.; Moore, A. L.; Moore, T. A. "[FeFe]-hydrogenase-catalyzed H₂ production in a photoelectrochemical biofuel cell". *J Am Chem Soc* **2008**, *130*, 2015-2022, doi:10.1021/ja077691k.
- (103) Li, L.; Duan, L.; Wen, F.; Li, C.; Wang, M.; Hagfeldt, A.; Sun, L. "Visible light driven hydrogen production from a photo-active cathode based on a molecular catalyst and organic dye-sensitized p-type nanostructured NiO". *Chem. Commun.* **2012**, *48*, 988-990, doi:10.1039/c2cc16101j.
- (104) Lakadamyali, F.; Reisner, E. "Photocatalytic H₂ evolution from neutral water with a molecular cobalt catalyst on a dye-sensitised TiO₂ nanoparticle". *Chem. Commun.* **2011**, *47*, 1695-1697, doi:10.1039/c0cc04658b.
- (105) Reece, S. Y.; Hamel, J. A.; Sung, K.; Jarvi, T. D.; Esswein, A. J.; Pijpers, J. J.; Nocera, D. G. "Wireless solar water splitting using silicon-based semiconductors and earth-abundant catalysts". *Science* **2011**, *334*, 645-648, doi:10.1126/science.1209816.

(106) Hardin, B. E.; Snaith, H. J.; McGehee, M. D. "The renaissance of dye-sensitized solar cells". *Nat Photon* **2012**, *6*, 162-169.

(107) Li, X.; Yu, J.; Low, J.; Fang, Y.; Xiao, J.; Chen, X. "Engineering heterogeneous semiconductors for solar water splitting". *J. Mater. Chem. A* **2015**, *3*, 2485-2534, doi:10.1039/C4TA04461D.

Chapter 2

Dye sensitized solar cells

*“Great things are done by a series
of small things brought together.”¹*

Vincent Van Gogh, Artist, 1853 - 1890

Aim of this section

The first part of this PhD research project has been dedicated to the study of new sensitizers and material in the field of dye sensitized solar cells. As mentioned before, the dye-sensitized solar cells are easy tuneable devices. In fact, the photovoltaic response of the device can be easily modified not just changing the sensitizers, but also changing the morphology of the semiconductor, or the electrolyte. In this section we will focus our consideration on the study of two different classes of sensitizers with a particular attention to the tuning of their optical properties. The first class of sensitizers has been developed in collaboration with the group of Prof. Baldoli at the University of Milan.² The peculiar feature of these new dyes lies in the use of an uncommon π -spacer such as a functionalized benzodithiophene in combination with a variously functionalized triarylamine donor group and cyano acetic as acceptor/anchoring moiety. A general structure of the investigated dyes is depicted in Figure 2. 1.

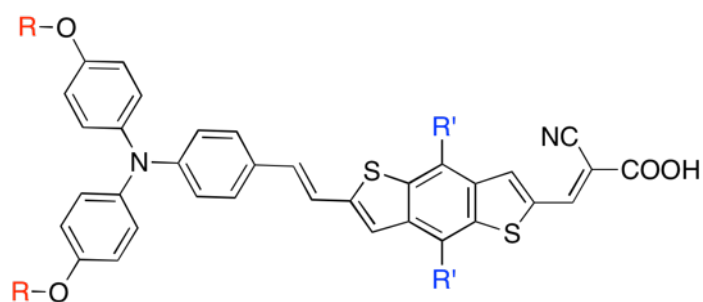


Figure 2. 1: general structure of a functionalized benzodithiophene based organic dye for DSSCs.

The second class of sensitizers has been developed in our laboratory in collaboration with another PhD research project. The new dyes uses the branched geometry, previously developed and deeply studied from our group (Figure 2. 2). This molecular structure, using a phenothiazine (**PTZ**) donor core instead of a common triphenylamine, allow to obtain molecules that show a more firmly bond with the titanium dioxide, useful feature in case of long term stability or in case of water based application.

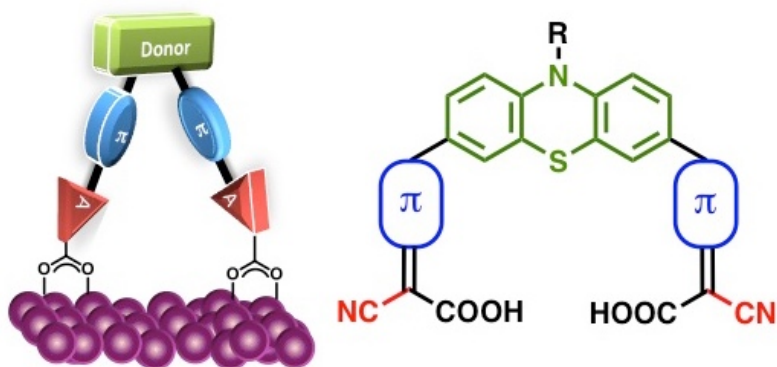


Figure 2. 2: general structure of a **PTZ**-based multibranching dyes

The studies on these molecules started, as usual, with the investigation of the photovoltaic response upon the variation of the optical properties as a result of the increase of the conjugation through the molecular structure. We synthesised a numbers of new dyes varying the π -spacer, exploiting different heteroaromatic rings such as functionalized thiophene derivatives or thiophene fused rings (Figure 2. 3).³

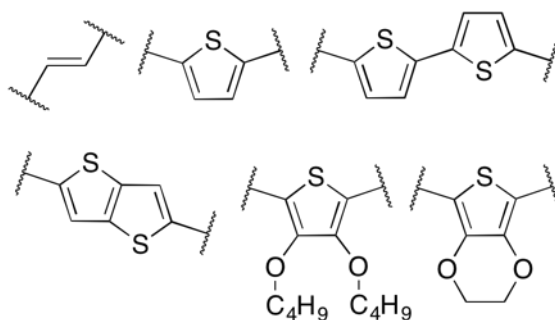


Figure 2. 3: π -spacer investigated in this research.

Moreover, the effect of the side functionalization, and the resulting variation of water affinity, has been exploited upon functionalization of the **PTZ** donor core with different hydrophobic and hydrophilic functionalities (Figure 2. 4).⁴ We have tested the photovoltaic characteristic of devices prepared using the water compatible functionalized dyes with either organic-based or water-based electrolyte.

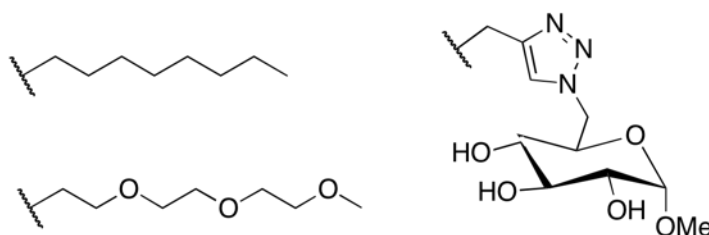


Figure 2. 4: side functionalities investigated in this research.

Last but not least, we have studied the photovoltaic properties of different carbon doped titanium dioxide nanoparticles (C-TiO₂-Np) produced at the university of Padova (Prof. G. Brusatin). These new materials have been tested in different devices configuration, either in double or single layer architecture, with or without a commercial scattering TiO₂ paste in order to study the photovoltaic response and compared to the most widely used commercially available TiO₂ paste.

Benzodithiophene based organic dyes for DSSC

In the last decade, the scientific community have been attracted by organic photovoltaic; and in particular DSSCs have attracted lots of interest due to their interesting good cost/efficiency ratio.⁵ In these years a large number of sensitizers have been studied in order to tune and eventually improve the efficiency of the device in relation to its final application. Since the very beginning, the most efficient dyes were happen to be the well known ruthenium complexes presented by Graezel and co-workers,^{6,7} nonetheless the researchers have focus their attention on the development of metal free organic dyes. In fact, metal free organic dyes allow a great number of diverse structures can be easily prepared using well established synthetic methodologies and, through appropriate molecular design, their optical, electronic and electrochemical properties can be finely modulated.⁸⁻¹⁰ The most widely investigated design for pure organic dyes is the push-pull structure in which an electron-rich donor group is conjugated through a π -spacer with an acceptor/anchoring group linked to the TiO_2 . The nature of the different components of the molecule is able to determine the optical properties as well as the electrochemical and photovoltaic properties.^{11,12} A number of conjugated aromatic and heteroaromatic systems have been investigated as spacers and dyes containing substituted thiophene or thienothiophene bridges have already shown remarkable efficiencies when employed in DSSC.¹³ On the contrary benzodithiophene systems, which own structural and electronic properties that match the π -spacer requests, have been widely employed in photovoltaic polymers¹⁴ but less used in DSSCs dye structures.¹⁵⁻¹⁷ In a previous work of Baldoli and co-workers, it has been demonstrated that the dye containing a benzo[1,2-b:4,5-b']dithiophene moiety as conjugated π -spacer, showed a better efficiency in DSSCs in respect of the other containing benzo[1,2-b:4,3-b']dithiophene π -spacer.¹⁸

On the basis of this work, a new series of push-pull dyes containing benzo[1,2-b:4,5-b']dithiophene (**BDT**₁) have been designed and synthesized to improve the performances (Figure 2. 5). The new dyes have been synthesized in the group of Prof Baldoli and the synthesis will be just presented because not a part of this PhD thesis, as well as electrochemistry and DFT calculation. We have deeply investigated the optical properties and the photovoltaic performances.

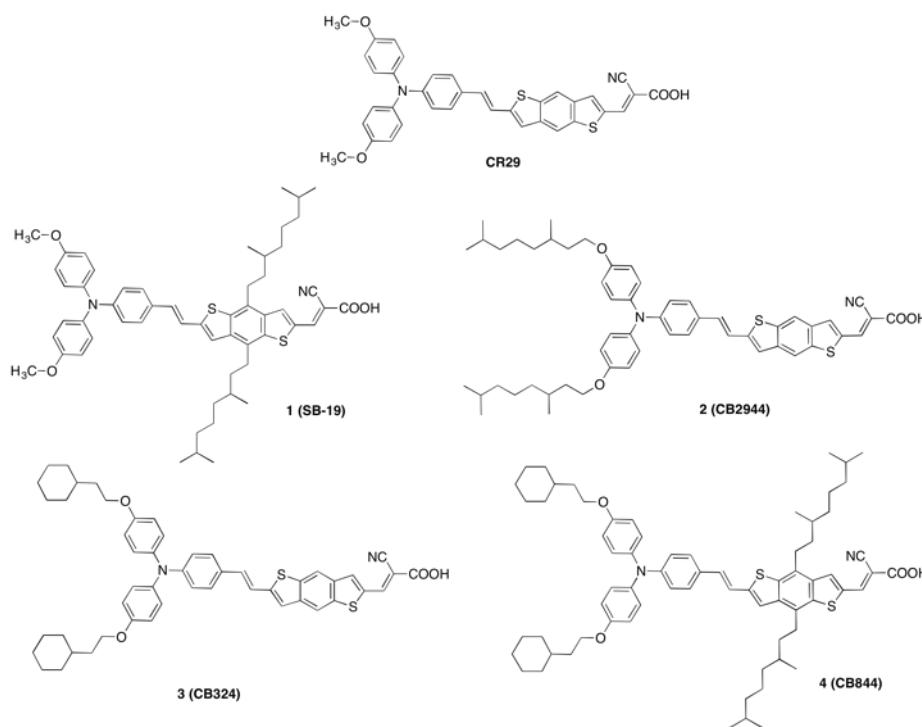
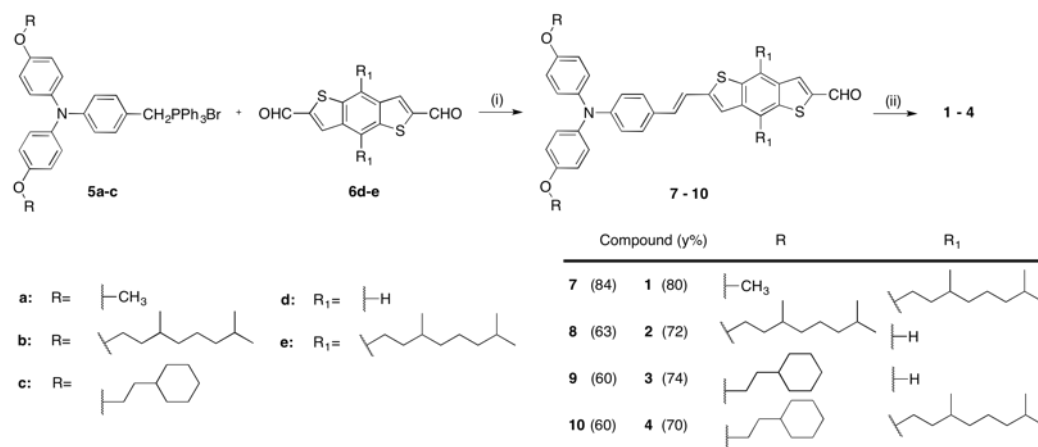


Figure 2. 5: **BDT**₁ based dyes investigated in this work.

The new dye shows the linear geometry, common in push-pull dyes, bearing a triarylamine donor group functionalized with different alkyl chains. The **BDT**₁ moiety connects the donor unit to the acceptor/anchoring cyanoacetic group. The use of bulky alkyl chains, such as 3,7-dimethyloctyl- and/or cyclohexylethyl functionalities, are meant to reduce some detrimental process such as dye aggregation at the TiO₂ surface and charge recombination at the TiO₂/electrolyte interface.¹⁹⁻²¹

SYNTHESIS, DFT CALCULATION AND ELECTROCHEMICAL PROPERTIES

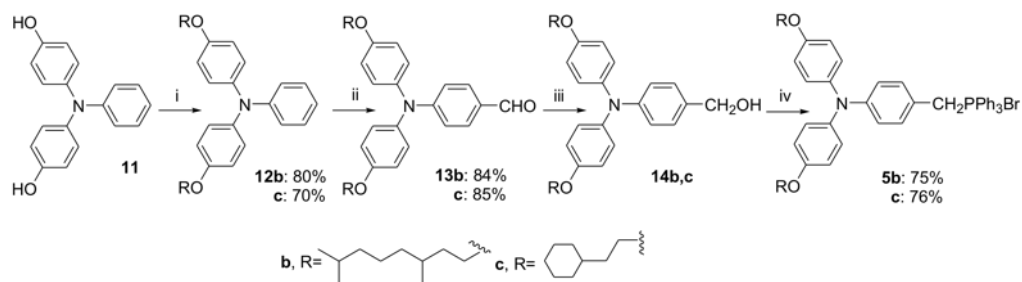
The detailed synthetic procedure for the new **BDT**₁-based dyes is reported in literature.² Here we present a general description of the synthetic pathway and the synthetic scheme for the four new dyes in Scheme 2. 1



Scheme 2. 1: general synthetic scheme for **BDT**₁-base dyes **1-4**. Reagents and conditions: (i) K_2CO_3 , 18-crown-6, DMF, r.t., 12 h; (ii) cyanoacetic acid, piperidine, THF, reflux, 8 h.

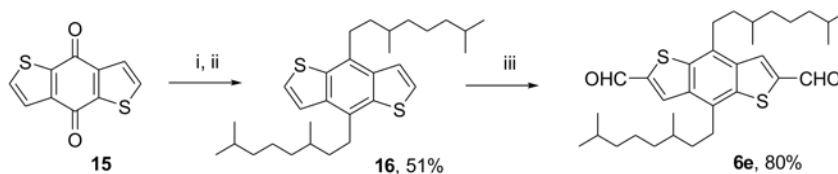
The properly functionalized phosphonium salt of the triphenylamine has been reacted with the **BDT**₁ di-aldehyde under Wittig condition in DMF at room temperature under phase transfer catalysis with 18-crown-6 ether and K_2CO_3 as a base, and gave formyl derivatives **7 - 10** in rather good yields. The final push-pull dyes have been prepared through reaction of the aldehyde with cyanoacetic acid in presence of a catalytic amount of piperidine in refluxing THF to give the crude product. After chromatography over silica gel and treatment with an aqueous solution of HCl (0.5 N), the pure products have been isolated with good yield. Phosphonium salts **5b** and **c** are new compounds and their synthesis is depicted in Scheme 2. 2. 4,4'-dihydroxytriphenylamine (**11**)²² was reacted with the proper alkylbromide, in the presence of K_2CO_3 and 18-crown-6 at reflux in CH_3CN , to give the corresponding alkoxy substituted triarylamine **12b,c**. Their subsequent formylation under Vilsmeier conditions gave aldehydes **13b,c** in good yields. The reduction of the formyl group with $NaBH_4$ gave the corresponding alcohols **14b,c**

in quantitative yields and their treatment with PPh_3 hydrobromide, at reflux in CHCl_3 gave phosphonium salts **5b, c** in rather good yields.



Scheme 2. 2: synthesis of functionalized triphenylamine donor core. Reagents and conditions: R-Br, K_2CO_3 , 18-crown-6, CH_3CN , 80°C 10 h; ii) DMF , POCl_3 , dichloroethane, 80°C 6h. iii) NaBH_4 , MeOH r.t. 4h iv) PPh_3HBr , CHCl_3 , 62°C 5 h.

Benzodithiophene bis-aldehyde **6d** was prepared as already reported¹⁸ while the new 3,7-dimethyloctyl disubstituted **BDT**₁ bis-aldehyde **6e** was synthesized starting from benzo[1,2-b:4,5-b']dithiophene-4,8-dione **15** (Scheme 3), which was reacted with 3,7-dimethyloctylmagnesium bromide, heating in THF solution followed by the addition of tin(II) chloride that gave 4,8-bis-(dimethyloctyl)benzodithiophene **16** in 51% yield. This was treated with 3 equivalents of butyllithium, followed by the addition of DMF to give the new bis-aldehyde **6e** in 80% yield.



Scheme 2. 3: synthesis of functionalized **BDT**₁ π -spacer. Reagents and conditions:

The new chromophores were completely characterized. The optical and redox properties as well as DSSC performances of dyes **1-4** and their dependence on the nature and position of the alkyl chains have been investigated. In addition, as a complement to the experimental work the molecular and electronic structures and the excited states of dyes **1-4** were investigated by achieving DFT/TDDFT calculations.

Optimized geometries of the considered dyes, compared with the reference **CR29** dye, have been calculated and are reported in Figure 3. All the molecules have been simulated in their protonated form, and are characterized by a planar donor-acceptor geometries, except for the two *O*-alkyl substituted phenyl rings in the donor part of the structures. The presence of lateral alkyl chains on **BDT₁** spacer (dye **1** and **4**) causes a consistent steric hindrance near the molecule, but does not modify the structure geometry. This arrangement suggests a strong conjugation between the donor, the **BDT₁** spacer and cyanoacrylic anchoring group, as previously found for this kind of structures.

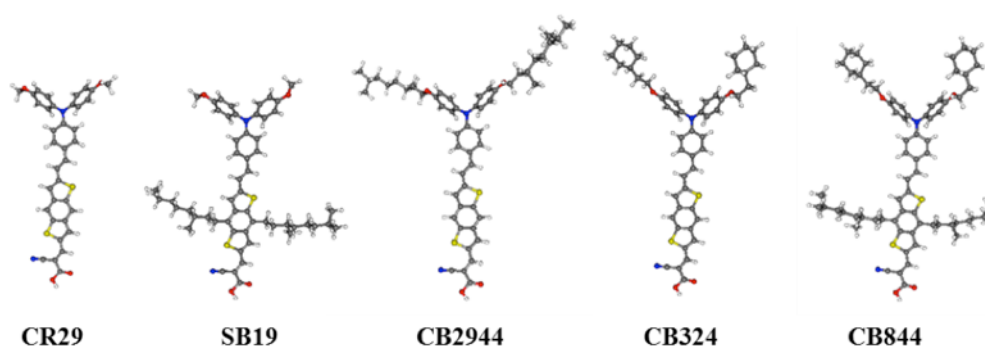


Figure 2. 6: optimized geometries of the investigated dyes.

All the investigated dyes exhibit a strong push-pull behaviour, characteristic for these D- π -A compounds in which the HOMO is mainly localized on the triphenylamine donor moiety, and the LUMO extends over the p-bridge and the acceptor cyanoacrylic acid with the largest component localized on the latter (Fig. 4). The calculated HOMO and LUMO energy levels are in quite good agreement with their experimental analogues, obtained by electrochemical characterization discussed afterwards.

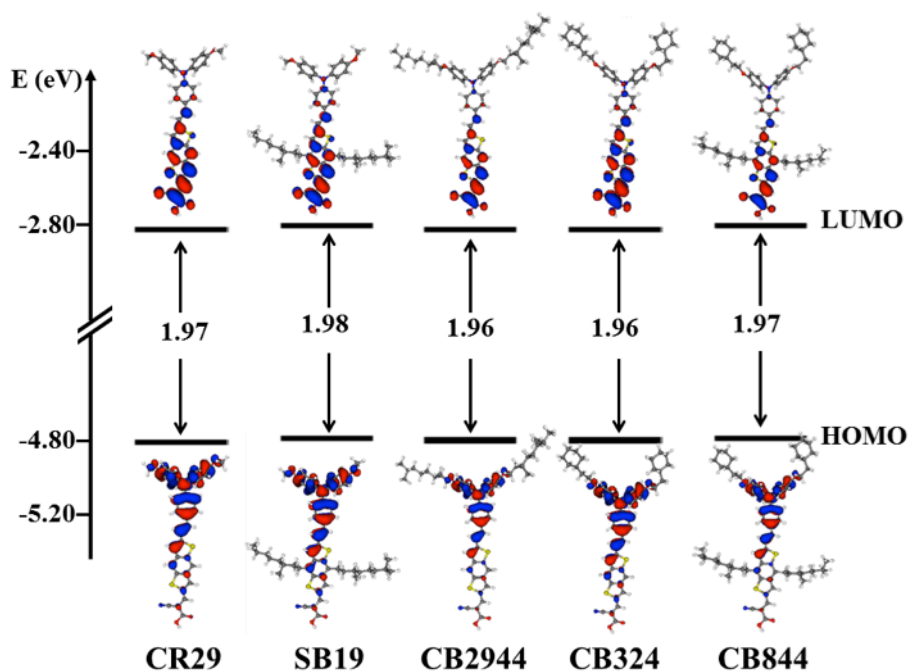


Figure 2. 7: HOMO-LUMO energy levels and isodensity plots for the considered dyes.

The energy gaps are comprised in a 0.02 eV range, between 1.96 eV and 1.98 eV. The slight differences among the dyes are due to the fact that the dye backbone structure is essentially the same along all the series, while the alkoxy substituents little affect the electronic properties of the sensitizers.

To evaluate the possibility of electron-transfer from the dye **1-4** excited state to the conductive band of TiO_2 , their redox behavior and experimental HOMO/LUMO energy levels were determined by using cyclic voltammetry technique. The CV patterns for dyes **1-4** are reported in Figure 2. 8 and the calculated experimental HOMO/LUMO energies are reported in Table 2. 1, and compared to the theoretical ones.

Concerning the energy parameters, since the first reduction is practically unaffected by the alkyl presence (-1.99 V in **1** vs -1.98 V in **CR29**; -2.05 V in **4** vs -2.06 V in **3**) and the first oxidation only slightly affected (0.24 V in **1** vs 0.26 V in **CR29**; 0.25 V in **4** vs 0.29 V in **3**).

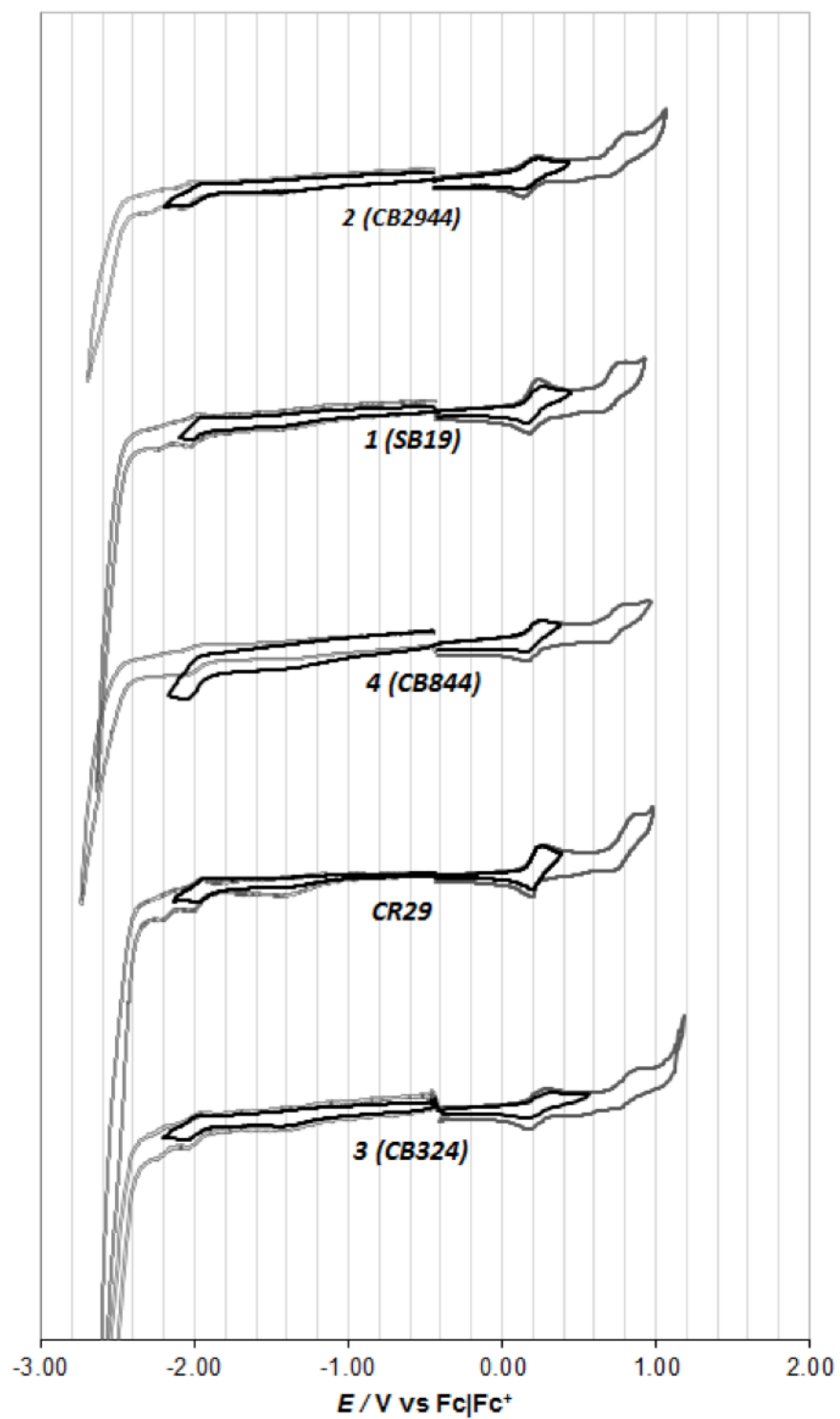


Figure 2. 8: CV profiles of dyes 1-4 in $CH_2Cl_2 + 0.1 M TBAPF_6$ at 0.2 V/s.

The alkylation of **BDT**₁ unit leaves the LUMOs practically constant, while the HOMOs are slightly higher and the energy gaps slightly decrease. This small effect is not observed in the computation results, which however do not take into account the creation of net charges in the polar (solvent + supporting electrolyte) medium. The effect of increasing the bulkiness of the *O*-alkyl chains on the amino site can be instead evaluated comparing dye **CR29** and **1** bearing *O*-Me substituent to **2** (*O*-3,7-dimethyloctyl), **3** and **4** (*O*-2-cyclohexylethyl). Surprisingly, in all cases the most conspicuous effect is the negative shift of both the reduction peaks.

Table 2. 1: experimental and theoretical energy parameters of dyes **1-4**

Dye	HOMO [eV]		LUMO [eV]		Egap [eV]	
	Exp.	Theo.	Exp.	Theo.	Exp.	Theo.
1	-5.04	-4.79	-2.81	-2.81	2.23	1.98
2	-5.09	-4.80	-2.74	-2.44	2.35	1.96
3	-5.05	-4.78	-2.75	-2.81	2.30	1.97
4	-5.03	-4.80	-2.77	-2.84	2.26	1.96

OPTICAL PROPERTIES

A study of the absorption profile of dyes **1-4** in different solvents were carried out: UV-Vis spectra in solvents with increasing polarity namely: dichloromethane (DCM), tetrahydrofuran (THF), EtOH and acetonitrile (ACN) are reported in Figure 2. 9. All the dyes display broad absorptions covering a wide wavelength range in the visible region and exhibit two prominent absorption peaks, (Table 2. 1) well reproduced by the TDDFT calculations, despite a slight shift toward lower energies for the calculation in solution.

The absorption bands at the shorter wavelength region (<400 nm) originate from the π - π^* electronic excitations localized within the triarylamine and π -bridge segments while the bands at the longer wavelength correspond to the intramolecular charge transfer (ICT) transition from triarylamine donor (HOMO) to the cyanoacrylic acid acceptor (LUMO), and is mainly influenced by the solvent polarity.^{18,21,23} In fact, as known for many push-pull dyes,²⁴ this absorption band is slightly blue-shifted in polar solvents (EtOH, ACN) with respect to that in DCM.

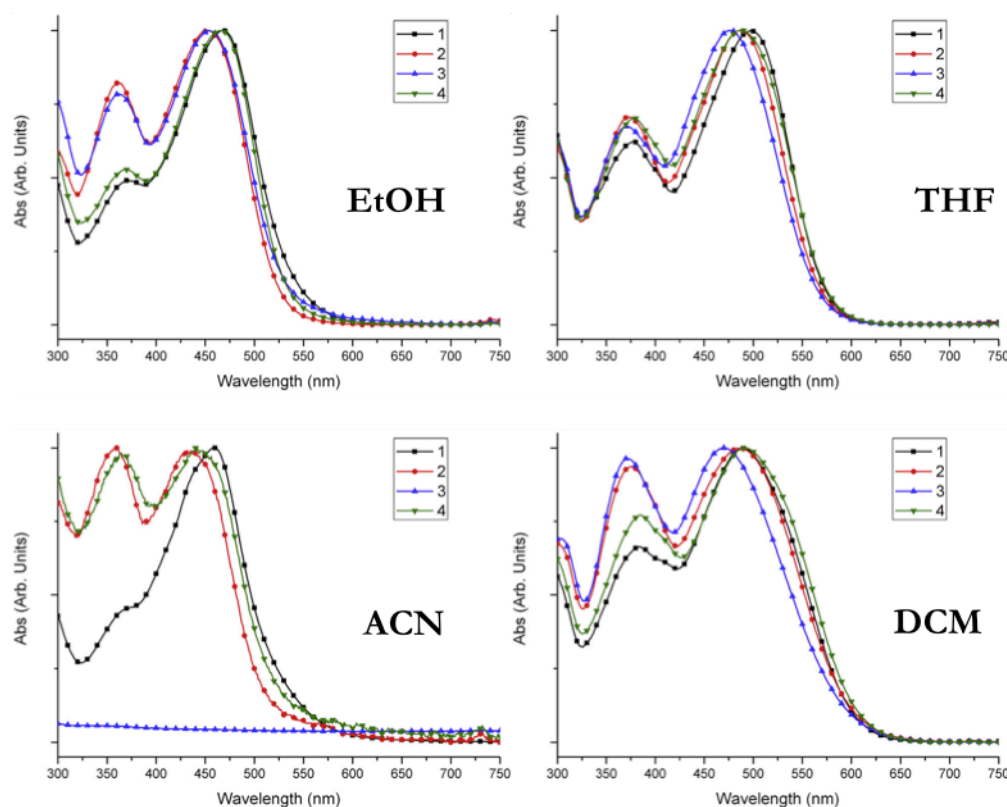


Figure 2. 9: normalized UV-Vis spectra of dye **1-4** in different solvents.

In addition dyes **1-4** bear a carboxylic group, whose ionization equilibrium is known to be affected by solvent parameters²⁵ e.g. acid/base properties, solvating ability and relative permittivity (ϵ_r). For acids with a comparable pK_a, as can be assumed for **1-4**, an increase in relative permittivity of the solvent (from DCM to

ACN) increases the ionization, shifting acid/base equilibrium toward the deprotonated form of the dye, in which a reduced donor-acceptor interaction causes a blue shift in absorption. This hypothesis was further confirmed by the addition of triethylamine (TEA) or trifluoroacetic acid (TFA) to the dye solutions that respectively caused a hypsochromic or bathochromic effect in UV absorption. (Figure 2. 10) Thus we can partially attribute the calculated red shift of the lowest transition with respect to the experimental values to the effect of the protonation, that have been shown to affect the calculated absorption maxima up to 0.3-0.4 eV for similar push-pull dyes at the same computational level.²⁶

Moreover considering the influence of alkyl substituents on dye optical properties, as expected, the absorption wavelengths (λ_{max}) of dyes increase as the alkyl chain is longer and in particular 3,7-dimethyloctyl group appears as the best substituent both when inserted on **BDT**₁ ring (**SB19**) and on triarylamine (**CB2944**) unit. The effect of cyclohexylethyl as substituent of triarylamine unit is comparable to that of OCH₃. The presence of both alkyl chains as in dye **CB844** don't make any significative improvement of dye optical features, thus **SB19** can be considered as the best molecule in term of light absorption.

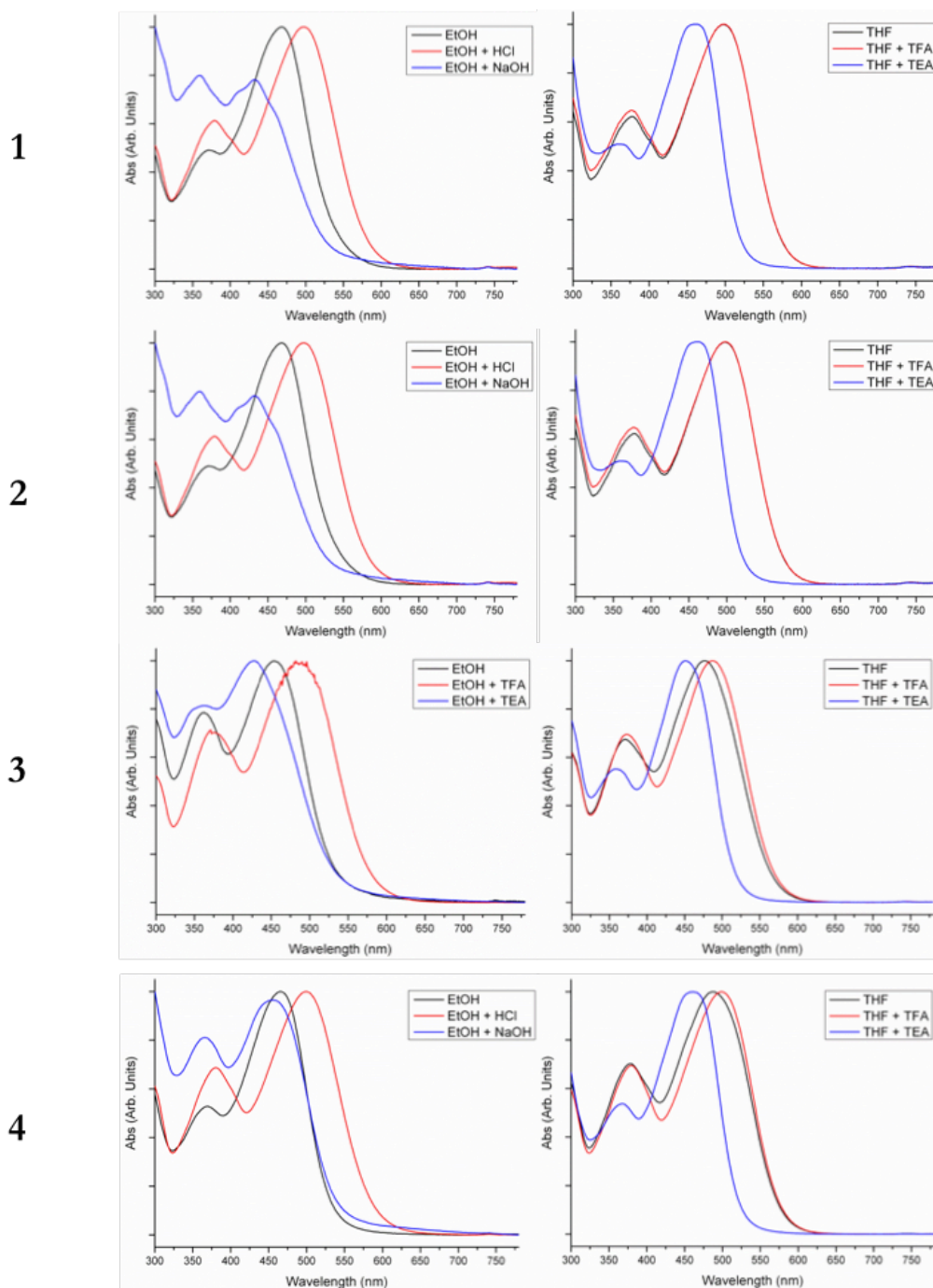


Figure 2. 10: comparison of the normalized UV-Vis spectra of the dyes **1-4** in presence of TFA or TEA in EtOH and THF to evaluate the acid/base equilibrium.

Table 2. 2: optical properties of dyes **1-4** in solvents with increasing polarity and ϵ_r .

Dye	λ_{\max} [nm]			
	$(\epsilon \cdot 10^3)$ [M ⁻¹ cm ⁻¹]			
solvent ^a	DCM	THF	EtOH	ACN
1	384; 489	377; 499	370; 468	370; 459
	(40.0; 59.8)	(31.6; 51.7)	(23.8; 50.1)	(21.0; 34.7)
2	376; 488	373; 486	371; 454	359; 430 ^b
	(32.3; 34.9)	(30.2; 51.8)	(23.8; 24.8)	(22.1; 31.0) ^b
3	371; 469	371; 476	369; 454 ^b	346; 436 ^b
	(30.7; 32.0)	(39.7; 68.6)	(28.7; 41.5) ^b	(25.2; 38.1) ^b
4	384; 491	378; 487	369; 465 ^b	363; 472 ^b
	(34.7; 46.1)	(32.0; 44.5)	(35.6; 46.0) ^b	(24.8; 44.1) ^b

^a [C] ~ 2 · 10⁻⁵; ^b traces of TFA to solubilize the compound.

PHOTOVOLTAIC PROPERTIES

The four new dyes have been used as sensitizers in liquid DSSCs. Solar devices were prepared using a double layer film consisting of a transparent 20-nm particles layer (10 μm) of anatase TiO₂ and a scattering layer (5 μm) containing optically dispersing anatase > 100 nm particles. The liquid electrolytes **Z960** (1.0 M dimethyl imidazolium iodide, 0.03 M I₂, 0.05 M LiI, 0.1 M guanidinium thiocyanate and 0.5 M 4-*t*-butylpyridine in acetonitrile/valeronitrile 85/15)²⁷ and **A6986** (0.6 M 1-Butyl-3-methylimidazolium iodide, 0.05 M I₂, 0.1 M LiI, and 0.05 M 4-*t*-butylpyridine in acetonitrile/valeronitrile 85/15)²⁸ were used for testing the photovoltaic properties of devices. In addition, we have investigated the photovoltaic response of the devices by varying the amount of chenodeoxycholic acid (CDCA) as a de-aggregating co-adsorbent agent²⁹ in the sensitizer solution (CDCA:dye = 0:1, 1:1, and 30:1) finding that the best performances were reached using a relative concentration of 30:1 in the case of **2**, **3** and **4** (**CB2944**, **C324**, **CB844**) and 1:1 for **1** (**SB19**).

The measured photovoltaic performances under AM 1.5 solar standard conditions and double-layer TiO₂ films with a 0:1, 1:1, and 30:1 CDCA:dye ratio are listed in Table 2. 3, Table 2. 4, Table 2. 5.

The overall power conversion efficiencies PCE were derived from the equation: $PCE = J_{sc} \times V_{oc} \times FF$, where J_{sc} is the short circuit current density, V_{oc} the open circuit voltage, and FF the fill factor, as described in previous chapter. Figure 2. 11 shows the photocurrent-voltage curves of DSSCs based on the new dyes.

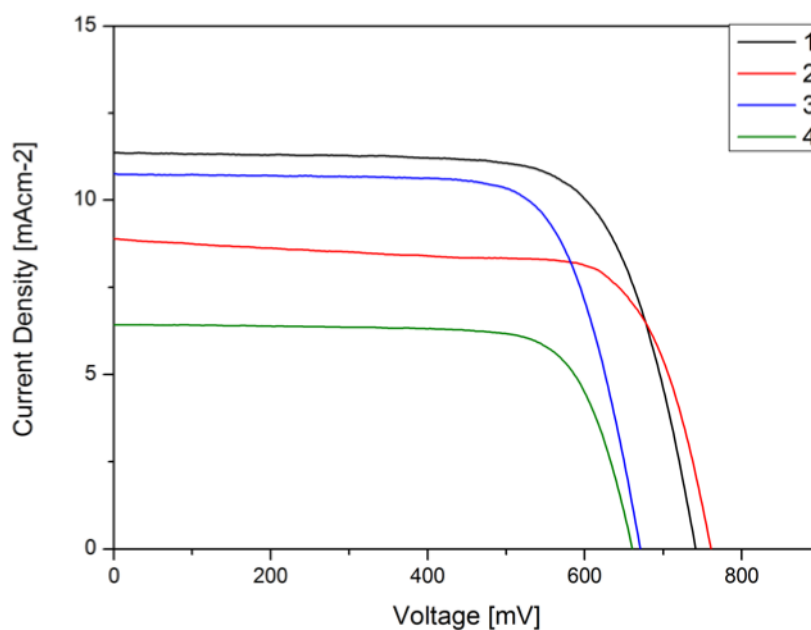


Figure 2. 11: Comparison of the J - V curves of dye sensitized solar cells under full AM 1.5 solar intensity.

The best PCE was recorded for **1**, where notable values of 6.6 and 8.4% (with and without a black tape shading mask, 0.40 mm², on top of devices mask, respectively) were measured at 0.5 sun irradiation.

Table 2. 3: Detailed photovoltaic parameters of the devices using dyes **1-4** and with 0:1 CDCA at different light intensities.

Chapter 2

Device ^[a]	Irradiance	J_{sc}		V_{oc}		FF		PCE	
	[sun]	[mA cm ⁻²]		[mV]		[%]		[%]	
1(SB19) ^[c]	1	11.8	(14.1)	754	(765)	72	(70)	6.4	(7.5)
	0.8	9.2	(11.1)	746	(755)	72	(70)	6.3	(7.5)
	0.5	6.5	(7.8)	736	(745)	73	(71)	7.0	(8.3)
	0.2	2.8	(3.4)	713	(720)	74	(72)	6.4	(7.7)
2(CB2944) ^[b]	1	8.4	(10.1)	678	(686)	74	(73)	4.3	(5.0)
	0.8	6.7	(8.0)	668	(680)	75	(74)	4.2	(5.0)
	0.5	4.7	(5.6)	658	(669)	76	(75)	4.7	(5.6)
	0.2	1.9	(2.4)	633	(644)	77	(76)	4.6	(6.0)
3(CB324) ^[b]	1	5.2	(6.8)	667	(677)	75	(73)	2.6	(3.4)
	0.8	4.0	(5.5)	654	(663)	74	(73)	2.5	(3.4)
	0.5	2.7	(3.8)	642	(655)	75	(73)	2.6	(3.6)
	0.2	1.2	(1.5)	618	(628)	75	(73)	2.3	(3.0)
4(CB844) ^[b]	1	5.7	(7.1)	670	(682)	74	(73)	2.8	(3.5)
	0.8	4.4	(5.6)	663	(673)	74	(74)	2.7	(3.4)
	0.5	3.0	(3.8)	652	(662)	75	(74)	3.0	(3.7)
	0.2	1.3	(1.6)	627	(636)	74	(74)	3.1	(3.8)
N719 ^[d]	1	15.6	(17.9)	720	(722)	72	(71)	8.1	(9.2)

^a Incident intensity of AM1.5 solar light; values without mask are in brackets; double TiO₂ layer (10+5 μm). ^b Dye solution of 2 x 10⁻⁴ M in EtOH/THF 1:1; electrolyte Z960. ^c Dye solution of 2 x 10⁻⁴ M in EtOH; electrolyte A6986 ^d Dye solution of 5 x 10⁻⁴ M in EtOH solution with 1:1 CDCA; electrolyte A6141 (0.6 M N-butyl-N-methyl imidazolium iodide, 0.03 M I₂, 0.10 M guanidinium thiocyanate, and 0.5 M 4-*t*-butylpyridine in acetonitrile/valeronitrile 85:15).

Table 2. 4: Detailed photovoltaic parameters of the devices using dyes **1-4** and with 1:1 CDCA at different light intensities.

Dye sensitized solar cells

Device ^[a]	Irradiance	J_{sc}		V_{oc}		FF		PCE	
	[sun]	[mA cm ⁻²]		[mV]		[%]		[%]	
1(SB19) ^[c]	1	11.4	(14.4)	741	(757)	72	(70)	6.1	(7.6)
	0.8	9.1	(11.5)	732	(749)	73	(70)	6.1	(7.7)
	0.5	6.3	(8.0)	721	(738)	73	(71)	6.7	(8.4)
	0.2	2.7	(3.5)	703	(713)	73	(72)	5.9	(7.8)
2(CB2944) ^[b]	1	8.1	(9.8)	677	(689)	73	(72)	4.0	(4.9)
	0.8	6.4	(7.7)	669	(681)	74	(73)	4.0	(4.8)
	0.5	4.4	(5.4)	660	(672)	75	(74)	4.4	(5.5)
	0.2	1.9	(2.3)	636	(647)	76	(76)	4.6	(5.7)
3(CB324) ^[b]	1	6.6	(8.9)	657	(671)	75	(74)	3.3	(4.4)
	0.8	5.3	(6.9)	644	(658)	75	(74)	3.2	(4.3)
	0.5	3.5	(4.9)	632	(649)	76	(75)	3.4	(4.8)
	0.2	1.5	(2.0)	607	(623)	76	(76)	3.0	(4.1)
4(CB844) ^[b]	1	6.2	(7.5)	661	(672)	74	(75)	3.0	(3.8)
	0.8	4.5	(5.8)	650	(663)	76	(75)	2.8	(3.6)
	0.5	3.1	(4.0)	640	(653)	76	(76)	3.1	(4.0)
	0.2	1.3	(1.7)	616	(628)	76	(76)	3.1	(4.1)
N719 ^[d]	1	15.6	(17.9)	720	(722)	72	(71)	8.1	(9.2)

^a Incident intensity of AM1.5 solar light; values without mask are in brackets; double TiO₂ layer (10+5 μm). ^b Dye solution of 2 x 10⁻⁴ M in EtOH/THF 1:1; electrolyte Z960. ^c Dye solution of 2 x 10⁻⁴ M in EtOH; electrolyte A6986. ^d Dye solution of 5 x 10⁻⁴ M in EtOH solution with 1:1 CDCA; electrolyte A6141 (0.6 M *N*-butyl-*N*-methyl imidazolium iodide, 0.03 M I₂, 0.10 M guanidinium thiocyanate, and 0.5 M 4-*t*-butylpyridine in acetonitrile/valeronitrile 85:15).

Table 2. 5: Detailed photovoltaic parameters of the devices made with the dyes 1-4 and with 30:1 CDCA at different light intensities.

Chapter 2

Device ^[a]	Irradiance	J_{sc}		V_{oc}		FF		PCE	
	[sun]	[mA cm ⁻²]		[mV]		[%]		[%]	
1(SB19) ^[c]	1	11.2	(14.0)	738	(748)	72	(70)	6.0	(7.3)
	0.8	9.0	(11.0)	729	(738)	73	(71)	6.0	(7.3)
	0.5	6.3	(8.0)	717	(728)	73	(72)	6.6	(8.4)
	0.2	2.7	(3.4)	691	(701)	75	(73)	6.0	(7.6)
2(CB2944) ^[b]	1	8.8	(11.2)	664	(680)	73	(74)	4.3	(5.6)
	0.8	6.6	(8.7)	661	(672)	76	(75)	4.2	(5.5)
	0.5	4.6	(6.2)	649	(662)	77	(76)	4.6	(6.2)
	0.2	2.0	(2.6)	627	(638)	78	(77)	5.0	(6.5)
3(CB324) ^[b]	1	10.7	(13.9)	671	(684)	73	(71)	5.3	(6.8)
	0.8	8.4	(11.1)	659	(674)	74	(72)	5.2	(6.8)
	0.5	6.0	(7.8)	648	(662)	75	(74)	5.8	(7.7)
	0.2	2.5	(3.2)	620	(632)	76	(76)	5.1	(6.6)
4(CB844) ^[b]	1	6.5	(7.8)	657	(668)	76	(76)	3.2	(3.9)
	0.8	5.0	(6.1)	646	(658)	76	(76)	3.1	(3.8)
	0.5	3.4	(4.2)	635	(646)	76	(76)	3.3	(4.1)
	0.2	1.5	(1.7)	612	(620)	76	(77)	3.4	(4.1)
N719 ^[d]	1	15.6	(17.9)	720	(722)	72	(71)	8.1	(9.2)

^a Incident intensity of AM1.5 solar light; values without mask are in brackets; double TiO₂ layer (10+5 μm). ^b Dye solution of 2 x 10⁻⁴ M in EtOH/THF 1:1; electrolyte Z960. ^c Dye solution of 2 x 10⁻⁴ M in EtOH; electrolyte A6986. ^d Dye solution of 5 x 10⁻⁴ M in EtOH solution with 1:1 CDCA; electrolyte A6141 (0.6 M *N*-butyl-*N*-methyl imidazolium iodide, 0.03 M I₂, 0.10 M guanidinium thiocyanate, and 0.5 M 4-*t*-butylpyridine in acetonitrile/valeronitrile 85:15).

It is worth noting that dye **1** is the molecule with the simplest donor core, where methoxy substituents are present on the triphenylamine scaffold. The long alkyl chains on the BDT₁ spacer are likely responsible for a minimized interaction TiO₂-electrolyte and, thus, decreased charge recombination from the semiconductor oxide to the oxidized form of the electrolyte. This is confirmed by the highest

measured photovoltage, being the only dye of the series with values > 0.7 V. Though molecule **4** has the same substituted pattern on the spacer, much lower PCE were recorded. In this case the lowest efficiency originates from the lower photocurrent. Once more, sensitizer **1** is the best system of the investigated series, with photocurrent reaching values over 11 mA cm^{-2} in presence of a device mask.

To gain further insights incident monochromatic photon-to-current conversion efficiencies (IPCE) were investigated (Figure 2. 12).

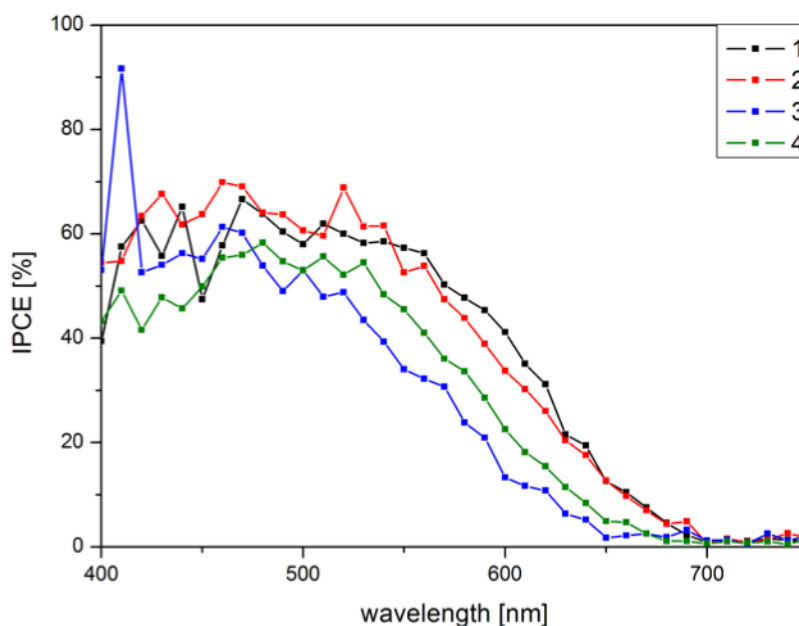


Figure 2. 12: incident monochromatic photon-to-current conversion efficiencies (IPCE) spectra comparison for dyes 1 – 4

The shape of these spectra follows those of the corresponding absorption spectra. The photocurrent values calculated by integrating the IPCE spectra and using the AM 1.5G spectrum nicely matched those measured with masked solar cells.³⁰ IPCE peaks ranged from 60% for **4** (CB844) to 70% for **1** (SB19). In order to elucidate the different IPCE responses we separately examined the two components expressed in the Equation 6 of $IPCE(\lambda)$ (chapter 1.2). The contribute of light-harvesting efficiency (LHE), associated to the ability of the cell of harvesting the light, and the absorbed monochromatic photon-to-current conversion efficiency

(APCE), that is the internal quantum efficiency associated to the ability of the cell of generating electric current, are shown in Figure 2. 13 and Figure 2. 14, respectively.

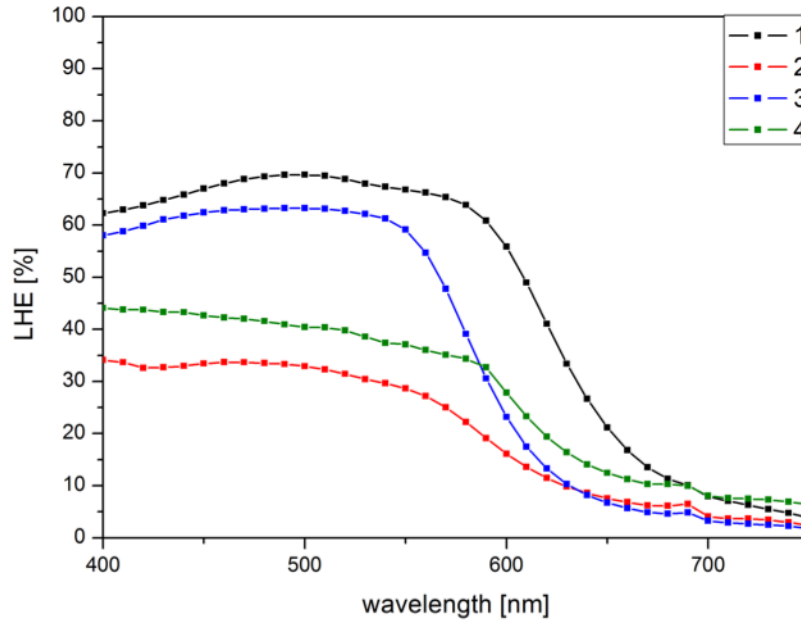


Figure 2. 13: LHE spectra obtained using a 10- μm transparent TiO_2 film sensitized using dye **1** - **4**.

The best LHE profile, which directly originates from the absorption spectra as films, was recorded for dye **1** and is in agreement with the higher measured photocurrent. The APCE of **1** is greater than 80% for a broad spectral region spanning from 400 to 550 nm. APCE_{max} reached values greater than 80 % for **3** as well but for a less extended wavelength range. Therefore we can conclude that the highest photovoltaic response, and thus the overall efficiency, of **1** originates both from an efficient and broad light harvesting and from an improved ability to convert photons to electrons. In the case of **3** the lower IPCE is either due to a decreased ability to harvest light over a broad range or to a lower internal quantum efficiency.

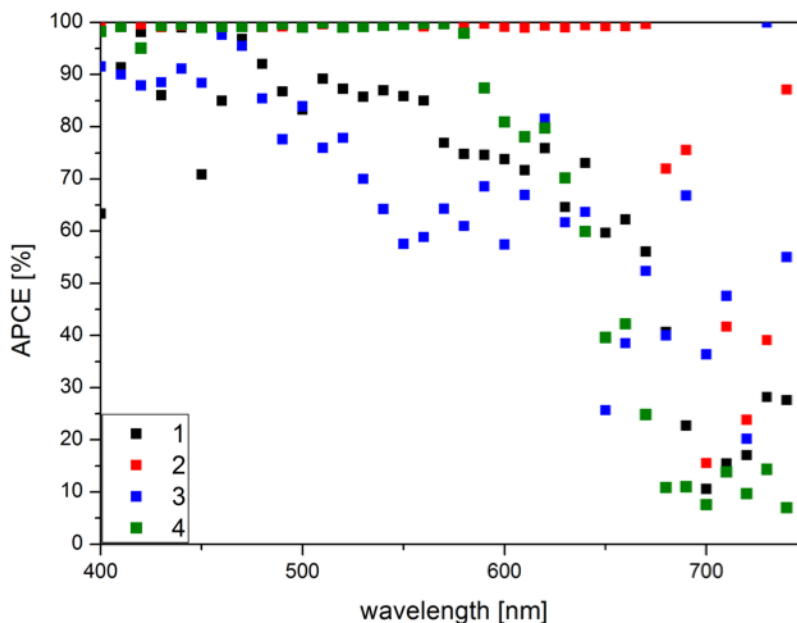


Figure 2. 14: APCE spectra obtained from IPCE and LHE for dyes 1 – 4

The protonation equilibrium COO^-/COOH of the dyes greatly affected the optical properties and the corresponding photovoltaic characteristics. In particular, we observed, for **2** and **4**, that when devices were prepared using a EtOH solution of the dyes, where the protonation equilibrium are shifted towards the deprotonated carboxylate form, photocurrents were very low and PCE close to 0% (Table 2. 6).

The detailed UV-Vis investigation of the protonation equilibria allowed us to select a more proper solvent with the dye in the protonated COOH form (Figure 2. 1). We identified THF as the best solvent where the protonated COOH form is predominant and thus used EtOH/THF 1:1 solutions of the dyes to sensitize the photoanodes. In this case much higher photocurrents, and efficiencies, were obtained. It is then clear that the equilibrium between the deprotonated COO^- and protonated COOH is critical to afford higher cell efficiencies. The use of 30:1 CDCA:dye EtOH solutions clearly support this hypothesis.

Table 2. 6: Photovoltaic performances of DSSC using solutions of sensitizers **2** (CB2944) and **4** (CB844) in EtOH at different CDCA:dye ratios

Chapter 2

Device ^[a]	CDCA:dye ratios	J_{sc}	V_{oc}	FF	PCE
		[mA cm ⁻²]	[mV]	[%]	[%]
2(CB2944) ^[b]	0:1	1.09	642	59	0.4
	1:1	1.13	617	55	0.4
	30:1	12.6	693	73	6.4
4(CB844) ^[b]	0:1	0.09	364	58	0.02
	1:1	0.7	524	57	0.2
	30:1	7.8	673	73	3.8

^a Incident intensity of AM1.5 solar light; double TiO₂ layer (10+5 μm). ^b Dye solution of 2 x 10⁻⁴ M in EtOH; electrolyte Z960.

In fact, in this case, the presence of a larger molar amount of CDCA is enough to shift the equilibrium towards COOH even in the ethanolic solution, whereas the presence of higher CDCA:dye ratios in the EtOH:THF solution afforded similar photocurrents and PCE. To the best of our knowledge this is the first time where the nature of the solvent used for the dye-sensitization bath is clearly found to be critical for reaching much higher efficiencies. These data clearly show that when an unsuitable, though very common, solvent as EtOH is used for dye solutions misleading PCEs even close to 0% may be obtained, although in the presence of performing sensitizers, as ascertained when proper conditions are alternatively selected.

Thiophene-base phenothiazine branched dye for dye-sensitized solar cells

In recent years, metal-free organic chromophores have been extensively investigated as alternative sensitizers to noble metal-complexes due to their high molar extinction coefficients, ease of structure tailoring as well as low-cost synthesis processes and compliance with environmental issues.³¹ To date, hundreds of organic dyes have been explored to act as sensitizers for DSSCs and remarkable efficiencies, over 14%, have been obtained.³²⁻³⁸ Organic dyes possessing a rod-like configuration with the electron-donating and electron-accepting groups bridged by a π -spacer molecular systems are the most used. The most common donor moiety is a triphenylamine (TPA) derivative.^{39,40} This donor scaffold has been widely used in the synthesis of sensitizers commonly bearing a long terminal alkoxy chain on peripherals phenyl rings⁴¹ to reduce detrimental charge recombination or to enhance electron donation capabilities. A few years ago we have proposed a new molecular architecture for metal-free organic dyes based on a multi-branched geometry.³⁸ In this first report, we have demonstrated that the new molecular architecture provided enhanced photoinduced intramolecular electron transfer, device photocurrent, and stability under light and thermal stress. Furthermore, the photophysical properties of the multi-branched dyes can be widely tuned upon varying donor, spacer, and acceptor moieties. Based on our previous work we decided to modify specific structural characteristics of di-branched dyes mainly directed at improving the critical interface between dye-decorated TiO_2 and the liquid electrolyte. Indeed, the electron recombination from TiO_2 to the oxidized form of the electrolyte represents one of the major drawbacks of the present device architecture and is responsible for lower photovoltage and fill factor and, eventually, PCE.⁴²⁻⁴⁶ Electron recombination is conveniently investigated via Electrochemical Impedance Spectroscopy (EIS), which is able to determine the recombination resistance between TiO_2 and the electrolyte and other parameters

related to the electron lifetime in the semiconductor.⁴⁷⁻⁴⁹ One of the most effective strategies to limit charge recombination is to make more difficult the approach of the liquid electrolyte to the semiconductor surface by chemical modification of the dye.

Triggered by the some recent studies on phenothiazines (**PTZ**) derivatives as DSSC sensitizers⁵⁰⁻⁵³ and by their first uses as light harvesters in the photo-driven production of hydrogen,⁵⁴ we decided to systematically investigate this promising class of dyes by designing a series of organic sensitizers containing the phenothiazine core as a donor scaffolds in donor- π -acceptor molecules. Interestingly, a very recent report on a class of benzo[b]phenothiazines confirms the increasing relevance of dye-sensitized hydrogen production using organic dyes and phenothiazine derivatives.⁵⁵ The phenothiazine core carries peculiar features associated to its non-planar butterfly conformation along the S-N axis. Such arrangement avoids fully planar geometries which could be detrimental by promoting self-quenching molecular aggregates on the TiO₂ surface. Moreover, the phenothiazine structure contains two symmetric benzene rings which can be conveniently functionalized allowing the design of symmetric di-branched dyes, a recently important class of photosensitizers endowed with higher anchoring stability and electron injection efficiency, improved optical properties, and enhanced device stability which was introduced by us in the DSSC field of investigation and later used by many research groups.^{10,38,56,57} Lastly, the nitrogen atom of the central core of the phenothiazine groups can be conveniently functionalized with alkyl or aryl groups of different chemical nature, in order to provide a further derivatization site able to induce additional properties such as proper solubility in specific media (with particular attention to water) or affinity to bio-inspired molecules. In order to systematically investigate this class of molecules, here we have focused our attention on the effect of the π -spacer group. In particular, thiophene rings have been widely used in materials science due to their peculiar structural and electronic properties.⁵⁸ Thiophene is a π -excessive

heteroaromatic five-membered ring with a lower resonance energy than benzene,⁵⁹ thus facilitating charge transfer between the donor and the acceptor core of the organic dyes. For these reasons thiophene-based spacers have been commonly applied in the design of dyes for solar applications.^{7,9,13,60,61} We have here exploited different mono-, poly-, and fused polycyclic thiophene-based groups as π -spacers between the phenothiazine donor core and the acceptor/anchoring groups based on cyanoacrylic acid (Figure 2. 2). As a reference system the previously investigated dye **PTZ1** (named P3 in Ref. ⁵⁴) has been included in our work, also because the hydrophobic octyl chain is supposed to raise detrimental charge recombination lifetimes.⁵⁴

SYNTHESIS

The new phenothiazines **PTZ2-6** (Figure 2. 15) have been designed and synthesized. Phenothiazines **PTZ2-6** differ in their thiophene-based π -spacers. The selection of the simple thiophene in **PTZ2** was made to improve optical properties of the dye by both red-shifted and more intense. With the same target in mind **PTZ3** and **PTZ4** have been designed where somewhat more sophisticated heteroaromatic cores have been employed to further modulate optical and electronic characteristics. **PTZ5** was prepared both to study the influence of electron-rich alkoxy functionalities in the electronic communication between the dye and TiO₂ surface, and to limit dye aggregation thanks to the four butyl chains, that should prevent π -stacking processes. Finally, the 3,4-ethylenedioxythiophene (EDOT) derivative **PTZ6** was synthesized to study the net electronic role of the alkoxy groups without any steric effect as in **PTZ5**. The overall synthetic approach for **PTZ2-6** is depicted in Scheme 2. 4.

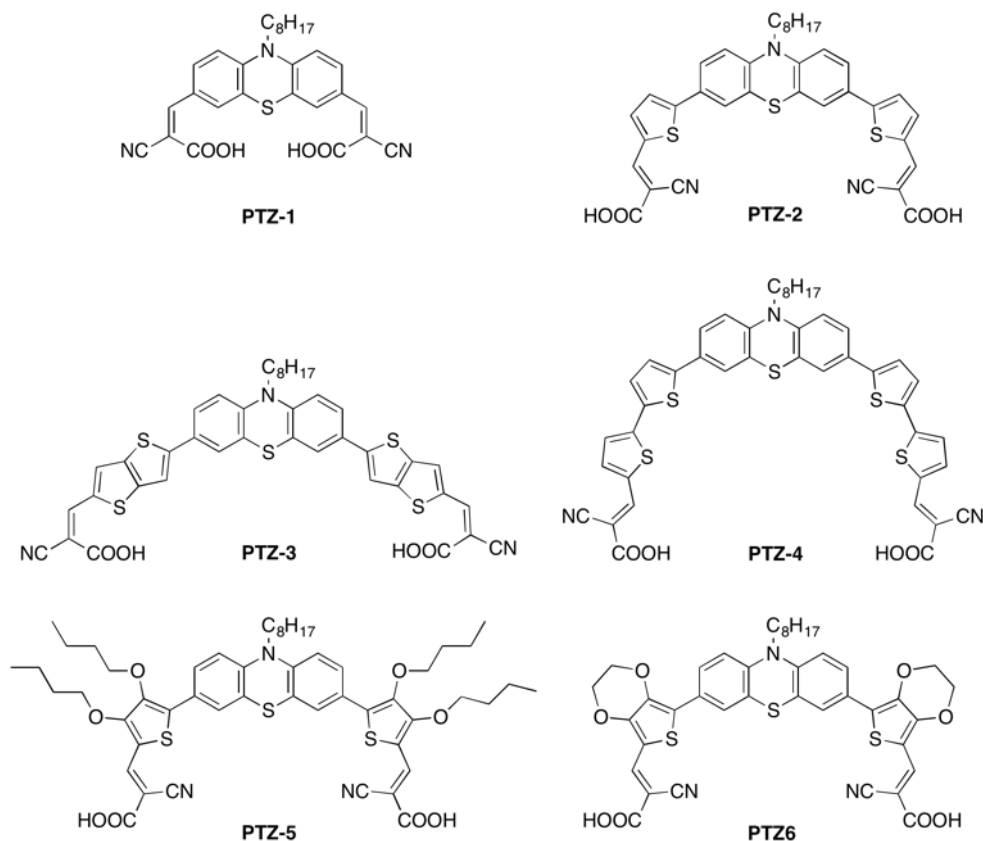
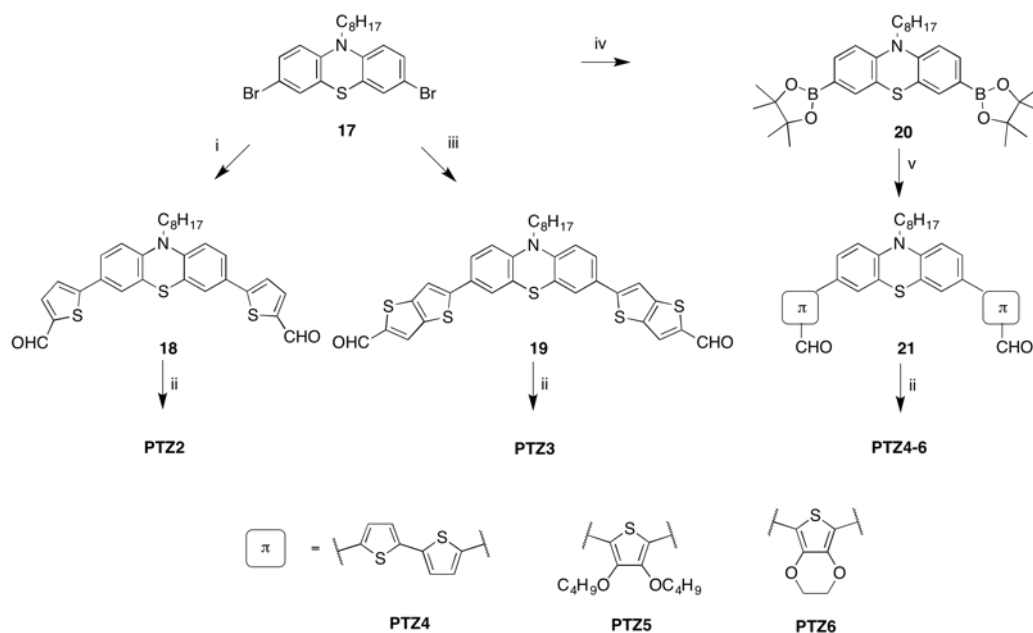


Figure 2. 15: Structure of the investigated phenothiazine based branched dyes.

Dye **PTZ1** has been synthesized according to literature methods starting from commercial 10*H*-phenothiazine. Alkylation at nitrogen was carried out with NaH as a base and 1-bromooctane as the alkylating agent followed by a Vilsmeier-Haack formylation of the aromatic core and Knoevenagel condensation with cyanoacetic acid.⁵⁴ Bromination of 10-octyl-10*H*-phenothiazine with NBS in classical conditions gave very low yields (~30 %); thus bromine in acetic acid was preferred (up to 95 % of yield) to synthesize molecule **17**.⁶² The Suzuki-Miyaura cross coupling reaction, since using boron derivatives is more sustainable than the alternative Stille reaction, was preferred to insert the thiophene-based spacer.⁶³ Two alternative strategies were used, according to the availability of precursors. The bromo-derivative **17** was coupled to 2-thiophene-aldehyde-5-boronic acid and 4,4,5,5-tetramethyl-2-(thieno[3,2- b]thiophen-2-yl)-1,3,2-dioxaborolan⁶⁴ for the

synthesis of **PTZ2** and **PTZ3**, respectively. A Vilsmeier-Haack formylation on the thieno[3,2-b]thiophene derivative allowed to isolate molecule **19**. In the case of **PTZ4-6**, for which the bromo-derivatives of the corresponding π -spacers were more readily available, the boronic functionality was placed on phenothiazine core through halogen-metal exchange by *n*-BuLi and subsequent quenching by 2-isopropoxy-4,4,5,5-tetramethyl-1,3,2-dioxaborolane to give the intermediate **20**.



Scheme 2. 4: Synthetic routes for **PTZ2-6**. Reagents and conditions: (i) 5-Formyl-2-thienylboronic acid, Pd(dppf)Cl₂·CH₂Cl₂ [dppf = 1,1'-bis(diphenylphosphino)ferrocene], K₂CO₃, DME/MeOH, microwave 90 °C, 90 min; (ii) cyanoacetic acid, piperidine, CHCl₃, 80 °C, 5 h; (iii) a. 4,4,5,5-tetramethyl-2-(thieno[3,2-b]thiophen-2-yl)-1,3,2-dioxaborolane, Pd(dppf)Cl₂·CH₂Cl₂, K₂CO₃, DME/MeOH, microwave 90 °C, 90 min, b. POCl₃, DMF, -5 °C to 100 °C, 8h; (iv) a. BuLi, THF, -78 °C, 60 min, b. 2-isopropoxy-4,4,5,5-tetramethyl-1,3,2-dioxaborolane, r.t., 15 h; (v) 5'-bromo-(2,2'-bithiophene)-5-carbaldehyde (**PTZ4**), or 5-bromo-3,4-dibutoxythiophene-2-carbaldehyde (**PTZ5**), or 7-bromo-2,3-dihydrothieno[3,4-b][1,4]dioxine-5-carbaldehyde (**PTZ6**), Pd(dppf)Cl₂·CH₂Cl₂, K₂CO₃, microwave, 90 °C, 90 min.

The π -precursors for **PTZ4-6** were synthesized according to reported methods in the case of bithienyl,⁶⁵ and EDOT.⁶⁶ To synthesize 5-bromo-3,4-dibutoxythiophene-2-carbaldehyde, similar conditions as that for the EDOT derivative were chosen. 3,4-Dimethoxythiophene was treated with PTSA and butanol to insert the butyl chains^{67,68} followed by formylation and bromination with NBS allowed to afford the desired intermediate. Boronic ester **20** was then allowed

to react with the corresponding bromo-derivatives under microwave assisted Suzuki-Miyaura cross coupling conditions to isolate carbaldehyde precursors of **PTZ4-6** in comparable yields. Final Knoevenagel condensation with cyanoacetic acid in basic conditions afforded **PTZ2-6** in good yields.

OPTICAL AND ELECTROCHEMICAL CHARACTERIZATION

Optical characterization of dyes **PTZ1-6** was performed in 10^{-5} M THF solution. Absorption spectra normalized to molar extinction coefficients are shown in Figure 2. 16.

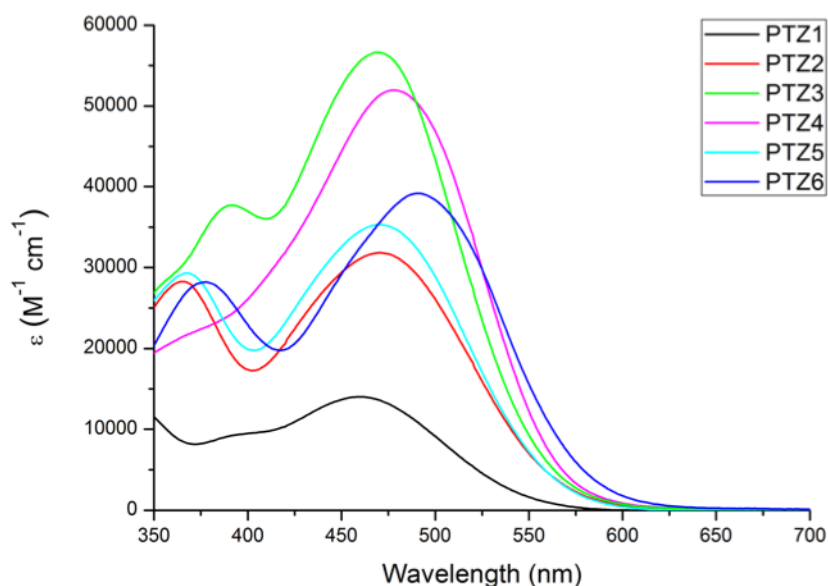


Figure 2. 16: Absorption spectra of dyes **PTZ1-6** in THF.

All the dyes showed a classical pattern, with an intense absorption band in the Vis region attributed to the intramolecular donor to acceptor charge-transfer transition. Validating the target of this work, the introduction of thienyl π -spacers led to a substantial qualitative and/or quantitative improvement of the optical properties of **PTZ2-6** compared to reference **PTZ1**. Moreover, an additional band at higher energies, likely attributed to the local thiophene transitions, is present in the thienyl dyes **PTZ2-6**. The introduction of more structured thiophene-based π -cores resulted to substantial bathochromic and/or hyperchromic effects, thus allowing a

more efficient photon harvesting. Such important property is compatible with the use of thinner nanocrystalline films as those required by solid-state devices and in solid-state DSSC. It is worth noting that even the introduction of a single thiophene ring in the π -framework afforded a molar extinction coefficient twice as large as in **PTZ1** (from 13700 to 34000 $\text{M}^{-1}\text{cm}^{-1}$ in **PTZ2**) and a 11-nm red-shifting. The use of spacers with longer conjugation paths confirmed this optical trend allowing us to achieve molar absorptivities up to 60000 $\text{M}^{-1}\text{cm}^{-1}$ as in **PTZ3** and **PTZ4**, that is more than four times larger than in the reference dye, and, in some cases, absorption peaks at significantly longer wavelengths. In the case of **PTZ3** the introduction of the more π -extended thienothiophene spacer compared to simple thiophene in **PTZ2** was not associated to a bathochromic effect but a substantial hyperchromic effect, with a peak molar absorptivity almost twice as larger than that of the thiophene derivative. A different behaviour is recorded for the 3,4-alkoxythienyl derivatives **PTZ5** and **PTZ6** where molar absorptivities are ultimately comparable to that of **PTZ2**, though the presence of the auxochrome groups further shifted the absorption maximum to longer wavelength, reaching a top value of 490 nm for **PTZ6**, to be compared with 460 nm in **PTZ1**. In summary, the introduction of the thiophene-based spacers in **PTZ2-PTZ6** resulted in either significantly red-shifted absorption peaks or enhanced molar absorptivities or a combination of the two effects. Optical bandgaps were calculated by means of the Tauc plots⁶⁹ (Figure 2. 17) and listed in Table 2. 7: Optical characterization of dye **PTZ1-6** in 10^{-5} M THF solution. together with their main optical parameters.

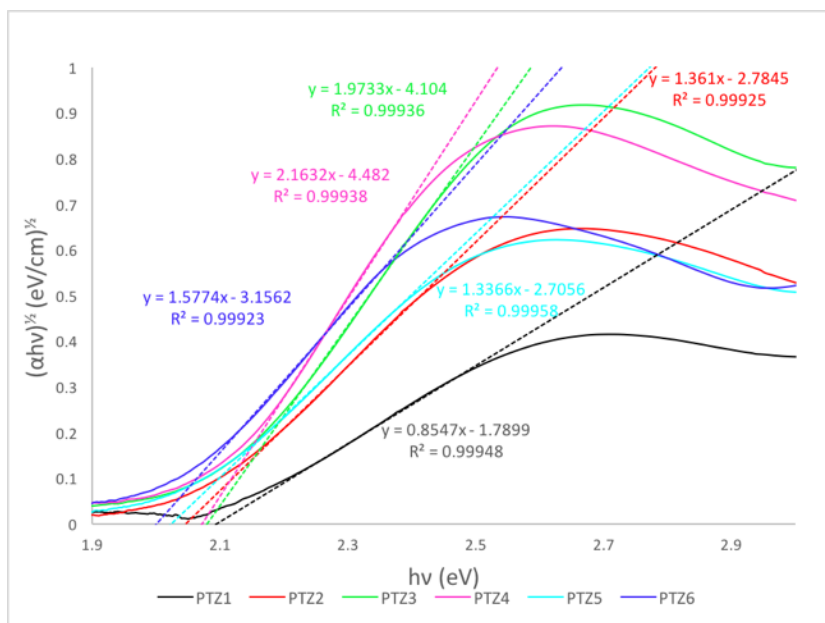


Figure 2. 17: Tauc plots calculated for **PTZ1-6** for optical band gap evaluation.

The dyes have very low emission intensity and were not considered reliable enough to calculate zeroth-zeroth energies from the intercept with the normalized absorption spectra. In fact, the shape of the emission spectra is rather broad compared to the absorption bands, likely due to aggregation and intermolecular energy exchange reasons.

Table 2. 7: Optical characterization of dye **PTZ1-6** in 10^{-5} M THF solution.

Dye	λ_{\max} [nm]	ϵ [$M^{-1}cm^{-1}$]	λ_{onset} [nm]	λ_{em} [nm]	$E_{\text{gap}}^{\text{opt}}$ [eV]
PTZ1	460	13700 ± 300	590	613	2.10
PTZ2	471	34000 ± 1800	605	654	2.05
PTZ3	470	57800 ± 2900	596	605	2.08
PTZ4	478	56200 ± 2200	598	583	2.07
PTZ5	477	35400 ± 1300	613	598	2.02
PTZ6	490	39200 ± 600	617	654	2.01

ELECTROCHEMICAL CHARACTERIZATION

Saturated solutions of **PTZ1-6** in CH_2Cl_2 were used for the electrochemical characterization by dissolving each derivate in the supporting electrolyte (0.1 M TBAClO_4). The cyclic voltammetry (CV) study (Figure 2. 18) showed a quasi-reversible behaviour at oxidative potentials (potential > 0 V) and several irreversible reduction waves at the lowest potentials (potential < -1.0 V) for all the dyes.

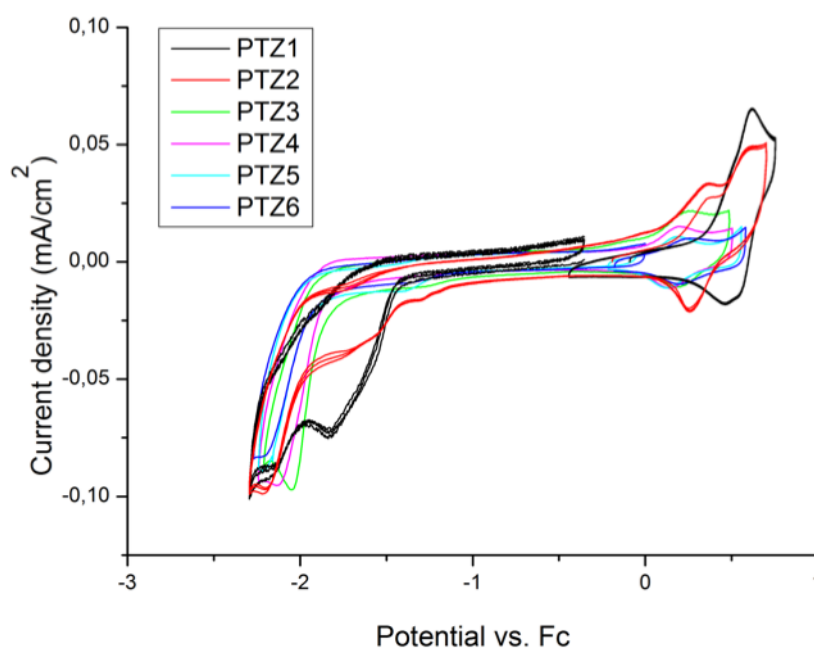


Figure 2. 18: CV traces for **PTZ** dyes in solution.

In this latter potential region, the main source of current raising was due to the electrolyte decomposition. In fact, the CH_2Cl_2 electrochemical stability window is reported in literature⁷⁰ to be between +1.5 and -2.5 V vs. Fc. These limits are measured by CV considering the potential values at which the current density reaches 1 mA cm^{-2} . We point out that this is a kinetic, not a thermodynamic, limit.

In our case, we noticed that below -2.0 V the current started raising due to the reduction of the solvent. For example, at -2.25 V a current density of 0.1 mA cm^{-2} has been reached, a value which is compatible with the initial stages of the

decomposition reaction of CH_2Cl_2 . Moreover, being the active species concentration rather low, the current associated to the reduction of dyes is comparable with that of the CH_2Cl_2 decomposition.

Differential pulse voltammetry (DPV) was preferred for the accurate estimation of the oxidation (E^{ox}) and reduction (E^{red}) potentials and HOMO/LUMO energy levels (Figure 2. 19 and Table 2. 8). HOMO/LUMO energies are pictorially depicted in Figure 2. 20 relative to the conduction band level of TiO_2 .⁴⁷

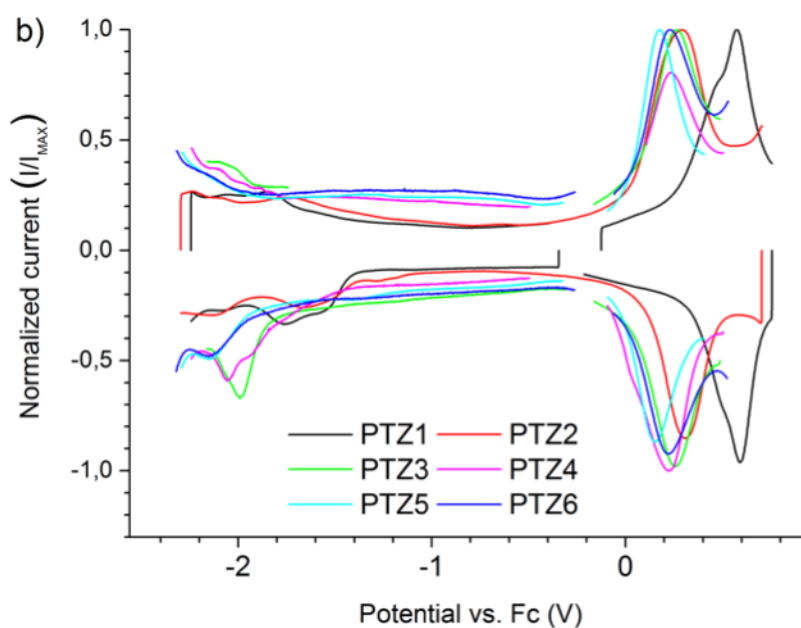


Figure 2. 19: DPV traces for PTZ dyes in solution.

All the oxidative processes seem to be constituted by two different waves; the first wave is a shoulder in the case of **PTZ1**. By using DPV the decomposition effect of the electrolyte is minimized and the waves can be more accurately attributed to the investigated molecules. The oxidation potentials of the molecules are similar to each other, as expected for the presence of the same phenothiazine donor core, whereas differences are recorded in their properties at cathodic potentials. All of the thiophene-substituted dyes were found easier to oxidize than **PTZ1** (lower oxidation potential) by 120 to 240 mV, in agreement with the donor character of

the thiophene ring.⁷¹ No substantial differences were found within the thiophene derivatives **PTZ2-PTZ6**, with oxidation potentials being within a range of 120 mV, in agreement with literature data on similar compounds.⁵⁰⁻⁵³ This suggests that the presence of different thiophene spacers and ring substituents did not significantly affect the oxidation potential, and thus the HOMO energy level, of the corresponding dyes. This is in agreement with the spacer character, rather than a donor nature represented by the phenothiazine core, of the thiophene moieties in the donor- π -acceptor dyes.

Table 2. 8: Electrochemical characterization of PTZ dyes.^a

Sample	E^{ox} (V) \pm 5 mV	HOMO (eV) \pm 50 meV	E^{red} (V) \pm 5 mV	LUMO (eV) \pm 50 meV
PTZ1	0.39	-5.62	-	-3.52 ^b
PTZ2	0.15	-5.38	-	-3.33 ^b
PTZ3	0.26	-5.49	-1.99	-3.25
PTZ4	0.27	-5.50	-2.06	-3.17
PTZ5	0.16	-5.39	-2.15	-3.08
PTZ6	0.22	-5.45	-2.16	-3.07

^a All potentials are reported vs. Fc/Fc⁺, and the HOMO and LUMO energies are derived from the electrochemical data based on the assumption that the Fc/Fc⁺ redox couple is 5.23 eV relative to a vacuum (Ref.⁷²). ^b Calculated from electrochemical HOMO energies and optical bandgap.

However, we note that the bis-alkoxythiophene derivative **PTZ5**, carrying two electronrich substituents on each thiophene ring, is amongst the most easily oxidized dyes. The presence of broad current profiles and two reduction waves, one of which appears as a shoulder, in the reduction range of **PTZ1** and **PTZ2** (see Figure 2. 19) suggests the presence of more than one reduction process, which is attributed to the reductive chemisorption of the acidic protons onto the electrode surface and to the electron injection in the LUMO orbital.⁷³ The observation that a simple washing step is not enough to detach the dye from the electrode suggested

that a strong interaction between the molecules and the glassy carbon surface, after the reductive step, takes place. Due to the multi-wave profile of the reduction processes LUMO energies were not evaluated for **PTZ1** and **PTZ2**. In these cases, the LUMO was evaluated from the corresponding HOMO energies and optical bandgaps. The cathodic electrochemistry of **PTZ3-6** molecules is somewhat more regular and the current peak positions were used to calculate their LUMO energy values. As can be seen from Figure 2. 20 all of the LUMO energies of the new thiophene-based dyes were higher than that of **PTZ1**, increasing from **PTZ2** to **PTZ5** and **PTZ6**, once again in agreement with the presence of the electron-rich thiophene spacer.

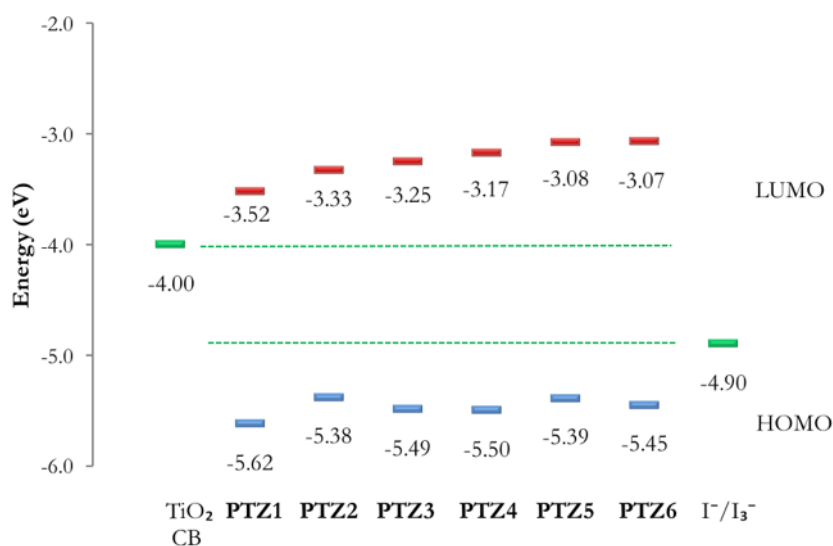


Figure 2. 20: HOMO/LUMO energies of dyes **PTZ1-PTZ6** in comparison with the conduction band (CB) level of TiO₂ and redox potential of the couple I⁻/I₃⁻.

PHOTOVOLTAIC INVESTIGATION

PTZ1-6 dyes were tested in DSSCs in order to have a proper evaluation of the new dyes as photosensitizers. DSSCs have been prepared using a single layer film (10

μm) consisting of a blend of active 20-nm up to 450-nm scattering nanoparticles of TiO_2 anatase and **Z960** (1.0 M dimethyl imidazolium iodide, 0.03 M I_2 , 0.05 M LiI, 0.1 M guanidinium thiocyanate and 0.5 M 4-*t*-butylpyridine in acetonitrile/valeronitrile 85/15)²⁷ as the liquid electrolyte. Chenodeoxycholic acid (CDCA) was added as a de-aggregating co-adsorbent agent²⁹ (CDCA:dye = 1:1). The recorded parameters are reported in Table 2. 9, current (J)/voltage (V) curves and incident photon-to-current conversion efficiencies (IPCE) are shown in Figure 2. 21 and Figure 2. 22, respectively.

Table 2. 9: photovoltaic characteristics of DSSCs containing phenothiazine-based dyes **PTZ1-6** (AM1.5 solar light).^a

Dye ^b	J_{sc} [mA cm ⁻²]		V_{oc} [mV]		FF [%]		PCE [%]	
PTZ1	8.76	(11.1)	656	(667)	74	(74)	4.3	(5.5)
PTZ2	10.8	(13.4)	632	(649)	72	(70)	4.9	(6.1)
PTZ3	10.2	(13.1)	622	(632)	67	(66)	4.3	(5.5)
PTZ4	9.71	(12.7)	622	(632)	70	(67)	4.2	(5.3)
PTZ5	10.3	(12.0)	682	(690)	74	(74)	5.2	(6.1)
PTZ6	6.58	(9.00)	604	(614)	69	(68)	2.8	(3.7)
N719 ^c	14.7	(17.4)	768	(753)	73	(71)	8.3	(9.3)

^a Values without a black mask on the top of the cell are listed in brackets. ^b Dye solution of 2×10^{-4} M in EtOH with 1:1 CDCA; electrolyte Z960 (see text), single TiO_2 layer (10 μm); surface area 0.20 cm². ^c Dye solution of 5×10^{-4} M in EtOH solution with 1:1 CDCA; electrolyte A6141 (0.6 M *N*-butyl-*N*-methyl imidazolium iodide, 0.03 M I_2 , 0.10 M guanidinium thiocyanate, and 0.5 M 4-*t*-butylpyridine in acetonitrile/valeronitrile 85:15).

Except for **PTZ6**, for which low current and voltage values were recorded, photocurrent values and corresponding PCE of the devices sensitized by the thiophene-based dyes were larger than **PTZ1**-based DSSC, in agreement with the enhanced optical properties.

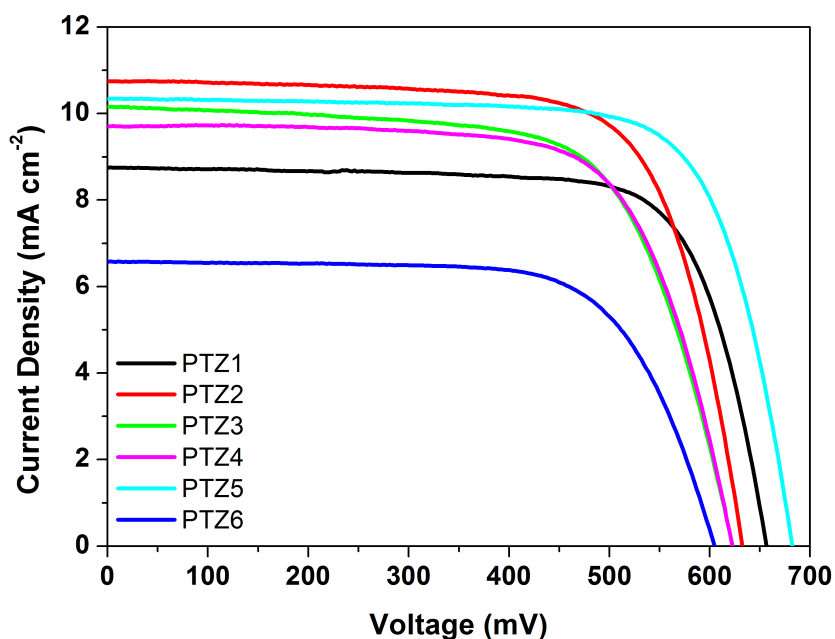


Figure 2. 21: comparison of the J - V curves of dyes sensitized solar cells using **PTZ1-6** dyes under full AM 1.5 solar intensity.

Devices based on dyes **PTZ1-6** exhibited different photovoltages, spanning from 604 to 682 mV. Dye **PTZ5** yielded the highest photovoltage, which in turn determined the largest PCE ($> 6\%$) in the series.

To gain further insights incident monochromatic photon-to-current conversion efficiencies (IPCE) were studied. The shape of these spectra follows those of the corresponding absorption spectra. The photocurrent values calculated by integrating the IPCE spectra and using the AM 1.5G spectrum nicely matched those measured with masked solar cells.³⁰ IPCE peaks ranged from 60% to 70% for all the **PTZ**-dyes except for **PTZ3** and **PTZ6** where the values are about 30%.

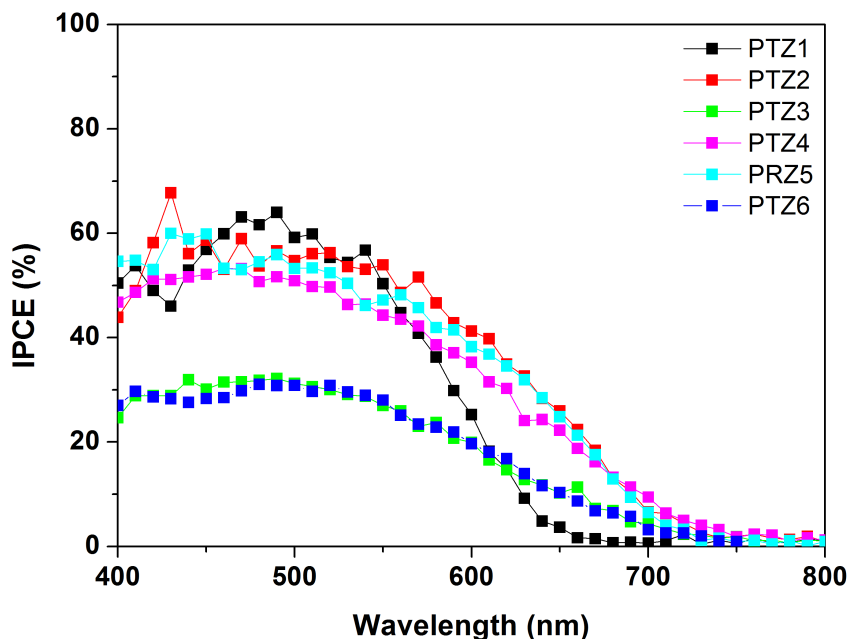


Figure 2. 22: incident monochromatic photon-to-current conversion efficiencies (IPCE) spectra comparison for dyes **PTZ1-6**

Electrochemical impedance spectroscopy (EIS) was used to further investigate the comparative behaviour, in particular in terms of different photovoltages, of the DSSC based on the dyes **PTZ1-6**.⁴⁷ The analysis of the impedance spectra was performed in terms of Nyquist plots (see Figure 2. 23) where the imaginary part of the impedance is plotted as a function of the real part over the range of frequencies. The impedance of the cell can be described by an equivalent circuit model (see inset Figure 2. 23) in which the different cell components and their interfaces are treated as discrete electrical elements. Under illumination at open circuit voltage conditions, in order to have direct current equal to zero and force the device to mainly describe recombination phenomena, the properties of the TiO_2 /electrolyte interface can be derived from the main (central) arc in terms of recombination resistance (R_{rec}), related to the recombination current, and chemical capacitance, associated to the density of states in the band gap of the oxide (C_{μ}).

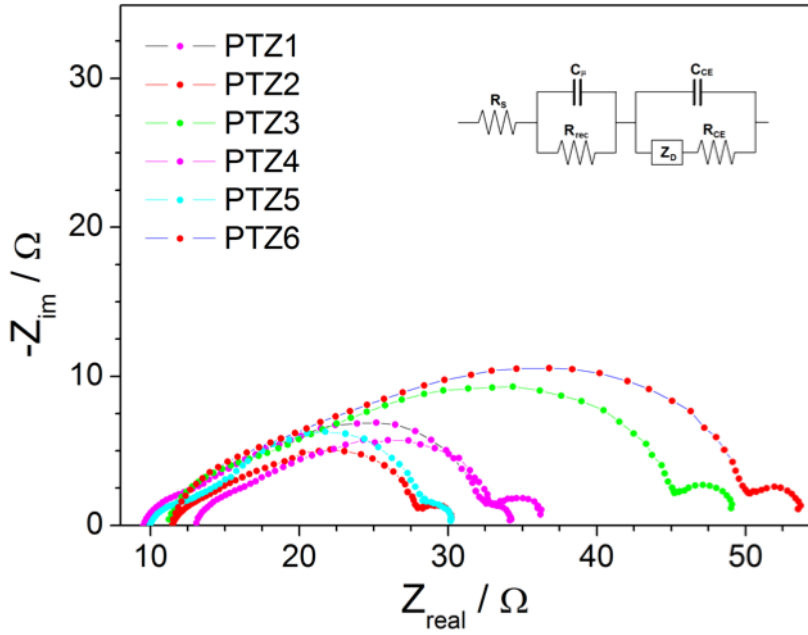


Figure 2. 23: Nyquist plots of DSSCs sensitized by **PTZ1-6**. Continuous lines represent the data fitting by using the equivalent circuit shown in the inset.

The apparent electron lifetime in the oxide τ_n can thus be calculated from Equation 12 and corresponds to the angular frequency at the top of the middle arc of the Nyquist plots.⁴⁷

$$\tau_n = R_{rec} \times C_\mu \quad (\text{Eq. 12})$$

All of these parameters are therefore associated to charge transfer (recombination) phenomena representing detrimental back-processes between the injected electrons in the semiconductor oxide and the oxidized form of the electrolyte. According to the benchmark Shockley–Queisser model the most important limitations to the cell photovoltage are carrier recombination phenomena, which are thus summarized in the τ_n values, reported in with R_{rec} and C_μ values. Indeed, we observe that the τ_n values were closely associated to the measured photovoltages. Accordingly, the cell based on **PTZ5**, which exhibited the highest carrier lifetime, showed the largest voltage, whereas the lowest voltages observed for DSSC sensitized by **PTZ3**, **PTZ4**, and **PTZ6** were associated to the smallest lifetimes.

Dye sensitized solar cells

Table 2. 10: Parameters calculated from EIS data plots of DSSC based on **PTZ1-6**.

Dye	R_{rec}	C_{μ}	τ_n
	[Ω]	[F]	[ms]
PTZ1	20	1.6×10^{-4}	3.1
PTZ2	13	2.0×10^{-4}	2.6
PTZ3	30	6.0×10^{-5}	1.8
PTZ4	18	1.2×10^{-4}	2.2
PTZ5	14	3.7×10^{-4}	5.0
PTZ6	35	4.9×10^{-5}	1.7

The analysis of the two components R_{rec} and C_{μ} showed that the highest electron lifetime measured for **PTZ5** was mainly due to the contribution of the chemical capacitance. Looking at the peculiar structural features of **PTZ5** we might therefore conclude that the most favourable conditions for the device photovoltage are associated to the presence of the alkyl groups on the thiophene rings, beneficial in terms of suppressing recombination reactions as widely reported in the literature,⁵² with particular emphasis on the position of the substituents in the dye central moiety.⁵³

Hydrophilic phenothiazine dyes for dye-sensitized solar cells using an water based electrolyte solution

One of the main issue related to the best performing DSSCs is the use of liquid electrolytes based on hazardous and volatile organic solvents (VOCs), such as acetonitrile. This clearly seriously hampers the widespread use of these devices in our society. In order to overcome these drawbacks, alternative solvents have been proposed as electrolyte media, such as ionic liquids (ILs),⁷⁴ liquid solutions adsorbed in polymeric matrixes,⁷⁵⁻⁷⁷ and solid state cells fully avoiding the use of solvents.^{78,79} Each of these configurations carries some disadvantages, such as higher costs, limited sustainability, and reduced power conversion efficiencies (PCEs). Therefore, the search for new electrolyte media combining ease of availability, low cost, high sustainability, while maintaining a comparable PCE as that of VOCs is in great demand in order to encourage a wider use of this solar technology.

In the last years, researchers started to investigate DSSCs in water as electrolyte media.⁸⁰ Water fully meets the aforementioned requirements since it is abundant, cheap and non-toxic. However, water is an atypical solvent for DSSCs and has been carefully avoided for years since it negatively affects the stability of the covalent grafting of the dye-sensitizer to the photoanode semiconductor oxide, typically TiO_2 , leading to dye desorption and corresponding shutdown of the device. Furthermore, pure water has a number of additional drawbacks such as shifting of the TiO_2 conduction band (CB) towards the wrong direction, interaction with additives and salts present in the electrolyte solution, and inhibition of interfacial contact between the electrolyte phase and the dye-coated semiconductor surface when common hydrophobic sensitizers are used.⁸¹ Although very exhaustive works have been recently published using water as the electrolyte solvent,^{80,82} PCEs are low, routinely spanning around values of 1-2%. These reports suggest that, although it successfully addresses some stringent requirements for the

industrialization of sustainable and cheap devices, water can be considered as a medium for DSSCs only in presence of water compatible components.

In DSSC working with a water-based electrolyte solvent, the dye acting as a sensitizer has to be carefully selected to offer good performance and good compatibility with an aqueous environment and with ultrathin (less than 5 μm) semiconductor layers. Taking into account these requirements, organic dyes are preferred since they exhibit higher molar extinction coefficient than conventional Ru(II) dyes such as N719.⁸³ One of the most common strategies to induce hydrophilicity to organic dyes is the introduction of a polyethylene glycol functionality, such as the widely used tris(ethylene glycol) monomethyl ether (TEG) group.⁸⁴ In fact, the TEG group has been successfully employed in many material science fields, including dye-sensitized solar cells⁸⁵ and nonlinear optics.⁸⁶ Despite these several reports, the TEG functionality cannot imply a more sophisticated design to further tune water affinity of sensitizers as well as induce additional properties such as intermolecular self-assembly. We have thus decided to check the use of a multifunctional scaffold derived from the natural monosaccharide D-glucose. Carbohydrates are excellent hydrogen bond donors and acceptors thanks to their multiple hydroxyl functions; sugar conjugation to hydrophobic molecular materials has been used in other research fields to enhance wettability⁸⁷

Here we report on the synthesis, characterization and comparative use of TEG (**PTZ-TEG**) and sugar (**PTZ-GLU**) derivatives of a thiophene-based phenothiazine dye (Figure 2. 24) belonging to the aforementioned **PTZ** family. In order to similarly compare with the small TEG substituent, we have selected the commercially available methyl α -D-glucopyranoside moiety. The series was completed by inserting in the comparative study an alkyl (n-octyl) derivative of the phenothiazine scaffold **PTZ-ALK** (named **PTZ2** in Ref. 3).

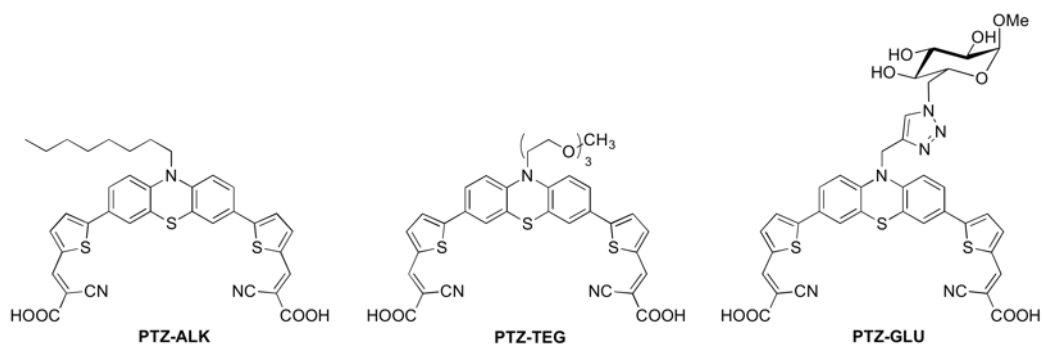
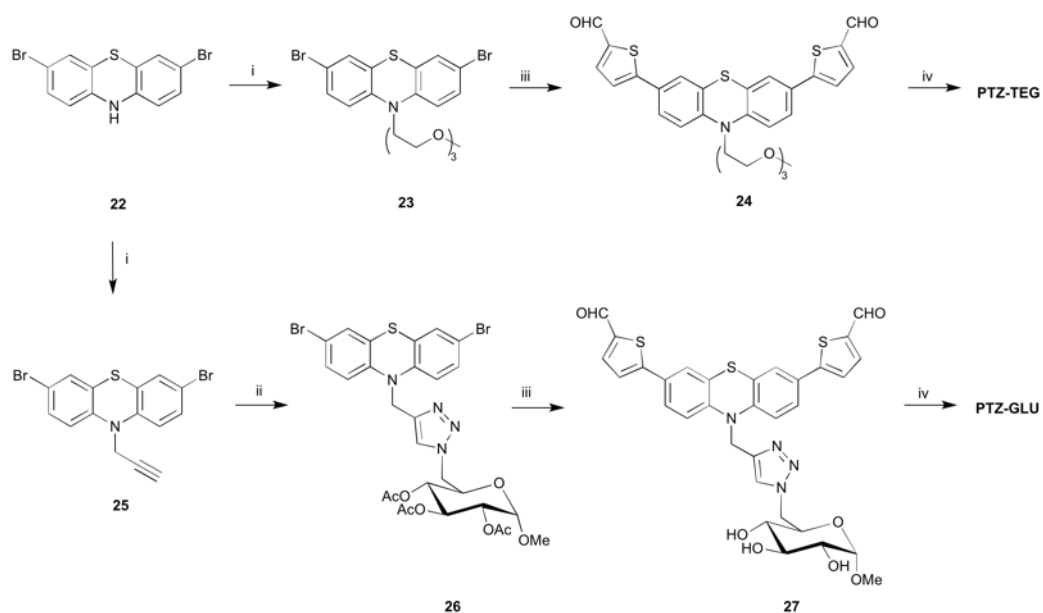


Figure 2. 24: hydrophilic sensitizers investigated in this work and reference hydrophobic dye.

SYNTHESIS

The designed procedure to synthesize **PTZ-TEG** and **PTZ-GLU** is depicted in Scheme 2. 5.



Scheme 2. 5: Synthetic routes for PTZ7 and 8. Reagents and conditions: (i) a. NaH 60%, DMF, 0°C, b. TEG-OTs for 2 and propargyl bromide for 4, rt, 24 h; (ii) methyl 2,3,4-tri-*O*-acetyl-6-azido-6-deoxy- α -D-glucopyranoside, Cu₂SO₄·5H₂O, sodium ascorbate, THF/H₂O, rt, 4 h; (iii) 5-formyl-2-thienylboronic acid, Pd(dppf)Cl₂·CH₂Cl₂ [dppf = 1,1'-bis(diphenylphosphino)ferrocene], K₂CO₃, DME/MeOH, microwave, 70 °C, 90 min; (iv) cyanoacetic acid, piperidine, CHCl₃, reflux, 5 h.

The synthetic procedure for achieving **PTZ-TEG** is similar to the one used for **PTZ-ALK**,³ the alkylating reagent was prepared according to a known procedure starting from triethylene glycol monomethyl ether and *p*-TsOH.⁸⁸ Phenothiazine

was brominated with Br₂ following the reported procedure⁶², and then the anilinic nitrogen was deprotonated with NaH 60 % in DMF and added the prepared tosylate. A following Suzuki-Miyaura cross coupling to introduce the π portion and a Knoevenagel condensation to introduce the anchoring and accepting unit enabled to afford **PTZ-TEG** with a satisfactory yield.³

To obtain the glucose-functionalized dye **PTZ-GLU** we adopted the Cu-assisted azide-alkyne cycloaddition (CuAAC) “click” reaction,^{89,90} using the methyl 2,3,4-tri-O-acetyl-6-azido-6-deoxy- α -D-glucopyranoside, which was synthesized as reported in literature,⁹¹ and the alkyne-functionalized dye **25**. The advantage of azide-alkyne cycloadditions is their high chemoselectivity, which makes these reactions particularly attractive to conjugate highly functional molecules as for example carbohydrates.⁹² Moreover the versatility of the click reaction and the eventual easiness and high functional group tolerance in expanding the synthetic procedure to more complicated carbohydrates could be preferred in designing a library of glycoconjugated dyes. Azide functionality was introduced in C6 position of glucose through a substitution reaction; the glucose was previously protected in the OH functionalities as acetate and the anomeric carbon was blocked as methyl acetal. The anomeric carbon should be blocked in the final dye as well to prevent any possible redox interference with the photocatalytic cycle of the sensitizer. The triple bond has been introduced on the phenothiazine moiety through nucleophilic substitution in an analogous way as for **PTZ-TEG**, using NaH as base to deprotonate the nitrogen and propargyl bromide as alkylating reagent. Butynyl bromide has been tested as well for alkylation but the strong basic conditions precluded the achievement of the desired product because of likely side-reactions taking place on the butynyl chain. Anyway the presence of a sp³ carbon on the propargyl chain guarantees that no π conjugation of the molecule with the triazole ring will be present in the dye. Click reaction has been performed in standard conditions using CuSO₄ as copper source and sodium ascorbate as reducing agent in a THF and water mixture. The thienyl group was introduced with a Suzuki-

Miyaura cross-coupling, during such reaction step the basic conditions due to K_2CO_3 brought to the formation of the desired product with the simultaneous cleavage of the three acetate groups on the glucose. Such side reaction was not forecast but since the protecting groups were introduced to perform the previous steps there had been no problem in performing the final Knoevenagel condensation in basic conditions to afford the desired product.

OPTICAL AND ELECTROCHEMICAL PROPERTIES

Optical characterization of dyes **PTZ7-8** was performed in 10^{-5} M THF solution. Absorption spectra normalized to molar extinction coefficients are shown in Figure 2. 25. The optical and electrochemical parameters are listed in Table 2. 11.

Table 2. 11: Optical and electrochemical characterization of dye **PTZ-ALK**, **PTZ-TEG** and **PTZ-GLU**.

Sample	λ_{max}^a (nm)	ϵ ($M^{-1}cm^{-1}$)	V_{ox} (V vs. Fc) ± 10 mV	HOMO ^b eV ± 0.1 eV	V_{red} (V vs. Fc) ± 10 mV	LUMO ^b eV ± 0.1 eV
PTZ-ALK ^c	470	34000 ± 1000	0.15	-5.4	-	-3.3
PTZ-TEG	470	28000 ± 1000	0.33	-5.5	-1.52	-3.7
PTZ-GLU	471	32000 ± 1000	0.30	-5.5	-1.49	-3.7

^a Dye solution 10^{-5} M in THF. ^b Vacuum potential = Fc/Fc⁺ + 5.2 V. ^c Values from Ref 3

The three dyes showed a classical behaviour, with an intense $\pi-\pi^*$ absorption band in the UV region attributed to the local transition of the electron-rich donor core and a strong absorption band in the Vis region attributed to the intramolecular donor to acceptor charge-transfer transition (ICT). The position of the maximum of absorption is around 470 nm for all the dyes and the molar absorptivity is from 28000 to 32000 $M^{-1}cm^{-1}$. As expected (see molecular design), the absorption peak of the two dyes is not affected by the presence of the two different terminal moieties.

The molar absorptivity is slightly different though the deviation is approximately 20%.

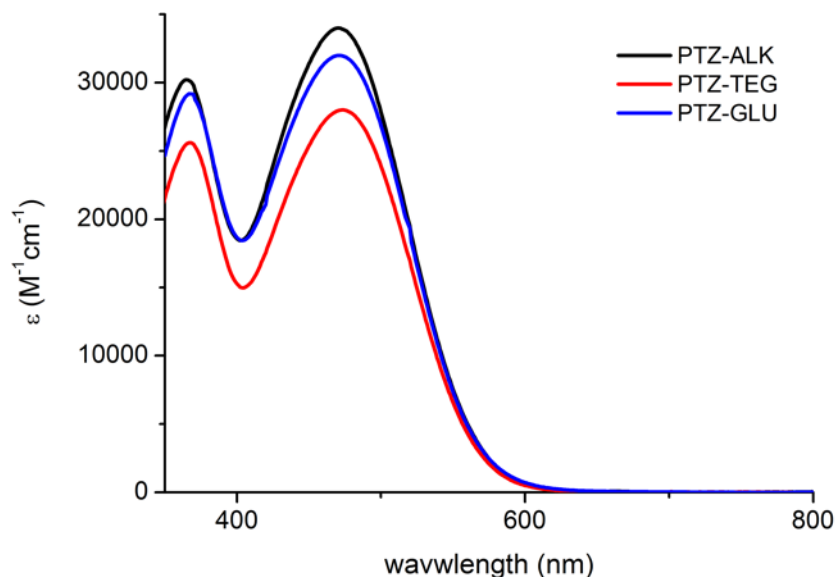


Figure 2. 25: absorption spectra of dyes PTZ-ALK, PTZ-TEG and PTZ-GLU in THF

The electrochemical characterization is summarized in Figure 2. 26 and Table 2. 11. Cyclic voltammetry profiles showed a quasi-reversible behaviour for the **PTZ-TEG** oxidation. The remaining investigated redox processes (**PTZ-TEG** reduction and **PTZ-GLU** oxidation and reductions) were irreversible. The **PTZ-TEG** oxidation showed two unresolved current signals (a peak and its shoulder), which made somewhat difficult the energy level calculation. For these reasons, Differential Pulsed Voltammetry (DPV) was employed. DPV was able to isolate the different electrochemical processes with the exception of the **PTZ-GLU** first oxidation, which appears as a shoulder of the main peak. In this case the HOMO energy level has been determined from the current onset rather than current peak.

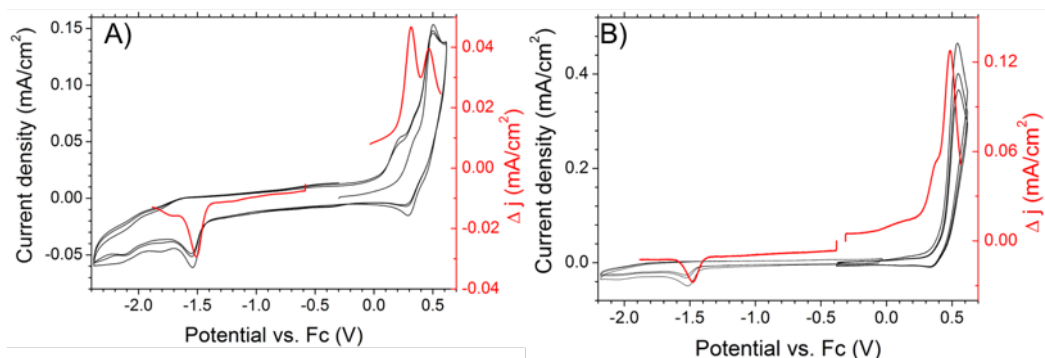


Figure 2. 26: CV (black line) and DPV (red line) measurements of a) **PTZ-TEG** and b) **PTZ-GLU**

WATER AFFINITY AND PHOTOVOLTAIC PROPERTIES

Contact angle analysis was used to investigate the hydrophilicity properties of the **PTZ-ALK**, **PTZ-TEG**, and **PTZ-GLU** sensitized TiO_2 nanoparticles. The contact angles of a deionized water drop on the surface of a film of sintered TiO_2 and the corresponding films sensitized with both dyes are shown in figure; data are summarized in Table 2. 12. The bare TiO_2 and the hydrophilic dyes-sensitized films have contact angles lower than 35° , compared to the value of 117° for the hydrophobic dye **PTZ-ALK**. Therefore, the introduction of the hydrophilic substituents clearly improves the wettability of the photocatalyst surface. More importantly, the sugar functionality in **PTZ-GLU** is able to improve water affinity by further decreasing the angle from 34° in the **PTZ-TEG** dye to 27° , thus going closer to the bare TiO_2 -NP surface character.

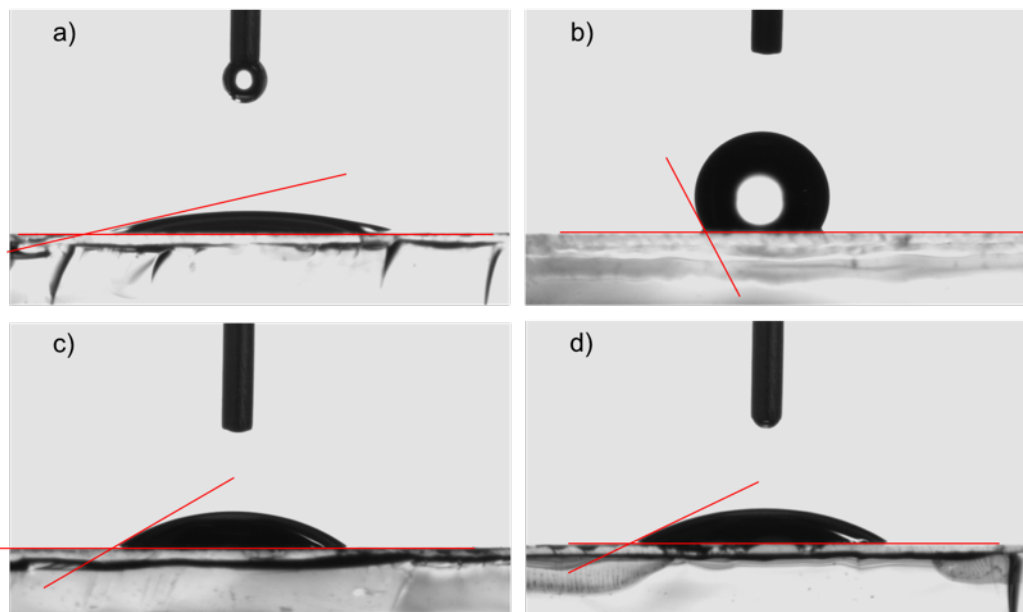


Figure 2. 27: Cross-sections of a) a film of sintered TiO_2 -NP; b) film of sintered TiO_2 -NP sensitized with **PTZ-ALK**; c) film of sintered TiO_2 -NP sensitized with **PTZ-TEG**; d) film of sintered TiO_2 -NP sensitized with **PTZ-GLU** and a drop of deionized water positioned on the top, which were used for the estimation of the contact angles ($\theta_c/^\circ$)

A preliminar investigation of the new hydrophilic dyes in DSSCs has been performed. DSSCs have been prepared using a single layer film ($10\ \mu\text{m}$) consisting of a blend of active 20-nm up to 450-nm scattering nanoparticles of TiO_2 anatase. Two electrolyte have been chosen to test the new dyes, **Z960** (1.0 M dimethyl imidazolium iodide, 0.03 M I_2 , 0.05 M LiI, 0.1 M guanidinium thiocyanate and 0.5 M 4-*t*-butylpyridine in acetonitrile/valeronitrile 85/15)²⁷ as organic liquid electrolyte, and **W1** (4 M KI, 0.02 M I_2 in deionized water)⁸⁵ as water base electrolyte. Chenodeoxycholic acid (CDCA) was added as a de-aggregating co-adsorbent agent²⁹ (CDCA:dye = 1:1). The recorded parameters are reported in Table 2. 12, current (J)/voltage (V) curves in Figure 2. 28.

Table 2. 12: photovoltaic characteristics of DSSCs containing phenothiazine-based dyes **PTZ-ALK**, **PTZ-TEG** and **PTZ-GLU** (AM1.5 solar light).^a

Chapter 2

Dye ^b	J_{sc} [mA cm ⁻²]	V_{oc} [mV]	FF [%]	PCE [%]	Electrolyte	Contact angle (θ_c /°)
TiO ₂	-	-	-	-	-	13.9
PTZ-ALK	10.8	632	72	4.9	Z960	-
PTZ-ALK	-	-	-	-	W1	117.3
PTZ-TEG	8.3	644	68	3.6	Z960	-
PTZ-TEG	-	-	-	-	W1	33.9
PTZ-GLU	9.0	654	70	4.1	Z960	-
PTZ-GLU	0.29	256	30	0.02	W1	26.8

^a Values with a black mask on the top of the cell. ^b Dye solution of 2×10^{-4} M in EtOH with 1:1 CDCA; single TiO₂ layer (10 μ m); surface area 0.20 cm².

The values recorded for the three dyes in presence of an organic based electrolyte are very similar. They basically follow the trend observed in the optical properties. The recorded photovoltage are really similar around 640 mV. In this case the difference between the recorded PCE is close to 30% but the difference between the measured current density is rather 20% in agreement with the difference in molar extinction coefficient. The residual difference can be explained by the dissimilar affinity of the sensitized titanium oxide with the electrolyte. By the other hand, the presence of a strong hydrophilic functionality allows to record a measurable value in presence of a water based electrolyte. While the water affinity of the two hydrophilic dyes is comparable, it is still not clear why it is impossible to measure any photocurrent when **PTZ-TEG** is used as sensitizers. A possible explanation can be related to the steric hindrance of the glucose functionality. In fact, even though both **PTZ-GLU** and **PTZ-TEG** have comparable behavior in presence of a water based electrolyte, the larger glucose functionality can more efficiently help to prevent the recombination between the electrolyte and the titanium dioxide. At the moment, this topic is being studied in another Ph.D. thesis in our research group.⁹³

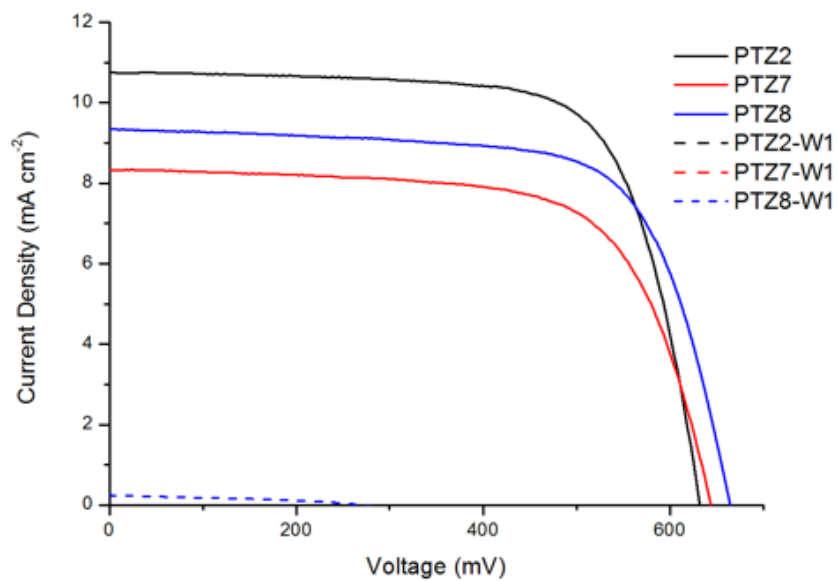


Figure 2. 28: comparison of the $J-V$ curves of dyes sensitized solar cells using **PTZ-ALK**, **PTZ-TEG** and **PTZ-GLU** dyes in presence of organic solvent based electrolyte (solid line) and water based electrolyte (dashed line) under full AM 1.5 solar intensity

C-Doped-titania paste for Dye-Sensitized Solar Cells

Titanium dioxide (TiO_2) has been extensively used as the photoanode n-type semiconductor, thanks to its low-cost, long-term stability, and non-toxicity. However, the main drawback of the use of TiO_2 lies in its intrinsic wide bandgap (3.2 eV), thus directly harvesting only 3-5% of the solar radiation. The strategies adopted for improving the harvesting efficiency of TiO_2 can be summarized as either morphological modifications, such as higher surface area and porosity, or as chemical modifications, by incorporation of additional components in the TiO_2 structure. Accordingly, many efforts have been dedicated to develop TiO_2 -based materials that could bridge both the UV (290-400 nm) and the visible (400-700 nm) radiation and reduce the recombination of electron/hole pairs, thereby enhancing the overall absorption efficiency.⁹⁴

Attempts toward achieving this goals have relied, in part, on photosensitizing the metal oxide by molecular visible-light-harvesters, such as suitable organic dyes^{95,96} and suitable metal-ion dopants.^{97,98} However, both approaches present serious drawbacks. Although organic dyes allowed DSSC record efficiencies,^{32,35} often undergo natural degradation thus permitting limited long-term stability under light soaking and thermal stress. On the other hand, metal dopants act as recombination centres for the photogenerated charge carriers. To overcome these limitations, researchers started to consider nonmetals-doping (N, C, S and F) as a prelude to increase the photoactivity of this metal,⁹⁹ following the pioneering work of Asahi et al. in 2001.¹⁰⁰

Visible-light activation of TiO_2 specimens (anion-doped or otherwise) have been attributed either to defects associated with oxygen vacancies that give rise to color centres^{99,101} or to a narrowing of the original band-gap of TiO_2 through mixing of dopant and oxygen 2p orbitals.¹⁰⁰ Nevertheless, the chemical nature of the doped species, responsible for the visible titania photoactivity, and the electronic structure of the doped material have not been yet fully exploited.¹⁰²

Among the anionic dopant, carbon¹⁰³⁻¹⁰⁵ and nitrogen¹⁰⁶⁻¹⁰⁸ are the most employed and are introduced into the titania structure in concentration ranging parts per thousand to parts per hundreds. The effects and the efficiency of doping greatly vary with the employed techniques and synthetic methods. A common observation among the studied techniques is the creation of localized extrinsic energy levels inside the band-gap of TiO₂.¹⁰⁹ The optical transitions between these levels and the Ti 3d levels (which are the main component of the CB edge), are responsible for the improve in the absorption properties of the material, and are traced by the shift of absorption threshold of TiO₂ in the form of shoulders or tails towards higher wavelength range of the radiation.

Aiming to overcome the current limits of DSSC and reach a higher PCE, this work investigate the device performances using easily obtainable and low cost carbon-doped TiO₂, synthesized through a sustainable and easily scalable chemical route, ready for fast industrialization. Intensive efforts have been made so far to develop methods for synthesizing nonmetal-doped TiO₂-based photocatalysts. The three most important methods for the synthesis of C-doped TiO₂ are: 1. high-temperature sintering of carbon-containing TiO₂ precursor, 2. CVD or pyrolysis, 3. solution-phase strategies.¹¹⁰⁻¹¹⁵ Most of the methods require high-temperature treatments (400-850 °C), use expensive, toxic, or unstable precursors, and are tedious to conduct, making difficult a large-scale application. Therefore, it is of particular importance to develop a facile, energy efficient, and environmentally friendly approach for the synthesis of C-doped TiO₂ nanomaterials with high visible photocatalytic activity.

Other synthetic routes, such as simple wet chemistry techniques, can solve the aforementioned issues. These approaches relies on its efficiency to afford pure products while minimizing the number of preparation steps and avoiding the use of either excessively harmful reagents or unstable precursors, with no generation of toxic by-products. Thus, such a method is efficient in scale-up procedures and benign to human health and the environment.

Herein, we have investigated the photovoltaic properties of DSSCs devices prepared using different C-doped TiO₂ pastes.

SYNTHESIS AND CHARACTERIZATION OF THE C-DOPED TiO₂ PASTE

The synthesis of the C-doped TiO₂ nanoparticle, their characterization and the preparation of the C-doped TiO₂ pastes has been done in the laboratory of the University of Padova in the group of Prof. Brusatin.

The novelty is the green approach based on a simple “multi-step” mild process, where low-cost titania nanoparticles, and glucose (C₆H₁₂O₆) as the C-dopant, are used.¹¹⁶ The C-doped titania nanoparticles have been prepared adding the proper amount of a solution of the carbon source (sucrose, C₁₂H₂₂O₁₁) to a dispersion of the desired TiO₂ nanoparticles (P25 or 100% Anatase). The sealed system was allowed to react at 85 °C overnight and then air dried, grinded and thermally treated at 255 °C for 4 h. The obtained nanoparticles have been characterized using XPS (X-Ray Photoelectron Spectroscopy). The photoemission peaks depend on the chemical environment of the atoms from which they generate and a shift is observable from the unperturbed atomic value if the chemical surrounding is changed. An extensive literature research did not present a univocal interpretation of XPS data regarding the assignment of the dopant peaks and the effectiveness of the doping treatment for TiO₂ nanoparticles. Notwithstanding, some signals are clear and unanimously assigned to the doping species we have employed in this work. In the case of carbon doping, the peak relative to the C 1s orbital extends for a interval in binding energy between 281-291eV and many contribution can be recognized. The signals are assigned as follow: 281,8 eV is the Ti-C bond, 284,6 eV is the C-C bond and 288,6eV are the Ti-O-C structures. Unfortunately, as it can be seen in Figure 2. 29, one should remember the ubiquitous carbon contamination present on the top of any sample. In this sense, with our preliminary data, it is unreliable any conclusion about the signal of doping atoms as it was difficult to separate the contribution from adventitious carbon contamination.

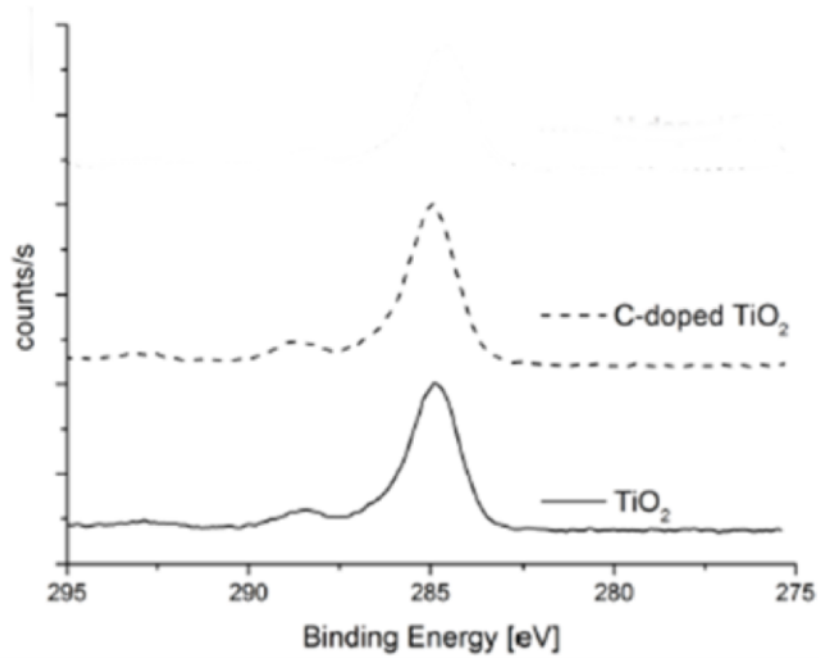


Figure 2. 29: Comparison of the C 1s XPS signal of the samples.

Finally, XPS spectra of both undoped and doped titania, in Figure 2. 30, exhibit two main contributions corresponding to Ti 2p_{3/2} and 2p_{1/2} at 458.5 - 458.7 eV and 464.4 eV, respectively, in good agreement with the previously reported XPS data on Ti⁴⁺-based oxides.¹¹⁷

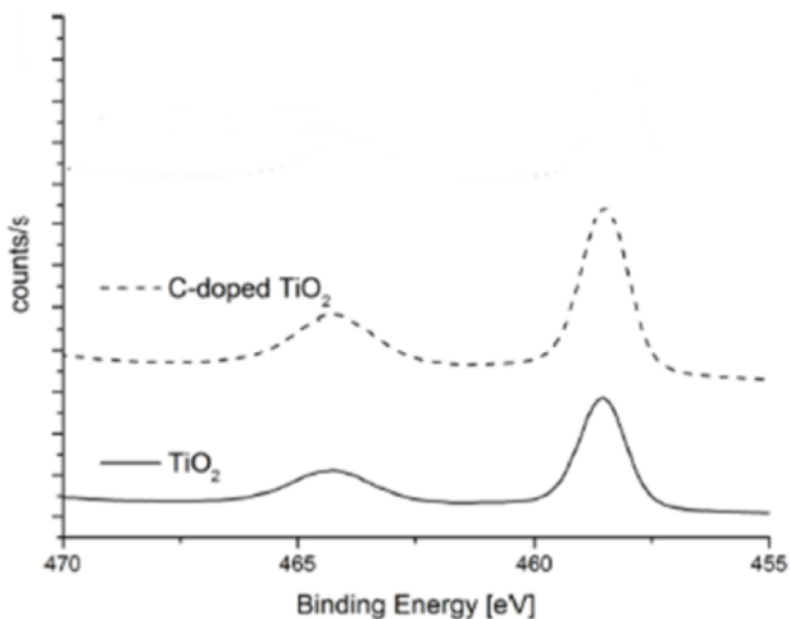


Figure 2. 30: Comparison of the Ti 2p XPS signal of the samples.

The titania paste has been prepared according to literature,¹¹⁸ and the morphology of anodic samples deposited on glass substrate was evaluated through SEM analysis. As a great part of the electronic transport properties of the anode is given by its morphology, not only a smoother texture allows for longer migrating distances and efficient separation of couples, but also a greater surface area allow for a more efficient loading of the dye, thus in general increasing the power density of the cell. Moreover, pore size and distribution should be as smooth as possible, since rougher morphology reduces available surface area.

As reported in Figure 2. 31, which show the TiO₂ electrode surface morphology obtained during doctor blade preparatory technique, there is no drastic change in the texture or porosity among the samples, both in the native P25 TiO₂ nanoparticles and in the C doped samples. This allow us to conclude that the proposed strategy, given its lower process temperature as compared to other doping methods, such as flame pyrolysis, do not modify the aggregation state of the nanoparticles which are thus suitable for the preparation of the anodic material.

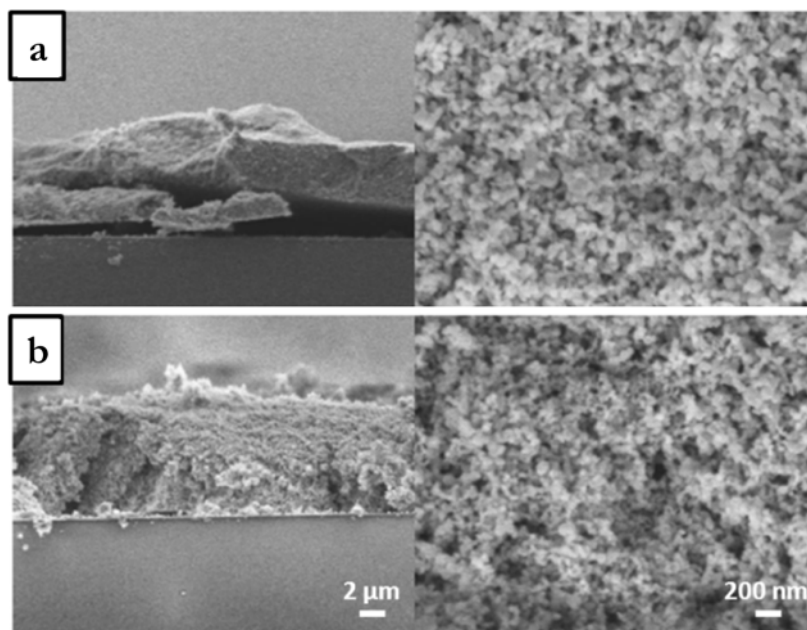


Figure 2. 31: SEM images of the TiO_2 pastes deposited with doctor blade technique. (a) Carbon-doped TiO_2 ; (b) P25.

Three different C-doped titanium oxide nanoparticles have been synthesized with an increasing carbon content, namely with 24% ($\text{TiO}_2\text{-C24}$), 32% ($\text{TiO}_2\text{-C32}$), and 40% ($\text{TiO}_2\text{-C40}$).

PHOTOVOLTAIC CHARACTERIZATION

The new titanium oxide pastes, with increasing amount of carbon dopant, have been investigated and the photovoltaic parameters have been reported in Table 2. 13, as well as the J/V curves of the devices in Figure 2. 32 and , respectively. The doped TiO_2 paste have been compared with the commercial analogous (Solaronix T/SP) and with a paste prepared using pure anatase- TiO_2 , the same used to prepare the doped systems.

Solar devices were prepared using either a single layer film consisting of a transparent 20-nm particles layer ($10\ \mu\text{m}$) of TiO_2 paste and a double in combination with the commercial scattering layer ($5\ \mu\text{m}$, Solaronix R/SP) containing optically dispersing anatase $> 100\ \text{nm}$ particles. The liquid electrolyte

A6141 (0.6 M *N*-butyl-*N*-methyl imidazolium iodide, 0.03 M I₂, 0.10 M guanidinium thiocyanate, and 0.5 M 4-*t*-butylpyridine in acetonitrile/valeronitrile 85:15)^{47,83} was used for testing the photovoltaic properties of devices. In addition, we have investigated the photovoltaic in presence of equimolar amount of chenodeoxycholic acid (CDCA) as a de-aggregating co-adsorbent agent²⁹ in the sensitizer solution (CDCA:dye = 1:1).

Table 2. 13: Photovoltaic characteristics and dye loading of DSSCs containing carbon-doped TiO₂ films and comparison with commercial TiO₂ pastes. (Value without mask are in brackets)

Device ^a	J _{sc}		V _{oc}		FF		PCE		Dye adsorbed ^d [10 ⁻⁸ mol cm ⁻²]
	[mA/cm ²]	[mV]	[mV]	[mV]	[%]	[%]	[%]	[%]	
Solaronix T/SP-R/SP ^b	15.6	(17.9)	720	(722)	72	(71)	8.1	(9.2)	15.9
Solaronix T/SP ^c	15.4	(15.7)	732	(758)	73	(75)	8.2	(8.9)	11.9
TiO ₂ -Anatase ^c	11.9	(13.6)	802	(780)	76	(75)	7.3	(7.9)	6.9
TiO ₂ -A + Solaronix R/SP ^b	11.5	(13.0)	758	(760)	74	(73)	6.4	(7.2)	6.5
TiO ₂ -C24 ^c	11.3	(14.5)	792	(797)	76	(74)	6.8	(8.5)	5.5
TiO ₂ -C24 + Solaronix R/SP ^b	13.2	(15.7)	778	(785)	75	(74)	7.7	(9.1)	6.3
TiO ₂ -C32 ^c	11.6	(13.5)	775	(778)	73	(74)	6.6	(7.8)	6.4
TiO ₂ -C32 + Solaronix R/SP ^b	11.7	(14.0)	778	(781)	76	(75)	6.9	(8.2)	5.9
TiO ₂ -C40 ^c	10.9	(12.1)	778	(778)	76	(75)	6.4	(7.1)	5.3
TiO ₂ -C40 + Solaronix R/SP ^b	10.9	(11.9)	762	(775)	75	(75)	6.2	(6.9)	6.1

^a Dye solution of 5 x 10⁻⁴ M in EtOH solution with 1:1 CDCA; electrolyte A6141 (see text); ^b Double TiO₂ layer (10+5 μm); ^c Single TiO₂ layer (10 μm); ^d surface area 0.20 cm²

The overall power conversion efficiencies PCE were derived from the equation: $PCE = J_{sc} \times V_{oc} \times FF$, where J_{sc} is the short circuit current density, V_{oc} the open circuit voltage, and FF the fill factor, as described in previous chapter.

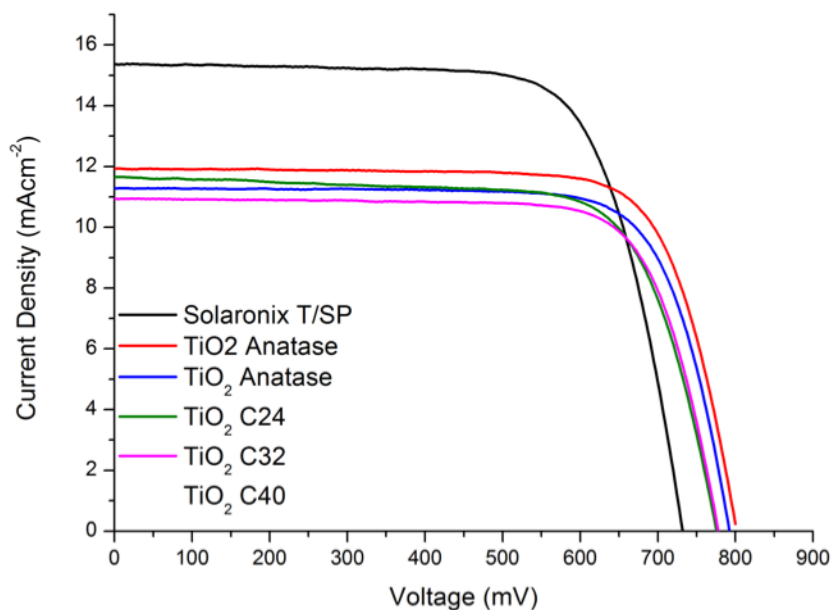


Figure 2. 32: Current–voltage characteristics of single layer DSCs containing carbon-doped TiO₂ films and comparison with commercial TiO₂ pastes. (full AM 1.5G solar intensity).

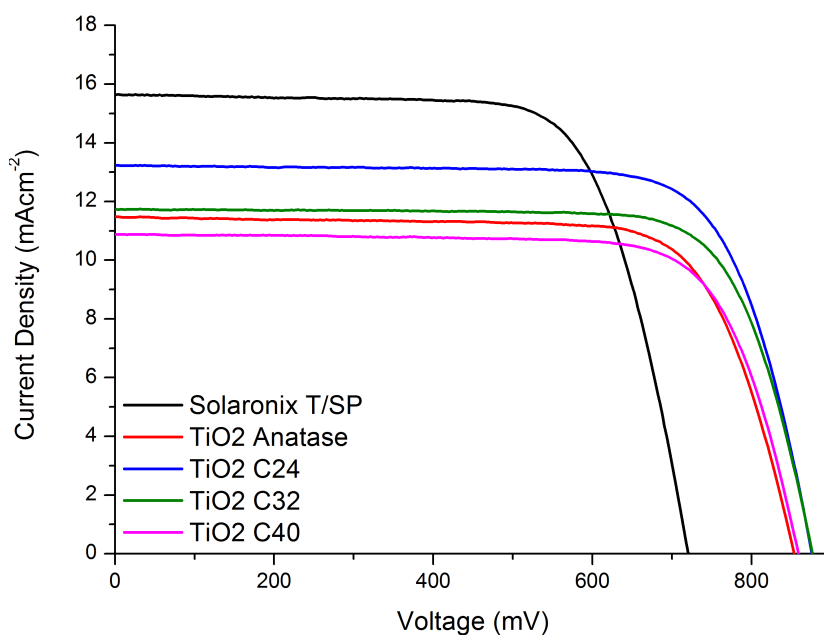


Figure 2. 33: Current–voltage characteristics of double layers DSCs containing carbon-doped TiO₂ films and comparison with commercial TiO₂ pastes. (full AM 1.5G solar intensity).

The highest recorded efficiency in these measurements has been achieved with the commercial paste in both configurations, single and double layer. The interesting

fact is that the photocurrent is slightly higher compared to the titania paste prepared using TiO_2 nanoparticles, but the photovoltage is 80 mV lower. The values recoded for the home made titania pastes are similar except for the best samples C24 which has allowed to record a PCE value almost equal to the commercial best paste both in case of single or double layer devices. This is obviously due to the carbon doping, in fact, the cells made with the pure anatase- TiO_2 used as reference, showed a lower efficiency. Whereas the cells use the same sensitizer, it is meaningless to analyse the IPCE characteristic, but it is more significant to consider the electrochemical characteristics and the dye loading.

The dye loading has been ascertained via optical absorption of a proper solution of the desorbed dyes from the photoanode as described in our previous works.¹¹⁹ The results are reported in Table 2. 13 and graphically depicted in Figure 2. 34.

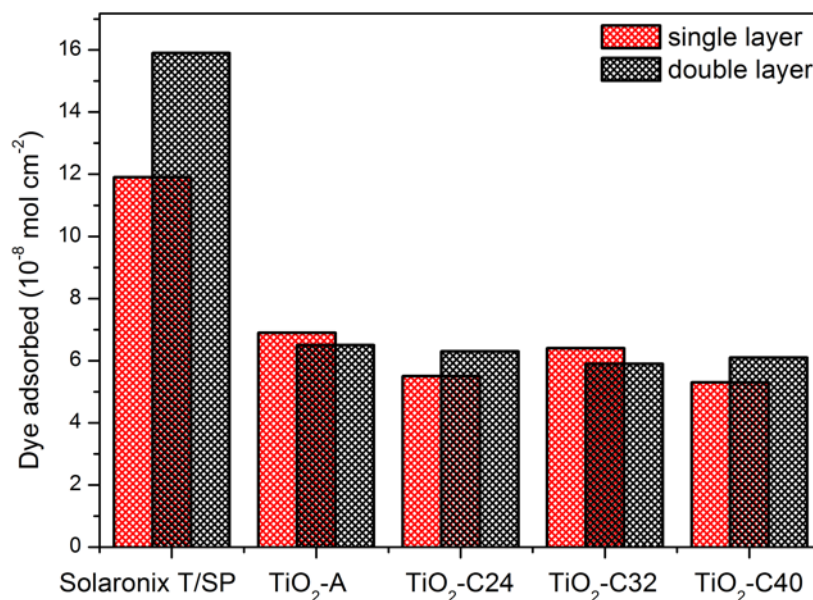



Figure 2. 34: Comparison of dye adsorbed on single layer (red pattern) and double layer (black pattern) DSCs containing carbon-doped TiO_2 films and comparison with commercial TiO_2 pastes.

The significant fact that emerges from this series of measurements is that the titania prepared from nanoparticles of anatase- TiO_2 absorbs a significantly lower amount (about 50% less) of dye than that prepared from commercial pastes.

Though it is not known the exact composition of the commercial pastes, what appears evident simply depositing them to prepare photoanodes, it is that are much more transparent compared with those prepared from nanoparticles. This is definitely related to scattering phenomena due to the formation of large aggregates in the pastes prepared from nanoparticles compared to the commercial. In other words, it is conceivable that the commercial pastes are prepared with nanoparticles of titanium dioxide functionalized for better remain dispersed in the organic environment that form the dough used to prepare the photoanodes, and to remain more transparent after the thermal treatments. In fact, the commercial paste Solaronix T/SP allows to realize devices with a high degree of transparency, which is impossible using the pastes prepared using bare TiO₂ nanoparticles. This effect could be considered negative in the case of devices used in smart windows (*i.e.* photovoltaic windows). However, if the devices are made as a double layer in combination with a scattering layer, this becomes meaningless. The formation of large aggregates can also explain such a substantial difference in the amount of absorbed dye. To get a clearer idea of such phenomena are at the basis of the different absorption of the dye it will be necessary to study the surface area and the porosity of the titania powder obtained from the different studied pastes. This will allow us to determine whether the difference in dye loading is due to a different morphology or other phenomena not yet taken into account.

However, it is possible an analysis of the electrical phenomena that occur within the devices made with the different pastes going to study the devices themselves by means of electrochemical impedance spectroscopy (EIS). The Nyquist plots (Figure 2. 35 and Figure 2. 36) show the characteristic feature of DSSC spectra. The electrochemical charge transfer process at the Pt electrode and the electron leaking at the photoanode/electrolyte interface correspond the high, and low frequency semicircles, respectively. Data were fitted using the equivalent circuit model shown in the inset of Figure 2. 23, the corresponding electrochemical parameters are reported in Table 2. 14.

Table 2. 14: Impedance characteristics of single and double layers DSCs containing carbon-doped TiO₂ films and comparison with commercial TiO₂ pastes, with a commercial TiO₂ scattering layer.

Device ^a	R _{rec} [Ω]	C _{dl,p} × 10 ⁴ [F]	 [ms]
Solaronix T/SP-R/SP	8.0	7.6	6.1
Solaronix T/SP	11	3.9	4.3
TiO ₂ -A	12	3.2	3.7
TiO ₂ -A + Solaronix R/SP	11	3.8	4.3
TiO ₂ -C24	16	2.5	4.0
TiO ₂ -C24 + Solaronix R/SP	13	3.6	4.3
TiO ₂ -C32	16	2.7	4.3
TiO ₂ -C32 + Solaronix R/SP	12	3.5	4.2
TiO ₂ -C40	12	3.5	4.1
TiO ₂ -C40 + Solaronix R/SP	11	3.7	4.3

Since we are interested in the effect of the carbon doping of titania on the cell performances, we will focus the attention only on the high frequency semicircle which depends on the interfacial feature of the titania/electrolyte inter-phase. The electron time life in the titania appears to be correlated to the quantity of adsorbed dye: the larger the amount of dye the longest the electron time life.

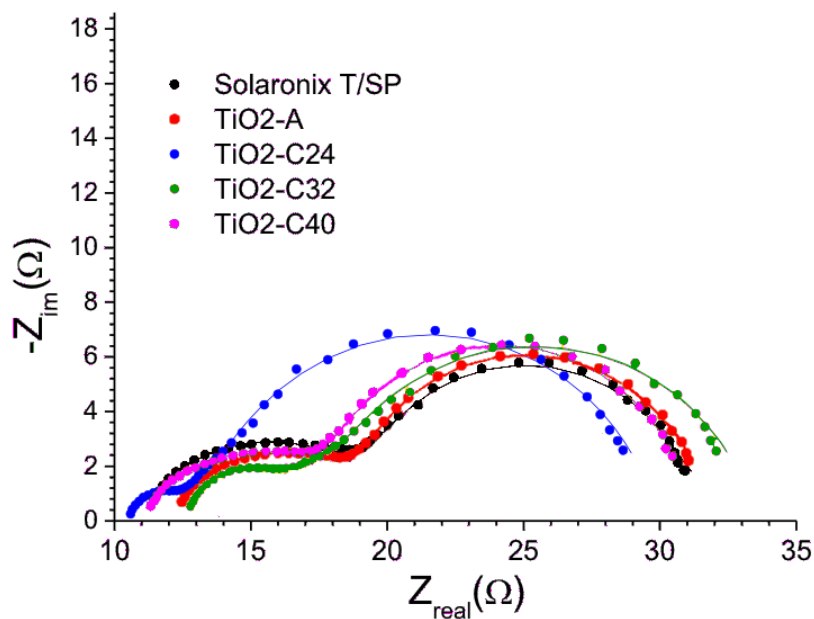


Figure 2. 35: Nyquist plots of and single layer DSCs containing carbon-doped TiO₂ films and comparison with commercial TiO₂ pastes. Dot points: experimental data; continuous line: fitted data.

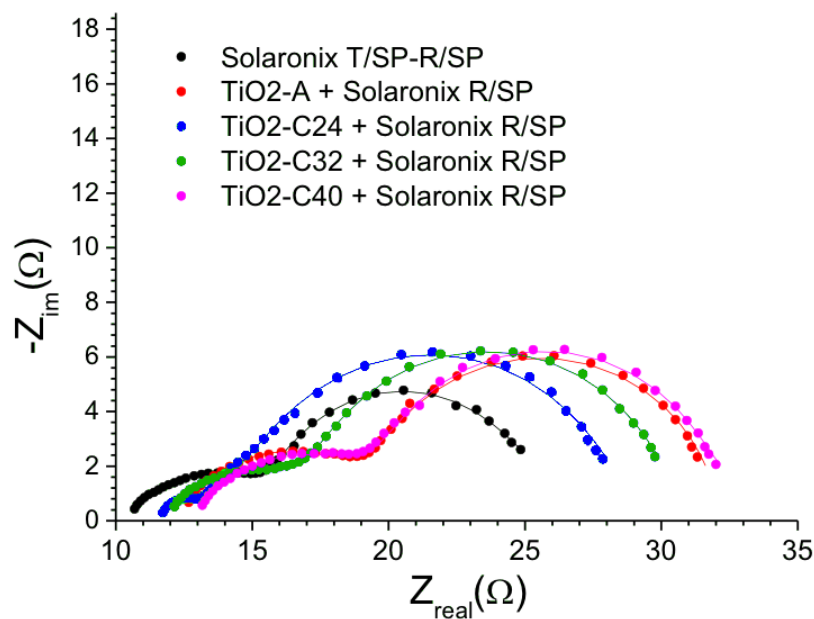


Figure 2. 36: Nyquist plots of double layers DSCs containing carbon-doped TiO₂ films and comparison with commercial TiO₂ pastes, with a commercial TiO₂ scattering layer. Dot points: experimental data; continuous line: fitted data.

Moreover, the decrease in electron time life does not depend from the recombination resistance while is mostly affected by the decrease of double layer capacitance; indeed, the dielectric permittivity of the interface is lower in sample with less amount of the neutral organic molecule onto the semiconductor surface.

Though the reasons why the efficiency values recorded by the devices prepared using the C-doped-TiO₂ are not yet completely understood, it is clear that their use can have a very positive effect on the final performance. Furthermore, the use of these pastes could be particularly interesting especially in double layer devices. In fact, in case the transparency of the device is not a requirement of primary importance, the use of these pastes allows us to drastically reduce the amount of dye per unit area, thus reducing costs and allowing us to also use the high-performance dyes whose synthesis may be long and costly.

Experimental section

GENERAL INFORMATION

NMR spectra were recorded with a Bruker AMX-500 spectrometer operating at 500.13 MHz (^1H) and 125.77 MHz (^{13}C). Coupling constants are given in Hz. Absorption spectra were recorded with a V-570 Jasco spectrophotometer. Infrared spectra (IR) were recorded with an ATR-FTIR Perkin–Elmer Spectrum100 spectrometer. Flash chromatography was performed with Merck grade 9385 silica gel 230–400 mesh (60 Å). Reactions performed under inert atmosphere were done in oven-dried glassware and a nitrogen atmosphere was generated with Schlenk technique. Conversion was monitored by thin-layer chromatography by using UV light (254 and 365 nm) as a visualizing agent. All reagents were obtained from commercial suppliers at the highest purity grade and used without further purification. Anhydrous solvents were purchased from Sigma-Aldrich and used without further purification. Extracts were dried with Na_2SO_4 and filtered before removal of the solvent by evaporation.

FTO-coated glass plates (2.2 mm thick; sheet resistance ~ 7 ohm per square; Solaronix), Dyesol 18NR-AO active opaque TiO_2 blend of active 20 nm anatase particles and up to 450 nm anatase scatter particles, Solaronix T/SP active 20-nm transparent TiO_2 paste, light scattering TiO_2 paste with particles > 100 nm Solaronix R/SP and N719 (Sigma-Aldrich) have been purchased from commercial.

ELECTROCHEMICAL CHARACTERIZATION

Pulsed Voltammetry (DPV) and Cyclic Voltammetry (CV) were carried out at scan rate of 20 and 50 mV/s, respectively, using a PARSTA2273 potentiostat in a two compartments, three electrode electrochemical cell in a glove box filled with N_2 ($[\text{O}_2]$ and $[\text{H}_2\text{O}] \leq 0.1$ ppm). The working, counter, and the pseudo-reference electrodes were a glassy carbon pin, a Pt flag and an Ag/AgCl wire, respectively. The working electrodes discs were well polished with alumina 0.1 μm suspension,

sonicated for 15 min in deionized water, washed with 2-propanol, and cycled for 50 times in 0.5 M H₂SO₄ before use. The Ag/AgCl pseudo-reference electrode was calibrated, by adding ferrocene (10⁻³ M) to the test solution after each measurement.

Oxidation potential values were determined using DPV traces by following the reference methods reported in the literature.¹²⁰ For mono-electronic well defined current wave, the potentials were calculated by the peak position. In the presence of overlapping peaks due to molecular additional oxidations potential values were calculated using the current onsets of the oxidation processes for both the standard (ferrocene) and the molecules.

DYE LOADING

The amount of adsorbed dye has been measured for each sample by desorbing the dye, after the photovoltaic investigation on the dye-coated films, using a 0.1 M solution of NaOH in ethanol–H₂O (1:1) and by measuring its UV-Vis spectrum in a known volume of the solution. Comparison with the spectra of freshly prepared solutions of the dye in the same solvent, at known concentrations, as used to determine the amounts of desorbed dye.

GENERAL PROCEDURE FOR THE PREPARATION OF THE TiO₂ PASTES

The preparation of TiO₂ pastes roots in the optimization of published procedures.^{118,121} In this way a dense, viscous paste is prepared that facilitate the deposition through the doctor blade or screen printing technique. The preparation procedure is as follows: 1. Ethyl Cellulose powders are separately dissolved in EtOH to prepare the desired solutions (#46070, #46080 10% m/m in EtOH, respectively); 2. A dispersion of Terpeneol and TiO₂ nanoparticles (1g of TiO₂ every 4.056g of Terpeneol) is prepared to which the Ethyl Cellulose solutions (2.813g of #46070 and 2.188g of #46080, respectively) are added during vigorous

magnetic stirring; 3. EtOH (5g) is slowly added and the solution is alternatively stirred and sonicated to facilitate homogenization (3 times).

The excess ethanol is eventually eliminated in a rotary evaporator to give the final product, which is then conserved at -18°C to slow phase separation. Product are stable for several months (>7 months).

DSSCs FABRICATION PROCEDURE

DSSCs have been prepared adapting a procedure reported in the literature.¹²¹ In order to exclude metal contamination all of the containers were in glass or Teflon and were treated with EtOH and 10% HCl prior to use. Plastic spatulas and tweezers have been used throughout the procedure. FTO glass plates were cleaned in a detergent solution for 15 min using an ultrasonic bath, rinsed with pure water and EtOH. After treatment in a UV- O_3 system for 18 min, the FTO plates were treated with a freshly prepared 40 mM aqueous solution of TiCl_4 for 30 min at 70°C and then rinsed with water and EtOH. A transparent layer of 0.20 cm^2 was screen-printed using the proper active TiO_2 paste (*i.e.* Solaronix T/SP, Dyesol 18NR-AO, C-doped- TiO_2). In case of double layer device, the coated transparent film was dried at 125°C for 6 min and then another layer was screen-printed by using a light scattering TiO_2 paste with particles $> 100\text{ nm}$ (Solaronix R-SP). The coated films were thermally treated at 125°C for 6 min, 325°C for 10 min, 450°C for 15 min, and 500°C for 15 min. The heating ramp rate was $5 - 10^{\circ}\text{C}/\text{min}$. The sintered layer was treated again with 40 mM aqueous TiCl_4 (70°C for 30 min), rinsed with EtOH and heated at 500°C for 30 min. After cooling down to 80°C the TiO_2 coated plate was immersed into a 0.5 mM solution of the dye for 20 h at room temperature in the dark.

Counter electrodes were prepared according to the following procedure: a 1-mm hole was made in a FTO plate, using diamond drill bits. The electrodes were then cleaned with a detergent solution for 15 min using an ultrasonic bath, 10% HCl, and finally acetone for 15 min using an ultrasonic bath. After thermal treatment at

500 °C for 30 min, a 15 μL of a 5×10^{-3} M solution of H_2PtCl_6 in EtOH was added and the thermal treatment at 500 °C for 30 min repeated. The dye adsorbed TiO_2 electrode and Pt-counter electrode were assembled into a sealed sandwich-type cell by heating with a hot-melt ionomer-class resin (Surlyn 30- μm thickness) as a spacer between the electrodes. A drop of the proper electrolyte solution was added to the hole and introduced inside the cell by vacuum backfilling. Finally, the hole was sealed with a sheet of Surlyn and a cover glass. A reflective foil at the back side of the counter electrode was taped to reflect unabsorbed light back to the photoanode.

DSSCs CHARACTERIZATION

The thickness of the layers was measured by means of a VEECO Dektak 8 Stylus Profiler. Photovoltaic measurements of DSSCs were carried out with an antireflective layer and with or without black mask on top of the photoanode of 0.38 cm^2 surface area under a 500 W Xenon light source. The power of the simulated light was calibrated to AM 1.5 (100 mW cm^{-2}) using a reference Si cell photodiode equipped with an IR-cutoff filter (KG-5) to reduce the mismatch in the region of 350-750 nm between the simulated light and the AM 1.5 spectrum. Values were recorded after 3 and 24 h, 3 and 6 days of ageing in the dark. $I-V$ curves were obtained by applying an external bias to the cell and measuring the generated photocurrent with a Keithley digital source meter. IPCE were recorded as a function of excitation wavelength by using a monochromator with single grating in Czerny-Turner optical design, in AC mode with a chopping frequency of 1 Hz and a bias of blue light (0.3 sun). Absorption spectra were recorded on a V-570 Jasco spectrophotometer.

Electrochemical Impedance Spectroscopy (EIS) measurements were performed using a EG&G 2263 potentiostat-galvanostat. The voltage amplitude was 15 mV at open circuit voltage (OCV) under 1 Sun and the frequency was scanned from 1 to 5×10^4 Hz. Data were fitted via a non-linear least square procedure using a simple

equivalent circuit model proposed by Fabregas et al¹²² for a DSSC at OCV under illumination to separate the contribute of the different interfaces to the total cell impedance. In particular, the model includes the charge transfer resistance ($R_{ct,Pt}$) and the double layer capacitance ($C_{dl,Pt}$) of the Pt/interface as well as the recombination resistance ($R_{rec,Pt}$) and the the double layer capacitance ($C_{TiO_2,Pt}$) of the photoanode/electrolyte interface. The electrons time life in the TiO_2 (τ) was also calculated.

SYNTHETIC PROCEDURES

This section reports experimental procedures for the synthesis of molecules prepared in this PhD work. Here are not presented the syntheses of the studied benzodithiophene-dyes, which instead are available in the literature,² and **PTZ1**.⁵⁴

General Procedure for Alkylation: Compound **22** (1 eq.) was dissolved in dry DMF under N_2 atmosphere, then the solution was cooled to $0^\circ C$ using an ice bath and NaH 60% (2 eq.) was slowly added. After stirring at $0^\circ C$ for 1 h, the appropriate tosylate or bromide (2 eq.) was added and the solution was stirred at rt for 4 h, when TLC revealed the complete conversion of the starting material. The reaction mixture was quenched with iced water, then extracted with Et_2O and the organic phase was dried with Na_2SO_4 and concentrated. The crude was purified using flash column chromatography on silica gel.

General Procedure A for Suzuki-Miyaura Cross-Coupling: Product **17** (1 eq.) and $Pd(dppf)Cl_2 \cdot CH_2Cl_2$ (10 % eq.) were dissolved in dimethoxyethane (0.1 M) and stirred for 15 minutes under nitrogen atmosphere. Then boronic acid/ester derivative (2.4 eq.) and K_2CO_3 (10 eq.) were added as suspension in methanol (0.1 M). The reaction was performed with microwave irradiation ($100^\circ C$, 200 W, 90 minutes) and then quenched by pouring into a saturated solution of NH_4Cl (50 mL). Filtration on Celite and extractions with organic solvent allowed to isolate the crude product, then purified through column chromatography on silica gel.

General Procedure B for Suzuki-Miyaura Cross-Coupling: Bromo-derivative (2.2 eq.) and Pd(dppf)Cl₂·CH₂Cl₂ (10 % eq.) were dissolved in dimethoxyethane (0.1 M) and stirred for 15 minutes under nitrogen atmosphere. Then product **20** (1 eq. of crude product) and K₂CO₃ (10 eq.) were added as suspension in methanol (0.1 M). The reaction was performed with microwave irradiation (100 °C, 200 W, 90 minutes) and then quenched by pouring into a saturated solution of NH₄Cl (50 mL). Filtration on Celite and extractions with organic solvent allowed to isolate the crude product, then purified through column chromatography on silica gel.

General Procedure C for Knoevenagel Condensation: Aldehyde precursor (1 eq.), cyanoacetic acid (10 eq.) and piperidine (10 eq. + catalytic) were dissolved in CHCl₃ (0.02 M) and warmed to reflux for 5 h. After having the solvent evaporated, a solution of HCl 1 M (~50 mL) was added and the mixture was left under magnetic stirring for 5 h at rt. The dark red solid that precipitated was filtered and washed with water (3x30 mL), PE (2x30 mL) and Et₂O (1x10 mL).

5,5'-(10-octyl-10*H*-phenothiazine-3,7-diyl)dithiophene-2-carbaldehyde (18). Product **18** was synthesized according to general procedure A for Suzuki-Miyaura cross-coupling, using product **17** (200 mg, 0.43 mmol), Pd(dppf)Cl₂·CH₂Cl₂ (35 mg, 0.043 mmol), (5-formylthiophen-2-yl)boronic acid (160 mg, 1.03 mmol), K₂CO₃ (600 mg, 4.3 mmol), DME (3 mL) and methanol (3 mL). Extractions were performed with AcOEt (3 x 50 mL) and a mixture of PE:AcOEt - 3:1 was used as eluent for purification. The desired product was isolated as a red solid (200 mg) with a 87% of yield. ¹H NMR (500 MHz, CDCl₃): δ 9.82 (s, 2H), 7.65 (d, *J* = 3.9 Hz, 2H), 7.38 (dd, *J* = 8.5, 2.0 Hz, 2H), 7.31 (d, *J* = 2.0 Hz, 2H), 7.24 (d, *J* = 3.9 Hz, 2H), 6.79 (d, *J* = 8.5 Hz, 2H), 3.79 (t, *J* = 7.2 Hz, 2H), 1.81 – 1.71 (m, 2H), 1.44 – 1.34 (m, 2H), 1.34 – 1.18 (m, 8H), 0.84 (t, *J* = 6.9 Hz, 3H). ¹³C NMR (126 MHz, CDCl₃): δ 182.5, 153.1, 145.1, 141.7, 137.6, 127.7, 125.7, 124.8, 124.4, 123.2, 115.6, 47.8, 31.7, 29.2, 29.1, 26.8, 26.6, 22.6, 14.1. Anal. Calcd for C₃₀H₂₉NO₂S₃: C, 67.76; H, 5.50; N, 2.63. Found: C, 67.69; H, 5.59; N, 2.72. IR: cm⁻¹ 2924, 2851, 1654, 1580, 1429, 1220, 1053, 792.

3,3'-(5,5'-(10-octyl-10*H*-phenothiazine-3,7-diyl)bis(thiophene-5,2-diyl))bis(2-cyanoacrylic acid) (PTZ2). PTZ2 was synthesized according to general procedure C for Knoevenagel condensation using product **18** (140 mg, 0.26 mmol), cyanoacetic acid (220 mg, 2.6 mmol), piperidine (270 mg, 3.16 mmol) and CHCl₃ (5 mL). A dark red solid (150 mg) has been isolated as the product with 87 % of yield. ¹H NMR (500 MHz, DMSO): δ 8.48 (s, 2H), 8.00 (d, *J* = 4.2 Hz, 2H), 7.72 (d, *J* = 4.0 Hz, 2H), 7.64 – 7.56 (m, 4H), 7.14 (d, *J* = 8.4 Hz, 2H), 3.95 (t, *J* = 6.7 Hz, 2H), 1.76 – 1.62 (m, 2H), 1.45 – 1.37 (m, 2H), 1.34 – 1.16 (m, 8H), 0.82 (t, *J* = 6.7 Hz, 3H). ¹³C NMR (126 MHz, DMSO): δ 164.1, 152.3, 147.0, 145.2, 142.0, 134.4, 127.6, 126.6, 125.0, 124.9, 124.0, 117.1, 117.0, 98.4, 63.3, 44.2, 31.5, 29.1, 28.9, 22.7, 22.5, 14.4. Anal. Calcd C₃₆H₃₁N₃O₄S₃: C, 64.94; H, 4.69; N, 6.31. Found: C, 64.71; H, 5.13; N, 6.26. IR: cm⁻¹ 2921, 2846, 2218, 1678, 1559, 1479, 1393, 1355, 1250, 1212, 1061, 788.

10-octyl-3,7-di(thieno[3,2-*b*]thiophen-2-yl)-10*H*-phenothiazine (19a). Product **19a** was synthesized according to general procedure A for Suzuki-Miyaura cross-coupling using product **17** (500 mg, 1.07 mmol), Pd(dppf)Cl₂·CH₂Cl₂ (90 mg, 0.107 mmol), 4,4,5,5-tetramethyl-2-(thieno(3,2-*b*)thiophen-2-yl)-1,3,2-dioxaborolane (660 mg, 2.46 mmol), K₂CO₃ (1.50 g, 10.7 mmol), DME (7 mL) and methanol (7 mL). Extractions with AcOEt and purification with PE:DCM - 8:1 as eluent gave product **19a** as a yellow solid with a 84 % yield (530 mg). ¹H NMR (500 MHz, CDCl₃): δ 7.39 – 7.34 (m, 6H), 7.33 (d, *J* = 5.2 Hz, 2H), 7.23 (d, *J* = 5.2 Hz, 2H), 6.81 (d, *J* = 9.1 Hz, 2H), 3.81 (t, *J* = 7.2 Hz, 2H), 1.85 – 1.76 (m, 2H), 1.48 – 1.39 (m, 2H), 1.38 – 1.21 (m, 8H), 0.90 (t, *J* = 6.9 Hz, 3H). ¹³C NMR (126 MHz, CDCl₃): δ 145.3, 144.2, 140.1, 138.0, 129.4, 126.5, 124.9, 124.6, 124.5, 119.6, 115.5, 114.4, 47.6, 31.8, 29.3, 29.2, 26.9, 26.8, 22.7, 14.2. Anal. Calcd for C₃₂H₂₉NS₃: C, 65.37; H, 4.97; N, 2.38. Found: C, 65.35; H, 4.83; N, 2.54. IR: cm⁻¹ 2923, 2849, 1467, 1451, 1329, 1243, 1155, 807.

5,5'-(10-octyl-10*H*-phenothiazine-3,7-diyl)dithieno[3,2-*b*]thiophene-2-carbaldehyde (19b). Distilled POCl₃ (250 mg, 1.63 mmol) was added dropwise to

DMF (120 mg, 1.63 mmol) at -15 °C under N₂ atmosphere; at the end of the addition a white solid formed, that, after 60 minutes, was dissolved in DMF (15 mL). Product **19a** (320 mg, 0.54 mmol) was added and the mixture warmed at 80 °C for 8 h. Then a saturated solution of NaOAc (30 mL) was added dropwise and the mixture was extracted with DCM (3 x 50 mL), the organic phases were combined and dried. Purification through column chromatography on silica gel, with PE:AcOEt - 3:1 as eluent, gave the product **19b** as orange solid with a 65 % yield (225 mg, 0.35 mmol). ¹H NMR (500 MHz, CDCl₃): δ 9.93 (s, 2H), 7.88 (s, 2H), 7.44 – 7.39 (m, 4H), 7.37 (d, *J* = 2.1 Hz, 2H), 6.87 (d, *J* = 8.5 Hz, 2H), 3.87 (t, *J* = 7.2 Hz, 2H), 1.88 – 1.79 (m, 2H), 1.50 – 1.42 (m, 2H), 1.37 – 1.22 (m, 8H), 0.87 (t, *J* = 6.9 Hz, 3H). ¹³C NMR (126 MHz, CDCl₃): δ 183.0, 151.8, 146.9, 145.0, 144.3, 137.7, 129.1, 128.5, 125.5, 124.8, 124.6, 115.7, 114.9, 47.8, 31.7, 29.2, 29.2, 26.8, 26.7, 22.6, 14.1. Anal. Calcd. For C₃₄H₂₉NO₂S₅: C, 63.42; H, 4.54; N, 2.18. Found: C, 63.41; H, 4.50; N, 1.83. IR: cm⁻¹ 2875, 1565, 1498, 1452, 1351, 1201, 1100, 1027, 920, 854, 729.

3,3'-(5,5'-(10-octyl-10*H*-phenothiazine-3,7-diyl)bis(thieno[3,2-*b*]thiophene-5,2-diyl))bis(2-cyanoacrylic acid) (PTZ3). **PTZ3** was synthesized according to general procedure C for Knoevenagel condensation using product **19b** (200 mg, 0.31 mmol), cyanoacetic acid (270 mg, 3.10 mmol), piperidine (320 mg, 3.70 mmol) and CHCl₃ (10 mL). A dark red solid (200 mg) has been isolated as the product with a 83 % of yield. ¹H NMR (500 MHz, DMSO): δ 8.55 (s, 2H), 8.29 (s, 2H), 7.96 (s, 2H), 7.63 – 7.44 (m, 4H), 7.10 (d, *J* = 8.4 Hz, 2H), 4.05 – 3.72 (m, 2H), 1.78 – 1.59 (m, 2H), 1.50 – 1.32 (m, 2H), 1.32 – 1.10 (m, 8H), 0.82 (t, *J* = 9.7 Hz, 3H). ¹³C NMR (126 MHz, DMSO): δ 164.2, 151.6, 147.9, 147.8, 144.8, 137.9, 137.1, 132.8, 128.4, 126.1, 124.5, 123.8, 117.0, 116.8, 116.5, 98.0, 63.3, 31.6, 29.1, 28.9, 26.5, 22.5, 14.4. Anal. Calcd. For C₄₀H₃₁N₃O₄S₅: C, 61.75; H, 4.02; N, 5.40. Found: C, 61.59; H, 4.29; N, 5.81. IR: cm⁻¹ 2920, 2850, 2216, 1678, 1565, 1454, 1396, 1236, 1158, 1132, 796.

10-octyl-3,7-bis(4,4,5,5-tetramethyl-1,3,2-dioxaborolan-2-yl)-10H-phenothiazine (20). Product **17** (1.00 g, 2.14 mmol) was dissolved in THF (30 mL) under inert atmosphere and the solution cooled down to -78 °C. *n*-BuLi (1.6 M solution in hexane, 3.4 mL, 5.36 mmol) was then added dropwise and the mixture was left under magnetic stirring for 60 min. Then 2-isopropoxy-4,4,5,5-tetramethyl-1,3,2-dioxaborolane (1.00 g, 5.36 mmol) was added at -78 °C and the mixture was left under magnetic stirring for 48 h at rt. The quench was performed by pouring into 50 mL of a saturated solution of NH₄Cl and extractions with Et₂O were performed, followed by anhydriification. The crude product was a sticky liquid that was used for cross-coupling step without any further purification. ¹H NMR (500 MHz, CDCl₃): δ 7.55 (dd, *J* = 8.1, 1.3 Hz, 2H), 7.51 (d, *J* = 1.3 Hz, 2H), 6.80 (d, *J* = 8.2 Hz, 2H), 3.84 (t, *J* = 7.2 Hz, 2H), 1.81 – 1.73 (m, 2H), 1.42 – 1.35 (m, 2H), 1.31 (s, 24H), 1.28 – 1.19 (m, 8H), 0.88 (t, *J* = 7.2 Hz, 3H).

5',5'''-(10-octyl-10H-phenothiazine-3,7-diyl)bis((2,2'-bithiophene)-5-carbaldehyde) (21a). Product **21a** was synthesized according to general procedure B for Suzuki-Miyaura cross-coupling using product **20** (115 mg, 0.20 mmol), Pd(dppf)Cl₂·CH₂Cl₂ (17 mg, 0.020 mmol), 5'-bromo-(2,2'-bithiophene)-5-carbaldehyde (120 mg, 0.44 mmol), K₂CO₃ (280mg, 2.0 mmol), DME (3 mL) and methanol (3 mL). Extractions with AcOEt and purification with DCM as eluent, gave product **21a** as an orange solid with a 64 % yield 90 mg). ¹H NMR (500 MHz, CDCl₃): δ 9.86 (s, 2H), 7.67 (d, *J* = 4.0 Hz, 2H), 7.39 (dd, *J* = 8.4, 2.2 Hz, 2H), 7.36 (d, *J* = 2.1 Hz, 2H), 7.31 (d, *J* = 3.8 Hz, 2H), 7.25 (d, *J* = 3.9 Hz, 2H), 7.17 (d, *J* = 3.8 Hz, 2H), 6.86 (d, *J* = 8.5 Hz, 2H), 3.87 (t, *J* = 7.2 Hz, 2H), 1.93 – 1.73 (m, 2H), 1.48 – 1.40 (m, 2H), 1.40 – 1.17 (m, 8H), 0.87 (t, *J* = 6.9 Hz, 3H). ¹³C NMR (126 MHz, CDCl₃): δ 182.4, 147.2, 145.1, 144.5, 141.5, 137.3, 134.4, 128.2, 127.2, 125.0, 124.7, 124.5, 123.8, 123.4, 115.6, 47.8, 31.7, 29.2, 26.9, 26.8, 22.6, 14.0. Anal. Calcd. For C₃₈H₃₃NO₂S₅: C, 65.58; H, 4.78; N, 2.01. Found: C, 65.38; H, 4.51; N, 1.28. IR: cm⁻¹ 2920, 2851, 1649, 1442, 1367, 1223, 1047, 791.

3,3'-(5',5'''-(10-octyl-10*H*-phenothiazine-3,7-diyl)bis([2,2'-bithiophene]-5',5-diyl))bis(2-cyanoacrylic acid) (PTZ4). PTZ4 was synthesized according to general procedure C for Knoevenagel condensation using product **21a** (60 mg, 0.086 mmol), cyanoacetic acid (75 mg, 0.86 mmol), piperidine (100 mg, 1.04 mmol) and CHCl₃ (3 mL). A dark red solid (60 mg) has been isolated as the product with a 86 % of yield. ¹H NMR (500 MHz, DMSO): δ 8.46 (s, 2H), 7.97 (d, *J* = 4.1 Hz, 2H), 7.61 (d, *J* = 3.9 Hz, 2H), 7.58 (d, *J* = 3.9 Hz, 2H), 7.57 – 7.50 (m, 6H), 7.06 (d, *J* = 8.3 Hz, 2H), 3.92 (t, *J* = 6.5 Hz, 2H), 1.75 – 1.60 (m, 2H), 1.45 – 1.35 (m, 2H), 1.33 – 1.06 (m, 8H), 0.82 (t, *J* = 6.6 Hz, 3H). ¹³C NMR (126 MHz, CDCl₃): δ 164.9, 147.3, 147.2, 146.8, 145.7, 145.3, 142.6, 135.3, 134.7, 129.7, 128.8, 126.5, 126.1, 125.1, 124.9, 118.1, 117.6, 99.9, 32.4, 30.0, 29.8, 27.4, 27.3, 23.6, 23.4, 15.3. Anal. Calcd. For 6C₃₈H₃₃NO₂S₅·H₂O: C, 63.41; H, 4.64; N, 5.04. Found: C, 62.81; H, 4.87; N, 5.35. IR: cm⁻¹ 2925, 2215, 1686, 1570, 1400, 1254, 1207, 1155, 1052, 788.

5-bromo-3,4-dibutoxythiophene-2-carbaldehyde. 3,4-dibutoxythiophene (1.25 g, 5.47 mmol) was solubilized in dry THF (30 mL) under nitrogen atmosphere. The mixture was cooled to -78 °C and *n*-BuLi (3.76 mL, 6.02 mmol) was added dropwise. After having stirred the mixture for 60 min, DMF (480 mg, 6.57 mmol) was added and the mixture was stirred at rt for 15 h. Then the solvent was evaporated and the mixture was quenched with 50 mL of a saturated solution of NH₄Cl, extracted with Et₂O (3x50 mL), and dried. The isolated product (850 mg, 3.32 mmol) was solubilized in DMF (7 mL), temperature was lowered to -5 °C and NBS (710 mg, 3.97 mmol) was added dropwise as DMF solution (7 mL). The color changed from yellow to brown-green. After 7 h of stirring at rt, 50 mL of water were added and Et₂O extractions performed (3x50 mL). Anhydrification and purification through column chromatography (mixture of PE:AcOEt – 10:1 as eluent) allowed isolating the desired product (1.06 g, 3.16 mmol) as yellow oil with an overall yield of 58 %. The product has been used without any further purification for the following step. ¹H NMR (500 MHz, CDCl₃): δ 9.85 (s, 1H), 4.27 (t, *J* = 6.5 Hz, 2H), 4.03 (t, *J* = 6.5 Hz, 2H), 1.78 – 1.67 (m, 4H), 1.52 – 1.42

(m, 4H), 1.00 – 0.90 (m, 6H). ^{13}C NMR (126 MHz, CDCl_3): δ 180.0, 155.7, 147.5, 124.3, 112.1, 74.5, 73.9, 31.9, 31.8, 19.0, 18.9, 13.7, 13.6.

5,5'-(10-octyl-10*H*-phenothiazine-3,7-diyl)bis(3,4-dibutoxythiophene-2-carbaldehyde) (21b). Product **21b** was synthesized according to general procedure B for Suzuki-Miyaura cross-coupling using product **20** (200 mg, 0.35 mmol), $\text{Pd}(\text{dppf})\text{Cl}_2 \cdot \text{CH}_2\text{Cl}_2$ (30 mg, 0.035 mmol), 5-bromo-3,4-dibutoxythiophene-2-carbaldehyde (200 mg, 0.71 mmol), K_2CO_3 (500mg, 3.5 mmol), DME (5 mL) and methanol (5 mL). Purification with PE:AcOEt - 10:1 as eluent gave product **21b** as an orange solid with a 45 % yield (130 mg). ^1H NMR (500 MHz, CDCl_3): δ 9.98 (s, 2H), 7.61 (d, $J = 2.1$ Hz, 2H), 7.53 (dd, $J = 8.6, 2.1$ Hz, 2H), 6.85 (d, $J = 8.6$ Hz, 2H), 4.34 (t, $J = 6.5$ Hz, 4H), 3.91 (t, $J = 6.5$ Hz, 4H), 3.87 (t, $J = 7.2, 2\text{H}$), 1.87 – 1.76 (m, 6H), 1.72 – 1.63 (m, 4H), 1.57 – 1.41 (m, 10H), 1.38 – 1.20 (m, 8H), 1.00 (t, $J = 7.4$ Hz, 6H), 0.94 (t, $J = 7.4$ Hz, 6H), 0.87 (t, $J = 6.9$ Hz, 3H). ^{13}C NMR (126 MHz, CDCl_3): δ 180.7, 157.4, 144.9, 144.7, 136.3, 126.7, 126.4, 125.9, 124.3, 121.3, 115.3, 74.5, 73.3, 47.8, 32.1, 32.0, 31.7, 29.2, 29.1, 26.8, 26.7, 22.6, 19.2, 19.0, 14.0, 13.8, 13.8. Anal. Calcd. For $\text{C}_{46}\text{H}_{61}\text{NO}_6\text{S}_3$: C, 67.36; H, 7.50; N, 1.71. Found: C, 67.69; H, 7.23; N, 2.00. IR: cm^{-1} 2956, 2927, 2871, 1647, 1578, 1459, 1417, 1401, 1350, 1254, 1105, 1062, 1029, 811.

3,3'-(5,5'-(10-octyl-10*H*-phenothiazine-3,7-diyl)bis(3,4-dibutoxythiophene-5,2-diyl))bis(2-cyanoacrylic acid) (PTZ5). **PTZ5** was synthesized according to general procedure C for Knoevenagel condensation using product **21b** (200 mg, 0.23 mmol), cyanoacetic acid (200 mg, 2.32 mmol), piperidine (240 mg, 2.79 mmol) and CHCl_3 (10 mL). A dark red solid (200 mg) has been isolated as the product with a 90 % of yield. ^1H NMR (500 MHz, DMSO): δ 8.26 (s, 2H), 7.59 – 7.47 (m, 4H), 7.16 – 7.02 (m, 2H), 4.28 (t, $J = 6.4$ Hz, 6H), 3.95 – 3.85 (m, 8H), 1.78 – 1.67 (m, 6H), 1.67 – 1.55 (m, 4H), 1.52 – 1.44 (m, 4H), 1.44 – 1.35 (m, 6H), 1.32 – 1.15 (m, 8H), 0.95 (t, $J = 7.4$ Hz, 6H), 0.87 (t, $J = 7.4$ Hz, 6H), 0.82 (t, $J = 6.8$ Hz, 3H). ^{13}C NMR (126 MHz, DMSO): δ 164.2, 157.1, 145.4, 144.9, 141.4, 134.6, 127.0, 126.2, 125.5, 123.5, 117.1, 116.8, 116.0, 96.2, 74.4, 73.4, 31.9, 31.5, 29.0, 28.9, 26.4,

22.5, 19.2, 19.0, 14.4, 14.0. Anal. Calcd. For $C_{52}H_{63}N_3O_8S_3$: C, 65.45; H, 6.65; N, 4.40. Found: C, 65.85; H, 6.06; N, 4.96. IR: cm^{-1} 2927, 2871, 2214, 1683, 1555, 1457, 1394, 1362, 1230, 1172, 1027, 794.

7,7'-(10-octyl-10H-phenothiazine-3,7-diyl)bis(2,3-dihydrothieno[3,4-b][1,4]dioxine-5-carbaldehyde) (21c). Product **21c** was synthesized according to general procedure B for Suzuki-Miyaura cross-coupling using product **20** (400 mg, 0.71 mmol), $Pd(dppf)Cl_2 \cdot CH_2Cl_2$ (58 mg, 0.071 mmol), 7-bromo-2,3-dihydrothieno[3,4-b][1,4]dioxine-5-carbaldehyde (400 mg, 1.56 mmol), K_2CO_3 (1.00 g, 7.10 mmol), DME (7 mL) and methanol (7 mL). Purification with DCM:Et₂O – 100:1 as eluent gave product **5c** as an orange solid with a 40 % yield (185 mg). ¹H NMR (500 MHz, CDCl₃): δ 9.90 (s, 2H), 7.57 (d, *J* = 2.1 Hz, 2H), 7.52 (dd, *J* = 8.6, 2.2 Hz, 2H), 6.82 (d, *J* = 8.6 Hz, 2H), 4.44 – 4.35 (m, 8H), 3.83 (t, *J* = 7.0 Hz, 2H), 1.80 – 1.75 (m, 2H), 1.47 – 1.06 (m, 10H), 0.86 (t, *J* = 6.5 Hz, 3H). ¹³C NMR (126 MHz, CDCl₃): δ 179.4, 149.0, 144.6, 137.2, 128.0, 126.4, 126.0, 125.5, 124.1, 115.3, 115.0, 65.1, 64.5, 47.7, 31.7, 29.2, 29.1, 26.8, 26.7, 22.6, 14.1. Anal. Calcd. For $C_{34}H_{33}NO_6S_3$: C, 63.04; H, 5.13; N, 2.16. Found: C, 63.12; H, 4.96; N, 2.40. IR: cm^{-1} 2926, 2851, 1638, 1438, 1357, 1254, 1217, 1080, 805.

3,3'-(7,7'-(10-octyl-10H-phenothiazine-3,7-diyl)bis(2,3-dihydrothieno[3,4-b][1,4]dioxine-7,5-diyl))bis(2-cyanoacrylic acid) (PTZ6). PTZ6 was synthesized according to general procedure C for Knoevenagel condensation using product **21c** (90 mg, 0.14 mmol), cyanoacetic acid (120 mg, 1.40 mmol), piperidine (140 mg, 1.67 mmol) and CHCl₃ (5 mL). A dark red solid (88 mg) has been isolated as the product with a 80 % of yield. ¹H NMR (500 MHz, DMSO): δ 8.14 (s, 2H), 7.48 (dd, *J* = 8.6, 1.7 Hz, 2H), 7.41 (d, *J* = 1.9 Hz, 2H), 6.97 (d, *J* = 8.8 Hz, 2H), 4.60 – 4.30 (m, 8H), 3.90 – 3.60 (m, 2H), 1.70 – 1.60 (m, 2H), 1.45 – 1.14 (m, 10H), 0.82 (t, *J* = 6.7 Hz, 3H). ¹³C NMR (126 MHz, DMSO): δ 164.5, 149.6, 144.2, 140.2, 138.2, 126.6, 126.2, 126.1, 124.9, 123.0, 117.5, 116.4, 108.8, 94.4, 66.1, 65.2, 47.4, 31.6, 29.1, 29.0, 26.5, 26.3, 22.5, 14.4. Anal. Calcd. For $C_{40}H_{35}N_3O_8S_3$: C, 61.44; H,

4.51; N, 5.37. Found: C, 61.48; H, 4.77; N, 5.47. IR: cm^{-1} 2924, 2210, 1676, 1561, 1545, 1438, 1396, 1356, 1225, 1069, 1024, 760.

3,7-dibromo-10-(2-(2-(2-methoxyethoxy)ethoxy)ethyl)-10H-phenothiazine

(23). Compound **23** was synthesized according to general procedure for alkylation using product **22** (0.20 g, 0.56 mmol), NaH 60% (0.13 g, 1.12 mmol) and TEG-OTs (0.35 g, 1.12 mmol) in 5 mL of dry DMF. Extraction with Et_2O and purification with petroleum ether/AcOEt 5:1 as eluent, gave product **23** as pale yellow oil in 80% yield (0.70 g). ^1H NMR (500 MHz, CDCl_3) δ 7.21 (dd, $J = 8.6, 2.2$ Hz, 2H), 7.17 (d, $J = 1.7$ Hz, 2H), 6.73 (d, $J = 8.7$ Hz, 2H), 3.99 (t, $J = 6.1$ Hz, 2H), 3.78 (t, $J = 6.1$ Hz, 2H), 3.67 – 3.57 (m, 6H), 3.55 – 3.48 (m, 2H), 3.35 (s, 3H). ^{13}C NMR (126 MHz, CDCl_3) δ 143.7, 130.2, 129.6, 126.0, 116.6, 115.0, 71.9, 70.7, 70.6 (x3), 68.1, 59.0, 47.9.

5,5'-(10-(2-(2-(2-methoxyethoxy)ethoxy)ethyl)-10H-phenothiazine-3,7-

diyl)bis(thiophene-2-carbaldehyde) (24). Compound **24** was synthesized according to general procedure A for Suzuki-Miyaura cross-coupling using product **23** (0.24 g, 0.48 mmol), $\text{Pd}(\text{dppf})\text{Cl}_2 \cdot \text{CH}_2\text{Cl}_2$ (0.04 g, 0.05 mmol), 5-formyl-2-thienylboronic acid (0.21 g, 1.15 mmol), K_2CO_3 (0.66 g, 4.80 mmol), DME (5 mL) and methanol (5 mL). Extractions with AcOEt and purification with petroleum ether/AcOEt 2:1 as eluent, gave product **24** as an orange solid in 75 % yield (0.19 g). ^1H NMR (500 MHz, DMSO-d_6) δ 9.76 (s, 2H), 7.60 (d, $J = 3.9$ Hz, 2H), 7.31 (dd, $J = 8.5, 2.1$ Hz, 2H), 7.22 (d, $J = 2.2$ Hz, 2H), 7.19 (d, $J = 3.9$ Hz, 2H), 6.81 (d, $J = 8.6$ Hz, 2H), 3.99 (t, $J = 6.0$ Hz, 2H), 3.78 (t, $J = 6.0$ Hz, 2H), 3.71 – 3.51 (m, 6H), 3.50 – 3.45 (m, 2H), 3.29 (s, 3H). ^{13}C NMR (126 MHz, DMSO-d_6) δ 182.4, 152.7, 144.6, 141.6, 137.5, 127.8, 125.7, 124.6, 123.9, 123.2, 115.5, 71.8, 70.7, 70.5, 70.4(x2), 67.9, 58.9, 47.9. HRMS (ESI) m/z : calcd. for $[\text{M}+\text{Na}]^+$ $\text{C}_{35}\text{H}_{29}\text{N}_3\text{NaO}_7\text{S}_3$: 588.0949; found 588.1081.

3,7-dibromo-10-(prop-2-yn-1-yl)-10H-phenothiazine (25). Compound **25** was synthesized according to general procedure for alkylation using product **22** (0.20 g, 0.56 mmol), NaH 60% (0.13 g, 1.12 mmol), propargyl bromide (0.04 g, 1.12 mmol) in 5 mL of dry DMF. Extraction with Et₂O and purification with petroleum ether/AcOEt 20:1 as eluent, gave product **25** as pale yellow solid in 77% yield (0.17 g). ¹H NMR (400 MHz, CDCl₃) δ 7.28 (dd, *J* = 8.6, 2.2 Hz, 2H), 7.22 (d, *J* = 2.2 Hz, 2H), 7.04 (d, *J* = 8.6 Hz, 2H), 4.43 (d, *J* = 2.3 Hz, 2H), 2.47 (t, *J* = 2.3 Hz, 1H). ¹³C NMR (101 MHz, CDCl₃) δ 143.1, 130.5, 129.5, 125.1, 116.1, 115.8, 78.2, 75.2, 38.8.

2*S*,4*R*,5*S*,6*S*)-2-(((4-((3,7-dibromo-10H-phenothiazin-10-yl)methyl)-1*H*-1,2,3-triazol-1-yl)methyl)-6-methoxytetrahydro-2*H*-pyran-3,4,5-triyl triacetate (**26**). Compound **26** was synthesized by mixing compound **25** (0.12 g, 0.30 mmol) and methyl 2,3,4-tri-*O*-acetyl-6-azido-6-deoxy- α -D-glucopyranoside (0.09 g, 0.27 mmol) in THF (6 mL), and adding a second solution of CuSO₄·5H₂O (0.08 g, 0.33 mmol) and sodium ascorbate (0.08 g, 0.41 mmol) in H₂O (2.5 mL), then the reaction mixture was stirred at rt in the dark for 4 h. TLC (petroleum ether/AcOEt 1:1) revealed the complete consumption of compound **25**, then the solvents were evaporated and the crude was dissolved in CH₂Cl₂ and washed with HCl 5% solution and brine. The crude was purified using flash chromatography (petroleum ether/AcOEt 8:2 then 4:6) affording compound **26** (0.19 g, 95%) as an oil. ¹H NMR (500 MHz, CDCl₃) δ 7.48 (s, 1H), 7.23 (d, *J* = 2.2 Hz, 2H), 7.15 (dd, *J* = 8.7, 2.3 Hz, 2H), 6.65 (d, *J* = 8.7 Hz, 2H), 5.42 (t, *J* = 10.0 Hz, 1H), 5.12 (s, 2H), 4.79 (d, *J* = 3.6 Hz, 1H), 4.67 – 4.58 (m, 2H), 4.51 (dd, *J* = 14.5, 2.1 Hz, 1H), 4.37 – 4.31 (m, 1H), 4.07 (td, *J* = 8.2, 4.1 Hz, 1H), 2.91 (s, 3H), 2.08 (s, 3H), 2.06 (s, 3H), 2.00 (s, 3H). ¹³C NMR (101 MHz, CDCl₃) δ 170.1, 169.9, 169.7, 144.1, 143.2, 130.2, 129.6, 125.7, 123.8, 116.6, 115.5, 96.5, 70.6, 69.5, 69.4, 67.6, 55.2, 50.8, 44.6, 20.7 (x3).

5,5'-(10-(((1-(((2*S*,4*R*,5*S*,6*S*)-3,4,5-trihydroxy-6-methoxytetrahydro-2*H*-pyran-2-yl)methyl)-1*H*-1,2,3-triazol-4-yl)methyl)-10H-phenothiazine-3,7-diyl)bis(thiophene-2-carbaldehyde) (**27**). Compound **27** was synthesized according to general procedure A for Suzuki-Miyaura cross-coupling using product **26** (0.10 g, 0.13

mmol), Pd(dppf)Cl₂·CH₂Cl₂ (0.01 g, 0.01 mmol), 5-formyl-2-thienylboronic acid (0.05 g, 0.31 mmol), K₂CO₃ (0.18 g, 1.35 mmol), DME (3 mL) and methanol (3 mL). Extraction with AcOEt and purification with AcOEt/*i*PrOH 10:1 as eluent, gave product 27 as an orange solid in 74% yield (0.07 g). ¹H NMR (500 MHz, DMSO-*d*₆) δ 9.88 (s, 2H), 8.01 (d, *J* = 3.8 Hz, 2H), 7.97 (s, 1H), 7.69 (d, *J* = 3.6 Hz, 2H), 7.61 (s, 2H), 7.53 (d, *J* = 8.5 Hz, 2H), 7.02 (d, *J* = 8.6 Hz, 2H), 5.33 (d, *J* = 5.8 Hz, 1H), 5.24 (s, 2H), 4.93 (d, *J* = 4.7 Hz, 1H), 4.77 (d, *J* = 6.5 Hz, 1H), 4.71 (d, *J* = 14.0 Hz, 1H), 4.46 – 4.29 (m, 2H), 3.61 (t, *J* = 9.2 Hz, 1H), 3.23 – 3.11 (m, 1H), 3.02 – 2.93 (m, 1H), 2.73 (s, 3H). ¹H NMR (500 MHz, DMSO-*d*₆ + D₂O) δ 9.83 (s, 2H), 7.96 (d, *J* = 3.8 Hz, 2H), 7.92 (s, 1H), 7.61 (d, *J* = 3.8 Hz, 2H), 7.55 (s, 2H), 7.49 (d, *J* = 8.2 Hz, 2H), 6.99 (d, *J* = 8.6 Hz, 2H), 5.20 (s, 2H), 4.68 (d, *J* = 13.4 Hz, 1H), 4.35 (d, *J* = 3.6 Hz, 2H), 3.56 (s, 1H), 3.32 (s, 1H), 3.15 (dd, *J* = 9.5, 3.6 Hz, 1H), 2.97 (s, 1H), 2.70 (d, *J* = 24.2 Hz, 3H). ¹³C NMR (126 MHz, DMSO-*d*₆) δ ¹³C NMR (126 MHz, DMSO) δ 184.1, 152.0, 144.5, 143.1, 141.8, 139.8, 127.9, 126.3, 125.1, 124.6, 123.1, 116.7, 100.1, 73.5, 72.2, 72.2, 71.0, 54.4, 51.6, 44.5. HRMS (ESI) *m/z*: calcd. for [M+H]⁺ C₃₂H₂₉N₄O₇S₃: 677.1198; found 677.1185; calcd. for [M+Na]⁺ C₃₂H₂₈N₄NaO₇S₃: 699.1018; found 699.1040.

3,3'-(5',5'''-(10-(2-(2-(2-methoxyethoxy)ethoxy)ethyl)-10*H*-phenothiazine-3,7-diyl)bis([2,2'-bithiophene]-5',5'-diyl))bis(2-cyanoacrylic acid) (PTZ-TEG). Compound PTZ-TEG was synthesized according to general for Knoevenagel condensation using product 24 (0.19 g, 0.34 mmol), cyanoacetic acid (0.29 g, 3.40 mmol), piperidine (0.34 g, 3.4 mmol) and CHCl₃ (6 mL). A dark red solid (0.22 g) has been isolated as the product in 92% yield. ¹H NMR (500 MHz, DMSO-*d*₆) δ 8.45 (s, 2H), 7.98 (d, *J* = 3.8 Hz, 2H), 7.71 (d, *J* = 3.8 Hz, 2H), 7.57 (m, 4H), 7.16 (d, *J* = 9.1 Hz, 2H), 4.13 (t, *J* = 5.3 Hz, 2H), 3.79 (t, *J* = 5.3 Hz, 2H), 3.66 – 3.43 (m, 6H), 3.43 – 3.29 (m, 2H), 3.20 (s, 3H). ¹³C NMR (126 MHz, DMSO-*d*₆) δ 164.2, 152.0, 146.0, 145.0, 141.0, 134.5, 127.7, 126.5, 125.0, 124.8, 123.8, 117.2, 116.9, 98.8, 71.7, 70.4, 70.2, 70.1, 67.8, 58.5, 44.1. HRMS (ESI) *m/z*: calcd. for [M+H]⁺

$C_{35}H_{30}N_3O_7S_3$: 700.1246; found 700.0552; calcd. for $[M+Na]^+$ $C_{35}H_{29}N_3NaO_7S_3$: 722.1065; found 722.0307. m.p.: 206-207 °C (deg)

5,5'-(10-((1-(((2S,4R,5S,6S)-3,4,5-trihydroxy-6-methoxytetrahydro-2H-pyran-2-yl)methyl)-1H-1,2,3-triazol-4-yl)methyl)-10H-phenothiazine-3,7-diyl)bis([2,2'-bithiophene]-5',5'-diyl))bis(2-cyanoacrylic acid) (PTZ-GLU). Compound PTZ-GLU was synthesized according to general for Knoevenagel condensation using product 27 (0.18 g, 0.27 mmol), cyanoacetic acid (0.11 g, 2.70 mmol), piperidine (0.22 g, 2.70 mmol) and $CHCl_3$ (5 mL). A dark red solid (0.19 g) has been isolated as the product in 90% yield. 1H NMR (500 MHz, DMSO- d_6) δ 8.47 (s, 2H), 7.99 (m, 3H), 7.71 (d, $J = 4.0$ Hz, 2H), 7.57 (d, $J = 2.1$ Hz, 2H), 7.50 (dd, $J = 8.5, 2.0$ Hz, 2H), 7.05 (d, $J = 8.7$ Hz, 2H), 5.24 (s, 2H), 4.71 (d, $J = 12.9$ Hz, 1H), 4.46 – 4.29 (m, 2H), 3.61 (t, $J = 9.5$ Hz, 1H), 3.36 (t, $J = 9.1$ Hz, 1H), 3.17 (dd, $J = 9.6, 3.6$ Hz, 1H), 2.98 (t, $J = 9.2$ Hz, 1H), 2.74 (s, 3H). ^{13}C NMR (126 MHz, DMSO- d_6) δ 164.1, 152.2, 147.0, 144.6, 143.0, 142.0, 134.4, 127.7, 126.3, 125.1, 124.6, 123.1, 117.0, 116.8, 100.1, 98.2, 73.5, 72.2, 72.1, 71.0, 54.4, 51.6, 44.4. HRMS (ESI) m/z : calcd. for $[M+H]^+$ $C_{38}H_{31}N_6O_9S_3$: 811.1315; found 811.0627; calcd. for $[M+Na]^+$ $C_{38}H_{30}N_6NaO_9S_3$: 833.1134; found 833.0417. m.p.: 283-284 °C (deg)

References

- (1) Vincent Van Gogh. (n.d.). BrainyQuote.com. Retrieved November 17, 2016, from BrainyQuote.com Web site: <https://www.brainyquote.com/quotes/quotes/v/vincentvan120866.html>
- (2) Baldoli, C.; Bertuolo, S.; Licandro, E.; Viglianti, L.; Mussini, P.; Marotta, G.; Salvatori, P.; De Angelis, F.; Manca, P.; Manfredi, N.; Abboto, A. "Benzodithiophene based organic dyes for DSSC: Effect of alkyl chain substitution on dye efficiency". *Dyes Pigm.* **2015**, *121*, 351-362, doi:<http://dx.doi.org/10.1016/j.dyepig.2015.04.028>.
- (3) Cecconi, B.; Manfredi, N.; Ruffo, R.; Montini, T.; Romero-Ocana, I.; Fornasiero, P.; Abboto, A. "Tuning Thiophene-Based Phenothiazines for Stable Photocatalytic Hydrogen Production". *ChemSusChem* **2015**, *8*, 4216-4228, doi:10.1002/cssc.201501040.
- (4) Manfredi, N.; Cecconi, B.; Calabrese, V.; Minotti, A.; Peri, F.; Ruffo, R.; Monai, M.; Romero-Ocana, I.; Montini, T.; Fornasiero, P.; Abboto, A. "Dye-sensitized photocatalytic hydrogen production: distinct activity in a glucose derivative of a phenothiazine dye". *Chem. Commun.* **2016**, *52*, 6977-6980, doi:10.1039/c6cc00390g.
- (5) Armaroli, N.; Balzani, V. "Towards an electricity-powered world". *Energy Environ. Sci.* **2011**, *4*, 3193-3222, doi:10.1039/c1ee01249e.
- (6) Nazeeruddin, M. K.; Zakeeruddin, S. M.; Humphry-Baker, R.; Jirousek, M.; Liska, P.; Vlachopoulos, N.; Shklover, V.; Fischer, C. H.; Gratzel, M. "Acid-base equilibria of (2,2'-bipyridyl-4,4'-dicarboxylic acid)ruthenium(II) complexes and the effect of protonation on charge-transfer sensitization of nanocrystalline titania". *Inorg. Chem.* **1999**, *38*, 6298-6305, doi:DOI 10.1021/ic990916a.
- (7) Abboto, A.; Sauvage, F.; Barolo, C.; De Angelis, F.; Fantacci, S.; Graetzel, M.; Manfredi, N.; Marinzi, C.; Nazeeruddin, M. K. "Panchromatic ruthenium sensitizer based on electron-rich heteroarylvinylene pi-conjugated quaterpyridine for dye-sensitized solar cells". *Dalton Transactions* **2011**, *40*, 234-242, doi:10.1039/c0dt01190h.
- (8) Hara, K.: Molecular Design of Sensitizers for Dye-Sensitized Solar Cells. In *Molecular Catalysts for Energy Conversion*; Okada, T., Kaneko, M., Eds.; Springer Berlin Heidelberg: Berlin, Heidelberg, 2009; pp 217-250.
- (9) Mishra, A.; Fischer, M. K.; Bauerle, P. "Metal-free organic dyes for dye-sensitized solar cells: from structure: property relationships to design rules". *Angew Chem Int Ed Engl* **2009**, *48*, 2474-2499, doi:10.1002/anie.200804709.

- (10) Manfredi, N.; Cecconi, B.; Abboto, A. "Multi-Branched Multi-Anchoring Metal-Free Dyes for Dye-Sensitized Solar Cells". *Eur. J. Org. Chem.* **2014**, 7069-7086, doi:10.1002/ejoc.201402422.
- (11) Al-Alwani, M. A. M.; Mohamad, A.; Ludin, N. A.; Kadhum, A. A. H.; Sopian, K. "Dye-sensitized solar cells: Development, structure, operation principles, electron kinetics, characterisation, synthesis materials and natural photosensitisers". *Renewable & Sustainable Energy Reviews* **2016**, *65*, 183-213, doi:10.1016/j.rser.2016.06.045.
- (12) Gong, J.; Sumathy, K.; Qiao, Q.; Zhou, Z. "Review on dye-sensitized solar cells (DSSCs): Advanced techniques and research trends". *Renewable and Sustainable Energy Reviews* **2017**, *68*, 234-246, doi:10.1016/j.rser.2016.09.097.
- (13) Liang, M.; Chen, J. "Arylamine organic dyes for dye-sensitized solar cells". *Chem. Soc. Rev.* **2013**, *42*, 3453-3488, doi:10.1039/C3CS35372A.
- (14) Ye, L.; Zhang, S.; Huo, L.; Zhang, M.; Hou, J. "Molecular design toward highly efficient photovoltaic polymers based on two-dimensional conjugated benzodithiophene". *Acc Chem Res* **2014**, *47*, 1595-1603, doi:10.1021/ar5000743.
- (15) Gao, P.; Tsao, H. N.; Gratzel, M.; Nazeeruddin, M. K. "Fine-tuning the electronic structure of organic dyes for dye-sensitized solar cells". *Org Lett* **2012**, *14*, 4330-4333, doi:10.1021/ol301730c.
- (16) Hao, X.; Liang, M.; Cheng, X.; Pian, X.; Sun, Z.; Xue, S. "Organic dyes incorporating the benzo[1,2-b:4,5-b']dithiophene moiety for efficient dye-sensitized solar cells". *Org Lett* **2011**, *13*, 5424-5427, doi:10.1021/ol201858b.
- (17) Lin, Y. Z.; Yeh, C. W.; Chou, P. T.; Watanabe, M.; Chang, Y. H.; Chang, Y. J.; Chow, T. J. "Benzo[1,2-b:4,5-b']dithiophene and benzo[1,2-b:4,5-b']difuran based organic dipolar compounds for sensitized solar cells". *Dyes Pigm.* **2014**, *109*, 81-89, doi:10.1016/j.dyepig.2014.04.043.
- (18) Longhi, E.; Bossi, A.; Di Carlo, G.; Maiorana, S.; De Angelis, F.; Salvatori, P.; Petrozza, A.; Binda, M.; Roiati, V.; Mussini, P. R.; Baldoli, C.; Licandro, E. "Metal-Free Benzodithiophene-Containing Organic Dyes for Dye-Sensitized Solar Cells". *Eur. J. Org. Chem.* **2013**, *2013*, 84-94, doi:10.1002/ejoc.201200958.
- (19) Koumura, N.; Wang, Z. S.; Mori, S.; Miyashita, M.; Suzuki, E.; Hara, K. "Alkyl-functionalized organic dyes for efficient molecular photovoltaics". *J Am Chem Soc* **2006**, *128*, 14256-14257, doi:10.1021/ja0645640.

- (20) Wang, X.; Guo, L.; Xia, P. F.; Zheng, F.; Wong, M. S.; Zhu, Z. "Dye-sensitized solar cells based on organic dyes with naphtho[2,1-b:3,4-b']dithiophene as the conjugated linker". *J. Mater. Chem. A* **2013**, *1*, 13328-13336, doi:10.1039/c3ta12901b.
- (21) Yu, Q. Y.; Liao, J. Y.; Zhou, S. M.; Shen, Y.; Liu, J. M.; Kuang, D. B.; Su, C. Y. "Effect of Hydrocarbon Chain Length of Disubstituted Triphenyl-amine-Based Organic Dyes on Dye-Sensitized Solar Cells". *J. Phys. Chem. C* **2011**, *115*, 22002-22008, doi:10.1021/jp2054519.
- (22) Faccini, M.; Balakrishnan, M.; Diemeer, M. B. J.; Hu, Z. P.; Clays, K.; Asselberghs, I.; Leinse, A.; Driessen, A.; Reinhoudt, D. N.; Verboom, W. "Enhanced poling efficiency in highly thermal and photostable nonlinear optical chromophores". *J. Mater. Chem.* **2008**, *18*, 2141-2149, doi:10.1039/b801728j.
- (23) Shen, P.; Liu, Y.; Huang, X.; Zhao, B.; Xiang, N.; Fei, J.; Liu, L.; Wang, X.; Huang, H.; Tan, S. "Efficient triphenylamine dyes for solar cells: Effects of alkyl-substituents and π -conjugated thiophene unit". *Dyes Pigm.* **2009**, *83*, 187-197, doi:10.1016/j.dyepig.2009.04.005.
- (24) Kim, B. G.; Chung, K.; Kim, J. "Molecular design principle of all-organic dyes for dye-sensitized solar cells". *Chemistry* **2013**, *19*, 5220-5230, doi:10.1002/chem.201204343.
- (25) Reichardt, C.; Welton, T.: *Solvents and Solvent Effects in Organic Chemistry, 4th Edition*, Wiley-VCH Verlag GmbH & Co. KGaA, Weinheim, Germany, 2010.
- (26) Pastore, M.; Mosconi, E.; De Angelis, F.; Gratzel, M. "A Computational Investigation of Organic Dyes for Dye-Sensitized Solar Cells: Benchmark, Strategies, and Open Issues". *J. Phys. Chem. C* **2010**, *114*, 7205-7212, doi:10.1021/jp100713r.
- (27) Bessho, T.; Zakeeruddin, S. M.; Yeh, C.-Y.; Diau, E. W.-G.; Grätzel, M. "Highly Efficient Mesoscopic Dye-Sensitized Solar Cells Based on Donor-Acceptor-Substituted Porphyrins". *Angew. Chem. Int. Ed.* **2010**, *49*, 6646-6649, doi:10.1002/anie.201002118.
- (28) Abboto, A.; Barolo, C.; Bellotto, L.; De Angelis, F.; Gratzel, M.; Manfredi, N.; Maranzi, C.; Fantacci, S.; Yum, J. H.; Nazeeruddin, M. K. "Electron-rich heteroaromatic conjugated bipyridine based ruthenium sensitizer for efficient dye-sensitized solar cells". *Chem. Commun.* **2008**, 5318-5320, doi:10.1039/b811378e.
- (29) Marinado, T.; Hahlin, M.; Jiang, X.; Quintana, M.; Johansson, E. M. J.; Gabrielsson, E.; Plogmaker, S.; Hagberg, D. P.; Boschloo, G.; Zakeeruddin, S. M.; Grätzel, M.; Siegbahn, H.; Sun, L.; Hagfeldt, A.; Rensmo, H. "Surface Molecular Quantification and Photoelectrochemical Characterization of Mixed Organic Dye and Coadsorbent Layers on

TiO₂ for Dye-Sensitized Solar Cells". *J. Phys. Chem. C* **2010**, *114*, 11903-11910, doi:10.1021/jp102381x.

(30) Ito, S.; Nazeeruddin, M. K.; Liska, P.; Comte, P.; Charvet, R.; Péchy, P.; Jirousek, M.; Kay, A.; Zakeeruddin, S. M.; Grätzel, M. "Photovoltaic characterization of dye-sensitized solar cells: effect of device masking on conversion efficiency". *Progr. Photovolt: Res. Appl.* **2006**, *14*, 589-601, doi:10.1002/pip.683.

(31) Lee, D. H.; Lee, M. J.; Song, H. M.; Song, B. J.; Seo, K. D.; Pastore, M.; Anselmi, C.; Fantacci, S.; De Angelis, F.; Nazeeruddin, M. K.; Grätzel, M.; Kim, H. K. "Organic dyes incorporating low-band-gap chromophores based on π -extended benzothiadiazole for dye-sensitized solar cells". *Dyes and Pigments* **2011**, *91*, 192-198, doi:10.1016/j.dyepig.2011.03.015.

(32) Yao, Z.; Zhang, M.; Wu, H.; Yang, L.; Li, R.; Wang, P. "Donor/Acceptor Indenoperylene Dye for Highly Efficient Organic Dye-Sensitized Solar Cells". *J. Am. Chem. Soc.* **2015**, *137*, 3799-3802, doi:10.1021/jacs.5b01537.

(33) Yang, X.; Yanagida, M.; Han, L. "Reliable evaluation of dye-sensitized solar cells". *Energy Environ. Sci.* **2012**.

(34) Kakiage, K.; Aoyama, Y.; Yano, T.; Oya, K.; Kyomen, T.; Hanaya, M. "Fabrication of a high-performance dye-sensitized solar cell with 12.8% conversion efficiency using organic silyl-anchor dyes". *Chemical Communications* **2015**, *51*, 6315-6317, doi:10.1039/C5CC00464K.

(35) Kakiage, K.; Aoyama, Y.; Yano, T.; Oya, K.; Fujisawa, J.-i.; Hanaya, M. "Highly-efficient dye-sensitized solar cells with collaborative sensitization by silyl-anchor and carboxy-anchor dyes". *Chem. Commun.* **2015**, *51*, 15894-15897, doi:10.1039/C5CC06759F.

(36) Abboto, A.; Leandri, V.; Manfredi, N.; De Angelis, F.; Pastore, M.; Yum, J. H.; Nazeeruddin, M. K.; Grätzel, M. "Bis-Donor-Bis-Acceptor Tribranched Organic Sensitizers for Dye-Sensitized Solar Cells". *Eur. J. Org. Chem.* **2011**, 6195-6205, doi:10.1002/Ejoc.201100821.

(37) Hong, Y.; Liao, J.-Y.; Fu, J.; Kuang, D.-B.; Meier, H.; Su, C.-Y.; Cao, D. "Performance of dye-sensitized solar cells based on novel sensitizers bearing asymmetric double D- π -A chains with arylamines as donors". *Dyes Pigm.* **2012**, *94*, 481-489, doi:10.1016/j.dyepig.2012.02.011.

(38) Abboto, A.; Manfredi, N.; Marinzi, C.; De Angelis, F.; Mosconi, E.; Yum, J. H.; Zhang, X. X.; Nazeeruddin, M. K.; Grätzel, M. "Di-branched di-anchoring organic

dyes for dye-sensitized solar cells". *Energy Environ. Sci.* **2009**, *2*, 1094-1101, doi:10.1039/b910654e.

(39) Ning, Z.; Tian, H. "Triarylamine: a promising core unit for efficient photovoltaic materials". *Chemical Communications* **2009**, 5483-5495, doi:10.1039/B908802D.

(40) Mahmood, A. "Triphenylamine based dyes for dye sensitized solar cells: A review". *Solar Energy* **2016**, *123*, 127-144, doi:<http://dx.doi.org/10.1016/j.solener.2015.11.015>.

(41) Zhang, G.; Bala, H.; Cheng, Y.; Shi, D.; Lv, X.; Yu, Q.; Wang, P. "High efficiency and stable dye-sensitized solar cells with an organic chromophore featuring a binary [small pi]-conjugated spacer". *Chemical Communications* **2009**.

(42) Ning, Z.; Fu, Y.; Tian, H. "Improvement of dye-sensitized solar cells: what we know and what we need to know". *Energy & Environmental Science* **2010**, *3*, 1170-1181, doi:Doi 10.1039/C003841e.

(43) Daeneke, T.; Mozer, A. J.; Kwon, T. H.; Duffy, N. W.; Holmes, A. B.; Bach, U.; Spiccia, L. "Dye regeneration and charge recombination in dye-sensitized solar cells with ferrocene derivatives as redox mediators". *Energy Environ. Sci.* **2012**, *5*, 7090-7099, doi:Doi 10.1039/C2ee21257a.

(44) Luo, Y.; Li, D.; Meng, Q. "Towards Optimization of Materials for Dye-Sensitized Solar Cells". *Adv Mater* **2009**, *21*, 4647-4651, doi:DOI 10.1002/adma.200901078.

(45) Listorti, A.; O'Regan, B.; Durrant, J. R. "Electron Transfer Dynamics in Dye-Sensitized Solar Cells". *Chem Mater* **2011**, *23*, 3381-3399, doi:Doi 10.1021/Cm200651e.

(46) Gregg, B. A.; Pichot, F.; Ferrere, S.; Fields, C. L. "Interfacial Recombination Processes in Dye-Sensitized Solar Cells and Methods To Passivate the Interfaces". *J. Phys. Chem. B* **2001**, *105*, 1422-1429, doi:10.1021/jp003000u.

(47) Fabregat-Santiago, F.; Garcia-Belmonte, G.; Mora-Sero, I.; Bisquert, J. "Characterization of nanostructured hybrid and organic solar cells by impedance spectroscopy". *Phys. Chem. Chem. Phys.* **2011**, *13*, 9083-9118, doi:10.1039/C0CP02249G.

(48) Bisquert, J.; Fabregat-Santiago, F.; Mora-Seró, I.; Garcia-Belmonte, G.; Giménez, S. "Electron Lifetime in Dye-Sensitized Solar Cells: Theory and Interpretation of Measurements". *J. Phys. Chem. C* **2009**, *113*, 17278-17290, doi:10.1021/jp9037649.

- (49) Halme, J.; Vahermaa, P.; Miettunen, K.; Lund, P. "Device Physics of Dye Solar Cells". *Adv. Mater.* **2010**, *22*, E210-E234, doi:10.1002/adma.201000726.
- (50) Hua, Y.; Chang, S.; Huang, D.; Zhou, X.; Zhu, X.; Zhao, J.; Chen, T.; Wong, W.-Y.; Wong, W.-K. "Significant Improvement of Dye-Sensitized Solar Cell Performance Using Simple Phenothiazine-Based Dyes". *Chem. Mater.* **2013**, *25*, 2146-2153, doi:10.1021/cm400800h.
- (51) Kim, S. H.; Kim, H. W.; Sakong, C.; Namgoong, J.; Park, S. W.; Ko, M. J.; Lee, C. H.; Lee, W. I.; Kim, J. P. "Effect of Five-Membered Heteroaromatic Linkers to the Performance of Phenothiazine-Based Dye-Sensitized Solar Cells". *Organic Letters* **2011**, *13*, 5784-5787, doi:10.1021/ol2023517.
- (52) Cheng, M.; Yang, X.; Zhao, J.; Chen, C.; Tan, Q.; Zhang, F.; Sun, L. "Efficient Organic Dye-Sensitized Solar Cells: Molecular Engineering of Donor-Acceptor-Acceptor cationic dyes". *ChemSusChem* **2013**, *6*, 2322-2329, doi:10.1002/cssc.201300481.
- (53) Hung, W.-I.; Liao, Y.-Y.; Hsu, C.-Y.; Chou, H.-H.; Lee, T.-H.; Kao, W.-S.; Lin, J. T. "High-Performance Dye-Sensitized Solar Cells Based on Phenothiazine Dyes Containing Double Anchors and Thiophene Spacers". *Chem. Asian J.* **2014**, *9*, 357-366, doi:10.1002/asia.201301228.
- (54) Lee, J.; Kwak, J.; Ko, K. C.; Park, J. H.; Ko, J. H.; Park, N.; Kim, E.; Ryu, D. H.; Ahn, T. K.; Lee, J. Y.; Son, S. U. "Phenothiazine-based organic dyes with two anchoring groups on TiO₂ for highly efficient visible light-induced water splitting". *Chem. Commun.* **2012**, *48*, 11431-11433, doi:10.1039/C2CC36501D.
- (55) Watanabe, M.; Hagiwara, H.; Iribe, A.; Ogata, Y.; Shiomi, K.; Staykov, A.; Ida, S.; Tanaka, K.; Ishihara, T. "Spacer effects in metal-free organic dyes for visible-light-driven dye-sensitized photocatalytic hydrogen production". *J. Mater. Chem. A* **2014**, *2*, 12952-12961, doi:10.1039/c4ta02720e.
- (56) Lin, R. Y. Y.; Wu, F. L.; Chang, C. H.; Chou, H. H.; Chuang, T. M.; Chu, T. C.; Hsu, C. Y.; Chen, P. W.; Ho, K. C.; Lo, Y. H.; Lin, J. T. "Y-shaped metal-free D-pi-(A)(2) sensitizers for high-performance dye-sensitized solar cells". *Journal of Materials Chemistry A* **2014**, *2*, 3092-3101, doi:Doi 10.1039/C3ta14404f.
- (57) Iqbal, Z.; Wu, W.-Q.; Zhang, H.; Han, L.; Fang, X.; Wang, L.; Kuang, D.-B.; Meier, H.; Cao, D. "Influence of spatial arrangements of π -spacer and acceptor of phenothiazine based dyes on the performance of dye-sensitized solar cells". *Org. Electron.* **2013**, *14*, 2662-2672, doi:<http://dx.doi.org/10.1016/j.orgel.2013.07.007>.

- (58) Albert, I. D. L.; Marks, T. J.; Ratner, M. A. "Large Molecular Hyperpolarizabilities. Quantitative Analysis of Aromaticity and Auxiliary Donor–Acceptor Effects". *J. Am. Chem. Soc.* **1997**, *119*, 6575-6582, doi:10.1021/ja962968u.
- (59) Albert, A.: *Heterocyclic Chemistry*; Oxford University Press: New York, 1968.
- (60) Kim, B.-G.; Chung, K.; Kim, J. "Molecular Design Principle of All-organic Dyes for Dye-Sensitized Solar Cells". *Chem. Eur. J.* **2013**, *19*, 5220-5230, doi:10.1002/chem.201204343.
- (61) Ahmad, S.; Guillen, E.; Kavan, L.; Gratzel, M.; Nazeeruddin, M. K. "Metal free sensitizer and catalyst for dye sensitized solar cells". *Energy Environ. Sci.* **2013**, *6*, 3439-3466, doi:10.1039/C3EE41888J.
- (62) Sailer, M.; Franz, A. W.; Müller, T. J. J. "Synthesis and Electronic Properties of Monodisperse Oligophenothiazines". *Chem. Eur. J.* **2008**, *14*, 2602-2614, doi:10.1002/chem.200701341.
- (63) de Meijere, A.; Diederich, F.: *Metal-Catalyzed Cross-Coupling Reactions*; Wiley-VCH Verlag GmbH, 2008.
- (64) Alesi, S.; Di Maria, F.; Melucci, M.; Macquarrie, D. J.; Luque, R.; Barbarella, G. "Microwave-assisted synthesis of oligothiophene semiconductors in aqueous media using silica and chitosan supported Pd catalysts". *Green Chemistry* **2008**, *10*, 517-523.
- (65) Kuo, C.-Y.; Huang, Y.-C.; Hsiow, C.-Y.; Yang, Y.-W.; Huang, C.-I.; Rwei, S.-P.; Wang, H.-L.; Wang, L. "Effect of Side-Chain Architecture on the Optical and Crystalline Properties of Two-Dimensional Polythiophenes". *Macromolecules* **2013**, *46*, 5985-5997, doi:10.1021/ma4007945.
- (66) Liu, W.-H.; Wu, I. C.; Lai, C.-H.; Lai, C.-H.; Chou, P.-T.; Li, Y.-T.; Chen, C.-L.; Hsu, Y.-Y.; Chi, Y. "Simple organic molecules bearing a 3,4-ethylenedioxythiophene linker for efficient dye-sensitized solar cells". *Chem. Commun.* **2008**, 5152-5154, doi:10.1039/B808535H.
- (67) Agarwal, N.; Hung, C. H.; Ravikanth, M. "Synthesis and crystal structures of 2,3,12,13-tetraalkoxy-21,23-dithiaporphyrins and 2,3-dialkoxy-21-monothiaporphyrins". *Tetrahedron* **2004**, *60*, 10671-10680, doi:<http://dx.doi.org/10.1016/j.tet.2004.09.008>.
- (68) Agarwal, N.; Mishra, S. P.; Kumar, A.; Hung, C. H.; Ravikanth, M. "Synthesis and crystal structure of 2,3,12,13-tetraalkoxy-21, 23-dithiaporphyrins". *Chem. Commun.* **2002**, 2642-2643, doi:10.1039/B208017F.

- (69) Tauc, J. "Optical properties and electronic structure of amorphous Ge and Si". *Mater. Res. Bull.* **1968**, *3*, 37-46, doi:[http://dx.doi.org/10.1016/0025-5408\(68\)90023-8](http://dx.doi.org/10.1016/0025-5408(68)90023-8).
- (70) Izutsu, K.: In *Electrochemistry in Nonaqueous Solutions*; Wiley-VCH Verlag GmbH & Co. KGaA, 2009.
- (71) Katritzky, A. R.; Rees, C. W.: *Comprehensive Heterocyclic Chemistry*; Pergamon: Oxford, 1984.
- (72) Using a potential value of 4.6 ± 0.2 eV for NHE vs. vacuum (J. O. M. Bockris, S. U. M. Khan, *Surface Electrochemistry – A Molecular Level Approach*, Kluwer Academic/Plenum Publishers, New York, 1993) and 0.63 eV for Fc/Fc+ vs. NHE (V. V. Pavlishchuk, A. W. Addison, *Inorg. Chim. Acta* **2000**, *298*, 97).
- (73) Barolo, C.; Nazeeruddin, M. K.; Fantacci, S.; Di Censo, D.; Comte, P.; Liska, P.; Viscardi, G.; Quagliotto, P.; De Angelis, F.; Ito, S.; Grätzel, M. "Synthesis, Characterization, and DFT-TDDFT Computational Study of a Ruthenium Complex Containing a Functionalized Tetradentate Ligand". *Inorg. Chem.* **2006**, *45*, 4642-4653, doi:10.1021/ic051970w.
- (74) Zakeeruddin, S. M.; Grätzel, M. "Solvent-Free Ionic Liquid Electrolytes for Mesoscopic Dye-Sensitized Solar Cells". *Advanced Functional Materials* **2009**, *19*, 2187-2202, doi:10.1002/adfm.200900390.
- (75) Dong, R.-X.; Shen, S.-Y.; Chen, H.-W.; Wang, C.-C.; Shih, P.-T.; Liu, C.-T.; Vittal, R.; Lin, J.-J.; Ho, K.-C. "A novel polymer gel electrolyte for highly efficient dye-sensitized solar cells". *J. Mater. Chem. A* **2013**, *1*, 8471-8478, doi:10.1039/C3TA11331K.
- (76) Kalyanasundaram, K.: *Dye-sensitized Solar Cells*; EFPL Press, 2010.
- (77) Manfredi, N.; Bianchi, A.; Causin, V.; Ruffo, R.; Simonutti, R.; Abboto, A. "Electrolytes for Quasi Solid-State Dye-Sensitized Solar Cells Based on Block Copolymers". *J Polym Sci Pol Chem* **2014**, *52*, 719-727.
- (78) Wang, M.; Gratzel, C.; Zakeeruddin, S. M.; Gratzel, M. "Recent developments in redox electrolytes for dye-sensitized solar cells". *Energy Environ. Sci.* **2012**, *5*, 9394-9405.
- (79) Docampo, P.; Guldin, S.; Leijtens, T.; Noel, N. K.; Steiner, U.; Snaith, H. J. "Lessons Learned: From Dye-Sensitized Solar Cells to All-Solid-State Hybrid Devices". *Adv. Mater.* **2014**, *26*, 4013-4030, doi:Doi 10.1002/Adma.201400486.

(80) Bella, F.; Gerbaldi, C.; Barolo, C.; Gratzel, M. "Aqueous dye-sensitized solar cells". *Chem. Soc. Rev.* **2015**, *44*, 3431-3473, doi:10.1039/C4CS00456F.

(81) Liu, Y.; Hagfeldt, A.; Xiao, X. R.; Lindquist, S. E. "Investigation of influence of redox species on the interfacial energetics of a dye-sensitized nanoporous TiO₂ solar cell". *Sol. Energy Mater. Sol. Cells* **1998**, *55*, 267-281, doi:10.1016/s0927-0248(98)00111-1.

(82) Bella, F.; Galliano, S.; Falco, M.; Viscardi, G.; Barolo, C.; Grätzel, M.; Gerbaldi, C. "Unveiling iodine-based electrolytes chemistry in aqueous dye-sensitized solar cells". *Chemical Science* **2016**, doi:10.1039/C6SC01145D.

(83) Nazeeruddin, M. K.; De Angelis, F.; Fantacci, S.; Selloni, A.; Viscardi, G.; Liska, P.; Ito, S.; Takeru, B.; Grätzel, M. "Combined Experimental and DFT-TDDFT Computational Study of Photoelectrochemical Cell Ruthenium Sensitizers". *J. Am. Chem. Soc.* **2005**, *127*, 16835-16847, doi:10.1021/ja052467l.

(84) Lin, R. Y.-Y.; Wu, F.-L.; Li, C.-T.; Chen, P.-Y.; Ho, K.-C.; Lin, J. T. "High-Performance Aqueous/Organic Dye-Sensitized Solar Cells Based on Sensitizers Containing Triethylene Oxide Methyl Ether". *ChemSusChem* **2015**, *8*, 2503-2513, doi:10.1002/cssc.201500589.

(85) Leandri, V.; Ellis, H.; Gabrielsson, E.; Sun, L.; Boschloo, G.; Hagfeldt, A. "An organic hydrophilic dye for water-based dye-sensitized solar cells". *Phys. Chem. Chem. Phys.* **2014**, *16*, 19964-19971, doi:10.1039/C4cp02774d.

(86) Berti, L.; Cucini, M.; Di Stasio, F.; Comoretto, D.; Galli, M.; Marabelli, F.; Manfredi, N.; Marinzi, C.; Abboto, A. "Spectroscopic Investigation of Artificial Opals Infiltrated with a Heteroaromatic Quadrupolar Dye". *J. Phys. Chem. C* **2010**, *114*, 2403-2413, doi:10.1021/jp906002q.

(87) Narain, R.: *Engineered Carbohydrate-Based Materials for Biomedical Applications*; John Wiley & Sons, Inc., 2011.

(88) Brunner, H.; Gruber, N. "Carboplatin-containing porphyrin-platinum complexes as cytotoxic and phototoxic antitumor agents". *Inorg. Chim. Acta* **2004**, *357*, 4423-4451, doi:<http://dx.doi.org/10.1016/j.ica.2004.03.061>.

(89) Rostovtsev, V. V.; Green, L. G.; Fokin, V. V.; Sharpless, K. B. "A Stepwise Huisgen Cycloaddition Process: Copper(I)-Catalyzed Regioselective "Ligation" of Azides and Terminal Alkynes". *Angew. Chem. Int. Ed.* **2002**, *41*, 2596-2599, doi:10.1002/1521-3773(20020715)41:14<2596::AID-ANIE2596>3.0.CO;2-4.

(90) Tornøe, C. W.; Christensen, C.; Meldal, M. "Peptidotriazoles on Solid Phase: [1,2,3]-Triazoles by Regiospecific Copper(I)-Catalyzed 1,3-Dipolar Cycloadditions of Terminal Alkynes to Azides". *J. Org. Chem.* **2002**, *67*, 3057-3064, doi:10.1021/jo011148j.

(91) Chakrabarty, S. P.; Ramapanicker, R.; Mishra, R.; Chandrasekaran, S.; Balaram, H. "Development and characterization of lysine based tripeptide analogues as inhibitors of Sir2 activity". *Biorg. Med. Chem.* **2009**, *17*, 8060-8072, doi:<http://dx.doi.org/10.1016/j.bmc.2009.10.003>.

(92) Dirks, A. J.; Cornelissen, J. J. L. M.; van Delft, F. L.; van Hest, J. C. M.; Nolte, R. J. M.; Rowan, A. E.; Rutjes, F. P. J. T. "From (bio)Molecules to Biohybrid Materials with the Click Chemistry Approach". *QSAR & Combinatorial Science* **2007**, *26*, 1200-1210, doi:10.1002/qsar.200740085.

(93) Abbotto, A.; Boldrini, C. L.; Manfredi, N.; Perna, F. M.; Capriati, V.; Trifiletti, V. "Dye-sensitized solar cells using an aqueous choline chloride-based deep eutectic solvent as an effective electrolyte solution". *Energy Technology* **2016**, n/a-n/a, doi:10.1002/ente.201600420.

(94) Pelaez, M.; Nolan, N. T.; Pillai, S. C.; Seery, M. K.; Falaras, P.; Kontos, A. G.; Dunlop, P. S. M.; Hamilton, J. W. J.; Byrne, J. A.; O'Shea, K.; Entezari, M. H.; Dionysiou, D. D. "A review on the visible light active titanium dioxide photocatalysts for environmental applications". *Appl. Catal., B-Environ* **2012**, *125*, 331-349, doi:<http://dx.doi.org/10.1016/j.apcatb.2012.05.036>.

(95) Afzal, S.; Daoud, W. A.; Langford, S. J. "Photostable Self-Cleaning Cotton by a Copper(II) Porphyrin/TiO₂ Visible-Light Photocatalytic System". *ACS Appl. Mater. Interfaces* **2013**, *5*, 4753-4759, doi:10.1021/am400002k.

(96) Wu, S.-H.; Wu, J.-L.; Jia, S.-Y.; Chang, Q.-W.; Ren, H.-T.; Liu, Y. "Cobalt(II) phthalocyanine-sensitized hollow Fe₃O₄@SiO₂@TiO₂ hierarchical nanostructures: Fabrication and enhanced photocatalytic properties". *Appl. Surf. Sci.* **2013**, *287*, 389-396, doi:<http://dx.doi.org/10.1016/j.apsusc.2013.09.164>.

(97) Inturi, S. N. R.; Boningari, T.; Suidan, M.; Smirniotis, P. G. "Visible-light-induced photodegradation of gas phase acetonitrile using aerosol-made transition metal (V, Cr, Fe, Co, Mn, Mo, Ni, Cu, Y, Ce, and Zr) doped TiO₂". *Appl. Catal., B-Environ* **2014**, *144*, 333-342, doi:<http://dx.doi.org/10.1016/j.apcatb.2013.07.032>.

(98) Serpone, N.; Lawless, D.; Disdier, J.; Herrmann, J.-M. "Spectroscopic, Photoconductivity, and Photocatalytic Studies of TiO₂ Colloids: Naked and with the Lattice Doped with Cr³⁺, Fe³⁺, and V⁵⁺ Cations". *Langmuir* **1994**, *10*, 643-652, doi:10.1021/la00015a010.

- (99) Serpone, N. "Is the Band Gap of Pristine TiO₂ Narrowed by Anion- and Cation-Doping of Titanium Dioxide in Second-Generation Photocatalysts?". *J. Phys. Chem. B* **2006**, *110*, 24287-24293, doi:10.1021/jp065659r.
- (100) Asahi, R.; Morikawa, T.; Ohwaki, T.; Aoki, K.; Taga, Y. "Visible-Light Photocatalysis in Nitrogen-Doped Titanium Oxides". *Science* **2001**, *293*, 269-271, doi:10.1126/science.1061051.
- (101) Kuznetsov, V. N.; Serpone, N. "Visible Light Absorption by Various Titanium Dioxide Specimens". *J. Phys. Chem. B* **2006**, *110*, 25203-25209, doi:10.1021/jp064253b.
- (102) Banerjee, S.; Pillai, S. C.; Falaras, P.; O'Shea, K. E.; Byrne, J. A.; Dionysiou, D. D. "New Insights into the Mechanism of Visible Light Photocatalysis". *J. Phys. Chem. Lett.* **2014**, *5*, 2543-2554, doi:10.1021/jz501030x.
- (103) Sakthivel, S.; Kisch, H. "Daylight Photocatalysis by Carbon-Modified Titanium Dioxide". *Angew. Chem. Int. Ed.* **2003**, *42*, 4908-4911, doi:10.1002/anie.200351577.
- (104) Taziwa, R.; Meyer, E. L.; Sideras-Haddad, E.; Erasmus, R. M.; Manikandan, E.; Mwakikunga, B. W. "Effect of Carbon Modification on the Electrical, Structural, and Optical Properties of Electrodes and Their Performance in Labscale Dye-Sensitized Solar Cells". *Int J Photoenergy* **2012**, *2012*, 9, doi:10.1155/2012/904323.
- (105) Hiroshi, I.; Yuka, W.; Kazuhito, H. "Carbon-doped Anatase TiO₂ Powders as a Visible-light Sensitive Photocatalyst". *Chem. Lett.* **2003**, *32*, 772-773, doi:doi:10.1246/cl.2003.772.
- (106) Kang, S. H.; Kim, H. S.; Kim, J.-Y.; Sung, Y.-E. "Enhanced photocurrent of nitrogen-doped TiO₂ film for dye-sensitized solar cells". *Mater. Chem. Phys.* **2010**, *124*, 422-426, doi:<http://dx.doi.org/10.1016/j.matchemphys.2010.06.059>.
- (107) Kushwaha, R.; Chauhan, R.; Srivastava, P.; Bahadur, L. "Synthesis and characterization of nitrogen-doped TiO₂ samples and their application as thin film electrodes in dye-sensitized solar cells". *J. Solid State Electrochem.* **2015**, *19*, 507-517, doi:10.1007/s10008-014-2623-8.
- (108) Diker, H.; Varlikli, C.; Stathatos, E. "N-doped titania powders prepared by different nitrogen sources and their application in quasi-solid state dye-sensitized solar cells". *Int. J. Energy Res.* **2014**, *38*, 908-917, doi:10.1002/er.3091.

(109) Chen, X.; Burda, C. "The Electronic Origin of the Visible-Light Absorption Properties of C-, N- and S-Doped TiO₂ Nanomaterials". *J. Am. Chem. Soc.* **2008**, *130*, 5018-5019, doi:10.1021/ja711023z.

(110) Martyanov, I. N.; Uma, S.; Rodrigues, S.; Klabunde, K. J. "Structural defects cause TiO₂-based photocatalysts to be active in visible light". *Chem. Commun.* **2004**, 2476-2477, doi:10.1039/B409730K.

(111) Wu, G.; Nishikawa, T.; Ohtani, B.; Chen, A. "Synthesis and Characterization of Carbon-Doped TiO₂ Nanostructures with Enhanced Visible Light Response". *Chem. Mater.* **2007**, *19*, 4530-4537, doi:10.1021/cm071244m.

(112) Shen, M.; Wu, Z.; Huang, H.; Du, Y.; Zou, Z.; Yang, P. "Carbon-doped anatase TiO₂ obtained from TiC for photocatalysis under visible light irradiation". *MatL* **2006**, *60*, 693-697, doi:<http://dx.doi.org/10.1016/j.matlet.2005.09.068>.

(113) Kuo, C.-S.; Tseng, Y.-H.; Huang, C.-H.; Li, Y.-Y. "Carbon-containing nano-titania prepared by chemical vapor deposition and its visible-light-responsive photocatalytic activity". *J. Mol. Catal. A: Chem.* **2007**, *270*, 93-100, doi:<http://dx.doi.org/10.1016/j.molcata.2007.01.031>.

(114) Park, Y.; Kim, W.; Park, H.; Tachikawa, T.; Majima, T.; Choi, W. "Carbon-doped TiO₂ photocatalyst synthesized without using an external carbon precursor and the visible light activity". *Appl. Catal., B-Environ* **2009**, *91*, 355-361, doi:<http://dx.doi.org/10.1016/j.apcatb.2009.06.001>.

(115) Huang, Y.; Ho, W.; Lee, S.; Zhang, L.; Li, G.; Yu, J. C. "Effect of Carbon Doping on the Mesoporous Structure of Nanocrystalline Titanium Dioxide and Its Solar-Light-Driven Photocatalytic Degradation of NO_x". *Langmuir* **2008**, *24*, 3510-3516, doi:10.1021/la703333z.

(116) Dong, F.; Guo, S.; Wang, H.; Li, X.; Wu, Z. "Enhancement of the Visible Light Photocatalytic Activity of C-Doped TiO₂ Nanomaterials Prepared by a Green Synthetic Approach". *J. Phys. Chem. C* **2011**, *115*, 13285-13292, doi:10.1021/jp111916q.

(117) Szot, K.; Rogala, M.; Speier, W.; Klusek, Z.; Besmehn, A.; Waser, R. "TiO₂ — a prototypical memristive material". *Nanot* **2011**, *22*, 254001.

(118) Ito, S.; Chen, P.; Comte, P.; Nazeeruddin, M. K.; Liska, P.; Péchy, P.; Grätzel, M. "Fabrication of screen-printing pastes from TiO₂ powders for dye-sensitised solar cells". *Progr. Photovolt: Res. Appl.* **2007**, *15*, 603-612, doi:10.1002/pip.768.

(119) Dell'Orto, E.; Raimondo, L.; Sassella, A.; Abboto, A. "Dye-sensitized solar cells: spectroscopic evaluation of dye loading on TiO₂". *J. Mater. Chem.* **2012**, *22*, 11364-11369, doi:10.1039/C2JM30481C.

(120) Bard, A. J.; Faulkner, L. R.: *Electrochemical Methods, Fundamentals and Applications, 2nd Ed.*; John Wiley & Sons, INC.

: New York, Chichester, Weinheim, Brisbane, Singapore, Toronto, 2001.

(121) Ito, S.; Murakami, T. N.; Comte, P.; Liska, P.; Grätzel, C.; Nazeeruddin, M. K.; Grätzel, M. "Fabrication of thin film dye sensitized solar cells with solar to electric power conversion efficiency over 10%". *Thin Solid Films* **2008**, *516*, 4613-4619, doi:10.1016/j.tsf.2007.05.090.

(122) Fabregat-Santiago, F.; Bisquert, J.; Garcia-Belmonte, G.; Boschloo, G.; Hagfeldt, A. "Influence of electrolyte in transport and recombination in dye-sensitized solar cells studied by impedance spectroscopy". *Sol. Energy Mater. Sol. Cells* **2005**, *87*, 117-131, doi:<http://dx.doi.org/10.1016/j.solmat.2004.07.017>.

Chapter 3

Perovskite solar cells

“Success is not final, failure is not fatal:

it is the courage to continue that counts.”¹

Winston Churchill, Statesman, 1874 - 1965

Aim of this work

The second part of this PhD research project has been dedicated to the study of solid state perovskite based solar cells (PSCs). This new technology became very popular in the last 5 years and it is attracting a lot of interest amongst the researcher due to its astonishing increasing achievements. The perovskite used in these devices are hybrid organic-inorganic material, namely a blend of lead halide (*i.e.* PbI_2 , PbCl_2) and an ammonium salt ($\text{CH}_3\text{NH}_3\text{I}$). None of these materials own a perovskite crystal structure, but mixed together they form a crystal with the structure of perovskite with unique properties. Even though the cells prepared using this perovskite material are promising in terms of photovoltaic efficiency, the working mechanism is still not completely clear. Moreover, despite the huge numbers of articles present in literature (more than 1500 in 2016 over more than 3200 in the last 10 years), there is still not a standard procedure to prepare these devices. Aim of this part of the work is to develop a procedure to prepare PSC with a good and reproducible efficiency. Further work can be done in preparing

prototype cells evaluating different geometries and non-standard material for more complex structure such as multijunction solar cell in combination with silicon or CIGS bottom cells, to boost their efficiency and improve optical properties (Figure 3. 1).

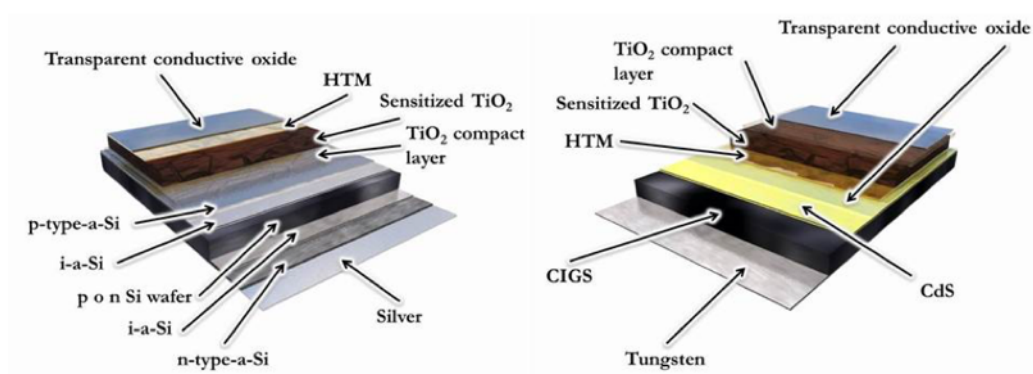


Figure 3. 1: scheme of construction of tandem devices. (left) tandem cell formed on a silicon-based device; (right) Tandem cell made of thin film second generation type CIGS

Another important part of this work has been done in collaboration with the group of Prof. N. Stingelin at the Imperial College London. In the PSCs, one of the most important component is the hole transport material (HTM) that is the equivalent of the electrolyte in liquid solar cells. The benchmark HTM is a commercial electron-rich molecule named Spiro-OMeTAD (Figure 3. 2).

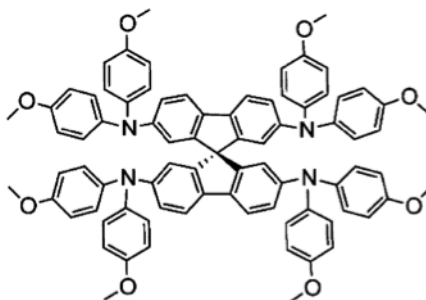


Figure 3. 2: Spiro-OMeTAD

This molecule, based on a tetra-diphenylamino-(spirobifluorene), allows to reach high efficiency but the synthetic procedure to prepare it is complicated and expensive. We have focussed our attention to a new class of electron-rich

molecules bearing an electron-donor hydrazone moieties. The general structure of the investigated molecule is depicted in Figure 3. 3. This class of molecule is well-known and widely used in chemistry and material science, with an easy and cheap synthetic access. A complete electrochemical investigation has been done and the carriers mobility has been evaluated in an organic field effect transistor device.

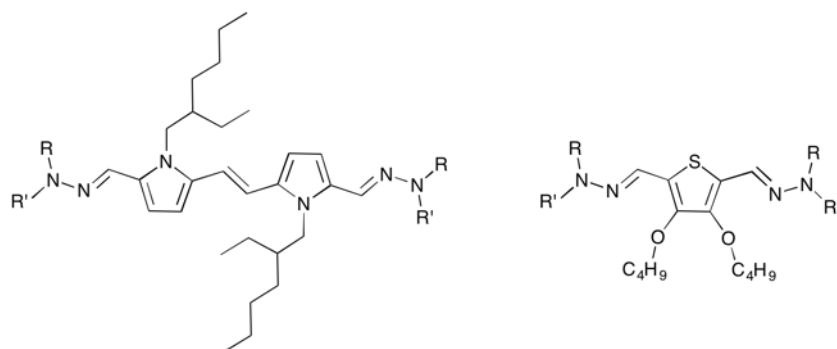


Figure 3. 3: general structure of investigated hydrazone-based HTM for PSCs.

Multijunction perovskite base hybrid solar cells

In the last decade, third generation perovskite-based solar cells have attracted interest of many researched, almost replacing the other organic-based solar cells.²⁻⁴ This novel and exciting light-harvesting material in an hybrid halide perovskite with the typical perovskite structure ABX_3 (where, $A = CH_3NH_3$ or $CH(NH_2)_2$, $B = Pb$, Sn and $X = Cl, Br, I$). The perovskite is a well-known material, discovered by Rose, in Russia's Ural Mountains in the late 19th century and the most common mineral wild type is calcium titanate ($CaTiO_3$), but perovskite's structure is observed in a wide range of elements, making it quite versatile Figure 3. 4 Usually A is 12-fold cuboctahedral coordinated with the X anions and B is located in the $[BX_6]^{4-}$ octahedral center.

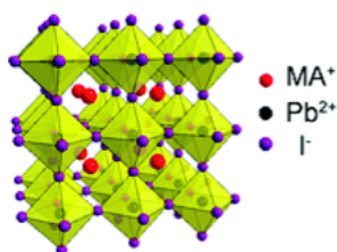


Figure 3. 4: typical structure of a perovskite crystal.

This class of perovskite material has been presented in the late '90 by Mitzi who was interested in studying the conductivity in layered tin-based perovskite materials.⁵ The capacity to change the electronic properties of these materials, by insulating to semiconductor, simply changing an organic cation through a simple solution process method, makes these new materials the perfect candidates for multiple applications in the field of solution processed optoelectronic devices, sweeping from the photovoltaic field⁶⁻¹⁰ to lasing devices,¹¹⁻¹³ and light-emitting diodes.¹⁴⁻¹⁸ This feature allowed the research community to develop highly performing devices at affordable costs. These crystalline semiconductors greatly satisfy these needs, combining excellent processability from solution with outstanding optoelectronic and electrical properties.¹⁹⁻²¹ This class of materials has

been innovative especially in the field of solution processable photovoltaic, reaching the astonishing efficiency of 22.1% in just a few years after their discovery.^{7,19,22-27} Very recently, Graetzel and co-workers at the EPFL research center in Lausanne, proved that employing a vacuum flash–assisted solution processing method, they were capable to produce high electronic quality crystalline perovskite film, with area exceeding 1 cm² and with an efficiency of 20.5%.²⁸ The fast increase of perovskite-based solar cell performances are correlated to the unique photophysical properties, such as remarkable optical absorption across a wide range of the solar spectrum, ambipolar charge transport and long charge-carrier diffusion lengths.^{7,12,21,25,29-33}

The impressive increase in performances is more related with the device architecture than to a development of the material itself. Indeed, hybrid halide perovskite has been originally used as sensitizer in a liquid DSC,²⁶ with poor efficiency due to interaction of the liquid component with the perovskite material. Since then, the community moved to a solid state architecture, at the beginning using the perovskite as light absorber in presence of a semiconductor as electron carrier to the complete removal of the semiconductor where the perovskite itself act as carrier to transfer the charge to the electrode. (Figure 3. 5).^{8,22,23,26,27,34} It should be noted that at that moment solid-state DSSC were actively investigated for their relevant use in practical devices but efficiency barely surpassed 5%. Since then, various device architectures have been made, and in all configurations, the hybrid halide perovskite proved major performances.

Moreover, in recent years, several research groups have proposed the interesting idea of preparing a multi-junction solar cell by combining traditional photovoltaic devices, such as silicon solar cells, with PSC in order to achieve higher performance, using low cost processes rather than sophisticated and expensive evaporation systems, commonly used in the manufacture of inorganic analogues.³⁵⁻

39

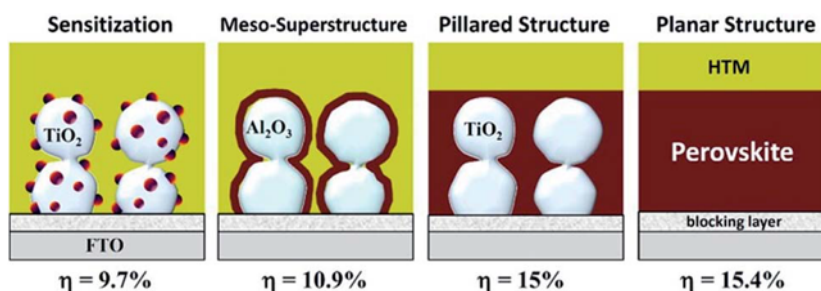


Figure 3. 5: The structures of hybrid perovskite solar cells in which (left to right) quantum dot shape perovskite was applied as a sensitizer, and a thin continuous layer as a light absorber and an electron conductor, overlapped perovskite functions additionally as a hole conductor, and planar perovskite as a heterojunction. Reproduced from ref 40, with permission of the Royal Society of Chemistry.

In this section, our goal is to develop a manufacturing protocol for PSC cells that allows us to obtain stable and reproducible results. In addition, particular attention will be given to the development of a device of the appropriate geometry to the need to develop an integrated system or, in the best case, a monolithic. The development of an integrated system (Figure 3. 1) will necessarily move through the study and development of a transparent or semi-transparent contacts to allow the bottom cell to absorb enough light order to work properly.

DEVICE FABRICATION

The first step has been to make a series of devices whit performances comparable to best average values reported in literature (PCE = 11-13%), although lower than absolute record values in champion cells (PCE ca. 20%). In order to achieve this, we have tried to optimize each production process of the manufacture of the device. Two main architectures have been exploited in search of higher performances. The first is the mesoporous (Ms-PSC) and the second is the planar (Pl-PSC), depicted in Figure 3. 6.

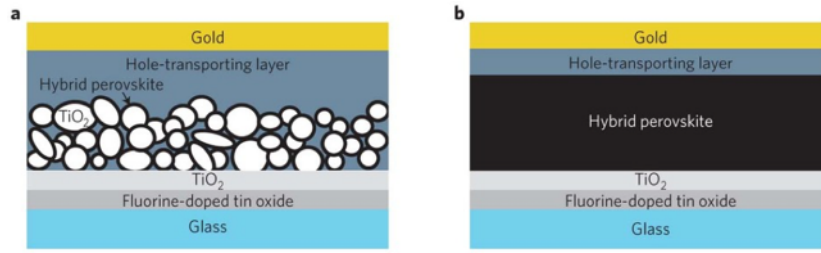


Figure 3. 6: Schematic of the investigated PSC configuration, (a) Ms-PSC and (b) PI-PSC

In the Ms-PSC configuration, the perovskite $\text{CH}_3\text{NH}_3\text{PbI}_3$ acts as absorber and transfers the electrons to the semiconductor mesoporous (TiO_2) deposited on the transparent conducting anode. These electrons move through the semiconductor reaching the anode where, through the circuit, they move towards the counter electrode. The counter electrode, typically gold or silver, is put in contact with the active anodic (perovskite and titania) through a hole conducting material (HTM).

In the PI-PSC configuration, the perovskite $\text{CH}_3\text{NH}_3\text{PbI}_3$ acts as absorber and n-type and semiconductor. Following the formation of an exciton produced by photoexcitation, the electrons produced passing through the material reaching the transparent conducting anode where, through the circuit are transferred to the counter electrode. The counter electrode, typically gold or silver, is put in contact with the active anodic (perovskite) through a hole conducting material (HTM).

Both configurations share the oxide semiconductor used as a selective layer, namely compact TiO_2 (c- TiO_2), the HTM and the counter electrode.

The first layer that composes the device is a thin layer a few tens of nanometers (30-50 nm) of c- TiO_2 called blocking layer (BL). The presence of this titania layer is necessary because in its absence, between the FTO and HTM, it would form an ohmic contact, so that the charge carriers would give recombination at the interface, leading to have an inherently inefficient solar cell. The presence of the BL thus avoids short circuit and current leakage for recombination so that the output current due to this arrangement increases up to three or four orders of magnitude.⁴¹ Generally, the compact layer is deposited by spin coating or spray pyrolysis from a

solution of a titania precursor. In literature, also other techniques have been reported such as the atomic layer deposition (ALD).⁴²The main difficulty in obtaining a BL that functions properly is due to the ability to control the thickness and the morphology of the same; in fact the non-homogeneity, the presence of holes (pinhole) and the defects generally lead to having contact areas between the electrode and HTM which as mentioned, are detrimental. The presence of holes (defect A) and inhomogeneity (defect B) is depicted in Figure 3. 7

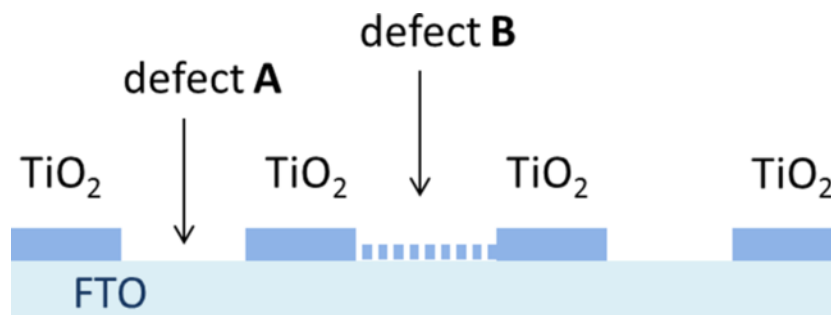


Figure 3. 7: Type of defects on the surface of a c-TiO₂ BL. Reprinted with permission from ref. ⁴³ Copyright (2014) American Chemical Society.

Also morphological analysis is not trivial and we chose to exploit typically electrochemical techniques to assess the deficiencies of the compact we deposited layer.⁴⁴ In particular we used cyclic voltammetry (CV) on multiple samples, consisting of the glass only with FTO and BL deposited by different methods, to compare the quality of the BL measuring the passage of current between the electrodes which, as easily understood, is proportional to the amount defects on the layer itself.⁴³

A set of samples was prepared by depositing via spin coating two different formulations of the same precursor, a commercial paste "Dyesol BL-1 Blocking Layer", undiluted or diluted 1:1 *w/w* in EtOH. Subsequently the samples were thermally treated at 450 °C for 30 min to make the titania solid and compact.

The electrochemical measurements have allowed us to understand that the technique of spin coating does not produce a BL compact enough; in fact, as it can

be seen in Figure 3. 8 compared to bare FTO glass, the passage of current is almost the same. The one remark to be highlighted is that by diluting the paste with the precursor to the BL turns out to be less defective resulting in lower current flow.

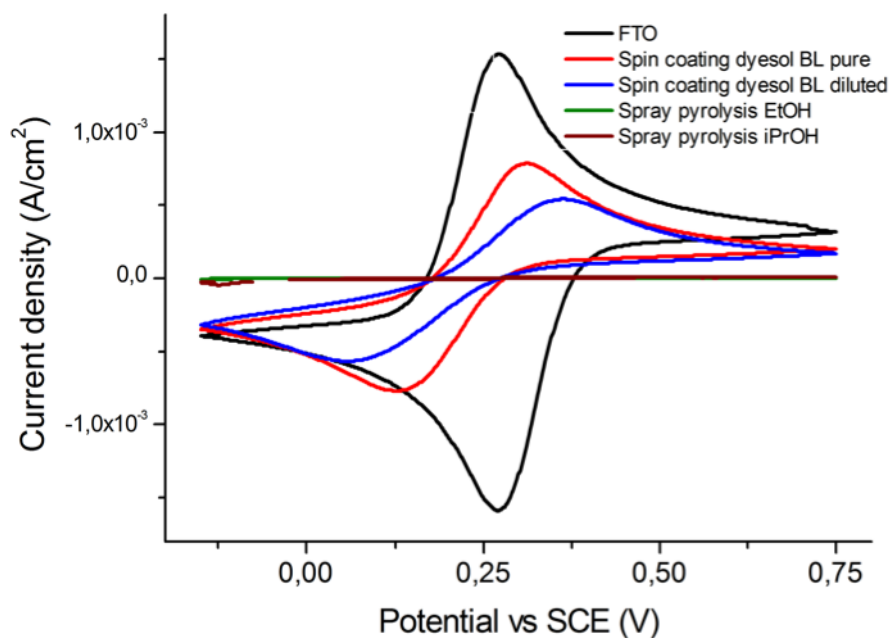


Figure 3. 8: CV traces of electrode with BL prepared using different techniques.

Another experiment was performed by depositing the BL via spray pyrolysis. In particular, the glasses were heated to about 450 °C on a hot-plate and, using an airbrush, two different precursors were applied: titanium diisopropoxide bis (acetylacetonate) diluted 1:10 in EtOH,³⁶ or a solution in isopropanol (iPrOH) of Ti-isopropoxide and 2 M acetylacetonate.⁴⁵ This time, there was obtained a much more powerful BL and suitable for the purpose of separating the FTO and HTM. In fact, as it can be seen in Figure 3. 8, the comparison between the currents recorded on the FTO untreated sample, the one with the BL deposited via spin coating and finally the two samples deposited via spray pyrolysis, makes evident the qualitative difference between the various materials and techniques with which they have been prepared. We then studied the BL thickness obtained using the spray pyrolysis technique, by depositing various amounts of the precursor by varying the

number of steps of airbrush. Subsequently, the thicknesses were measured by means of scanning electron microscopy (SEM). We observed a fair linearity between thickness and amount of deposited precursor, as shown in Figure 3. 9 and Figure 3. 10, where the steps of airbrush have been doubled (20 to 40). This analysis allowed to optimize the amount of material to be deposited to obtain a BL as close as possible to the characteristics estimated by comparing the parameters reported in the literature. For all the devices prepared in this work, it used the solution 1:10 in EtOH.

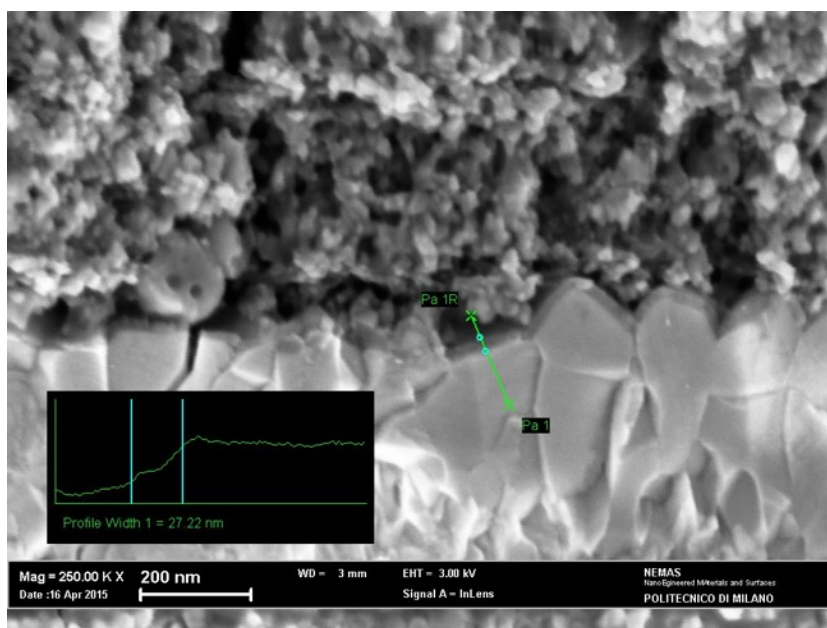


Figure 3. 9: SEM image with detail on the thickness of the BL (27 nm). FTO layer and mesoporous TiO₂ are also depicted.

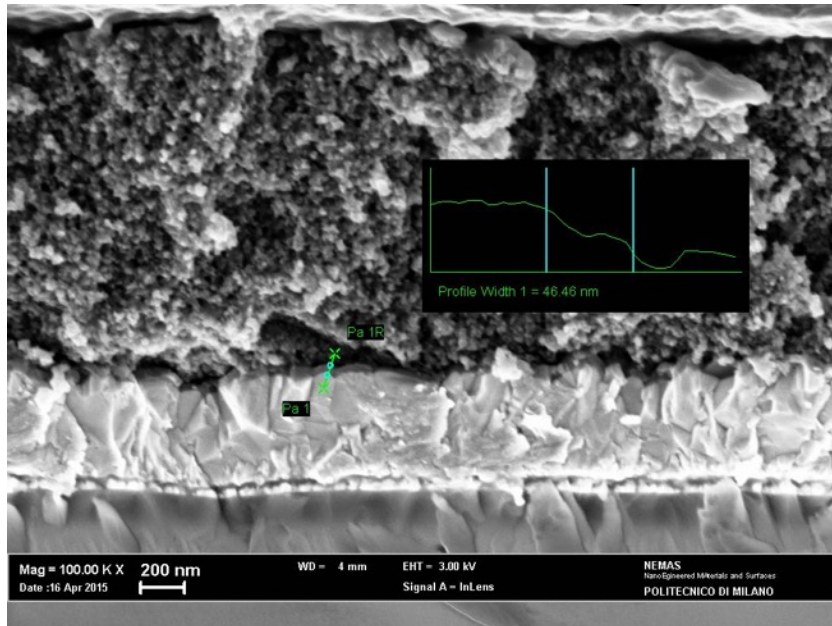


Figure 3. 10: SEM image with detail on the thickness of the BL (46 nm). FTO layer and mesoporous TiO₂ are also depicted.

MESOPOROUS ARCHITECTURE

Therefore, we moved on to study the first class of device, those mesoporous in which the perovskite is deposited on a semiconductor oxide (TiO₂) and acts as an absorber (Ms-PSC). The scheme of a typical device and its geometry (*four-in-a-row*) are shown in Figure 3. 11.

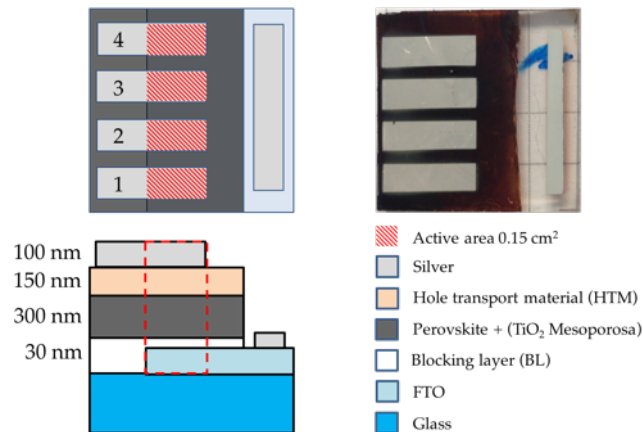


Figure 3. 11: Schematic architecture (bottom left), geometry *four-in-a-row* (top left), and picture (top right) of a Ms-PSC.

To facilitate the comprehension of the data reported in this section, we need to explain the nomenclature used to designate a particular cell. In general, it is used a code like $PX-m-n$, where X is a progressive uppercase letter (A, B, C, etc) that indicates the set of a given experiment glasses, m is a number indicating in which of the set of glasses it is referenced, and n is a number (1 to 4) that determines exactly one of the four cells present on each glass. Every cell shows an active area of 0.15 cm^2 .

The standard procedure used by us for the preparation of mesoporous PSC relies on the article published by Grätzel et al. 2013.⁴⁶ This has been used as a base on which to perform experiments in order to optimize the production process. A critical point concerns the environmental conditions in which it operates during the preparation of the devices. The level of humidity of the air, and then the concentration of H_2O , in fact, can affect both positively and negatively on the quality of perovskite crystals that are produced, and thus the performance of the photovoltaic device.⁴⁷ The presence of H_2O not only influences the formation of the $\text{CH}_3\text{NH}_3\text{PbI}_3$ crystal, but has negative effects perovskite films already formed, degrading it to a two-dimensional structure such as PbI_2 (rhombohedral crystalline structure) by removing the methylammonium molecule (MA) from its lattice position. This occurs through the formation of intermediate structures of the type $\text{MAPbI}_3\text{-H}_2\text{O}$ and $\text{MA}_4\text{PbI}_6\text{-2H}_2\text{O}$.⁴⁸ It is clear then that having a perfect control on the concentration in the environment is critical. On each glass, after preparing the BL as described previously, it was deposited a layer of mesoporous titania by spin coating and annealing at $500 \text{ }^\circ\text{C}$ ($\sim 500 \text{ nm}$). On the anode thus prepared is deposited a PbI_2 film, always via spin coating. Then, it is dipped into a solution of methylammonium iodide (MAI) in isopropanol that allows the formation of the perovskite layer. This technique is called in situ dipping reaction. As a final active layer was deposited via spin coating the HTM, on which finally were evaporated in a vacuum chamber, the silver metal contacts. A schematic representation of the procedure is depicted in Figure 3. 12.

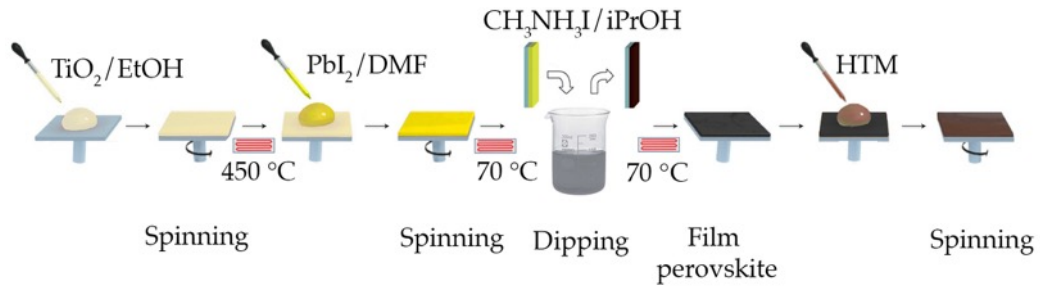


Figure 3. 12: Schematic representation of the fabrication method of a Ms-PSC.

These devices, whose geometry has been displayed previously, showed highly variable performance, from sample to sample. However, after many steps of optimization of the operating conditions, we were able to reach the desired efficiency targets and the J/V curve obtained by the best device is shown in Figure 15.

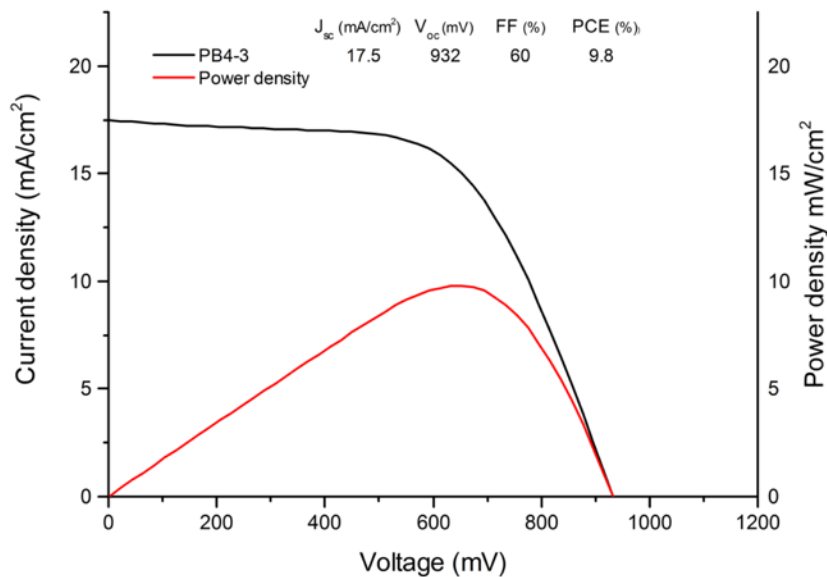


Figure 3. 13: (red line) J/V and (black line) power density characteristic curves of a Ms-PSC device under full AM 1.5 solar intensity.

The production of high-quality devices requires some major attention. First of all, it is important to note that the relative humidity present in the working area must be less than 30% at $20\text{ }^\circ\text{C}$. This parameter affects primarily the fabrication of devices. First critical step is the preparation of the 1.0 M PbI_2 solution. This solution must

be prepared using anhydrous solvents (in our case DMF), and must be maintained at 70 ° C to enable the dissolution of the PbI_2 . The dissolution of the PbI_2 in anhydrous solvents occurs slowly, usually a few hours, but in case of humid solvent, the dissolution is much faster but the film obtained does not give any working device. Furthermore, it is important to maintain photoanodes at 70 ° C even before the deposition of the PbI_2 solution. In fact, as said before, precipitation of the solute is observed, in this case on the layer of TiO_2 , leading once again to non-functioning devices. After spin-coating deposition, the so prepared substrate is annealed at 70 °C, after which it must be allowed to cool down to room temperature before the dipping procedure. The dipping must be done in a solution of MAI in anhydrous *i*-prOH. After drying at room temperature, the HTM layer is deposited and the silver contact (~ 120 nm) is evaporated at ($\sim 10^{-6}$ mbar). The devices are allowed to stand in dry air overnight to allow an oxygen doping of the HTM to improve the performances.⁴⁹ The best thus manufactured devices, have also been studied using cross-section SEM microscopy to evaluate the thickness and the uniformity of the layers. A SEM image characteristic of this class of cells is shown in Figure 3. 14.

As a final consideration, it is important to note the large distribution of efficiency values obtained from devices made with this architecture and geometry (Figure 3. 15).

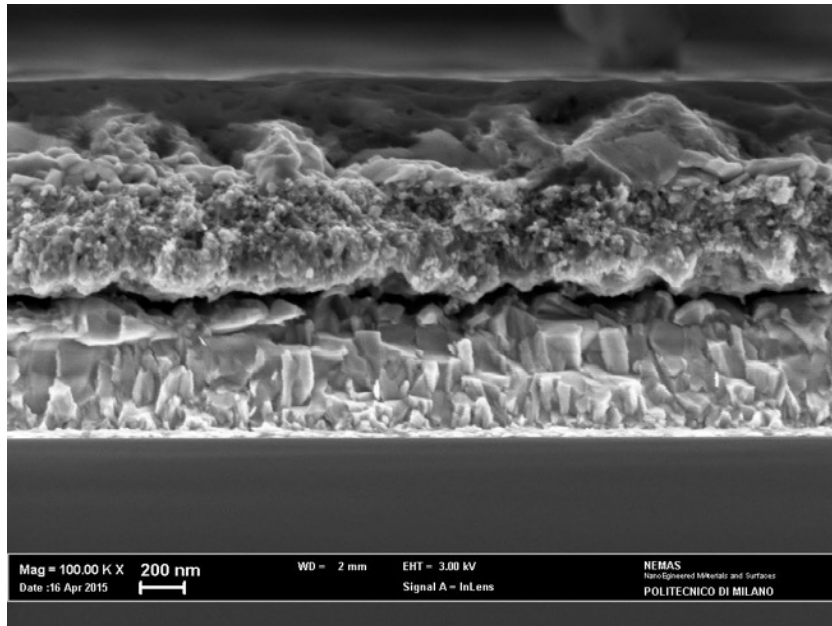


Figure 3. 14: cross-section SEM image of a Ms-PSC device.

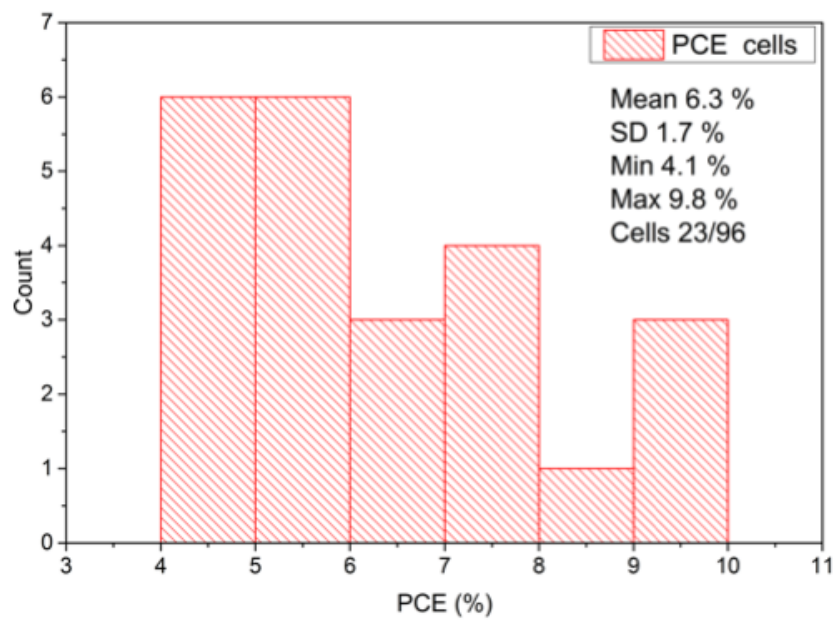


Figure 3. 15: Statistic distribution of the efficiency obtained with Ms-PSC devices.

As can be seen, on more than ninety devices realized only just over 20 showed the characteristic curve of a photovoltaic cell with acceptable values.

Given the great variability of results and the complexity of the realization of the devices themselves with this architecture, we moved to study the planar cell architecture. This structure allows us to remove the layer of mesoporous TiO₂ and use of the perovskite as a photoactive material and an electron transporter.

PLANAR ARCHITECTURE

PSC can exploit an interesting alternative to the architecture so far described: the planar architecture (Figure 3. 6b). The latter allows to avoid problems that result from poor pore filling of the perovskite itself and the HTM within the pores of the mesoporous layer. It also reduces the recombination due to the larger crystals size (also confirmed by SEM analysis below) and thus a lower density of defects. The cells with this architecture show better reproducibility and ease of fabrication, considered they have an active layer less than mesoporous.⁵⁰

The study of this type of cells is based on the procedure developed by Docampo et al.⁵¹ In this procedure are applied some changes to suit our needs. Overall, in comparison with the previously described fabrication procedure for the cells described so far, we can speak of a simplification which results from the lack of deposition of the mesoporous titania layers and the deposition of the perovskite layer in a single step. The layer of perovskite is prepared by spin coating of a solution consisting of 1.25 M PbI₂ and 1.25 M MAI in DMF followed by a recrystallization in situ (Figure 2.16) promoted by the addition of a non-solvent (eg chlorobenzene, chloroform, toluene) which favours the removal of residual traces of the solvent which is used for the deposition.

During deposition of the precursor of the perovskite layer solution, as said, it is necessary to add a non-solvent to promote the nucleation and growth of crystals. What is of fundamental importance is the choice of non-solvent and to establish with accuracy, the time in which it must be added.

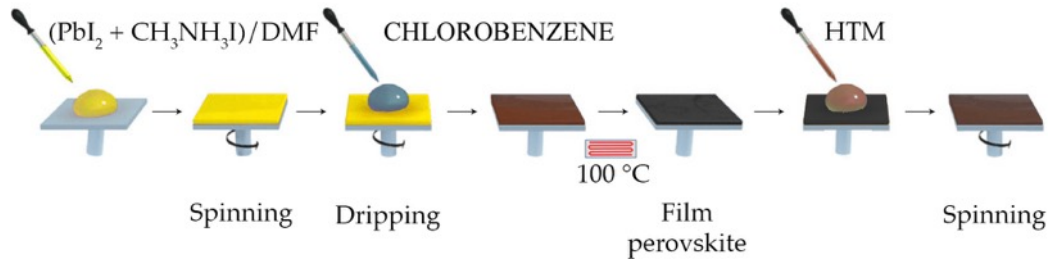


Figure 3. 16: Schematic representation of the fabrication method of a PI-PSC.

According to a study published by Spiccia et al., the formation of perovskite crystals during the spin coating process can be divided into three phases.⁵² The first phase takes place during the first 3 seconds from the beginning of rotation of the substrate: in these moments, the excess of the precursor solution is removed. The addition of non-solvent in this phase when the condition of supersaturation is not yet being reached, will determine the incomplete coverage of the substrate by the crystals. The second phase can be considered of between 4 and 6 seconds of the rotation and is now that, by adding the non-solvent, there is the formation of a good polycrystalline film. In the next step, over 6 seconds, the precursor film is practically dry and the addition of non-solvent causes an inhomogeneous crystallization. Using chlorobenzene as a solvent, we have obtained better results than that obtained with the MS-PSC cells. The J/V curve of the best device realized with PI-PSC architecture is shown in Figure 3. 17. This device has achieved an efficiency greater than 12% at 1 sun, and even higher than 13% at 0.5 sun.

Also in the case of PI-PSC, it was made a thorough study on the thicknesses of the different active layers present in the cell in order to accurately determine the actual size of our devices. As already done for the MS-PSC, for this analysis we performed cross section SEM images of which an example is reported in Figure 3.

18

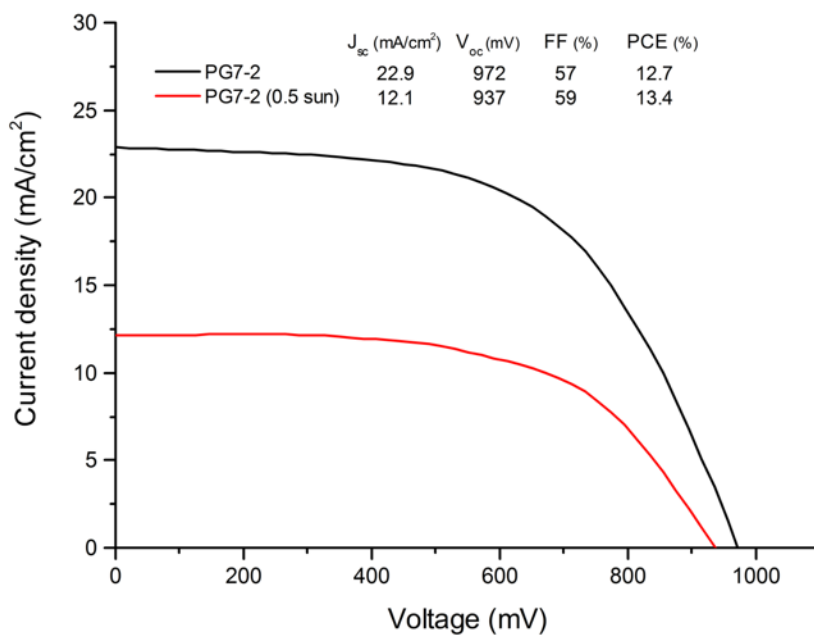


Figure 3. 17: J/V characteristic curves of a PI-PSC device under full AM 1.5 solar intensity (black line) and 0.5 AM 1.5 solar intensity (red line).

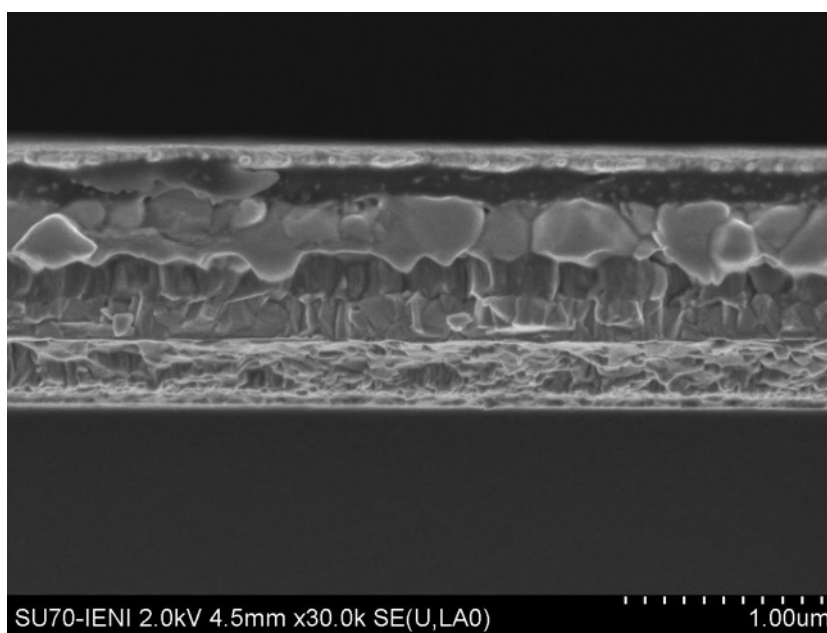


Figure 3. 18: cross-section SEM image of a Ms-PSC device.

It has been measured that the layer of perovskite crystals show a thickness of ~ 300 nm, while the layer of HTM, unlike in the mesoporous PSC, is very homogeneous

result but not thick enough; In fact, unlike the ~ 250 nm required was found to have a thickness of ~ 150 nm.

OPTIMIZED GEOMETRY

Common feature of the *four-in-a-row* geometry is that, among the four cells present on each glass, those that offer better performance and reproducibility are the central ones (the 2 and 3 in Figure 3. 11 and Figure 3. 19). This fact can be explained considering that the devices are manufactured mainly by depositing materials by spin coating which, as already mentioned, easily leads to films not perfectly homogeneous between the central and the peripheral area of the substrate.

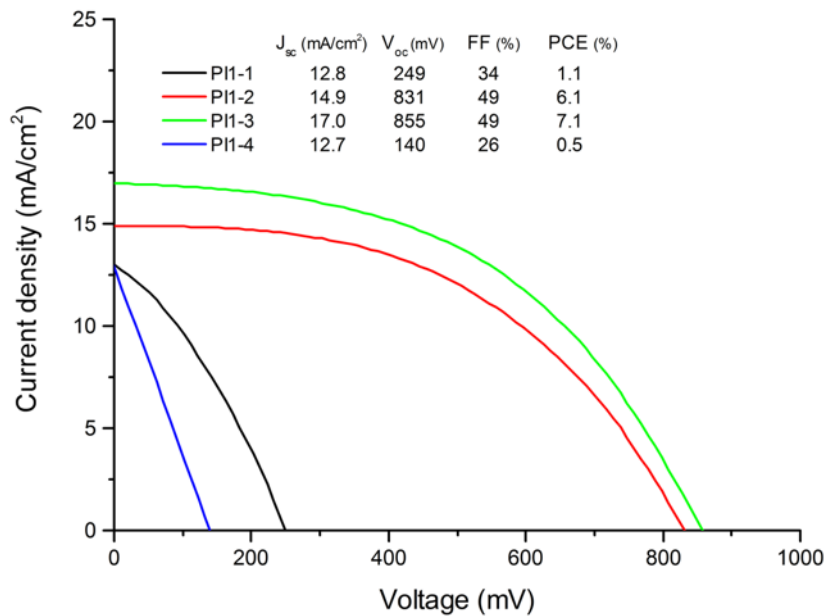


Figure 3. 19: J/V characteristic curves of 4 cells on a single PI-PSC device with *four-in-a-row* geometry under full AM 1.5 solar intensity.

For this reason, it was decided to further exploit the central area of the substrate by modifying the geometry of the device. The new *centred* geometry is shown in Figure 3. 20

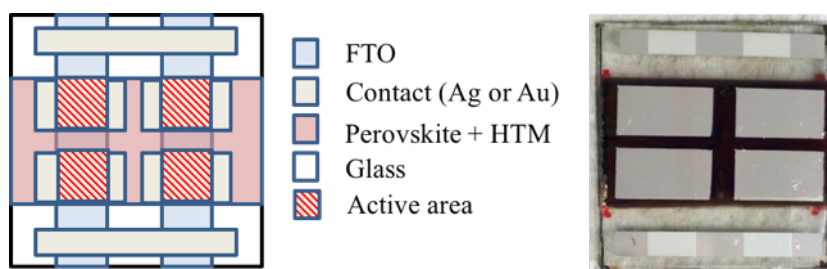


Figure 3. 20: (left) schematic representation of the *centred* geometry, (right) PI-PSC device with this geometry.

It is important to notice that the active area in this new geometry was set at 0.16 cm^2 but during measurement each cell has been masked in order to reduce the active area to about 0.10 cm^2 . The choice of the new geometry gave, as expected, excellent results in terms of reproducibility and performance. As can be seen from Figure 3. 21, relative to the four cells on a single device, unlike the measurements carried out previously on the other geometry, there has been very good homogeneity between the performance of the different cells on the same glass.

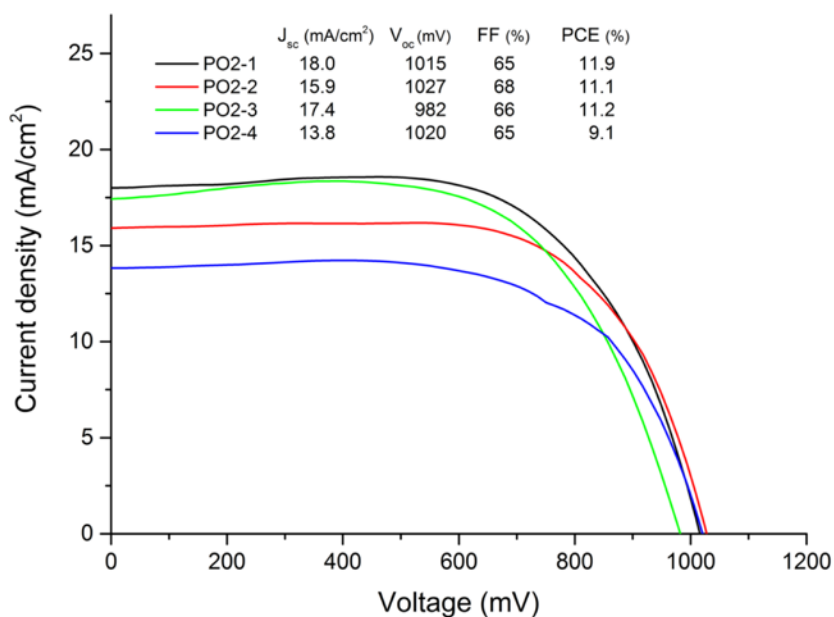


Figure 3. 21: J/V characteristic curves of 4 cells on a single PI-PSC device with *centred* geometry under full AM 1.5 solar intensity.

Upon completion of the optimization of the PI-PSC work, it has been done a statistical study of operational parameters (V_{oc} , J_{sc} , FF, PCE) relative to almost all

the cells prepared during the process itself. In particular, statistical data are based on 100 cells on 35 different devices. Should be noted that on these devices, the total cells are 140 but it is limited to only 100 cells with PCE greater than 3.5%. It has been noted that the mean value measured that deviates more negatively than that of the literature has the FF, being likely cause of PCE values not particularly high. The FF is determined primarily by two factors: the recombination of the charges and the electrical resistance of the device.^{37,53} This analysis has enabled us to better understand the level of manufacturing quality achieved and to be able to plan more effectively future work. The data are reported in table and depicted in Figure 3. 22.

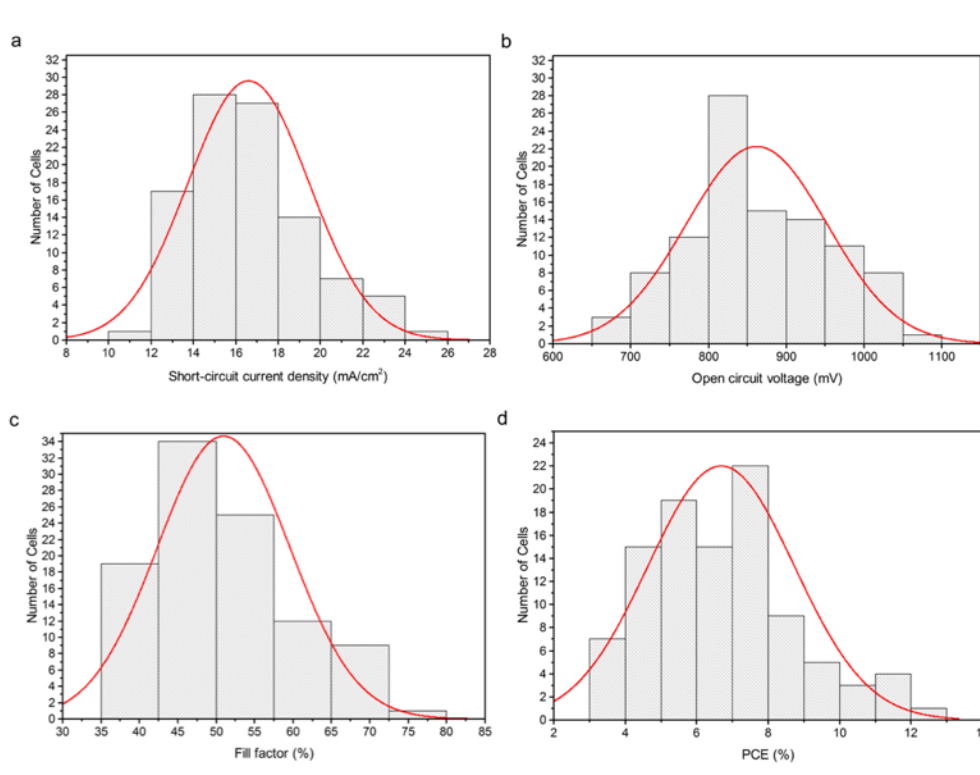


Figure 3. 22: Bar charts and relative Gaussian curve referred to the statistical distribution of the PI-PSC operating parameters produced and measured: (a) J_{sc} (b) V_{oc} (c), FF, and (d) PCE

Table 3. 1: Operating parameters and statistics on PI-PSC cells.

Perovskite solar cells

Parameters ^a	Average value	Std. dev.	Min value	Max value
J_{sc} (mA cm ⁻²)	16.6	2.8	11.9	25.2
V_{oc} (mV)	862	90	687	1055
FF (%)	51	9	39	73
PCE (%)	6.7	2.0	3.5	12.7

^a active area 0.16 cm², measured under full AM 1.5 solar intensity.

MULTIJUNCTION TANDEM DEVICE

By having developed a fairly stable process for the production of PSC-PI cells with *centred* geometry, we proceeded with the feasibility study for the integration of PSC with the first or second generation photovoltaic technologies. (Figure 3. 23) The theoretical advantage that this approach allows to obtain is a significant increase in efficiency of photovoltaic conversion: to date the best single junction PSC PCE show around 20% which would be far overcome by multi-junction tandem reaching PCE even close to 30%.³⁷

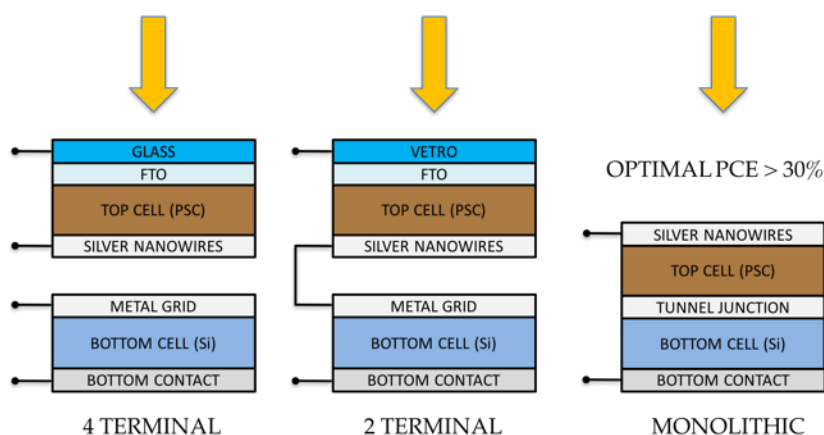


Figure 3. 23: Schematic representation of (left) 4-terminal, (centre) 2-terminal, and (right) monolithic integrated tandem device.

Given that the interest is to develop tandem solar cells with PSC top cell and a bottom one of silicon or other semiconductor, it was necessary to undertake a

study to develop semi-transparent PSC. For this reason, we have tried to replace the metal contacts, used until now, with contacts as transparent as possible; in particular the study was directed to contacts made from silver nanowires (Ag-NWs). The optimization of the deposition method of this type of contacts is very important in order to obtain devices which have performance not too much lower than those with more conventional metal contacts. The procedure on which it was based is described in the literature in an article by McGehee et al. of 2015.³⁶ the deposition method used is mechanical: the NW are deposited by spray coating on a plastic substrate and subsequently transferred by contact on the PSC. During several experiments conducted, two main critical issues have been identified. At first, we had to figure out what would be the best substrate to ensure a good transfer of Ag-NWs and, at the same time, avoid damaging the PSC during the operation. Afterwards it was necessary to establish a compromise between the amount of Ag-NWs deposited and the degree of transparency of the contact; in fact, they must be deposited Ag-NWs enough to establish a good electrical contact, so as to conduct more electrical current possible without too many resistive losses, on the other hand the greater the amount of NWs present the lower the transparency of the contacts. After a number of attempts, we have chosen to deposit the Ag-NWs on a PTFE support for spray coating maintaining the support at 100 ° C. The Ag-NWs are transferred mechanically to the cell, properly masked in order to define the shape of the contact. As aforementioned, we have tried to optimize the thickness of the Ag-NWs film so as to obtain a sufficient transparency without compromising the performance of the photovoltaic cell. It must be noted that the use of Ag-NWs, replacing the metal contacts, leads to a significant worsening in the measured current values, in particular because the interface that is formed between Ag-NWs and HTM, rich in defects due mainly to the somewhat invasive deposition method. To modify in a controlled manner the transparency of the contacts, the amount of suspension deposited on the substrate was varied, and the transmittance and the PCE measured. To maintain acceptable efficiency (PCE > 4%) it was not possible to reach very high levels of transparency, as can be

seen in Figure 3. 24 where is shows the measurement of transmittance of a contacts-free cell and of one with Ag-NWs semi-transparent contacts.

Finally, a preliminary study was carried out on the integration of the semi-transparent PSC with a mc-Si cell. Of the latter, it was measured the curve J/V under illumination with and without the semi-transparent PSC positioned above, by measuring a PCE of 4.8% and 14%. (Figure 3. 25 and Table 3. 2)

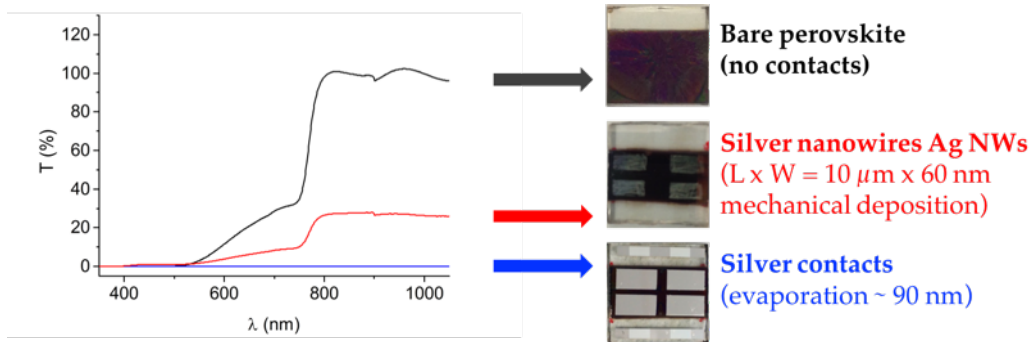


Figure 3. 24: UV-VIS transmittance spectra of PI-PSC (black) contacts-free, (red) semi-transparent Ag-NWs contacts and (blue) evaporated metal contact.

In accordance with recent publications, we have thus been able to calculate the efficiency of the 4 terminals tandem device (Figure 3. 23) as the sum of the PCE of the top and bottom cells.^{36,54-56} The calculated value is not very significant from a performance point of view because of the fact that it does not improve the characteristics of the starting mc-Si cell. Nevertheless, it is necessary to consider that the main limitation of this system comes from the lack of transparency of the top cell PSC caused by Ag-NWs.

At the moment, new transparent electrodes made of semiconductor oxides are under investigation, which should ensure high performance maintaining high transparency.

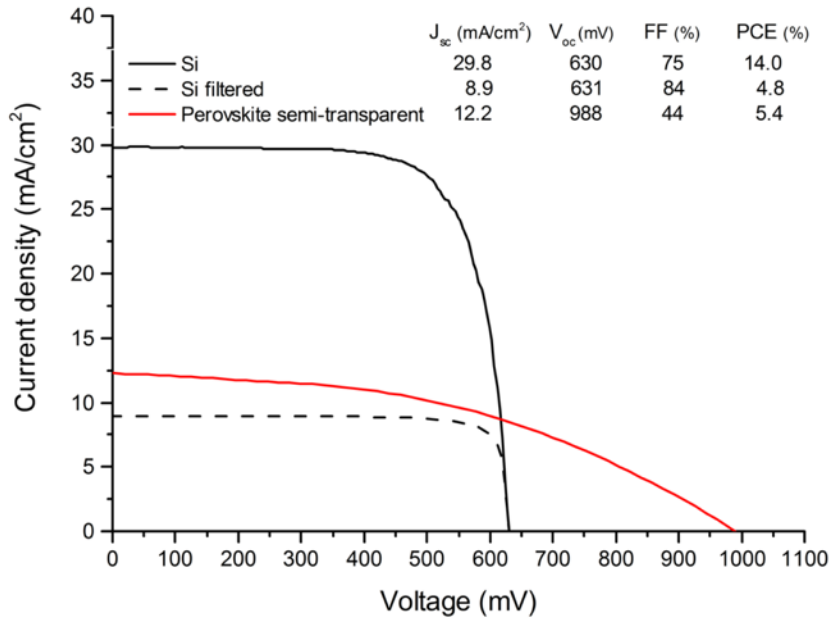


Figure 3. 25: J/V plots measured under full AM1.5 irradiation. Are reported the data related to a mc-Si cell (solid black curves), the same cell filter by a semi-transparent PI-PSC (dashed black curve) and to a semi-transparent PI-PSC (red line). Active area for each cell equal to 0.16 cm².

Table 3. 2: Operating parameters of PI-PSC and mc-Si cells in standard and tandem configuration.

Cell type ^a	J_{sc} (mA×cm ⁻²)	V_{oc} (mV)	FF (%)	PCE (%)
PI-PSC (metal contact)	22.9	972	57	12.7
PI-PSC (Ag-NWs contact)	12.2	988	44	5.4
mc-Si	29.8	630	75	14.0
mc-Si (filtered)	8.9	631	84	4.8
4 terminal tandem configuration				10.2

^a active area 0.16 cm², measured under full AM 1.5 solar intensity.

New heteroaromatic hydrazone-based hole transporting material for perovskite solar cells

In the field of photovoltaic, PSC have gained interest due to their high efficiency and cheap preparation method. In fact, this type of solar cell can be produced via solution process that is really cheap and can be easily transferred to industry.^{19,24,57} Despite the rapid increase in efficiency associated with the evolution of different types of perovskites and device fabrication techniques, the development of HTM is still a critical issue. The recent researches are mainly focused on organic compounds. In particular, the bulky 3-D spiro-OMeTAD (Figure 3. 2) with the twisted spirobifluorene centre has been proven as the most effective HTM for PSC devices since it was firstly presented in 1998 for ss-DSSCs.⁵⁸ However, the synthetic procedure to prepare it is complicated and expensive. This procedure uses noble metals and it is not suitable for large-scale production. Therefore, the need to develop new HTM systems appears to be a topic of primary relevance for the commercialization of efficient PSC cells, with an affordable cost. To make this possible, new kinds of alternative HTMs to spiro-OMeTAD with a simpler synthetic route, lower production cost and comparable device performance are needed. Also, a compatible HOMO energy level relative to perovskites and high charge-carrier mobility should also be considered. In the past two years, many new type HTMs, including organic small molecules and polymers,¹⁰ and inorganic materials,⁵⁹⁻⁶¹ have been used for perovskite solar cells and promising performance has been achieved for the corresponding devices.

The major effort has been made in the study of organic materials and, a series of different HTM based on electron-rich compounds, such as triphenylamine, thiophene, or thiophene derivatives has been published achieving good power conversion efficiency when used in substitution of the spiro-OMeTAD (Figure 3. 26).^{51,62-71}

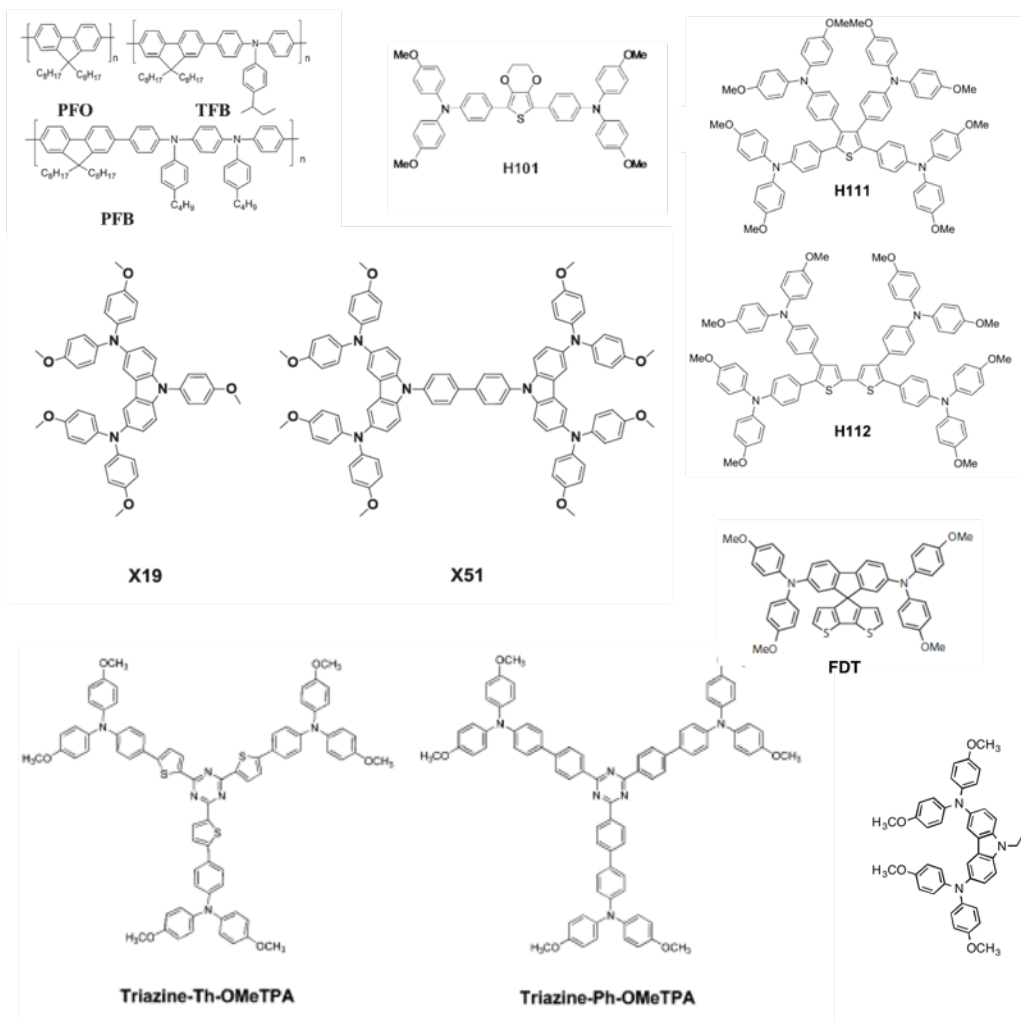


Figure 3. 26: Examples of alternative HTM reported in litterature.

An interesting approach towards the synthesis of low-cost, molecular HTMs (H101, Figure 3. 26) was recently introduced by Li et al.⁶⁴ They reported a EDOT based HTM with efficiencies up to 13.2%, which is comparable to Spiro-OMeTAD. However, also in this case, the synthesis involves the use of Pd-catalysed cross-coupling reactions, and extensive product purification; making it not suitable for large scale production.

More recently, Docampo et al. Here, described the synthesis of a simple azomethine-based conjugated small-molecule (EDOT-OMeTPA, Figure 3. 27) which is easily prepared in a cost effective Schiff base condensation reaction, with

water as only by-product, achieving efficiencies exceeding 11% in PI-PSC. The successful idea of this new HTM lies in a simple and inexpensive synthesis. Indeed, the the reaction can be performed at near ambient conditions and water is the only by-product, making product purification very straightforward.

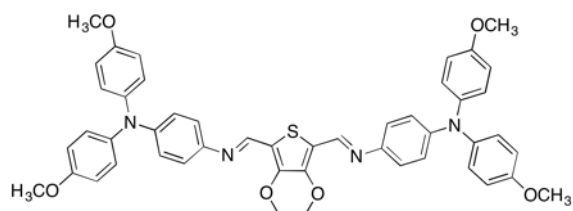


Figure 3. 27: Azomethine-based hole transporting presented by Docampo et al. In 2015

Inspired by this successful work, we decided to develop and study a new series of heteroaromatic HTM based on hydrazone moieties to be compared to the used in PI-PSC as alternative to Spiro-OMeTAD.

Hydrazone based compound⁷² are widely used in many field, from medicine⁷³ to biology,⁷⁴ from chemistry^{75,76} to material science.⁷⁷⁻⁷⁹ The synthesis of hydrazone-based compound is easy and, as well as the previous example, the only by-product is water.⁸⁰

The basic requirement for the hole-transport material is that its HOMO and LUMO levels are compatible with the HOMO level of the perovskite and the conduction band of TiO_2 to drive the charge-transfer process. In addition, the hole-transport material should be a transparent and amorphous thin film, as crystallization will prevent effective pore filling and thereby reduce its thermal and photochemical stability as well as carrier mobility. Spiro-OMeTAD displays a work function of about 4.9 eV and a hole mobility of $10^{-4} \text{ cm}^2 \text{ V}^{-1} \text{ s}^{-1}$.⁸¹ The high efficiency stems from the inherent properties of spiro-OMeTAD, that is, its amorphous structure, good solubility, and small size. Spiro-OMeTAD is an organic non-crystalline Another interesting feature is that the HTM materials are usually electron-rich materials and he typical structures reported are basically of two different categories: the first is a spiro-based structure, and the second is a D- π -D

structure or analogous. Herein, we report the synthesis, the optical and electrochemical characterization, as well as the photovoltaic investigation and hole mobility properties, of a series of electron-rich π -bridged symmetric hydrazone based HTM.

DESIGN AND SYNTHESIS

The new compound used as HTM in this project are depicted in Figure 3. 28 and their synthesis in scheme Scheme 3. 1.

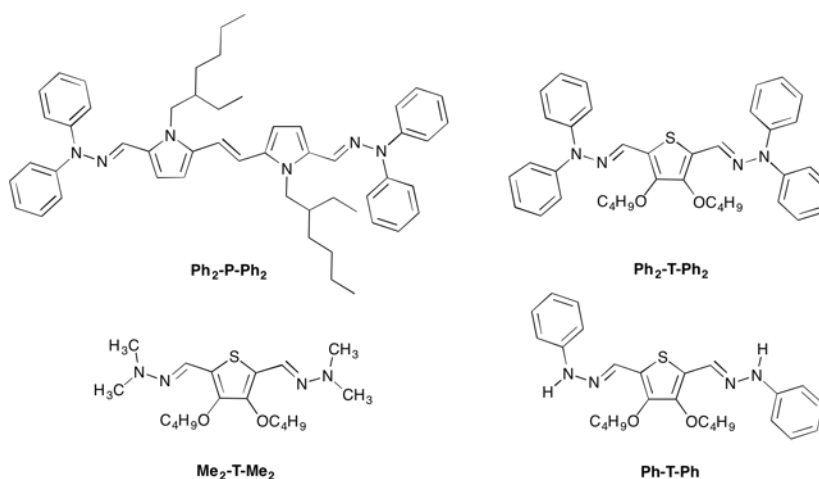
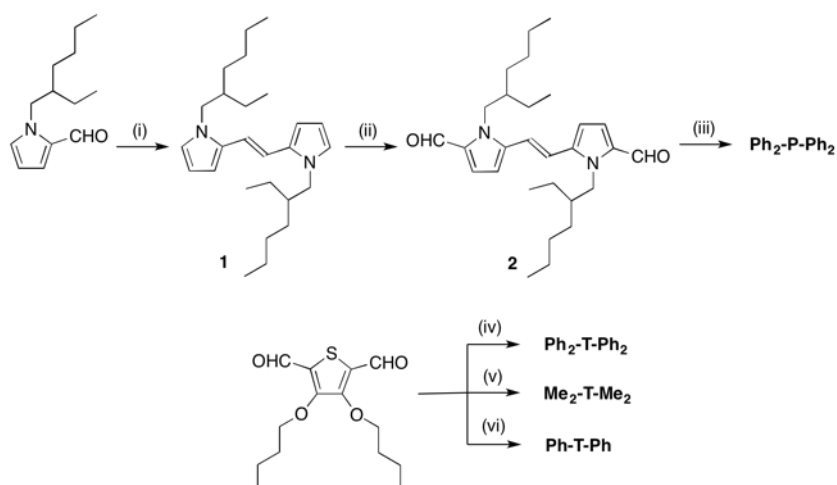


Figure 3. 28: Electron-rich π -bridged symmetric hydrazone based HTM investigated in this work.

In order to realize HTM that could be effectively transferred to a large-scale production we have opted to follow synthetic protocols as simple as possible.

On the basis of an unpublished study did in our lab, we knew that D- π -D derivatives of 1,2-di(2-pyrrolyl)ethenes based hydrazones showed a nicely reversible oxidation behaviour and can be easily prepared on a large scale in almost ambient conditions with straightforward purification. In some of the cases, they also showed a proper energetic alignment to be used as HTM in PI-PSC devices. Furthermore, a similar class of hydrazone-based compound have been successfully used as active material in BHJ solar cells.⁷⁹ To better exploit this series of compound we selected as donor moieties three different substituents on the hydrazones group, namely diphenyl, dimethyl and phenyl, have been employed. As

π -bridge, we have chosen a 1,2-di(2-pyrrolyl)ethenes functionalized with 2-ethylhexyl chains on the pyrrolic nitrogen and a 3-4-dibutoxythiophene. In both cases, the choice of the alkyl functionalities has been made to induce an amorphous character to the film.^{82,83}



Scheme 3. 1: Synthetic protocol for the preparation of electron-rich π -bridged symmetric hydrazone based HTM. Reagents and conditions. (i) TiCl_4 , Zn, Py, THF anhyd., N_2 , reflux, 4 h; (ii) POCl_3 , DMF, CH_3CN dry, rt, 17 h; (iii) N,N-diphenyl-hydrazine hydrochloride, THF, rt, 4 h; (iv) N,N-diphenyl-hydrazine hydrochloride, THF, rt, 4 h; (v) N,N-dimethyl-hydrazine, PTSA, THF, rt, 4 h; (vi) (iii) N-phenyl-hydrazine, PTSA, THF, rt, 4 h.

The synthesis of the **Ph₂-p-Ph₂** compound (Scheme 3. 1) is an easy three step process. Starting from the 1-(2-Ethylhexyl)-1H-pyrrole-2-carbaldehyde,⁸⁴ the dipyrrolyl-ethene core has been synthesized via McMurry reaction in presence of Zn and TiCl_4 . Pyridine was added to remove acid from the solution and prevent degradation of the product **1**. After flash chromatography, the pure product **1** has been submitted to Vilsmeier formylation to give the dialdehyde **2** with high yield. The obtained dialdehyde **2**, as well as the dialdehyde of the 3-4-dibutoxythiophene,⁸⁵ were used in the condensation with the proper hydrazine, in THF at room temperature in air, with stoichiometric amount of acid to give the corresponding product with yield ranging from 50% to 85%.

OPTICAL AND ELECTROCHEMICAL PROPERTIES

The new compounds have been characterized in their optical properties, both in solid and on a thin film prepared via spin coating (5×10^{-5} M in chlorobenzene, 2000 rpm, 30 s), and the results are reported respectively in Figure 3. 29 and Figure 3. 30, as well as the parameters reported in Table 3. 3.

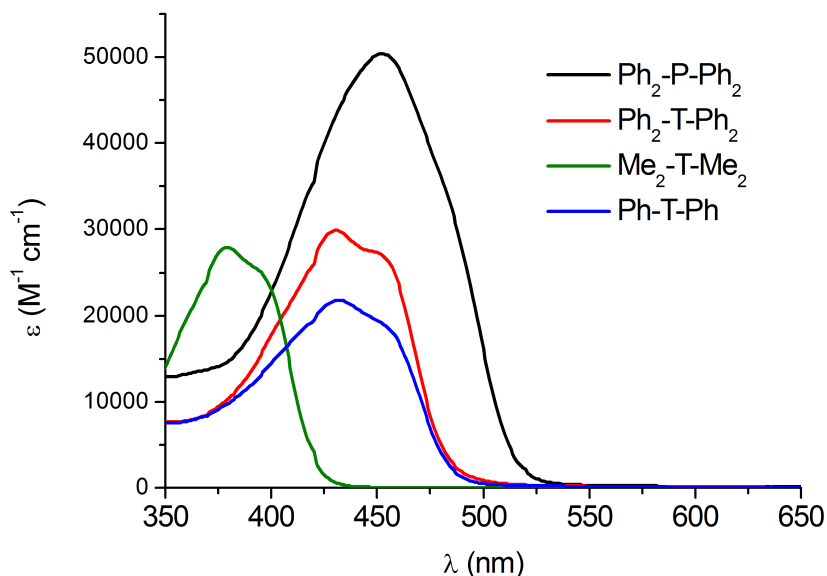


Figure 3. 29: Absorption spectra of hydrazone based HTM in THF.

The absorption spectra of the compounds showed an intense absorption peak related to the $\pi\text{-}\pi^*$ transition of the molecules at between 430 - 450 nm for the diphenyl- and phenyl-derivatives, and about 380 nm for the dimethyl-hydrazone. The molar extinction coefficients are similar in the homologous class of compound and seems related to the different π -bridge. The thienyl-based derivatives showed a molar extinction coefficients close to $29000 \text{ M}^{-1} \text{ cm}^{-1}$, a little lower for the phenyl-hydrazone around $21000 \text{ M}^{-1} \text{ cm}^{-1}$, whereas the dipyrrolil-ethene bridged showed a much higher value around $50000 \text{ M}^{-1} \text{ cm}^{-1}$.

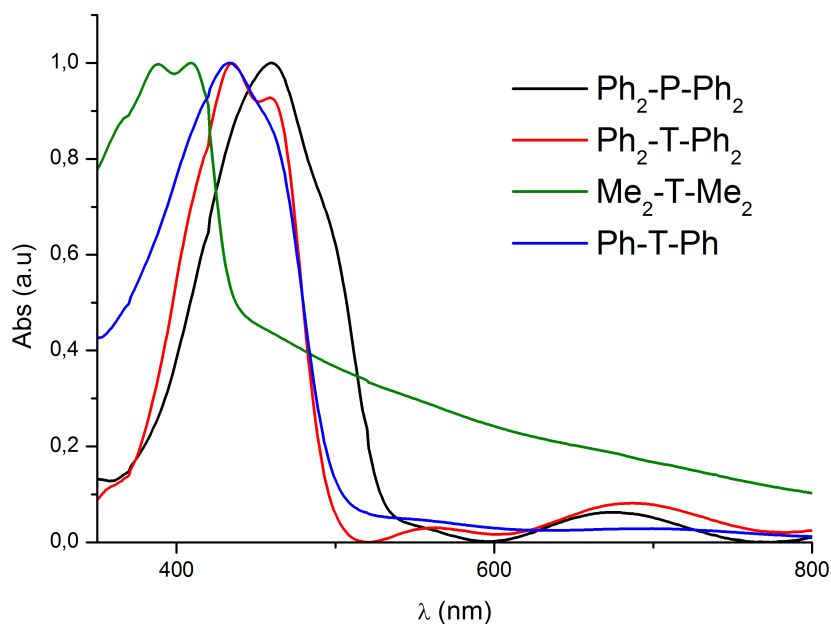


Figure 3. 30: Normalized absorption spectra of hydrazone based HTM on thin film.

Table 3. 3: Optical characterization of hydrazone based HTM in 10^{-5} M THF solution.

Compound	λ_{\max} sol [nm]	ϵ [M \cdot 1cm \cdot 1]	λ_{\max} film [nm]	$E_{\text{gap}}^{\text{opt}}$ [eV]
Ph ₂ -P-Ph ₂	452	50400 \pm 800	460	2.46
Ph ₂ -T-Ph ₂	431	29900 \pm 900	435	2.61
Me ₂ -T-Me ₂	379	27900 \pm 500	389	2.99
Ph-T-Ph	432	21800 \pm 800	434	2.60

In solid state, the absorption spectra are slightly red shifted (less than 10 nm) compared to the analogous in solution, as expected.

The electrochemical characterization is depicted in Figure 3. 31 and Figure 3. 32, and summarized table.

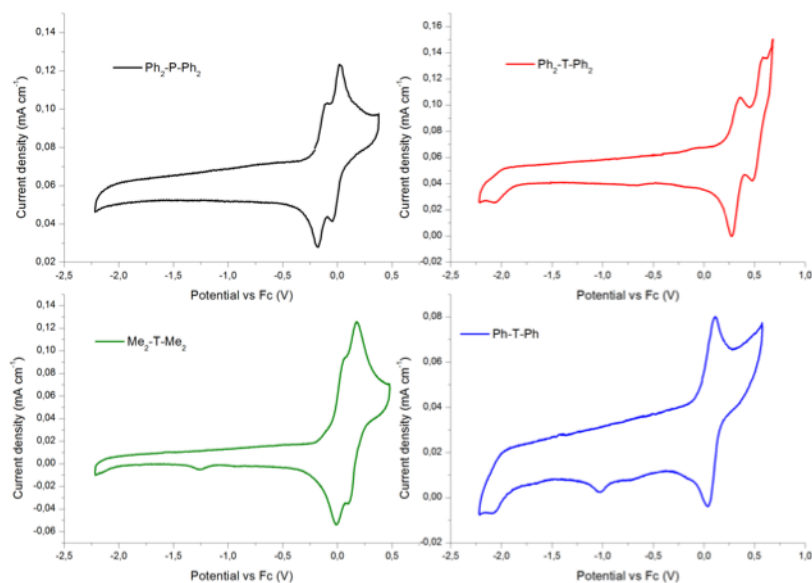


Figure 3. 31: CV plots of a 5×10^{-4} solution of hydrazone based HTM in 0.1 M TBAClO₄ in supporting electrolyte in THF. WE glassy carbon disk, CE Pt flag, RE Ag/AgCl, scan rate 50 mV/sec.

Cyclic voltammetry profiles showed a reversible behaviour for the all the investigated HTM oxidation. The investigated reduction process were irreversible. The HTMs oxidation showed two unresolved current signals (a peak and its shoulder) except in the case of **Ph₂-T-Ph₂**, which made somewhat difficult the energy level calculation. The first wave corresponds to the formation of a delocalized radical cation, whilst the second is associated with the formation of the dication. Both the position and the potential separation between the two peaks can be used to probe the electronic coupling between the end capping units and the electron-accepting core.⁷⁹ For these reasons, Differential Pulsed Voltammetry (DPV) was employed. DPV was able to isolate the different electrochemical processes with the exception of the **Ph-T-Ph** first oxidation, which appears as a shoulder over a broad peak. In this case the HOMO energy level has been determined from the current onset rather than current peak.

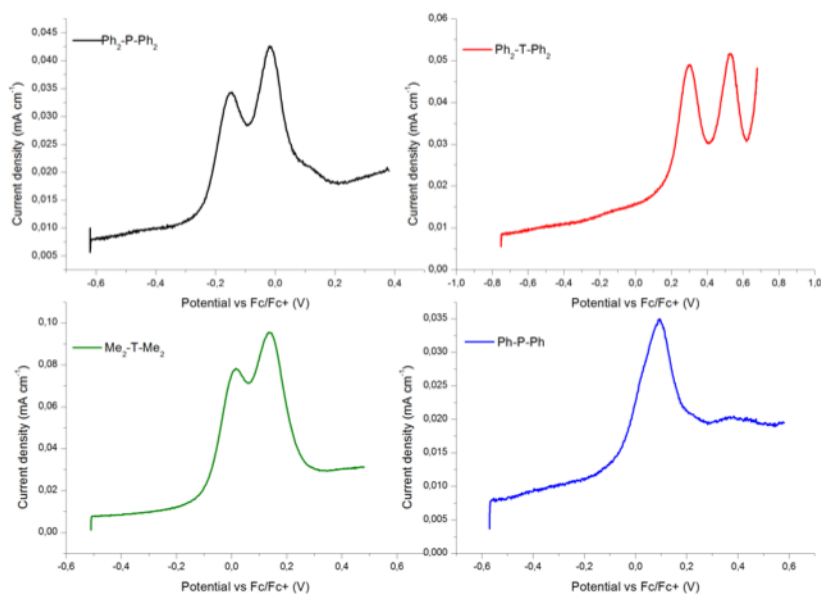


Figure 3. 32: DPV plots of a 5×10^{-4} solution of hydrazone based HTM in 0.1 M TBAClO₄ in supporting electrolyte in THF. WE glassy carbon disk, CE Pt flag, RE Ag/AgCl, scan rate 20 mV/sec.

Table 3. 4: Electrochemical characterization of hydrazone based HTM.

Sample	V_{ox} [V vs. Fc] \pm 10 mV	HOMO ^a [eV] \pm 0.1 eV	E_{gap}^{opt} [eV]	LUMO ^{a,b} [eV] \pm 0.1 eV
Ph ₂ -P-Ph ₂	-0.24	-4.98	2.46	-2.52
Ph ₂ -T-Ph ₂	0.17	-5.41	2.61	-2.80
Me ₂ -T-Me ₂	-0.09	-5.14	2.99	-2.15
Ph-T-Ph	-0.07	-5.15	2.60	-2.55

^a Vacuum potential = Fc/Fc⁺ + 5.2 V, ^b Calculated using optical band gap.

The new synthesized HTM showed a good energy levels alignments with the perovskite and are very close to the energy levels of the spiro-OMeTAD, except for the **Ph₂-T-Ph₂**, where the calculated HOMO level at a value of -5.41 eV seems to close to the HOMO level of the perovskite absorber. Considering that a minimal offset of 0.3 – 0.3 eV is generally required to ensure efficient electron injection,^{86,87} it is reasonable that electron donation is hampered and the whole mechanism negatively affected for this HTM.

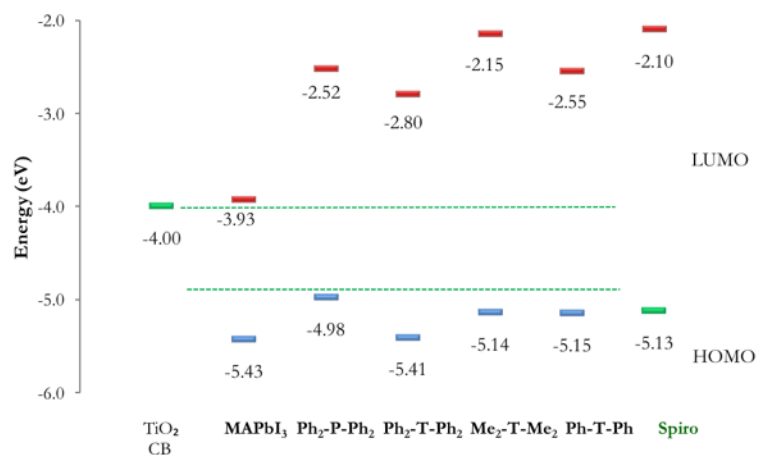


Figure 3. 33: Pictorial representation of calculated energy levels for the new hydrazone based HTM compared to TiO₂ CB, perovskite and Spiro-OMeTAD.

PHOTOVOLTAIC INVESTIGATION

Before starting with the cells preparation, we have investigated the deposition methods for the new HTM. In fact, as mentioned in the previous section, the thickness and the homogeneity of the layer is compulsory in order to achieve a good efficiency of the device. Furthermore, a well-defined thickness (about 50-70 nm) is required for the preparation of organic field effect transistor (OFET) used to measure the carrier mobility.

The HTM layer have been deposited on glass via spin coating. The glass have been cleaned with the same procedure employed in the fabrication of the PSC device. In this phase, we have changed different parameters to achieve the desired thickness and quality of the layer. Concentration, solvent, speed have been changed to ensure a proper deposition of the layer. But, the first thing we have noticed is that, regardless of the type of molecule deposited, a preliminary filtration through a 0.45 μm PTFE filter of the HTM solution is needed to have a homogeneous film (Figure 3. 34: Deposition of a (left) unfiltered solution, (b) filtered through a 0.45 μm PTFE filter of a 60 mM Spiro-OMeTAD solution in chlorobenzene.).

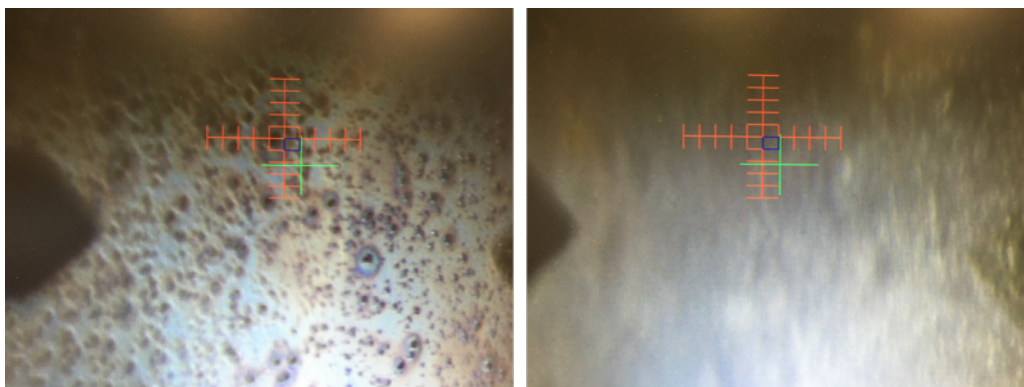


Figure 3. 34: Deposition of a (left) unfiltered solution, (b) filtered through a $0.45\ \mu\text{m}$ PTFE filter of a 60 mM Spiro-OMeTAD solution in chlorobenzene.

Thereafter, the solutions have been filtered before the deposition. The deposited HTM have been measured using a profilometer to ensure the thickness and optical microscopy to evaluate the quality of the deposited film. We choose to test the new HTM varying, one at a time, three spinning speeds (4000, 2000, 1000 rpm), and three solvents (chlorobenzene, toluene, chloroform). In table are reported the data collected for the good deposited film. In fact, in the case of the new HTM, some deposition conditions led to the formation of films of poor quality not suitable for the preparation of devices, or not enough homogeneous, making it impossible to evaluate the thickness. In particular, we noted that the new HTM, though highly soluble in chlorinated solvents, do not give appreciable quality film if deposited from solutions in chlorobenzene or chloroform. Another surprisingly feature seems to be that the thickness of the new hydrazone based HTM is not dependent by the spin coating parameters. To reduce the thickness of such films is therefore necessary to reduce the concentration of the solution of the precursor, leading to inhomogeneous films.

Table 3. 5: Deposition parameters and thickness of spin-coated films of new hydrazone based HTM compared to Spiro-OMeTAD.

Chapter 3

sample ^a	solvent	speed	time	thickness
		[rpm]	[sec]	[nm]
Spiro-OmeTAD	PhCl	4000	30	120
	PhCl	2000	30	180
	PhCl	1000	30	300
Ph ₂ -P-Ph ₂	toluene	6000	30	95 - 100
	toluene	4000	30	95 - 110
	toluene	2000	30	95 - 110
Ph ₂ -T-Ph ₂	toluene	6000	30	110 - 130
	toluene	4000	30	120 - 130
	toluene	2000	30	130 - 140
Me ₂ -T-Me ₂	toluene	6000	30	110 - 120
	toluene	4000	30	120 - 130
	toluene	2000	30	120 - 140
Ph-T-Ph	toluene	6000	30	110 - 130
	toluene	4000	30	130 - 140
	toluene	2000	30	130 - 140

^a 60 mM solution in the corresponding solvent. Films deposited on glass

With these data in mind, we tried to measure the mobility of these HTM materials and compare it with the one of the spiro-OMeTAD. We prepared some OFET in configuration bottom gate, bottom contact with a channel

length of $L = 1$ cm and different channel width $W = 2.5, 5, 10, 20$ μm , respectively. The surface of the devices have been previously treated with a solution of Octadecyltrichlorosilane (OTS) in toluene to make it hydrophobic and allow a better contact with the HTMs. The saturation mobility (μ_s) values were extracted

from the slope of the plot in ,⁸⁸ with an applied drain-source voltage $V_{DS} = -40$ V on a $W = 2.5$ μm device.

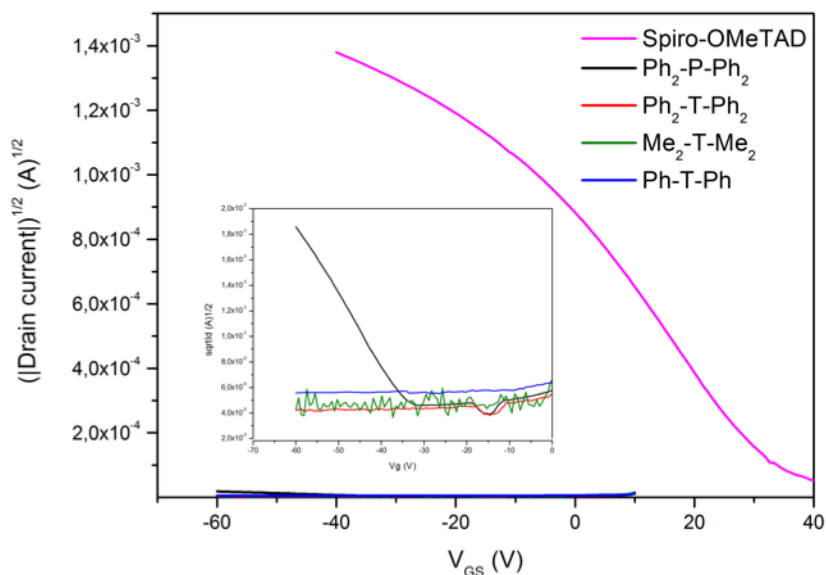


Figure 3.35: Square root of the absolute value of the drain current $(|I_{DS}|)^{1/2}$ as a function of gate voltage (for the $W = 2.5$ μm devices. (Inset) Enlargements of the new HTM region.

The calculated value of μ_s for the spiro-OMeTAD is $(2.4 \pm 0.1) \times 10^{-5}$ $\text{cm}^2/\text{V}\cdot\text{s}$. This value is lower to the best values reported in literature for this molecule but still comparable.^{81,88,89} Instead, what emerges from the study of the proposed new HTM, is that the thienyl derivatives did not show a semiconductor behaviour, namely there is not a threshold voltage beyond which begin to conduct charge, therefore for these systems was not possible to calculate a carrier mobility. In the case of the **Ph₂-P-Ph₂** derivative, an appropriate behaviour has been observed, even if with a rather high threshold voltage, and the carrier mobility has then been measured with a value of $\mu_s = (5.5 \pm 0.1) \times 10^{-7}$ $\text{cm}^2/\text{V}\cdot\text{s}$. A so low mobility value is definitely not encouraging. Nevertheless, the carrier mobility is not the only parameter that will have an impact on the performance of a PSC. In literature there are examples of materials with better mobility than the spiro-OMeTAD, underperforming once used in the final devices.⁹⁰

A first set of PI-PSC with the new HTM was made using the procedure presented in the previous section, but without use the Co(III) salt as dopant in the formulation of the HTM. The results are reported in Figure 3. 36 and Table 3. 6.

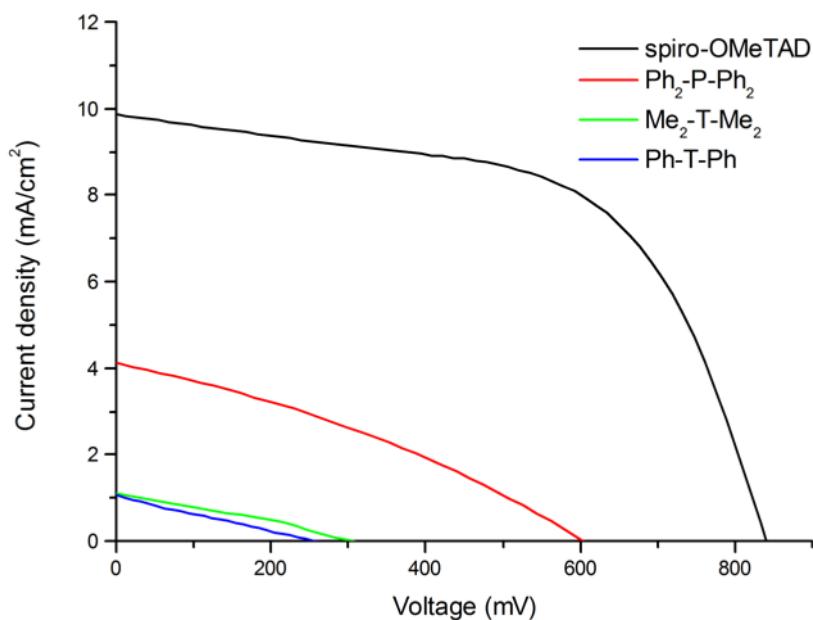


Figure 3. 36: J/V plots measured under full AM1.5 irradiation of PI-PSC cells made using the new HTM materials compared to Spiro-OMeTAD.

As expected, the **Ph₂-T-Ph₂** derivative did not exhibit any efficiency when used in combination with a MAPbI₃ perovskite because of the small difference in its HOMO level and the one of the perovskite.^{86,87} An extremely low activity has been measured for the other two thienyl based HTM, only the **Ph₂-P-Ph₂** showed a measurable current when used in a PI-PSC device.

Perovskite solar cells

Table 3. 6: Photovoltaic parameters of device prepared using the new HTM compared to Spiro-OMeTAD, under AM 1.5 full illumination.

Sample	J_{sc} [mA cm ⁻²]	V_{oc} [mV]	FF [%]	PCE [%]
Spiro-OMeTAD	9.9	836	58	4.8
Ph ₂ -P-Ph ₂	4.0	601	33	0.8
Ph ₂ -T-Ph ₂	-	-	-	-
Me ₂ -T-Me ₂	1.1	304	29	0.1
Ph-T-Ph	1.1	260	25	0.1

^a Active area 0.10 cm²,

The efficiency showed by the **Ph₂-P-Ph₂** derivative is not so low compared to the one obtained, in the same condition with the traditional spiro-OMeTAD. A such low efficiency registered for the reference device has to be ascribed to the poor environmental condition due to a major system failure in the lab. Indeed, the %RH at the moment of the measurements was too high (> 70%) to ensure safe measurement of the PSC. Further experiments will be performed to better instigate the properties of the **Ph₂-P-Ph₂** novel HTM.

Experimental section

GENERAL INFORMATION

NMR spectra were recorded with a Bruker AMX-500 spectrometer operating at 500.13 MHz (^1H) and 125.77 MHz (^{13}C). Coupling constants are given in Hz. Absorption spectra were recorded with a V-570 Jasco spectrophotometer. Infrared spectra (IR) were recorded with an ATR-FTIR Perkin–Elmer Spectrum100 spectrometer. Flash chromatography was performed with Merck grade 9385 silica gel 230–400 mesh (60 Å). Reactions performed under inert atmosphere were done in oven-dried glassware and a nitrogen atmosphere was generated with Schlenk technique. Conversion was monitored by thin-layer chromatography by using UV light (254 and 365 nm) as a visualizing agent. All reagents were obtained from commercial suppliers at the highest purity grade and used without further purification. Anhydrous solvents were purchased from Sigma-Aldrich and used without further purification. Extracts were dried with Na_2SO_4 and filtered before removal of the solvent by evaporation. Absorption spectra were recorded on a V-570 Jasco spectrophotometer.

FTO-coated glass plates (2.2 mm thick; sheet resistance ~ 7 ohm per square; Solaronix), Dyesol 18NR-T active 20-nm transparent TiO_2 paste, Dyesol BL-1 Blocking Layer paste, Titanium diisopropoxide bis(acetylacetonate) 75% wt. in isopropanol (Sigma Aldrich), Lead(II) iodide 99.999% trace metals basis, perovskite grade (Sigma Aldrich), Titanium(IV) isopropoxide (Sigma Aldrich), acetylacetone (Sigma Aldrich), Methylammonium iodide (Solaronix) and Silver nanowires (diam. \times L 60 nm \times 10 μm), 0.5% (isopropyl alcohol suspension) (Sigma Aldrich), spiro-MeOTAD (Sigma Aldrich and Solaronix), 4-tert-butylpyridine (Sigma Aldrich), lithium bis(trifluoromethylsulphonyl) imide (Sigma Aldrich), tris(2-(1H-pyrazol-1-yl)-4-tert-butylpyridine)cobalt(III) bis(trifluoromethylsulphonyl) FK102 (Dyesol), silver (Alfa Aesar) and all the solvents have been purchased from commercial.

ELECTROCHEMICAL CHARACTERIZATION

Pulsed Voltammetry (DPV) and Cyclic Voltammetry (CV) were carried out at scan rate of 20 and 50 mV/s, respectively, using a PARSTA2273 potentiostat in a two compartments, three electrode electrochemical cell in a glove box filled with N₂ ([O₂] and [H₂O] ≤ 0.1 ppm). The working, counter, and the pseudo-reference electrodes were a glassy carbon pin, a Pt flag and an Ag/AgCl wire, respectively. The working electrodes discs were well polished with alumina 0.1 μm suspension, sonicated for 15 min in deionized water, washed with 2-propanol, and cycled for 50 times in 0.5 M H₂SO₄ before use. The Ag/AgCl pseudo-reference electrode was calibrated, by adding ferrocene (10⁻³ M) to the test solution after each measurement.

Oxidation potential values were determined using DPV traces by following the reference methods reported in the literature.⁹¹ For mono-electronic well defined current wave, the potentials were calculated by the peak position. In the presence of overlapping peaks due to molecular additional oxidations potential values were calculated using the current onsets of the oxidation processes for both the standard (ferrocene) and the molecules.

For the characterization of the blocking layer. The working electrode was the sample, the counter a Pt net and the reference was SCE electrode. The electrolyte solution was 0.5 mM K₄Fe(CN)₆ + 0.5 mM K₃Fe(CN)₆ in aqueous 0.5 M KCl, pH 2.5, corrected with aqueous HCl. Scan rate 50 mV/s.

DEVICE FABRICATION

Ms-PSC have been prepared adapting a procedure reported in literature.⁴⁶ In order to exclude metal contamination all of the containers were in glass or Teflon and were treated with EtOH and 10% HCl prior to use. Plastic spatulas and tweezers have been used throughout the procedure. FTO glass plates etched with a Nd(YAG) laser to remove the FTO layer where needed. Then the substrates were

cleaned in a detergent solution for 15 min using an ultrasonic bath, rinsed with pure water and EtOH. The substrates were coated with a TiO₂ compact layer by aerosol spray pyrolysis of a solution titanium diisopropoxide bis (acetylacetonate) diluted 1:10 in EtOH on a hot plate at 450 °C (20 step for ~ 30 nm). A 450-nm-thick mesoporous TiO₂ layer composed of 20-nm-sized particles was then deposited by spin coating using a commercial paste (Dyesol 18NR-T diluted in EtOH 2:7 *w/w*, 5000 rpm, 30 s), and then sintered at 450 °C for 15 min. The mesoporous TiO₂ films were infiltrated with PbI₂ by spin-coating (6500 rpm, 30 s) with a PbI₂ solution in DMF (462 mg mL⁻¹) that was kept at 70 °C. After drying at 70 °C for 30 min, the films were allowed to cool down to room temperature and dipped in a solution of MAI in 2-propanol (10 mg mL⁻¹) for 20 to 60 s and rinsed with 2-propanol. After drying at 70 °C for 30 min, the films were allowed to cool down to room temperature and the HTM was deposited by spin-coating (2000 rpm, 30 s) using a solution of spiro-MeOTAD (72.3 mg/mL), 4-tert-butylpyridine (28.8 μL/mL), 17.5 μL of a solution of lithium bis(trifluoromethylsulphonyl) imide (520 mg/mL in acetonitrile) and 29 μL of a solution of tris(2-(1H-pyrazol-1-yl)-4-tert-butylpyridine)cobalt(III) bis(trifluoromethylsulphonyl) imide (300 mg/mL in acetonitrile) in chlorobenzene. Silver (120 nm) was thermally evaporated (~ 10⁻⁶ mbar) on top of the device to form the back contact.

PI-PSC have been prepared adapting a procedure reported in literature.⁵¹ In order to exclude metal contamination all of the containers were in glass or Teflon and were treated with EtOH and 10% HCl prior to use. Plastic spatulas and tweezers have been used throughout the procedure. FTO glass plates etched with a Nd(YAG) laser to remove the FTO layer where needed. Then the substrates were cleaned in a detergent solution for 15 min using an ultrasonic bath, rinsed with pure water and EtOH. The substrates were coated with a TiO₂ compact layer by aerosol spray pyrolysis of a solution titanium diisopropoxide bis (acetylacetonate) diluted 1:10 in EtOH on a hot plate at 450 °C (20 step for ~ 30 nm). A solution consisting of PbI₂ (1.25 M) and MAI (1.25 M) in DMF was deposited by spin-

coating (5000 rpm, 15 sec) onto the substrate. After ~ 5 seconds 100 μL of chlorobenzene was added on top of the spinning substrate and afterwards the substrates were placed on a hotplate (100 $^{\circ}\text{C}$ for 10 min). The films were allowed to cool down to room temperature and the HTM was deposited by spin-coating (2000 rpm, 30 s) using a solution of spiro-MeOTAD (72.3 mg/mL), 4-tert-butylpyridine (28.8 $\mu\text{L}/\text{mL}$), 17.5 μL of a solution of lithium bis(trifluoromethylsulphonyl) imide (520 mg/mL in acetonitrile) and 29 μL of a solution of tris(2-(1H-pyrazol-1-yl)-4-tert-butylpyridine)cobalt(III) bis(trifluoromethylsulphonyl) imide (300 mg/mL in acetonitrile) in chlorobenzene. Silver (120 nm) was thermally evaporated ($\sim 10^{-6}$ mbar) on top of the device to form the back contact.

Semitransparent PI-PSC: The cells have been prepared according to the procedure described above. As transparent contact, Silver nanowires (diam. \times L 60 nm \times 10 μm), 0.5% (isopropyl alcohol suspension) have been used. The suspension has been deposited onto a PTFE foil kept at 100 $^{\circ}\text{C}$ by spray coating (0.5 mL/cm²) and then, after cooling down to room temperature, mechanically transferred on the HTM layer of the cells with a mask (PTFE foil) to define the area.

DEVICE CHARACTERIZATION

Photovoltaic measurements of PSCs were carried out with or without black mask on top of the photoanode of 0.10 cm² surface area under a 500 W Xenon light source. The power of the simulated light was calibrated to AM 1.5 (100 mW cm⁻²) using a reference Si cell photodiode equipped with an IR-cutoff filter (KG-5) to reduce the mismatch in the region of 350-750 nm between the simulated light and the AM 1.5 spectrum. Values were recorded after 24 h of ageing in the dark in a dry cabinet (10-30% RH) applying a polarization ($V \approx 50 \text{ mV} < V_{oc}$) under illumination before the measurements, till stable photocurrent.

OFET FABRICATION

The silicon based patterned commercial bottom gate-bottom contact transistor substrate has been washed with acetone to remove the protective coating on the surface. Then, it has been treated in a UV-O₃ ozone cleaner for 30 min and moved to a nitrogen filled glove box. A layer of Octadecyltrichlorosilane (OTS) has been deposited after dipping the substrate in a solution of OTS in toluene (4 μL/mL) for 1 min., then rinsed with toluene, hexane and IPA. A solution of the precursor of the HTM in the proper solvent (see text) has been spin coated on the previously treated substrate and then dried in air for 4 h at room temperature in the dark.

Electrical characterization was carried out in vacuum (10⁻⁶ mbar) using an Agilent 4155C semiconductor parameter analyzer.

SYNTHESIS

The 1-(2-Ethylhexyl)-1H-pyrrole-2-carbaldehyde,⁸⁴ and 3-4-dibutoxythiophene-2,5-bisaldehyde⁸⁵ have been prepared according to literature.

(E)-1,2-bis(1-(2-ethylhexyl)-1H-pyrrol-2-yl)ethene (1). Zn (5.18 g, 79.0 mmol) was suspended in anhydrous THF (100 mL) and the suspension was cooled to -20 °C. TiCl₄ (7.50 g, 39.6 mmol) was added dropwise (formation of a yellow precipitate was observed). The suspension was heated to reflux for 30 min (gradual darkening was observed). The mixture was cooled to -15 °C and a solution of 1-(2-Ethylhexyl)-1H-pyrrole-2-carbaldehyde (4.10 g, 19.8 mmol) and anhydrous pyridine (4.10 g, 51.5 mmol) in anhydrous THF (50 mL) was added dropwise. The resulting suspension was heated to reflux for 2 h and then poured into a 3:2 mixture of water and CH₂Cl₂ (200 mL). The dark suspension was filtered through a pad of Celite. The organic phase was separated, extracted with water (3 x 50 mL), dried, and the solvent evaporated under reduced pressure to yield the pure product as a yellow solid (2.98 g, 7.8 mmol, 79%). ¹H NMR (500 MHz, CDCl₃) δ 7.33 (d, *J* = 4.3 Hz, 2H), 6.99 (s, 2H), 6.65 (d, *J* = 4.3 Hz, 2H), 6.15 (t, *J* = 4.5 Hz, 2H), 4.38 (d, *J* = 7.0 Hz, 4H), 1.73 (quintet, *J* = 6.5 Hz, 2H), 1.35 – 1.16 (m, 8H), 0.91 – 0.80 (m, 6H).

(E)-5,5'-(ethene-1,2-diyl)bis(1-(2-ethylhexyl)-1H-pyrrole-2-carbaldehyde) (2).

Anhydrous DMF (0.22 mL, 2.9 mmol) was added dropwise to freshly distilled POCl₃ (0.26 mL, 2.9 mmol) at 0 °C under nitrogen. The resulting solution was stirred at 0 °C for 15 min and a glassy white solid was obtained, which was taken up with anhydrous CH₃CN (10 mL). A solution of **1** (0.50 mg, 1.3 mmol) in anhydrous CH₃CN (30 mL) was added dropwise, and the resulting mixture was stirred at room temperature for 20 h. The mixture was then poured into aqueous K₂CO₃ (10%, 300 mL) and stirred for 1 h. After adding AcOEt (300 mL), the organic layer was separated, washed with brine (3 x 100 mL), dried, and the solvent was evaporated to dryness. The residue was submitted to flash chromatography (petroleum ether/ AcOEt, 7:3) to afford the pure compound as a orange oil (0.52 g, 1.2 mmol, 92%). ¹H NMR (500 MHz, CDCl₃) δ 9.49 (s, 2H), 6.97 (s, 2H), 6.93 (d, *J* = 4.3 Hz, 2H), 6.57 (d, *J* = 4.3 Hz, 2H), 4.38 (d, *J* = 7.0 Hz, 4H), 1.73 (quintet, *J* = 6.5 Hz, 2H), 1.35 – 1.16 (m, 8H), 0.91 – 0.80 (m, 6H). ¹³C NMR (126 MHz, CDCl₃) δ 178.77, 140.52, 133.16, 125.13, 118.85, 108.16, 48.86, 41.43, 30.37, 28.60, 23.76, 22.94, 13.91, 10.88.

(E)-1,2-bis(5-((E)-(2,2-diphenylhydrazono)methyl)-1-(2-ethylhexyl)-1H-pyrrol-2-yl)ethene (Ph₂-P-Ph₂).

A solution of *N,N*-diphenyl hydrazine hydrochloride (441 mg, 2.0 mmol) in anhydrous THF (10 mL) was added to a solution of **2** (430 mg, 1.0 mmol) in the same solvent under nitrogen, and stirred for 20 h at room temperature. The volume of the reaction mixture was reduced to ¼ and then poured in a saturates aqueous solution of K₂CO₃ (100 mL). CH₂Cl₂ (50 mL) was added, the organic layer was separated, dried, and the solvent was evaporated to dryness. The residue was dissolved in CH₂Cl₂ and precipitated with hexane to give the pure product as a dark orange solid (610 mg, 0.79 mmol, 79%). ¹H NMR (500 MHz, CDCl₃) δ 7.41 (t, *J* = 7.9 Hz, 8H), 7.20 – 7.12 (m, 12H), 6.78 (s, 2H), 6.45 (d, *J* = 4.0 Hz, 2H), 6.37 (d, *J* = 4.0 Hz, 2H), 4.28 (p, *J* = 14.6 Hz, 4H), 1.76 (d, *J* = 6.1 Hz, 2H), 1.33 – 1.13 (m, 8H), 0.94 – 0.76 (m, 6H). ¹³C NMR

(126 MHz, CDCl₃) δ 143.80, 135.97, 130.50, 130.38, 129.74, 124.07, 122.50, 115.39, 113.04, 106.44, 48.34, 41.20, 30.51, 28.68, 23.72, 23.11, 14.02, 11.00.

(2E,2'E)-2,2'-((3,4-dibutoxythiophene-2,5-diyl)bis(methanylylidene))bis(1,1-diphenylhydrazine) (Ph₂-T-Ph₂). A solution of *N,N*-diphenyl hydrazine hydrochloride (1015 mg, 4.6 mmol) in anhydrous THF (20 mL) was added to a solution of dibutoxythiophene-2,5-bisaldhyde (670 mg, 2.3 mmol) in the same solvent under nitrogen, and stirred for 20 h at room temperature. The volume of the reaction mixture was reduced to 1/4 and then poured in a saturates aqueous solution of K₂CO₃ (100 mL). CH₂Cl₂ (80 mL) was added, the organic layer was separated, dried, and the solvent was evaporated to dryness. The residue was dissolved in CH₂Cl₂ and precipitated with hexane to give the pure product as a light brown solid (1210 mg, 1.96 mmol, 85%). ¹H NMR (500 MHz, CDCl₃) δ 7.36 (t, *J* = 7.7 Hz, 8H), 7.13 (dd, *J* = 13.0, 7.5 Hz, 12H), 3.76 (t, *J* = 6.2 Hz, 4H), 1.42 – 1.33 (m, 4H), 1.10 (dq, *J* = 14.6, 7.2 Hz, 4H), 0.75 (t, *J* = 7.3 Hz, 6H). ¹³C NMR (126 MHz, CDCl₃) δ 147.77, 143.42, 130.00, 129.85, 128.42, 124.60, 123.92, 122.51, 73.74, 31.80, 19.06, 13.86.

(2E,2'E)-2,2'-((3,4-dibutoxythiophene-2,5-diyl)bis(methanylylidene))bis(1-phenylhydrazine) (Ph-T-Ph). A solution of *N*-phenyl hydrazine (0.50 mg, 4.6 mmol) in anhydrous THF (20 mL) was added to a solution of dibutoxythiophene-2,5-bisaldhyde (670 mg, 2.3 mmol) in the same solvent under nitrogen. PTSA (0.87 mg, 4.6 mmol) was then added as solid and stirred for 20 h at room temperature. The volume of the reaction mixture was reduced to 1/4 and then poured in a saturates aqueous solution of K₂CO₃ (100 mL). CH₂Cl₂ (80 mL) was added, the organic layer was separated, dried, and the solvent was evaporated to dryness. The residue was dissolved in CH₂Cl₂ and precipitated with hexane to give the pure product as a light brown solid (598 mg, 1.29 mmol, 56%). ¹H NMR (500 MHz, CDCl₃) δ 7.32 – 7.25 (t, *J* = 8.0 Hz, 4H), 7.10 (d, *J* = 7.8 Hz, 4H), 6.87 (s, 2H), 5.30 (s, 2H), 4.05 (t, *J* = 6.6 Hz, 4H), 1.73 (dt, *J* = 14.5, 6.7 Hz, 4H), 1.53 –

1.44 (m, 4H), 1.02 – 0.95 (m, 6H). ^{13}C NMR (126 MHz, CDCl_3) δ 149.77, 141.92, 131.07, 129.95, 128.53, 126.40, 123.22, 121.51, 73.74, 31.80, 19.06, 13.86.

(2E,2'E)-2,2'-((3,4-dibutoxythiophene-2,5-diyl)bis(methanylylidene))bis(1,1-dimethylhydrazine) ($\text{Me}_2\text{-T-Me}_2$). A solution of *N,N*-dimethyl hydrazine (0.35 mL, 4.6 mmol) in anhydrous THF (20 mL) was added to a solution of dibutoxythiophene-2,5-bisaldhyde (670 mg, 2.3 mmol) in the same solvent under nitrogen. PTSA (0.87 mg, 4.6 mmol) was then added as solid and stirred for 20 h at room temperature. The volume of the reaction mixture was reduced to $\frac{1}{4}$ and then poured in a saturates aqueous solution of K_2CO_3 (100 mL). CH_2Cl_2 (80 mL) was added, the organic layer was separated, dried, and the solvent was evaporated to dryness. The residue was dissolved in CH_2Cl_2 and precipitated with hexane to give the pure product as a light brown solid (652 mg, 1.77 mmol, 77%). ^1H NMR (500 MHz, CDCl_3) δ 3.99 (t, $J = 6.6$ Hz, 4H), 2.90 (s, 12H), 1.68 (m, 4H), 1.47 (dt, $J = 14.9, 7.4$ Hz, 4H), 0.95 (t, $J = 7.4$ Hz, 6H). ^{13}C NMR (126 MHz, CDCl_3) δ 146.11, 125.48, 123.49, 73.59, 43.25, 42.84, 31.99, 19.15, 13.86.

References

- (1) Winston Churchill. (n.d). BrainyQuote.com. Retrieved December 5, 2016, from BrainyQuote.com Web site: <https://www.brainyquote.com/quotes/quotes/w/winstonchu124653.html>
- (2) Di Giacomo, F.; Fakharuddin, A.; Jose, R.; Brown, T. M. "Progress, challenges and perspectives in flexible perovskite solar cells". *Energy Environ. Sci.* **2016**, *9*, 3007-3035, doi:10.1039/C6EE01137C.
- (3) Elumalai, N.; Mahmud, M.; Wang, D.; Uddin, A. "Perovskite Solar Cells: Progress and Advancements". *Energies* **2016**, *9*, 861.
- (4) Kim, H.-S.; Seo, J.-Y.; Park, N.-G. "Material and Device Stability in Perovskite Solar Cells". *ChemSusChem* **2016**, *9*, 2528-2540, doi:10.1002/cssc.201600915.
- (5) Mitzi, D. B.; Feild, C. A.; Harrison, W. T. A.; Guloy, A. M. "Conducting tin halides with a layered organic-based perovskite structure". *Nature* **1994**, *369*, 467-469.
- (6) Jung, H. S.; Park, N.-G. "Perovskite Solar Cells: From Materials to Devices". *Small* **2015**, *11*, 10-25, doi:10.1002/smll.201402767.
- (7) Green, M. A.; Ho-Baillie, A.; Snaith, H. J. "The emergence of perovskite solar cells". *Nat Photonics* **2014**, *8*, 506-514, doi:Doi 10.1038/Nphoton.2014.134.
- (8) Gao, P.; Gratzel, M.; Nazeeruddin, M. K. "Organohalide lead perovskites for photovoltaic applications". *Energy Environ. Sci.* **2014**, *7*, 2448-2463, doi:Doi 10.1039/C4ee00942h.
- (9) Jeon, N. J.; Noh, J. H.; Kim, Y. C.; Yang, W. S.; Ryu, S.; Il Seol, S. "Solvent engineering for high-performance inorganic-organic hybrid perovskite solar cells". *Nature Materials* **2014**, *13*, 897-903, doi:Doi 10.1038/Nmat4014.
- (10) Shi, S.; Li, Y.; Li, X.; Wang, H. "Advancements in all-solid-state hybrid solar cells based on organometal halide perovskites". *Materials Horizons* **2015**, *2*, 378-405, doi:10.1039/C4MH00236A.
- (11) Deschler, F.; Price, M.; Pathak, S.; Klintberg, L. E.; Jarausch, D.-D.; Higler, R.; Hüttner, S.; Leijtens, T.; Stranks, S. D.; Snaith, H. J.; Atatüre, M.; Phillips, R. T.; Friend, R. H. "High Photoluminescence Efficiency and Optically Pumped Lasing in Solution-Processed Mixed Halide Perovskite Semiconductors". *J. Phys. Chem. Lett.* **2014**, *5*, 1421-1426, doi:10.1021/jz5005285.

(12) Wehrenfennig, C.; Liu, M.; Snaith, H. J.; Johnston, M. B.; Herz, L. M. "Homogeneous Emission Line Broadening in the Organo Lead Halide Perovskite CH₃NH₃PbI_{3-x}Cl_x". *J. Phys. Chem. Lett.* **2014**, *5*, 1300-1306, doi:10.1021/jz500434p.

(13) Xing, G.; Mathews, N.; Lim, S. S.; Yantara, N.; Liu, X.; Sabba, D.; Grätzel, M.; Mhaisalkar, S.; Sum, T. C. "Low-temperature solution-processed wavelength-tunable perovskites for lasing". *Nat Mater* **2014**, *13*, 476-480, doi:10.1038/nmat3911

<http://www.nature.com/nmat/journal/v13/n5/abs/nmat3911.html> - [supplementary-information](#).

(14) Tan, Z.-K.; Moghaddam, R. S.; Lai, M. L.; Docampo, P.; Higler, R.; Deschler, F.; Price, M.; Sadhanala, A.; Pazos, L. M.; Credgington, D.; Hanusch, F.; Bein, T.; Snaith, H. J.; Friend, R. H. "Bright light-emitting diodes based on organometal halide perovskite". *Nat Nano* **2014**, *9*, 687-692, doi:10.1038/nnano.2014.149

<http://www.nature.com/nnano/journal/v9/n9/abs/nnano.2014.149.html> - [supplementary-information](#).

(15) Hoye, R. L. Z.; Chua, M. R.; Musselman, K. P.; Li, G.; Lai, M.-L.; Tan, Z.-K.; Greenham, N. C.; MacManus-Driscoll, J. L.; Friend, R. H.; Credgington, D. "Enhanced Performance in Fluorene-Free Organometal Halide Perovskite Light-Emitting Diodes using Tunable, Low Electron Affinity Oxide Electron Injectors". *Adv. Mater.* **2015**, *27*, 1414-1419, doi:10.1002/adma.201405044.

(16) Li, G.; Tan, Z.-K.; Di, D.; Lai, M. L.; Jiang, L.; Lim, J. H.-W.; Friend, R. H.; Greenham, N. C. "Efficient Light-Emitting Diodes Based on Nanocrystalline Perovskite in a Dielectric Polymer Matrix". *Nano Lett.* **2015**, *15*, 2640-2644, doi:10.1021/acs.nanolett.5b00235.

(17) Wang, J.; Wang, N.; Jin, Y.; Si, J.; Tan, Z.-K.; Du, H.; Cheng, L.; Dai, X.; Bai, S.; He, H.; Ye, Z.; Lai, M. L.; Friend, R. H.; Huang, W. "Interfacial Control Toward Efficient and Low-Voltage Perovskite Light-Emitting Diodes". *Adv. Mater.* **2015**, *27*, 2311-2316, doi:10.1002/adma.201405217.

(18) Sadhanala, A.; Kumar, A.; Pathak, S.; Rao, A.; Steiner, U.; Greenham, N. C.; Snaith, H. J.; Friend, R. H. "Electroluminescence from Organometallic Lead Halide Perovskite-Conjugated Polymer Diodes". *Advanced Electronic Materials* **2015**, *1*, 1500008-n/a, doi:10.1002/aelm.201500008.

(19) Snaith, H. J. "Perovskites: The Emergence of a New Era for Low-Cost, High-Efficiency Solar Cells". *J. Phys. Chem. Lett.* **2013**, *4*, 3623-3630, doi:10.1021/jz4020162.

- (20) Dong, Q.; Fang, Y.; Shao, Y.; Mulligan, P.; Qiu, J.; Cao, L.; Huang, J. "Electron-hole diffusion lengths > 175 μm in solution-grown $\text{CH}_3\text{NH}_3\text{PbI}_3$ single crystals". *Science* **2015**, *347*, 967-970, doi:10.1126/science.aaa5760.
- (21) Stranks, S. D.; Eperon, G. E.; Grancini, G.; Menelaou, C.; Alcocer, M. J. P.; Leijtens, T.; Herz, L. M.; Petrozza, A.; Snaith, H. J. "Electron-Hole Diffusion Lengths Exceeding 1 Micrometer in an Organometal Trihalide Perovskite Absorber". *Science* **2013**, *342*, 341-344, doi:10.1126/science.1243982.
- (22) Lee, M. M.; Teuscher, J.; Miyasaka, T.; Murakami, T. N.; Snaith, H. J. "Efficient Hybrid Solar Cells Based on Meso-Superstructured Organometal Halide Perovskites". *Science* **2012**, *338*, 643-647, doi:10.1126/science.1228604.
- (23) Park, N.-G. "Organometal Perovskite Light Absorbers Toward a 20% Efficiency Low-Cost Solid-State Mesoscopic Solar Cell". *J. Phys. Chem. Lett.* **2013**, *4*, 2423-2429, doi:10.1021/jz400892a.
- (24) Grätzel, M. "The light and shade of perovskite solar cells". *Nature Materials* **2014**, *13*, 838-842.
- (25) Green, M. A.; Emery, K.; Hishikawa, Y.; Warta, W.; Dunlop, E. D. "Solar cell efficiency tables (version 47)". *Prog. Photovolt: Res. Appl.* **2016**, *24*, 3-11, doi:10.1002/pip.2728.
- (26) Kojima, A.; Teshima, K.; Shirai, Y.; Miyasaka, T. "Organometal Halide Perovskites as Visible-Light Sensitizers for Photovoltaic Cells". *J. Am. Chem. Soc.* **2009**, *131*, 6050-6051, doi:10.1021/ja809598r.
- (27) Kim, H.-S.; Lee, C.-R.; Im, J.-H.; Lee, K.-B.; Moehl, T.; Marchioro, A.; Moon, S.-J.; Humphry-Baker, R.; Yum, J.-H.; Moser, J. E.; Grätzel, M.; Park, N.-G. "Lead Iodide Perovskite Sensitized All-Solid-State Submicron Thin Film Mesoscopic Solar Cell with Efficiency Exceeding 9%". *Sci Rep-Uk* **2012**, *2*, 591, doi:10.1038/srep00591
<http://www.nature.com/articles/srep00591-supplementary-information>.
- (28) Li, X.; Bi, D.; Yi, C.; Décoppet, J.-D.; Luo, J.; Zakeeruddin, S. M.; Hagfeldt, A.; Grätzel, M. "A vacuum flash-assisted solution process for high-efficiency large-area perovskite solar cells". *Science* **2016**, doi:10.1126/science.aaf8060.
- (29) Green, M. A.; Bein, T. "Photovoltaics: Perovskite cells charge forward". *Nat Mater* **2015**, *14*, 559-561, doi:10.1038/nmat4301.

(30) Sum, T. C.; Mathews, N. "Advancements in perovskite solar cells: photophysics behind the photovoltaics". *Energy Environ. Sci.* **2014**, *7*, 2518-2534, doi:10.1039/C4EE00673A.

(31) Heo, J. H.; Im, S. H.; Noh, J. H.; Mandal, T. N.; Lim, C.-S.; Chang, J. A.; Lee, Y. H.; Kim, H.-j.; Sarkar, A.; Nazeeruddin, K.; Gratzel, M.; Seok, S. I. "Efficient inorganic-organic hybrid heterojunction solar cells containing perovskite compound and polymeric hole conductors". *Nat Photon* **2013**, *7*, 486-491, doi:10.1038/nphoton.2013.80

<http://www.nature.com/nphoton/journal/v7/n6/abs/nphoton.2013.80.html> - [supplementary information.](#)

(32) Salim, T.; Sun, S.; Abe, Y.; Krishna, A.; Grimsdale, A. C.; Lam, Y. M. "Perovskite-based solar cells: impact of morphology and device architecture on device performance". *J. Mater. Chem. A* **2015**, *3*, 8943-8969, doi:10.1039/C4TA05226A.

(33) McGehee, M. D. "Perovskite solar cells: Continuing to soar". *Nat Mater* **2014**, *13*, 845-846, doi:10.1038/nmat4050.

(34) Im, J.-H.; Lee, C.-R.; Lee, J.-W.; Park, S.-W.; Park, N.-G. "6.5% efficient perovskite quantum-dot-sensitized solar cell". *Nanoscale* **2011**, *3*, 4088-4093, doi:10.1039/C1NR10867K.

(35) Mailoa, J. P.; Bailie, C. D.; Johlin, E. C.; Hoke, E. T.; Akey, A. J.; Nguyen, W. H.; McGehee, M. D.; Buonassisi, T. "A 2-terminal perovskite/silicon multijunction solar cell enabled by a silicon tunnel junction". *ApPhL* **2015**, *106*, 121105, doi:doi:<http://dx.doi.org/10.1063/1.4914179>.

(36) Bailie, C. D.; Christoforo, M. G.; Mailoa, J. P.; Bowring, A. R.; Unger, E. L.; Nguyen, W. H.; Burschka, J.; Pellet, N.; Lee, J. Z.; Gratzel, M.; Noufi, R.; Buonassisi, T.; Salleo, A.; McGehee, M. D. "Semi-transparent perovskite solar cells for tandems with silicon and CIGS". *Energy Environ. Sci.* **2015**, *8*, 956-963, doi:10.1039/C4EE03322A.

(37) Loper, P.; Moon, S.-J.; Martin de Nicolas, S.; Niesen, B.; Ledinsky, M.; Nicolay, S.; Bailat, J.; Yum, J.-H.; De Wolf, S.; Ballif, C. "Organic-inorganic halide perovskite/crystalline silicon four-terminal tandem solar cells". *Phys. Chem. Chem. Phys.* **2015**, *17*, 1619-1629, doi:10.1039/C4CP03788J.

(38) Albrecht, S.; Saliba, M.; Correa Baena, J. P.; Lang, F.; Kegelmann, L.; Mews, M.; Steier, L.; Abate, A.; Rappich, J.; Korte, L.; Schlattmann, R.; Nazeeruddin, M. K.; Hagfeldt, A.; Gratzel, M.; Rech, B. "Monolithic perovskite/silicon-heterojunction tandem solar cells processed at low temperature". *Energy Environ. Sci.* **2016**, *9*, 81-88, doi:10.1039/C5EE02965A.

(39) Bailie, C. D.; McGehee, M. D. "High-efficiency tandem perovskite solar cells". *MRS Bull.* **2015**, *40*, 681-686, doi:doi:10.1557/mrs.2015.167.

(40) Luo, S.; Daoud, W. A. "Recent progress in organic-inorganic halide perovskite solar cells: mechanisms and material design". *J. Mater. Chem. A* **2015**, doi:10.1039/C4TA04953E.

(41) Peng, B.; Jungmann, G.; Jäger, C.; Haarer, D.; Schmidt, H.-W.; Thelakkat, M. "Systematic investigation of the role of compact TiO₂ layer in solid state dye-sensitized TiO₂ solar cells". *Coord. Chem. Rev.* **2004**, *248*, 1479-1489, doi:<http://dx.doi.org/10.1016/j.ccr.2004.02.008>.

(42) Yongzhen, W.; Xudong, Y.; Han, C.; Kun, Z.; Chuanjiang, Q.; Jian, L.; Wenqin, P.; Ashraful, I.; Enbing, B.; Fei, Y.; Maoshu, Y.; Peng, Z.; Liyuan, H. "Highly compact TiO₂ layer for efficient hole-blocking in perovskite solar cells". *Applied Physics Express* **2014**, *7*, 052301.

(43) Kavan, L.; Tétreault, N.; Moehl, T.; Grätzel, M. "Electrochemical Characterization of TiO₂ Blocking Layers for Dye-Sensitized Solar Cells". *J. Phys. Chem. C* **2014**, *118*, 16408-16418, doi:10.1021/jp4103614.

(44) Moehl, T.; Im, J. H.; Lee, Y. H.; Domanski, K.; Giordano, F.; Zakeeruddin, S. M.; Dar, M. I.; Heiniger, L.-P.; Nazeeruddin, M. K.; Park, N.-G.; Grätzel, M. "Strong Photocurrent Amplification in Perovskite Solar Cells with a Porous TiO₂ Blocking Layer under Reverse Bias". *J. Phys. Chem. Lett.* **2014**, *5*, 3931-3936, doi:10.1021/jz502039k.

(45) Yang, L.; Cappel, U. B.; Unger, E. L.; Karlsson, M.; Karlsson, K. M.; Gabrielsson, E.; Sun, L.; Boschloo, G.; Hagfeldt, A.; Johansson, E. M. J. "Comparing spiro-OMeTAD and P3HT hole conductors in efficient solid state dye-sensitized solar cells". *Phys. Chem. Chem. Phys.* **2012**, *14*, 779-789, doi:10.1039/c1cp23031j.

(46) Burschka, J.; Pellet, N.; Moon, S.-J.; Humphry-Baker, R.; Gao, P.; Nazeeruddin, M. K.; Grätzel, M. "Sequential deposition as a route to high-performance perovskite-sensitized solar cells". *Nature* **2013**, *499*, 316-319, doi:10.1038/nature12340.

(47) Christians, J. A.; Miranda Herrera, P. A.; Kamat, P. V. "Transformation of the Excited State and Photovoltaic Efficiency of CH₃NH₃PbI₃ Perovskite upon Controlled Exposure to Humidified Air". *J. Am. Chem. Soc.* **2015**, *137*, 1530-1538, doi:10.1021/ja511132a.

(48) Eperon, G. E.; Habisreutinger, S. N.; Leijtens, T.; Bruijns, B. J.; van Franeker, J. J.; deQuilettes, D. W.; Pathak, S.; Sutton, R. J.; Grancini, G.; Ginger, D. S.; Janssen, R. A. J.; Petrozza, A.; Snaith, H. J. "The Importance of Moisture in Hybrid Lead

Halide Perovskite Thin Film Fabrication". *ACS Nano* **2015**, *9*, 9380-9393, doi:10.1021/acsnano.5b03626.

(49) Xu, B.; Huang, J.; Ågren, H.; Kloo, L.; Hagfeldt, A.; Sun, L. "AgTFSI as p-Type Dopant for Efficient and Stable Solid-State Dye-Sensitized and Perovskite Solar Cells". *ChemSusChem* **2014**, *7*, 3252-3256, doi:10.1002/cssc.201402678.

(50) Gamliel, S.; Etgar, L. "Organo-metal perovskite based solar cells: sensitized versus planar architecture". *RSC Adv.* **2014**, *4*, 29012-29021, doi:Doi 10.1039/C4ra03981e.

(51) Petrus, M. L.; Bein, T.; Dingemans, T. J.; Docampo, P. "A low cost azomethine-based hole transporting material for perovskite photovoltaics". *J. Mater. Chem. A* **2015**, *3*, 12159-12162, doi:10.1039/C5TA03046C.

(52) Xiao, M. D.; Huang, F. Z.; Huang, W. C.; Dkhissi, Y.; Zhu, Y.; Etheridge, J.; Gray-Weale, A.; Bach, U.; Cheng, Y. B.; Spiccia, L. "A Fast Deposition-Crystallization Procedure for Highly Efficient Lead Iodide Perovskite Thin-Film Solar Cells". *Angew Chem Int Edit* **2014**, *53*, 9898-9903, doi:Doi 10.1002/Anie.201405334.

(53) Krishnamoorthy, T.; Kunwu, F.; Boix, P. P.; Li, H.; Koh, T. M.; Leong, W. L.; Powar, S.; Grimsdale, A.; Grätzel, M.; Mathews, N.; Mhaisalkar, S. G. "A swivel-cruciform thiophene based hole-transporting material for efficient perovskite solar cells". *J. Mater. Chem. A* **2014**, *2*, 6305-6309, doi:10.1039/C4TA00486H.

(54) McMeekin, D. P.; Sadoughi, G.; Rehman, W.; Eperon, G. E.; Saliba, M.; Hörlantner, M. T.; Haghighirad, A.; Sakai, N.; Korte, L.; Rech, B.; Johnston, M. B.; Herz, L. M.; Snaith, H. J. "A mixed-cation lead mixed-halide perovskite absorber for tandem solar cells". *Science* **2016**, *351*, 151-155, doi:10.1126/science.aad5845.

(55) Kranz, L.; Abate, A.; Feurer, T.; Fu, F.; Avancini, E.; Löckinger, J.; Reinhard, P.; Zakeeruddin, S. M.; Grätzel, M.; Buecheler, S.; Tiwari, A. N. "High-Efficiency Polycrystalline Thin Film Tandem Solar Cells". *J. Phys. Chem. Lett.* **2015**, *6*, 2676-2681, doi:10.1021/acs.jpcllett.5b01108.

(56) Yang, Y.; Chen, Q.; Hsieh, Y.-T.; Song, T.-B.; Marco, N. D.; Zhou, H.; Yang, Y. "Multilayer Transparent Top Electrode for Solution Processed Perovskite/Cu(In,Ga)(Se,S)₂ Four Terminal Tandem Solar Cells". *ACS Nano* **2015**, *9*, 7714-7721, doi:10.1021/acsnano.5b03189.

(57) Hodes, G.; Cahen, D. "Perovskite cells roll forward". *Nat Photonics* **2014**, *8*, 87-88.

- (58) Bach, U.; Lupo, D.; Comte, P.; Moser, J. E.; Weissortel, F.; Salbeck, J.; Spreitzer, H.; Grätzel, M. "Solid-state dye-sensitized mesoporous TiO₂ solar cells with high photon-to-electron conversion efficiencies". *Nature* **1998**, *395*, 583-585.
- (59) Christians, J. A.; Fung, R. C. M.; Kamat, P. V. "An Inorganic Hole Conductor for Organo-Lead Halide Perovskite Solar Cells. Improved Hole Conductivity with Copper Iodide". *J. Am. Chem. Soc.* **2014**, *136*, 758-764, doi:10.1021/ja4111014k.
- (60) Ito, S.; Tanaka, S.; Manabe, K.; Nishino, H. "Effects of Surface Blocking Layer of Sb₂S₃ on Nanocrystalline TiO₂ for CH₃NH₃PbI₃ Perovskite Solar Cells". *J. Phys. Chem. C* **2014**, *118*, 16995-17000, doi:10.1021/jp500449z.
- (61) Qin, P.; Tanaka, S.; Ito, S.; Tetreault, N.; Manabe, K.; Nishino, H.; Nazeeruddin, M. K.; Grätzel, M. "Inorganic hole conductor-based lead halide perovskite solar cells with 12.4% conversion efficiency". *Nature Communications* **2014**, *5*, 3834, doi:10.1038/ncomms4834.
- (62) Zhu, Z.; Bai, Y.; Lee, H. K. H.; Mu, C.; Zhang, T.; Zhang, L.; Wang, J.; Yan, H.; So, S. K.; Yang, S. "Polyfluorene Derivatives are High-Performance Organic Hole-Transporting Materials for Inorganic–Organic Hybrid Perovskite Solar Cells". *Adv. Funct. Mater.* **2014**, *24*, 7357-7365, doi:10.1002/adfm.201401557.
- (63) Xu, B.; Sheibani, E.; Liu, P.; Zhang, J.; Tian, H.; Vlachopoulos, N.; Boschloo, G.; Kloo, L.; Hagfeldt, A.; Sun, L. "Carbazole-Based Hole-Transport Materials for Efficient Solid-State Dye-Sensitized Solar Cells and Perovskite Solar Cells". *Adv. Mater.* **2014**, *26*, 6629-6634, doi:10.1002/adma.201402415.
- (64) Li, H.; Fu, K.; Hagfeldt, A.; Grätzel, M.; Mhaisalkar, S. G.; Grimsdale, A. C. "A Simple 3,4-Ethylenedioxythiophene Based Hole-Transporting Material for Perovskite Solar Cells". *Angew. Chem. Int. Ed.* **2014**, *53*, 4085-4088, doi:10.1002/anie.201310877.
- (65) Do, K.; Choi, H.; Lim, K.; Jo, H.; Cho, J. W.; Nazeeruddin, M. K.; Ko, J. "Star-shaped hole transporting materials with a triazine unit for efficient perovskite solar cells". *Chem. Commun.* **2014**, *50*, 10971-10974, doi:Doi 10.1039/C4cc04550e.
- (66) Li, H.; Fu, K.; Boix, P. P.; Wong, L. H.; Hagfeldt, A.; Grätzel, M.; Mhaisalkar, S. G.; Grimsdale, A. C. "Hole-Transporting Small Molecules Based on Thiophene Cores for High Efficiency Perovskite Solar Cells". *ChemSusChem* **2014**, *7*, 3420-3425, doi:10.1002/cssc.201402587.
- (67) Jeon, N. J.; Lee, H. G.; Kim, Y. C.; Seo, J.; Noh, J. H.; Lee, J.; Seok, S. I. "o-Methoxy Substituents in Spiro-OMeTAD for Efficient Inorganic–Organic Hybrid Perovskite Solar Cells". *J. Am. Chem. Soc.* **2014**, *136*, 7837-7840, doi:10.1021/ja502824c.

(68) Saliba, M.; Orlandi, S.; Matsui, T.; Aghazada, S.; Cavazzini, M.; Correa-Baena, J.-P.; Gao, P.; Scopelliti, R.; Mosconi, E.; Dahmen, K.-H.; De Angelis, F.; Abate, A.; Hagfeldt, A.; Pozzi, G.; Graetzel, M.; Nazeeruddin, M. K. "A molecularly engineered hole-transporting material for efficient perovskite solar cells". *Nature Energy* **2016**, 15017, doi:10.1038/nenergy.2015.17

<http://www.nature.com/articles/nenergy201517-supplementary-information>.

(69) Lim, K.; Kang, M.-S.; Myung, Y.; Seo, J.-H.; Banerjee, P.; Marks, T. J.; Ko, J. "Star-shaped hole transport materials with indeno[1,2-b] thiophene or fluorene on a triazine core for efficient perovskite solar cells". *J. Mater. Chem. A* **2016**, doi:10.1039/C5TA07369C.

(70) Ganesan, P.; Fu, K.; Gao, P.; Raabe, I.; Schenk, K.; Scopelliti, R.; Luo, J.; Wong, L. H.; Grätzel, M.; Nazeeruddin, M. K. "A simple spiro-type hole transporting material for efficient perovskite solar cells". *Energy Environ. Sci.* **2015**, *8*, 1986-1991, doi:10.1039/c4ee03773a.

(71) Bui, T.-T.; Shah, S. K.; Abbas, M.; Sallenave, X.; Sini, G.; Hirsch, L.; Goubard, F. "Carbazole-Based Molecular Glasses as Hole-Transporting Materials in Solid State Dye-Sensitized Solar Cells". *ChemNanoMat* **2015**, *1*, 203-210, doi:10.1002/cnma.201500014.

(72) Lazny, R.; Nodzevska, A. "N,N-Dialkylhydrazones in Organic Synthesis. From Simple N,N-Dimethylhydrazones to Supported Chiral Auxiliaries". *Chem. Rev.* **2010**, *110*, 1386-1434, doi:10.1021/cr900067y.

(73) Neha, S.; Ritu, R.; Manju, K.; Birendra, K. "A review on biological activities of hydrazone derivatives". *Intl. J. Pharm. Clin. Res.* **2016**, *8*, 162-166.

(74) Verma, G.; Marella, A.; Shaquiquzzaman, M.; Akhtar, M.; Ali, M. R.; Alam, M. M. "A review exploring biological activities of hydrazones". *Journal of Pharmacy and Bioallied Sciences* **2014**, *6*, 69-80, doi:10.4103/0975-7406.129170.

(75) Barluenga, J.; Valdés, C. "Tosylhydrazones: New uses for classic reagents in palladium-catalyzed cross-coupling and metal-free reactions". *Angewandte Chemie - International Edition* **2011**, *50*, 7486-7500, doi:10.1002/anie.201007961.

(76) Sakai, N.; Matile, S. "Multistep organic synthesis of modular photosystems". *Beilstein Journal of Organic Chemistry* **2012**, *8*, 897-904, doi:10.3762/bjoc.8.102.

(77) Su, X.; Aprahamian, I. "Hydrazone-based switches, metallo-assemblies and sensors". *Chem. Soc. Rev.* **2014**, *43*, 1963-1981, doi:10.1039/c3cs60385g.

(78) Epstein, I. R.; Xu, B. "Reaction-diffusion processes at the nano- and microscales". *Nature Nanotechnology* **2016**, *11*, 312-319, doi:10.1038/nnano.2016.41.

(79) Sassi, M.; Crippa, M.; Ruffo, R.; Turrisi, R.; Drees, M.; Pandey, U. K.; Termine, R.; Golemme, A.; Facchetti, A.; Beverina, L. "Open circuit voltage tuning through molecular design in hydrazone end capped donors for bulk heterojunction solar cells". *J. Mater. Chem. A* **2013**, *1*, 2631-2638, doi:10.1039/C2TA00673A.

(80) March, J.: *Advanced organic chemistry: reactions, mechanisms, and structure*. Wiley: New York, 1985.

(81) Poplavskyy, D.; Nelson, J. "Nondispersive hole transport in amorphous films of methoxy-spirofluorene-arylamine organic compound". *J. Appl. Phys.* **2003**, *93*, 341-346, doi:10.1063/1.1525866.

(82) Balakrishnan, K.; Datar, A.; Naddo, T.; Huang, J.; Oitker, R.; Yen, M.; Zhao, J.; Zang, L. "Effect of Side-Chain Substituents on Self-Assembly of Perylene Diimide Molecules: Morphology Control". *J. Am. Chem. Soc.* **2006**, *128*, 7390-7398, doi:10.1021/ja061810z.

(83) Kim, C.; Liu, J.; Lin, J.; Tamayo, A. B.; Walker, B.; Wu, G.; Nguyen, T. Q. "Influence of structural variation on the solid-state properties of diketopyrrolopyrrole-based oligophenyleneethiophenes: Single-crystal structures, thermal properties, optical bandgaps, energy levels, film morphology, and hole mobility". *Chem. Mater.* **2012**, *24*, 1699-1709, doi:10.1021/cm202852f.

(84) Abboto, A.; Bellotto, L.; De Angelis, F.; Manfredi, N.; Marinzi, C. "Heteroaromatic Donor-Acceptor π -Conjugated 2,2'-Bipyridines". *Eur. J. Org. Chem.* **2008**, *2008*, 5047-5054, doi:10.1002/ejoc.200800692.

(85) Ono, N.; Okumura, H.; Murashima, T. "Synthesis of oligo(thienylenevinylenes) substituted with alkoxy groups". *Heteroat. Chem* **2001**, *12*, 414-417, doi:10.1002/hc.1062.

(86) Hagfeldt, A.; Boschloo, G.; Sun, L.; Kloo, L.; Pettersson, H. "Dye-sensitized solar cells". *Chem Rev* **2010**, *110*, 6595-6663, doi:10.1021/cr900356p.

(87) *Dye Sensitized Solar Cells*; K.Kalyanasundaram ed.; CRC Press: Boca Raton, FL, USA, 2010. pp. 320.

(88) Ono, L. K.; Schulz, P.; Endres, J. J.; Nikiforov, G. O.; Kato, Y.; Kahn, A.; Qi, Y. "Air-Exposure-Induced Gas-Molecule Incorporation into Spiro-MeOTAD Films". *J. Phys. Chem. Lett.* **2014**, *5*, 1374-1379, doi:10.1021/jz500414m.

(89) Kroeze, J. E.; Hirata, N.; Schmidt-Mende, L.; Orizu, C.; Ogier, S. D.; Carr, K.; Grätzel, M.; Durrant, J. R. "Parameters Influencing Charge Separation in Solid-State Dye-Sensitized Solar Cells Using Novel Hole Conductors". *Adv. Funct. Mater.* **2006**, *16*, 1832-1838, doi:10.1002/adfm.200500748.

(90) Yum, J.-H.; Chen, P.; Grätzel, M.; Nazeeruddin, M. K. "Recent Developments in Solid-State Dye-Sensitized Solar Cells". *ChemSusChem* **2008**, *1*, 699-707, doi:10.1002/cssc.200800084.

(91) Bard, A. J.; Faulkner, L. R.: *Electrochemical Methods, Fundamentals and Applications, 2nd Ed.*; John Wiley & Sons, INC.

: New York, Chichester, Weinheim, Brisbane, Singapore, Toronto, 2001.

Chapter 4

Dye-Sensitized Solar Hydrogen Production

*“The only way to discover the limits of the possible
is to go beyond them into the impossible.”^d*

Arthur C. Clarke, Writer, 1917 - 2008

Aim of this section

The third part of this PhD research project has been dedicated to the study of dye-sensitized hydrogen production. The production of hydrogen as alternative to carbon-based fuels is, at the present day, an interesting research topics. As mention before, current most diffused technology for H₂ production is the steam reforming of natural gas, which accounts for 80-90% of whole hydrogen production, while electrolysis, even if increasing, accounts only for a minor share (about 4%). Even if the electricity is produced using renewable sources, the overall efficiency of the process is not really satisfying due to the multi-step process.

In current market conditions, about 50 kWh of electricity are consumed to produce one kg of (compressed) hydrogen. A typical electrolysis cell has an efficiency of about 70–80%, but the real efficiency, however, is lower because of plant losses. Electrolysis requires DC power, so that the supplied

AC power must be inverted, resulting in as much as 10% additional energy losses. The photocatalytic or photoelectrochemical production of hydrogen is preferred because of the lower energy loss due to a single step process. In this context, a new class of sensitizers has been developed in our laboratory in collaboration with another PhD research project.² The new dyes use the branched geometry, previously developed and deeply studied from our group (Figure 4. 1). This molecular structure, using a phenothiazine (PTZ) donor core instead of a common triphenylamine, allow to obtain molecules that show a more firmly bond with the titanium dioxide, useful feature in case of long term stability or in case of water based application.

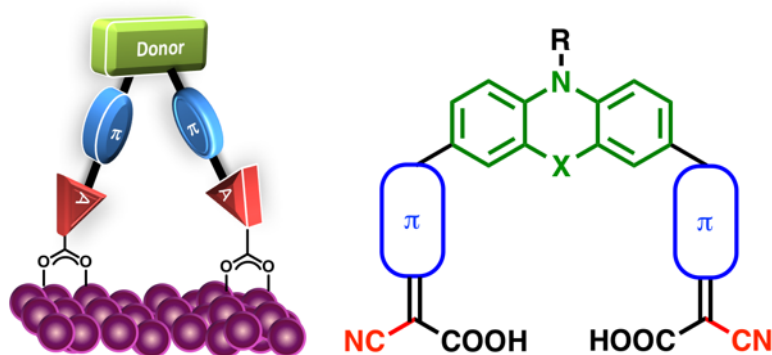


Figure 4. 1: general structure of a **PTZ**-based multibranching dyes

The studies on these molecules started, as usual, with the investigation of the photocatalytic response upon the variation of the optical properties as a result of the increase of the conjugation through the molecular structure. We synthesised a numbers of new dyes varying the π -spacer, exploiting different heteroaromatic rings such as functionalized thiophene derivatives or thiophene fused rings (Figure 4. 2).³

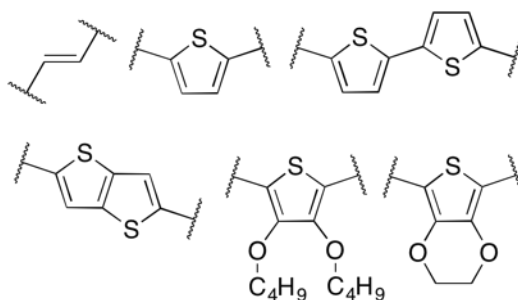


Figure 4. 2: π -spacer investigated in this research.

Moreover, the effect of the side functionalization, and the resulting variation of water affinity, has been exploited upon functionalization of the **PTZ** donor core with different hydrophobic and hydrophilic functionalities (Figure 4. 3).⁴ We have tested the photocatalytic properties at different dye loading on the surface of the photocatalyst and studied the effect of the presence of an optical inactive co-adsorbent.

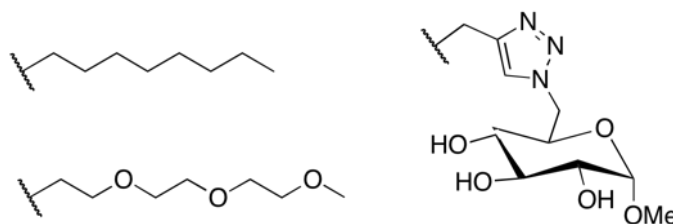


Figure 4. 3: side functionalities investigated in this research.

We have considered two different co-adsorbents, the first is the widely used chenodeoxycholic acid (**CDCA**), and as the second, we have selected glucuronic acid (**GLU**) since the presence of a similar sugar functionality should efficiently promote specific and directional co-adsorbent/dye intermolecular bonds.

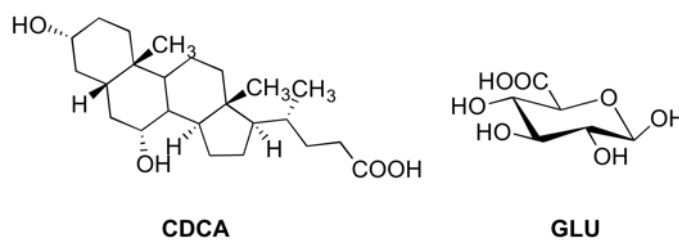


Figure 4. 4: Co-adsorbent agents tested in dye sensitized photocatalytic hydrogen production.

As a consequence of the unexpected results obtained with the first **PTZ** series of we decide to investigate the effect of the sulfur atoms in the backbone of the molecule. It is well known that the sulfur atoms can act as poisoning agent on the surface of noble metal (*i.e.* Pt, Pd), thus reducing their catalytic activity. To better investigate this phenomenon, we have synthesized an analogous series of dyes removing or replacing sulfur. We then replaced the **PTZ** donor core with carbazole (**CBZ**) and phenooazine (**POZ**), and the thiophene ring (**Th**) with furan (**Fu**).

Thiophene-based phenothiazines for long-term irradiation photocatalytic H₂ production

Hydrogen is particularly attractive as a fuel, since it has no carbon footprint when it is burnt to water and can be obtained through water splitting from an abundant and clean source. Unfortunately, water splitting is an up-hill and kinetically hindered process; the electromagnetic radiation can supply the energy needed to overcome ΔG only if a suitable catalyst is used to reduce the kinetic overpotential.

Fujishima and Honda first introduced in 1972 the use of titanium dioxide as a semiconductor, loaded with platinum nanoparticles on the surface as catalysts, to split water molecules using light.⁵ The efficiency of such a system is mainly associated to the fact that only a narrow portion of the sunlight, the ultraviolet region, is able to promote an electron into the conduction band (CB) of TiO₂ and to the fast electron-hole recombination process. Indeed, the minimum energy demand for water splitting, 1.23 eV at pH = 0 (corresponding to the near-IR region around 1000 nm), is much lower than the energy band gap in TiO₂ (3.0 – 3.2 eV depending on the polymorph, corresponding to a photon with $\lambda \sim 387 - 413$ nm). Nevertheless, TiO₂ has CB position suitable for proton reduction and remains a very attractive material due to its abundance, relatively low cost, stability against photo-corrosion and no toxicity in form of paste or thin films.⁶ Amongst the solutions to improve efficiency of these systems, the introduction of a sensitizer to extend the absorbed portion of solar spectrum is a challenging option.⁷ The working mechanism quite closely reminds that of natural photosynthesis, that is the reason why such technologies can be included in the group of the artificial photosynthetic methods.⁸ In such an artificial leaf, solar radiation is absorbed by a dye sensitizer D, which is promoted to its excited state D* through a HOMO-LUMO transition. Then, the electron in the dye LUMO is injected to the CB of TiO₂ on the surface of which Pt(0) is present and acts as an electron trap. Platinum is able to transfer two electrons to two protons to afford one molecule of H₂. After

electron injection, D^* has been converted to its radical cation $D^{\cdot+}$, which is then regenerated back to D . In a complete water splitting system the electrons for dye regeneration come from water oxidation to oxygen. If attention is focused only on water reduction to hydrogen, as in our case, a sacrificial electron donor (S) is commonly used, so that the reduction semi-reaction could be the rate determining step of the whole process.

Here we focused our attention on the role of the sensitizer D , which plays a central role both in DSSC and in H_2 photo-production being the first direct interface with the solar radiation. In contrast with the huge literature on DSSC sensitizers,^{9,10} few articles have studied the role of the dyes in the photocatalytic production of hydrogen. In the latter case the most important families of dyes are the same as in DSSC technology, mostly including organometallic molecules such as ruthenium complexes,^{11,12} porphyrins or phthalocyanines inspired by chlorophyll complex.¹³ Metal-free organic sensitizers have been gaining an increasing role in the scientific literature of hydrogen production,¹⁴⁻¹⁶ with record DSSC power conversion efficiencies (PCE) exceeding 12%.^{17,18} These dyes carry important advantages over metal complexes such as easier and cheaper synthesis and purification, larger structural variety, and wider tunability of optical and energetic properties, which are fundamental to optimize the corresponding solar devices.¹⁹⁻²² Triggered by the some recent studies on phenothiazines (**PTZ**) derivatives as DSSC sensitizers²³⁻²⁶ and by their first uses as light harvesters in the photo-driven production of hydrogen,²⁷ we decided to systematically investigate this promising class of dyes by designing a series of organic sensitizers containing the phenothiazine core as a donor scaffolds in donor- π -acceptor molecules. Interestingly, a very recent report on a class of benzo[*b*]phenothiazines confirms the increasing relevance of dye-sensitized hydrogen production using organic dyes and phenothiazine derivatives.²⁸ The phenothiazine core carries peculiar features associated to its non-planar butterfly conformation along the S-N axis. Such arrangement avoids fully planar geometries which could be detrimental by promoting self-quenching molecular

aggregates on the TiO_2 surface. Moreover, the phenothiazine structure contains two symmetric benzene rings which can be conveniently functionalized allowing the design of symmetric di-branched dyes, a recently important class of photosensitizers endowed with higher anchoring stability and electron injection efficiency, improved optical properties, and enhanced device stability which was introduced by us in the DSSC field of investigation and later used by many research groups.^{26,29-32} Lastly, the nitrogen atom of the central core of the phenothiazine groups can be conveniently functionalized with alkyl or aryl groups of different chemical nature, in order to provide a further derivatization site able to induce additional properties such as proper solubility in specific media (with particular attention to water) or affinity to bio-inspired molecules. In order to systematically investigate this class of molecules, here we have focused our attention on the effect of the π -spacer group. In particular, thiophene rings have been widely used in materials science due to their peculiar structural and electronic properties.³³ Thiophene is a π -excessive heteroaromatic five-membered ring with a lower resonance energy than benzene,³⁴ thus facilitating charge transfer between the donor and the acceptor core of the organic dyes. For these reasons thiophene-based spacers have been commonly applied in the design of dyes for solar applications.^{27,35} We have here exploited different mono-, poly-, and fused polycyclic thiophene-based groups as π -spacers between the phenothiazine donor core and the acceptor/anchoring groups based on cyanoacrylic acid (Figure 4. 5). As a reference system the previously investigated dye **PTZ1** (named P3 in Ref. 27) has been included in our work, also because the hydrophobic octyl chain is supposed to raise detrimental charge recombination lifetimes.²⁷

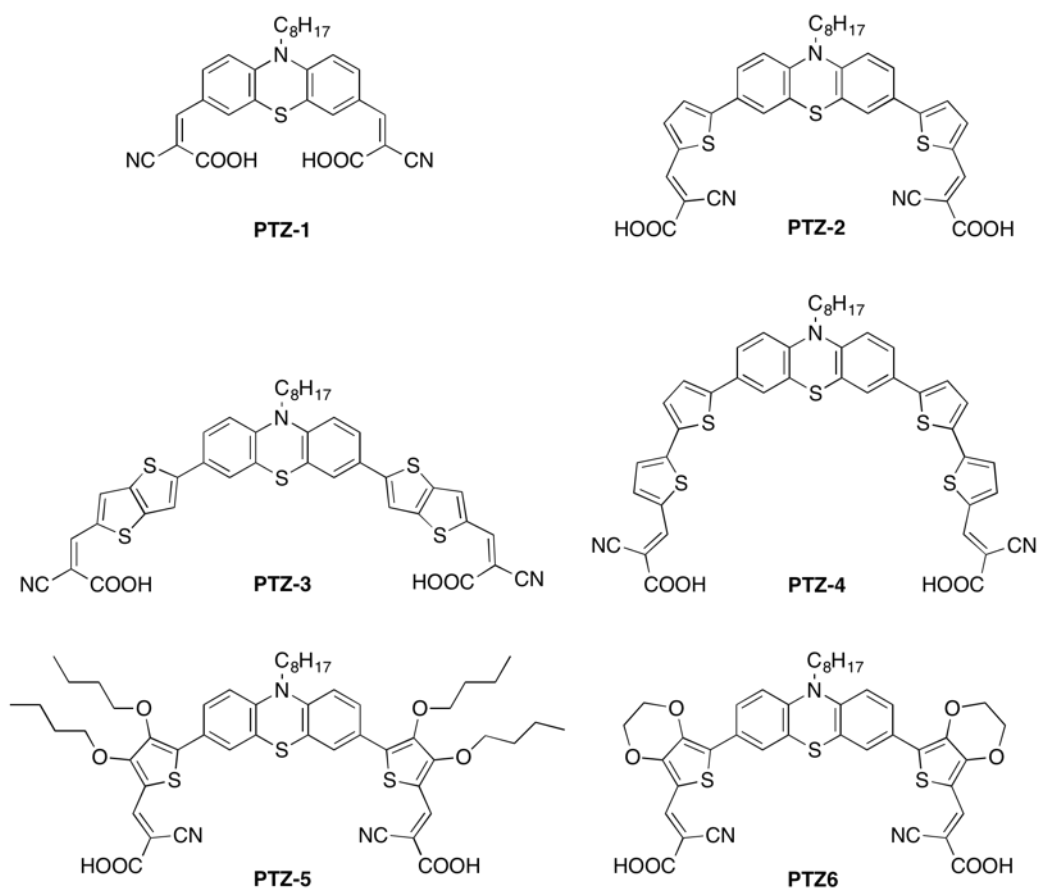


Figure 4. 5: Structure of the investigated phenothiazine based branched dyes.

Besides paying attention to harvesting visible light, we aimed at exploring the new dyes to overcome the problem of photo-induced degradation of the sensitizers. In particular, we have noticed that most of the reported studies on dye-sensitized production of hydrogen, with rare exceptions,²⁸ involve relatively short irradiation times (typically around 5 h).^{13-16,27,36,37} Such short irradiation periods limit the significance of these studies for realistic applications, not giving a true image of the photocatalytic activity of the dye-sensitized catalyst in the long term. In addition, to the best of our knowledge, no dye photo-degradation studies have been reported so far, though there are clear indications that hydrogen production rate decreases with time for these systems.^{27,28}

The new dyes have been synthesized, characterized in their optical and electrochemical properties and, in combination with TiO₂ and other proper components, investigated as photosensitizers in the photocatalytic H₂ production over 20 h irradiation times. Their activity as sensitizers in DSSC has been also tested. We examined the effect of the molecular design, namely that of the thiophene-based π spacer, on the efficiency of H₂. In particular, remarkably stable photocatalytic activity was observed with an H₂ evolution rate up to 250 $\mu\text{mol g}^{-1} \text{h}^{-1}$, and turnover number (TON) up to 75, making this class of compound particularly promising for solar-based devices. The highest efficiency of one of these dyes over long irradiation times was clearly associated to its higher stability under irradiation, in contrast with other previously reported dyes and with **PTZ1**, used as representative reference literature system in this work, which is strongly unstable under the same experimental conditions.

The synthesis, the optical and the electrochemical characterization, as well as DSSCS investigation, have been reported in the previous section (Chapter 2), herein we will discuss the photocatalytic investigation and the relative studies on their stability over long term irradiation.

HYDROGEN PRODUCTION USING DYE-SENSITIZED Pt/TiO₂

Hydrogen production using Pt/TiO₂ sensitized by dyes **PTZ1–6** was investigated using a Pt/TiO₂ nanocomposite catalyst prepared by irradiation of Degussa P25 TiO₂ suspended in a water/EtOH solution containing Pt(NO₃)₂. Irradiation with a UV-Vis lamp results in the reduction of Pt²⁺ ions and deposition of Pt(0) nanoparticles on the surface of the TiO₂ support. The powder X-ray diffraction (PXRD) analysis revealed that the material contains $\sim 68\%$ of anatase and $\sim 32\%$ of rutile (Figure 4. 6). The broadening of the main reflections of anatase and rutile phases indicates a mean crystallite size of 20 and 19 nm, respectively. No reflections related with Pt nanoparticles were observed in the PXRD pattern of the Pt/TiO₂ material because of their low amount and nanometric size.

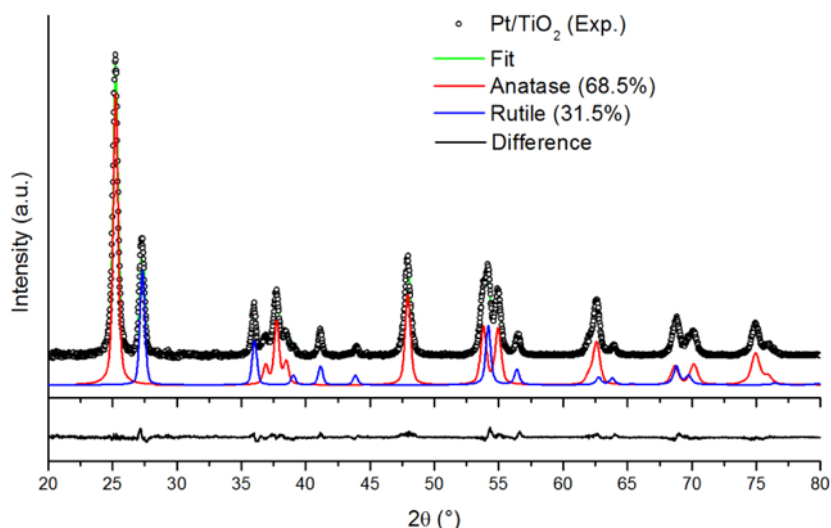


Figure 4. 6: Powder X-ray diffraction (PXRD) pattern of Pt/TiO₂ material with results of the Rietveld analysis to calculate the phase composition.

Textural analysis by means of N₂ physisorption revealed that the material shows a type IV isotherm, typical of mesoporous materials (Figure 4. 7a).³⁸ The specific surface area, calculated applying the Brunauer-Emmett-Teller (BET) equation, is 54 m² g⁻¹ while the Barrett-Joyner-Halenda (BJH) analysis showed that the pores of the materials have a maximum around 50 nm and a cumulative volume of 0.232 mL g⁻¹ (Figure 4. 7b).

Representative transmission electron microscopy (TEM) images acquired on the Pt/TiO₂ material are presented in Figure 4. 8a-b. TiO₂ particles show an irregular shape, with dimensions of 10-40 nm, in good agreement with the crystallite sizes calculated from line broadening in PXRD analysis. Pt nanoparticles, as highlighted in high-angle annular dark-field scanning TEM (HAADF-STEM) images (Figure 4. 8c), were homogeneously distributed on the surface of TiO₂ particles. Their size distribution (Figure 4. 8d) showed a mean particle size of 2.4 nm, in agreement with the size of metal nanoparticles obtained by photodeposition on multiphasic TiO₂ supports.^{11,14,39-42}

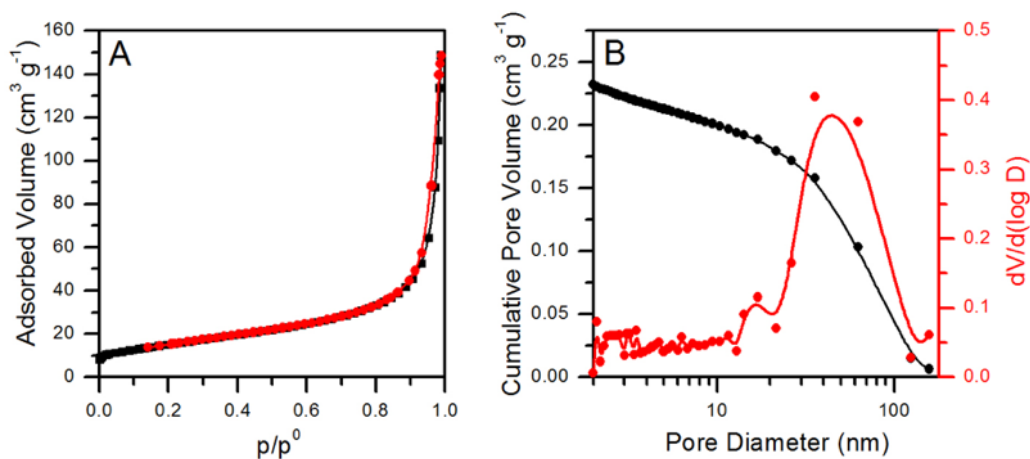


Figure 4. 7:a) N₂ physisorption isotherm obtained at the liquid nitrogen temperature for the Pt/TiO₂ material; b) Cumulative Pore Volume and pore size distribution obtained by the BJH analysis of the desorption branch of the N₂ physisorption isotherm.

The **PTZ1-6** dyes were used as sensitizers in the Pt/TiO₂ material for H₂ production under visible irradiation using triethanolamine (TEOA) as sacrificial agent at pH = 7.0. The **PTZ1-6** were quantitatively adsorbed on the Pt/TiO₂ catalyst from their solution in EtOH. After adsorption, the remaining solution was colourless. Under irradiation with visible light ($\lambda > 420$ nm), the H₂ production rates obtained using Pt/TiO₂ sensitized by **PTZ1-6** dyes are presented in Figure 4. 9 while the overall H₂ productivities are presented in Figure 4. 10. After optimization of the experimental conditions following the indications reported by Kisch and Bahnenmann,⁴³ the H₂ production rates are reported in Figure 4. 9 and in Figure 4. 10 after normalization to the mass of the catalyst. This is intended to give an indication of the scalability of the process under comparable experimental conditions.

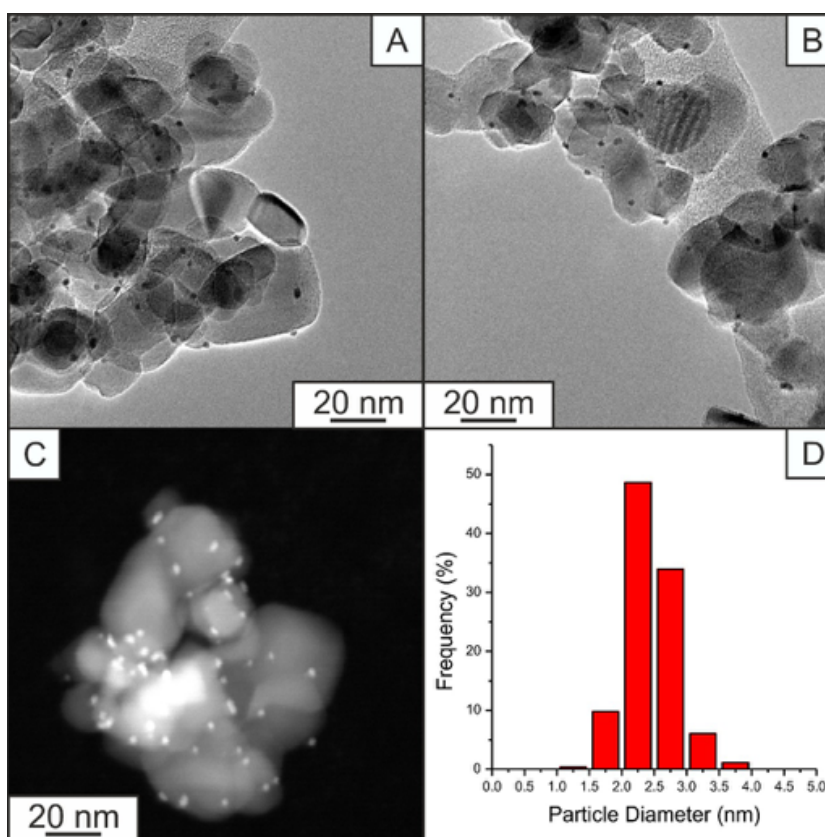


Figure 4. 8:a,b) Representative transmission electron microscopy (TEM) images acquired on the Pt/TiO₂ material; c) HAADF-STEM image showing distribution of Pt nanoparticles on the surface of TiO₂ support; d) Size distribution of the Pt nanoparticles.

Notably, unlike previous reports on phenothiazine-functionalized Pt/TiO₂,²⁷ in this study we extended the irradiation time up to 20 h in order to study the stability of the present photocatalysts under reaction conditions.

The data reported in Figure 4. 10 evidenced that the overall H₂ productivity of the photocatalysts functionalized with the new thiophene-based phenothiazine **PTZ2-6** were lower than that obtained using the reference dye **PTZ1** reported by Lee et al.,²⁷ though the dibutoxy-thiophene derivative **PTZ5** showed an H₂ productivity comparable to that of the **PTZ1**-based photocatalyst. The remaining dyes **PTZ2-4** and **PTZ6** showed a comparable activity.

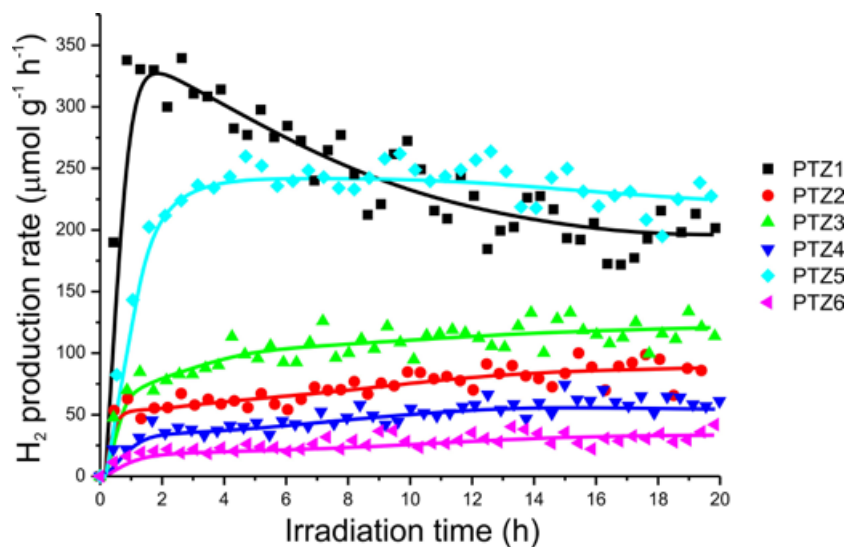


Figure 4. 9: H₂ production rates measured using the dye/Pt/TiO₂ materials in H₂ production from TEOA 10 v/v% solution at pH = 7.0 under irradiation with visible light ($\lambda > 420$ nm).

Despite the overall hydrogen production of the new dyes was lower than that of the reference system, the analysis of the H₂ production rates, presented in Figure 4. 9, put in evidence highly significant insights.

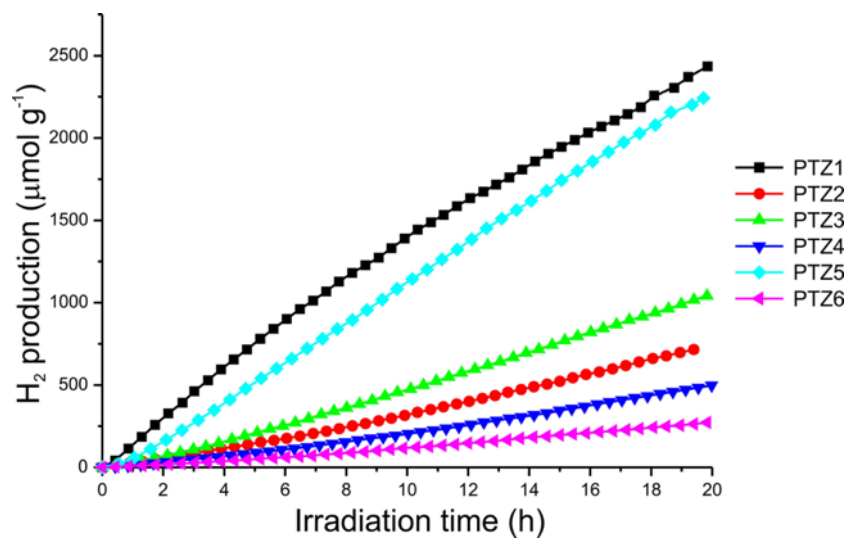


Figure 4. 10: H₂ production efficiency expressed as $\mu\text{mol/g}$ of material.

Despite the overall hydrogen production of the new dyes was lower than that of the reference system, the analysis of the H₂ production rates, presented in Figure 4. 9, put in evidence highly significant insights. Indeed, the **PTZ1**-based

photocatalysts showed a maximum in the H₂ production rate after 2 hours of irradiation, followed by a progressive decrease of its activity, in agreement with reports in the literature.^{27,28} On the contrary, the photocatalysts functionalized with the new **PTZ2-6** dyes showed an initial activation period of 4 – 6 h, resulting in an even low but constant H₂ production rates up to 20 h of irradiation under visible light, a behaviour which is unprecedented in the literature for this type of sensitizers. Notably, the H₂ production rate of the **PTZ5**-based photocatalyst surpassed that of the **PTZ1**-based one after 8 h of irradiation. The straightforward stability demonstrated by the photocatalysts functionalized with the new thiophene-based phenothiazines is particularly important in view of a medium-long term utilization of dye-sensitized photocatalysts for H₂ production.

Table 4. 1 summarizes the photocatalytic performance of the dye-sensitized material studied in this work. Turn-Over Numbers (TON), calculated accordingly to the procedure previously reported in the literature,^{27,44} indicate how many electrons generated by excitation of the dye are effective for proton reduction and H₂ production. The obtained data confirmed that the efficiency of the photocatalyst sensitized with **PTZ5** approaches that of the benchmark **PTZ1**, with all the other dyes showing lower TON values. This fact could be associated with the presence of thiophene spacers that could strongly interact with the surface of Pt nanoparticles, covering the catalytic sites responsible for H₂ evolution. In the case of **PTZ5**, adsorption of the sulphur sites on the Pt nanoparticles could be in some way hindered by the alkyl chains on the thiophene spacer. Moreover, degradation of the **PTZ1-6** dyes could contribute to the trend observed in the TON values (see below).

The TON obtained in this study are significantly lower with respect to those reported in the literature for photocatalysts sensitized using dyes with similar molecular structure.^{27,28} However, we note that the photocatalytic H₂ production is strongly dependent on many experimental conditions, including irradiation power, reactor geometry and dye loading on the photocatalysts.⁴³ Therefore, the direct

comparison of TON values is meaningful only when the same experimental conditions and apparatus are used.

Table 4. 1 Photocatalytic performance of the dye/Pt/TiO₂ materials in H₂ production from TEOA 10 v/v% solution at pH = 7.0 under irradiation with visible light ($\lambda > 420$ nm).

Sample	Dye loading ($\mu\text{mol}/50\text{mg}$)	H ₂ amount ^a (μmol)	TON ^b	LFE ₀₃ ^c	LFE ₂₀ ^d
PTZ1	2.97	121.7	81.8	0.144%	0.090%
PTZ2	2.98	35.8	24.0	0.026%	0.039%
PTZ3	3.01	52.1	34.6	0.037%	0.048%
PTZ4	2.99	24.9	16.6	0.017%	0.027%
PTZ5	2.98	111.6	74.9	0.104%	0.103%
PTZ6	2.98	13.6	9.1	0.010%	0.014%

^a Overall H₂ amount produced after 20 h of irradiation; ^b TON = (2 x H₂ amount) / (dye loading); ^c Light-to-Fuel Efficiency calculated after 3 h of irradiation; ^d Light-to-Fuel Efficiency calculated after 20 h of irradiation;

Light-to-Fuel Efficiency (LFE) has been introduced in order to quantitatively evaluate the fraction of energy from the light source that is stored in the form of H₂, defined in a similar manner as that previously proposed for H₂ production using PEC cells⁴⁵ or photocatalytic reforming of oxygenated compounds.⁴⁶ LFE listed in Table 4. 1 have been calculated from the H₂ flow produced at different irradiation times: 3 h (LFE₀₃) and 20 h (LFE₂₀). The LFE values confirmed the superior efficiency of **PTZ1** and **PTZ5** in storing light energy into chemical energy compared to the other dyes. Notably, LFE decreases with time for **PTZ1** while it is almost constant for the thiophene-derived dyes **PTZ2-6**. As a result, the LFE₂₀ is significantly higher for the thiophene-substituted dye **PTZ5** compared to the reference benchmark **PTZ1**.

DYE DEGRADATION STUDY AND INTRINSIC PHOTOCATALYTIC ACTIVITY

As aforementioned, we investigated the dye-sensitized production of hydrogen over irradiation times up to 20 h, in contrast with the much shorter irradiation periods commonly used in the literature, which, apart rare exceptions,²⁸ are typically around 5 h. The selected experimental time is a compromise between the need of performing longer stability tests and that of avoiding appreciable changes in the concentration of the sacrificial agent due to conversion of sacrificial agent, accumulation of by-products, and selective evaporation of the solvent in the used flow reactor. In particular, we were attracted by the anomalous behaviour of the reference dye **PTZ1** after the first irradiation hours, both in our investigation (Figure 4. 9) and in the literature reports.^{27,28} In order to get deeper insights into such experimental findings and previous literature studies, we decided to perform a detailed investigation of the stability of the **PTZ1-6** dye-sensitized Pt/TiO₂ catalysts over 20 h under the same conditions used during the hydrogen measurements (Figure 4. 9). The stability has been ascertained via optical absorption of a proper solution of the desorbed dyes from the Pt/TiO₂ catalyst at specific irradiation times and reported as relative residual absorbance compared to the absorbance before irradiation ($t = 0$ h). The results are summarized in Figure 4. 11.

The degradation study clearly shows that all of the dyes, with the notable exception of the catalyst sensitized by dye **PTZ5**, for which the best hydrogen production rates were recorded over longer irradiation times, are not stable under visible irradiation. Very importantly, the largest degradation over 20 h was observed for the reference literature dye **PTZ1**, for which the residual active catalyst after 20 h of irradiation is $\sim 30\%$. In other terms, the catalyst based on the literature dye **PTZ1** is mostly decomposed after 20 h.

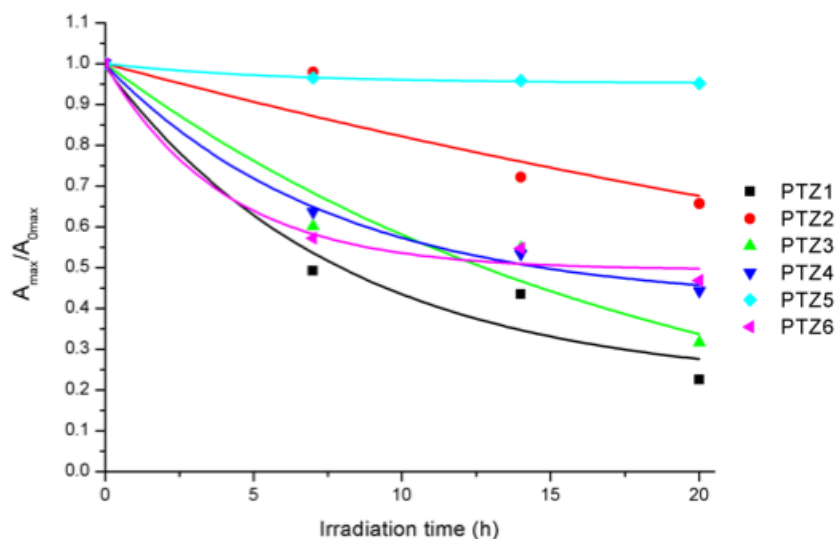


Figure 4. 11: Degradation plots of the **PTZ1-6** dye-sensitized Pt/TiO₂ catalysts under visible irradiation using TEOA as a sacrificial agent at pH = 7.0 in water under a nitrogen atmosphere.

This finding clearly explains the irregular behaviour recorded both in our investigation (Figure 4. 9) and in the literature,^{27,28} and visibly stresses the insufficient reliability of photocatalytic studies over short irradiation times (4-5 h). Apart the catalyst sensitized by **PTZ5**, those sensitized by the new dyes experiences photo-degradation as well, although the extent was smaller, with residual active catalyst being between ~35 and 70% after 20 h. While the reason of the superior stability of the dyes **PTZ2-6** compared to the dye **PTZ1** is not straightforward, it is evident that the presence of the thiophene spacer resulted beneficial for improved stability under light. This can be correlated both to the stronger interaction between the dyes and the Pt/TiO₂ catalyst mediated by the presence of the sulphur atoms of the thiophene-base spacer, somewhat inhibiting the degradation catalytic activity of the photocatalyst, and to the improved stability of the dye radical cation D⁺ following the electron photoinjection.⁴⁷

Very remarkably, the catalyst based on **PTZ5** is the only one stable over the whole irradiation period, thus elegantly validating the recorded superior performance of the hydrogen production over longer irradiation times (Figure 4. 11). The improved stability might be associated to the presence of the alkyl chains on the spacer

groups of **PTZ5**, being this the main peculiar structural difference with respect to the other thiophene derivatives. This conclusion is in full agreement with the EIS investigation on DSSC (Chapter 2) suggesting that interface interactions (e.g. dye regeneration or charge recombination) or intermolecular interactions (intermolecular self-quenching) may play a role in determining the stability in hydrogen production experiments. It is not evident if the stability of **PTZ5** is due to the peculiar D- π -A structure as a whole or rather to the presence of an inherently more stable spacer. The bis-alkoxythiophene groups do not induce a larger stability by itself, since, for instance, polycyclic thiophene cores, such as the thienothiophene groups in **PTZ3**, are more stable thanks to their larger structural rigidity.⁴⁸⁻⁵¹ We thus conclude that is the embedding of the bis-alkoxythiophene spacers in the phenothiazine donor-acceptor structure which accounts for the higher stability, with a key role of the four alkyl substituents strategically located in the middle portion of the molecular assembly, as previously discussed. Conversely, we exclude relevant electronic effects associated to the presence of the donor alkoxy groups on the thiophene ring, since these groups are present also in the EDOT derivative **PTZ6** where no improved stability was observed.

The present study indicates that the new dyes are less efficient than the reference dye **PTZ1**. This lower performance is reasonably associated to the strong and preferential interaction that sulfur atoms of the thiophene-based spacers can establish with surface Pt atoms, inhibiting the catalytic activity of Pt. However, the specific lower activity is well compensated by the improved stability of the dyes opening perspectives for real long-term applications by the design of new catalysts based on sulfur-free organic dyes. This is demonstrated by the remarkable constant H₂ production for over 90 h in the case of the **PTZ5** (Figure 4. 12). In addition, the measured TON, LFE₀₃, and LFE₂₀ can be correlated to dye stability.

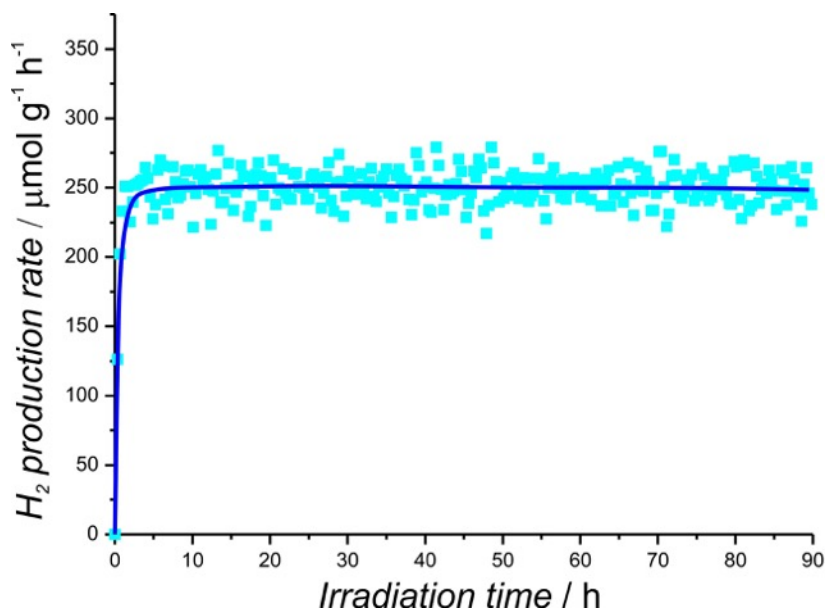


Figure 4. 12: H₂ production rates measured using the **PTZ5**/Pt/TiO₂ catalyst in H₂ production from TEOA 10 v/v% solution at pH = 7.0 under irradiation with visible light ($\lambda > 420$ nm).

The TON of a catalyst describes how many cycles it is able to cycle through before becoming inactive. Therefore, it is evident that the dye degradation plays a key role in defining the catalyst TON. In particular, in the thiophene-based series, the highest measured TON and LFE (**PTZ5**) are associated with the most stable dye.

Finally, and most importantly in terms of structure/property relations, the intrinsic H₂ production of the catalysts based on **PTZ2–6** can now be, at least in some cases, correlated to the optical properties of the dyes, though reminding that the light harvesting efficiency is only one of the components controlling the photocatalytic activity. Therefore, the new picture changes the unprocessed experimental H₂ production trend depicted in Figure 4. 9, in which no apparent correlation between H₂ evolution and optical properties is present. More specifically, the catalyst based on **PTZ3**, that is the dye with the highest ϵ in the thiophene-based series (Chapter 2, Table 2. 7), is now found as the most efficient system. Following the same analysis, the catalyst based on **PTZ2**, that is the dye with the lowest ϵ in the thiophene-based series, is found to be one of the least effective systems.

A final remark is needed to combine the reasonably constant H₂ production rates observed with the **PTZ2-6** dyes with the progressive dye degradation (Figure 4.11). Consistently with the mild reaction conditions and the inorganic nature of the remaining part of the photocatalysts, structural characterization does not evidence other modification of the investigated systems. This suggests that the slow and progressive dye degradation leaves still enough sensitizers to drive H₂ evolution at constant rate.

Enhanced photocatalytic hydrogen production in a glucose derivative of a phenothiazine dye: water affinity and self-organization

At the present time, rational design of dye-sensitizers is therefore urgently required to improve performances and stability of the photocatalytic system. We have recently described a series of new phenothiazine (**PTZ**) sensitizers containing thiophene-based spacers, showing that a careful design of the thiophene unit can afford improved long-term H₂ production rates and enhanced sensitizer stability under irradiation.³ The photocatalytic system comprised a two-component scheme where the dye-sensitizer is associated to a redox storing catalyst such as Pt/TiO₂. The **PTZ** series was characterized by the presence of a terminal alkyl substituent providing an hydrophobic nature to the sensitizers, which is not optimal for affinity to the aqueous working conditions.³

In this section, we prove the concept of improving the photocatalytic hydrogen production rate from aqueous solutions by enhancing the wettability of a dye-sensitized TiO₂ nanoparticles (TiO₂-NP) photocatalyst. One of the most common strategies to induce hydrophilicity to organic dyes is the introduction of a polyethylene glycol functionality, such as the widely used tris(ethylene glycol) monomethyl ether (TEG) group.⁵² In fact, the TEG group has been successfully employed in many material science fields, including dye-sensitized solar cells⁵³ and nonlinear optics.⁵⁴ More recently, the use of poly-glycolic functionalities as substituents in organic molecules for dye-sensitized hydrogen generation has been also reported.⁵⁶ Despite these several reports, the TEG functionality cannot imply a more sophisticated design to further tuning water affinity of sensitizers or induce additional properties such as intermolecular self-assembling. We have thus decided to check the use of a more refined and multifunctional functionality, such as the carbohydrate scaffold. Carbohydrates are excellent hydrogen bond donors and acceptors thanks to their multiple hydroxyl functions; sugar conjugation to

hydrophobic molecular materials has been used in other research fields to enhance wettability.⁵⁵ D-glucose derivatives have been recently used in material science to induce self-aggregation.⁵⁶

First, we report on the comparative use of TEG (**PTZ-TEG**) and sugar (**PTZ-GLU**) derivatives of a thiophene-based phenothiazine dye (Fig. 1) belonging to the aforementioned **PTZ** family. In order to similarly compare with the small TEG substituent, we have selected the commercially available methyl α -D-glucopyranoside moiety. The series was completed by inserting in the comparative study an alkyl (n-octyl) derivative of the phenothiazine scaffold (**PTZ-ALK**).³

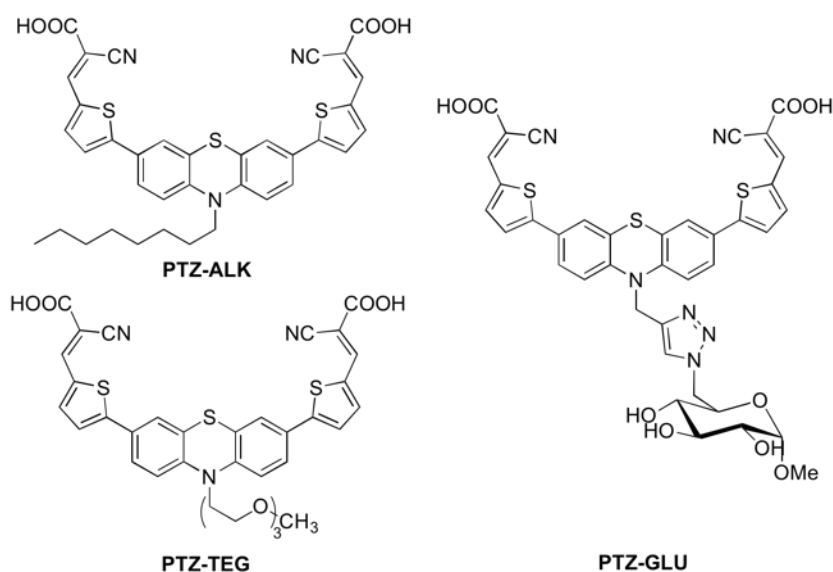


Figure 4. 13: Hydrophilic sensitizers (**PTZ-TEG** and **PTZ-GLU**) and reference dye (**PTZ-ALK**).

Otherwise, one of the major issues of dye-sensitized solar production of electricity (DSSCs) and fuels (photocatalytic hydrogen production) is the tendency of the quasi-planar π -conjugated organic dyes to aggregate on the surface of the n-type semiconductor (typically, TiO₂) causing the self-quenching of the photoexcited state and, accordingly, a decrease or even deactivation of the device.⁵⁷ For this reason, co-adsorbents, such as chenodeoxycholic acid (**CDCA**, Figure 4. 4), are commonly added to the dye solutions.⁵⁸ Exploiting its carboxylic functionality,

CDCA is able to co-graft on the semiconductor surface with the result of decreasing dye concentration and suppressing intermolecular dye-dye interaction, facilitating charge separation.⁵⁹ However, this effect is random since no specific intermolecular interaction is operating between the dye and **CDCA**, mostly limited to simple dipole-dipole forces with no directionality. This behaviour bounds the potential of the co-adsorbent and of the ultimate device.

We planned to exploit the peculiar features of **PTZ-GLU** dye, associated to the rigid geometry of the peripheral glucose functionality, in order to promote directional specific intermolecular interactions with proper co-adsorbents and therefore achieve enhanced device efficiencies in the photocatalytic hydrogen production. The glucose ring is optimal for this scope since, besides the rigid nature of the ring, the presence of three terminal –OH groups promotes the formation of strong directional hydrogen bonds with proper molecules. In particular, we have selected glucuronic acid (**GLU**, Figure 4. 4) as a co-adsorbent, since the presence of a similar sugar functionality should efficiently promote specific and directional co-adsorbent/dye intermolecular bonds. Though more sophisticated systems could be envisaged, **GLU** has been selected in reason of the simple structure, *i.e.* a glucose unit with the carbon atom in position 6 oxidized to a carboxylic acid, a functional group able to anchor onto TiO₂. Besides, **GLU** is widely available from natural gums (e.g. Gum Arabic) and is essential in the metabolism of animals and plants.⁶⁰⁻⁶⁴

Secondly, we present the investigation of the photocatalytic hydrogen production of the sugar derivative **PTZ-GLU** in the presence of **GLU** as a co-adsorbent. Not only do we show that the production of hydrogen sensitized by **PTZ-GLU** in presence of a 1:1 glucose co-adsorbent is significantly enhanced with respect to the experiment without co-adsorbent, but also that the presence of the conventional **CDCA** affords similar or even worse performances than without **CDCA**. When a hydrophobic **PTZ-ALK** sensitizer is used in place of **PTZ-GLU**, where the glucose functionality has been replaced by a simple alkyl chain, **GLU** and **CDCA**

gave similar results, demonstrating that the specific combination of the glucose dye **PTZ-GLU** and the glucose co-adsorbent **GLU** is responsible for the observed efficiency enhancement likely as a result of intermolecular self-assembly on the semiconductor surface promoted by directional hydrogen bonds.

H₂ PRODUCTION IN HYDROPHILIC PHENOTHAZINE BASED DYES

The synthesis, the optical and the electrochemical characterization, as well as DSSCs investigation, have been reported in the previous section (Chapter 2), herein we will discuss the photocatalytic investigation.

Contact angle analysis was used to investigate the hydrophilicity properties of the **PTZ-ALK**, **PTZ-TEG**, and **PTZ-GLU** sensitized TiO₂ nanoparticles. The contact angles of a deionized water drop on the surface of a film of sintered TiO₂ and the corresponding films sensitized with both dyes are shown in Figure 4. 14; data are summarized in Table 4. 2. The bare TiO₂ and the hydrophilic dyes-sensitized films have contact angles lower than 35°, compared to the value of 117° for the hydrophobic dye **PTZ-ALK**. Therefore the introduction of the hydrophilic substituents clearly improves the wettability of the semiconductor surface, as expected. More importantly, the sugar functionality in **PTZ-GLU** is able to improve water affinity by further decreasing the angle from 34° in the **PTZ-TEG** dye to 27°, thus going closer to the bare TiO₂-NP surface character.

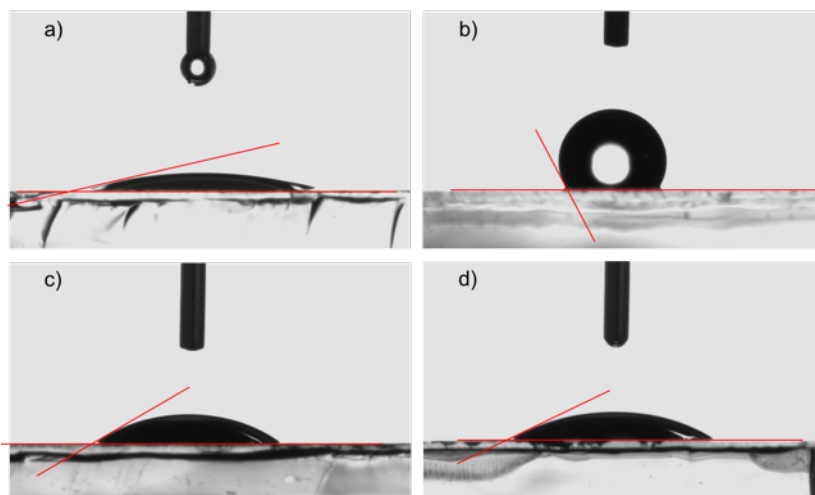


Figure 4. 14: Cross-sections of a) a film of sintered TiO_2 -NP; b) film of sintered TiO_2 -NP sensitized with **PTZ-ALK**; c) film of sintered TiO_2 -NP sensitized with **PTZ-TEG**; d) film of sintered TiO_2 -NP sensitized with **PTZ-GLU** and a drop of deionized water positioned on the top, which were used for the estimation of the contact angles ($\theta_c/^\circ$).

Pt/TiO_2 has been used as benchmark material to test the comparative sensitization ability of the new dyes under irradiation with visible light ($\lambda > 420 \text{ nm}$). The Pt/TiO_2 material (Pt loading of 1 wt%) has been prepared by photodeposition of Pt nanoparticles on the surface of TiO_2 P25 using a EtOH/water solution of $\text{Pt}(\text{NO}_3)_2$. The Pt/TiO_2 material is an anatase/rutile mixture ($\sim 70/30$ by weight) with mean crystallite sizes of 20 nm for both phases. Textural analysis revealed a surface area of $55 \text{ m}^2/\text{g}$ with pores diameters around 48 nm and a pore volume of 0.242 mL/g . HAADF-STEM analysis (Figure 4. 15) evidenced the irregular shape of TiO_2 particles (12 – 45 nm), with Pt nanoparticles with mean size of 2.4 nm homogeneously distributed on the surface of the support.

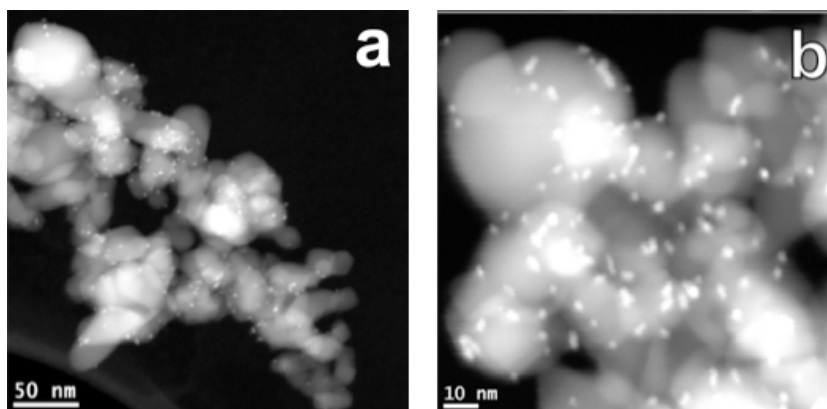


Figure 4. 15: Representative HAADF-STEM images of the Pt/TiO₂ nanocomposite.

The phenothiazine-based dyes (**PTZ-ALK**, **PTZ-TEG** and **PTZ-GLU**) have been adsorbed on Pt/TiO₂ nanocomposite by suspending the powder into an EtOH/DMSO solution of the dye in the dark for 12 h. The loading of the dye has been tuned from 1.0 to 30 $\mu\text{mol g}^{-1}$ upon varying the amount of dye added in the solution. After recovery of powder by filtration, the amount of residual dye in the solution was negligible in all of the cases, as assessed by UV-Vis spectroscopy.

Table 4. 2: Contact angle and photocatalytic performance of the dye/Pt/TiO₂ materials in H₂ production from TEOA 10% v/v solution at pH = 7.0 under irradiation with visible light ($\lambda > 420$ nm).

Sample	Dye loading ($\mu\text{mol g}^{-1}$)	Contact angle ($\theta_c/^\circ$)	H ₂ amount ^a ($\mu\text{mol g}^{-1}$)
TiO ₂ -NP	-	13.9	-
PTZ-ALK	30.0	117.3	1060
PTZ-TEG	30.0	33.9	421
PTZ-GLU	30.1	26.8	865

^a Overall H₂ amount produced after 20 h of irradiation .

The Pt/TiO₂ photocatalysts sensitized by **PTZ-ALK**, **PTZ-TEG** and **PTZ-GLU** were tested for H₂ production under Vis light ($\lambda > 420$ nm) from a triethanolamine (TEOA)/HCl aqueous buffer solution at pH = 7.0. Following the “best practice in

photocatalysis” reported by Kisch and Bahnenmann,⁴³ the experimental conditions have been optimized measuring the H₂ production rate after stabilization (see below) using different amounts of the photocatalyst. This preliminary optimization has been performed using the PTZ-GLU/Pt/TiO₂ photocatalyst with a dye loading of 30 μmol g⁻¹ (Figure 4. 16). Maintaining constant all the other experimental factors (geometry of irradiation and reactor, volume of the TEOA/HCl solution, temperature, etc.), the maximum H₂ production rate has been obtained using 60 mg of the photocatalyst, with a slight decrease for higher amounts likely due to increased scattering of the incoming photons.

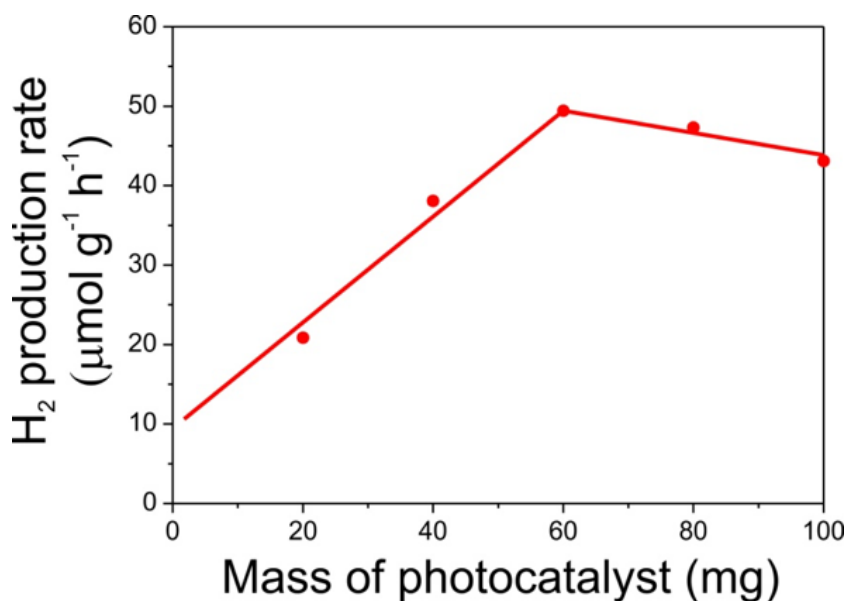


Figure 4. 16: Optimization of the experimental conditions for photocatalytic H₂ production.

Independently on the used dye, the H₂ production rates observed using the sensitized photocatalysts (Figure 4. 17) showed an initial increase in the first hours under irradiation. This phenomenon arises from the combination of two factors. First, diffusion of produced H₂ in the dead volume of the photoreactor resulted in the progressive increase of H₂ concentration in the gaseous effluent for the system, which typically accounts for the first 1-2 h.

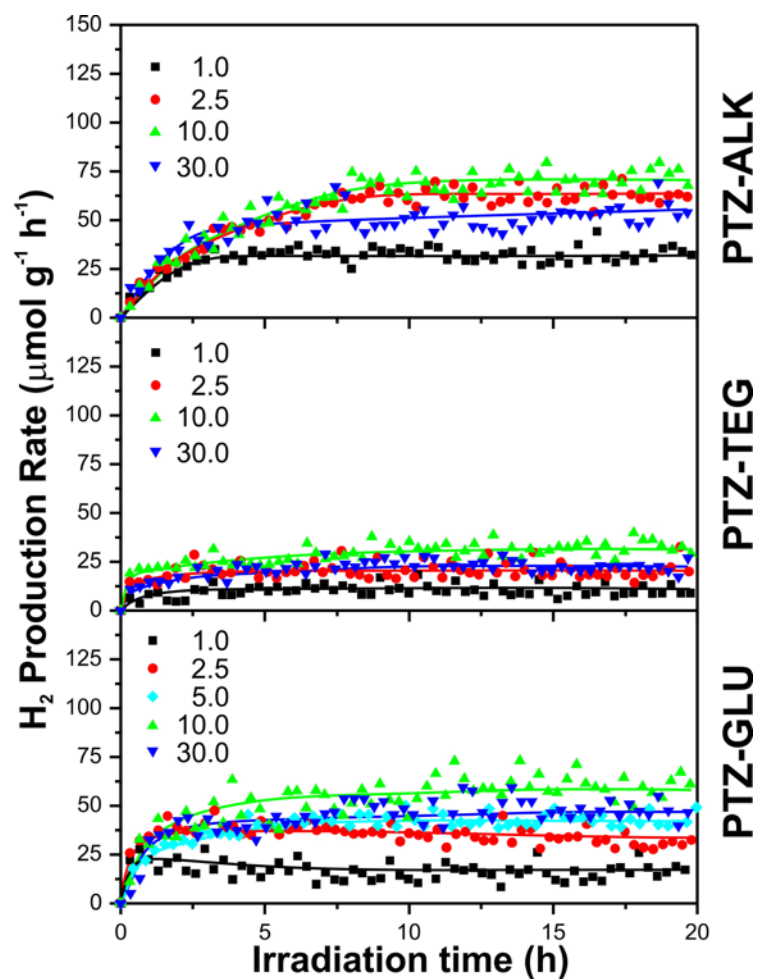


Figure 4. 17: H₂ production rates from TEOA 10% v/v solution at pH 7.0 under irradiation with visible light ($\lambda > 420$ nm) measured using the dye/Pt/TiO₂ materials. Numbers in the legends correspond to the dye loading in $\mu\text{mol g}^{-1}$.

Second, activation of the photocatalyst took place at the beginning of each photocatalytic experiment, likely because the Pt nanoparticles were passivated by the adsorbed oxygen resulting from exposure to air after photodeposition. This progressive activation of the photocatalysts resulted in an initial delay, as evident by plotting the amount of evolved gas (Figure 4. 18). It is interesting to underline that the activation period is significantly lower when hydrophilic dyes are used, probably because of the better interaction with the reactants in aqueous solution. Notably, no H₂ production was observed using the bare Pt/TiO₂ under the same experimental conditions.

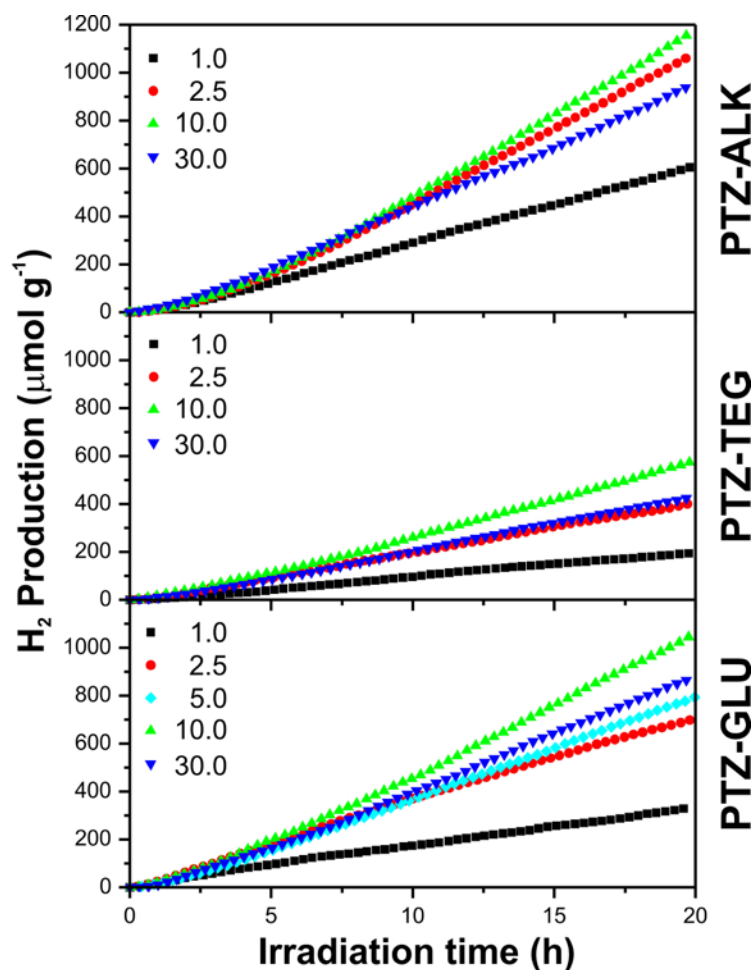


Figure 4. 18: H₂ production from TEOA 10% v/v solution at pH 7.0 under irradiation with visible light ($\lambda > 420$ nm) measured using the dye/Pt/TiO₂ materials. Numbers in the legends correspond to the dye loading in $\mu\text{mol g}^{-1}$.

The comparison of the H₂ production rates as a function of the dye loading showed different behavior for the photocatalysts sensitized with the investigated dyes (Figure 4. 19a). The effect of dye loading on the performance of photocatalysts with **PTZ-ALK** and **PTZ-TEG** shows the same trend, although the hydrophobic dye afforded a better performance: a sharp increase in the activity is observed for the lower dye loading while, above 2.5 $\mu\text{mol g}^{-1}$, the increment is modest. The photocatalysts sensitized by **PTZ-GLU** showed a different trend, with the H₂ productivity increasing up to the loading of 10 $\mu\text{mol g}^{-1}$.

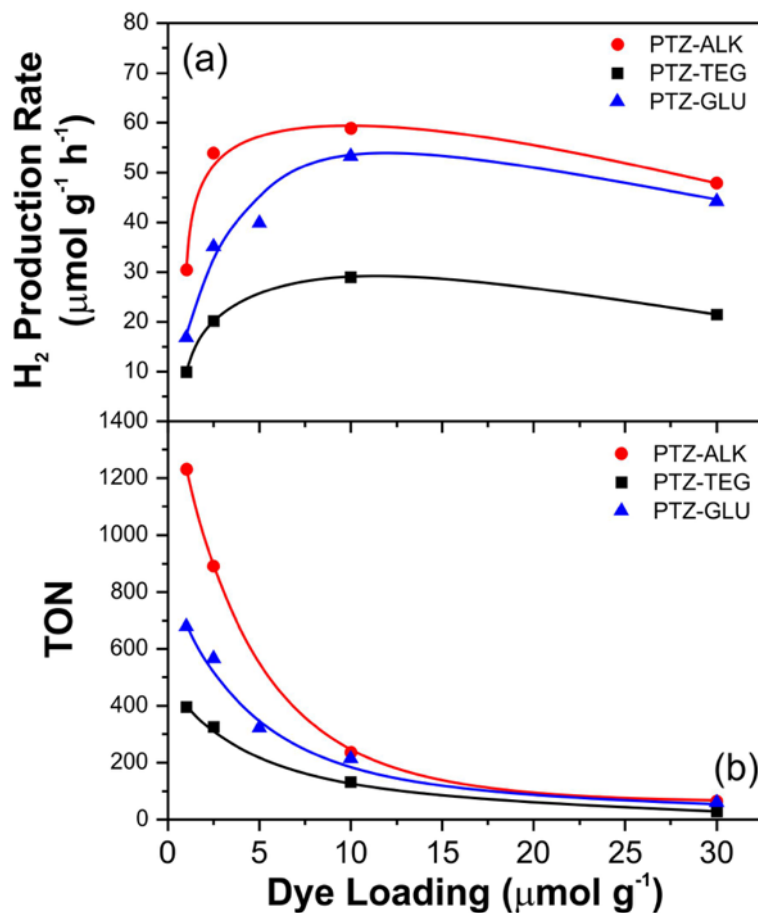


Figure 4. 19: Production rates (a) and TON (b) in H₂ evolution from TEOA 10% v/v solution at pH = 7.0 under irradiation with visible light ($\lambda > 420$ nm) using the Pt/TiO₂ materials sensitized with **PTZ-ALK**, **PTZ-TEG** and **PTZ-GLU**.

The different behavior of the dyes in sensitizing Pt/TiO₂ photocatalysts can be rationalized in terms of the molecular structure of the dyes, in particular the different chemical nature and geometry of the side functionality on the phenothiazine nitrogen site, and their possible 3D arrangement on the surface of the oxide material. Notably, considering the surface area of the Pt/TiO₂ material, a surface concentration of dye of 0.33 molecules nm⁻² can be calculated for the highest loading. Taking into account the size of the PTZ unit (length ~ 1 nm), it can be reasonably assumed that the coverage is always lower than one monolayer

and the contribution of multilayers is negligible, with all of the dyes molecules interacting with the surface through the PTZ unit.

The comparative trends are in agreement with the similar molecular geometry of **PTZ-ALK** and **PTZ-TEG**: a thiophene-PTZ unit connected to a terminal linear, flexible, chain. In the case of **PTZ-ALK**, the alkyl chain is reasonably coiled up because of repulsion from the aqueous solution, blocking the interactions between PTZ units and suppressing intermolecular quenching. This phenomenon does not take place in the case of the **PTZ-TEG** dye, in which the polar lateral chain can be considered unrolled within the aqueous solution allowing interaction of the heteroaromatic units by π - π stacking.

The photocatalysts sensitized by **PTZ-GLU** showed comparable H₂ production rates to **PTZ-ALK** for high loadings ($> 10 \mu\text{mol g}^{-1}$), while significantly depressed when lower amounts of dye were used. **PTZ-GLU** has a bulky side chain, with a considerably smaller degree of freedom compared to the ALK and TEG chains. In fact, whereas for **PTZ-GLU** a completely rigid cyclic substituent is present, for **PTZ-ALK** and **PTZ-TEG** the two side chains are endowed with free rotation along C-C and C-O single bonds, with the presence of infinite conformational isomers. This result suggests a distinct arrangement of the dye **PTZ-GLU** on the surface of the Pt/TiO₂ material. At high loadings, the organization of the **PTZ-GLU** becomes somewhat more similar to that of **PTZ-ALK**, with the PTZ units interacting with the Pt/TiO₂ surface and the bulky lateral chains avoiding intermolecular quenching. Notably, in the case of **PTZ-GLU**, the glucose functionality could also induce some sort of supramolecular organization of the dye on the surface.^{56,65} Upon decreasing the loading of PTZ-GLU, the glucose unit could interact directly with the TiO₂ surface through the remaining hydroxyl groups. The adsorption of the polar functionality on the surface might change the orientation of the PTZ scaffold with respect to the surface, affecting the electron transfer to the conduction band of TiO₂ and eventually decreasing the overall

activity. Very importantly, the contribution of degradation of the glucose group in the photocatalytic process can be reasonably ruled out. In fact, we have determined that a PTZ-GLU/Pt/TiO₂ suspension in water without the use of the sacrificial donor TEOA, using a loading of 10 μmol g⁻¹, afforded a H₂ production rate below the detection limit of the analytical apparatus (~ 3 μmol H₂ g⁻¹ h⁻¹). Indeed, dehydrogenation of alcohols and sugars are well known phenomena in H₂ production by photoreforming of oxygenated compounds, that are oxidized by the holes in the valence band of TiO₂. In the present case, no holes are formed in the valence band of the semiconductor since only visible light (λ > 420 nm) was employed.

TON values and Light-to-Fuel Efficiency (LFE₂₀) measured after 20 h of irradiation (Figure 4. 19b and Table 4. 3) showed that the efficiency of light conversion into effective electrons to produce H₂ increased as the dye loading decreased. This can be related to the suppression of intermolecular quenching at lower surface dye concentration. Similar trend have been measured for all of the three dyes, decreasing in the order **PTZ-ALK** > **PTZ-GLU** > **PTZ-TEG**, in agreement with the aforementioned discussion relating the molecular structure to the ability in sensitizing the Pt/TiO₂ photocatalysts.

Table 4. 3: TON values and Light-to-Fuel Efficiencies (LFE) of dye PTZ-ALK, PTZ-TEG and PTZ-GLU.

Dye Loading (μmol g ⁻¹)	TON			LFE (%)		
	PTZ-ALK	PTZ-TEG	PTZ-GLU	PTZ-ALK	PTZ-TEG	PTZ-GLU
1.0	1232	396	678	0.017	0.005	0.008
2.5	892	326	566	0.034	0.011	0.016
5.0	-	-	323	-	-	0.023
10.0	236	132	213	0.040	0.017	0.031
30.0	64	29	59	0.029	0.013	0.026

H₂ PRODUCTION IN GLUCOSE FUNCTIONALIZED PHENOTHAZINE BASED DYES IN PRESENCE OF TEMPLATING AGENT

The sensitizer systems listed in Table 4. 4 were investigated. In order to check different intermolecular interactions, co-adsorbent were added according to two dye:co-adsorbent ratios: 1:1 and 1:10.

Table 4. 4: Investigated sensitizers systems.

Sensitizer system	Dye-sensitizer	co-adsorbent
GLU	PTZ-GLU	-
GLU-GLU	PTZ-GLU	GLU
GLU-CDCA	PTZ-GLU	CDCA
ALK	PTZ-ALK	-
ALK-GLU	PTZ-ALK	GLU
ALK-CDCA	PTZ-ALK	CDCA

The Pt/TiO₂ photocatalysts sensitized by the **PTZ-ALK** and **PTZ-GLU** dyes were tested for H₂ production under Vis light irradiation ($\lambda > 420$ nm) from a triethanolamine (TEOA)/HCl aqueous buffer solution at pH = 7.0 in presence or in absence of **GLU** or **CDCA** as a co-adsorbent. In all cases, the remarkable stability previously observed for these **PTZ**-based dyes was maintained, even when a co-adsorbent was present.³ Indeed, the effect of the co-adsorbent on the H₂ production rate was remarkable. H₂ photogeneration over **PTZ-GLU** sensitized systems (Figure 4. 20) was enhanced by addition of the **GLU** co-adsorbent, while it was slightly hindered by addition of the **CDCA** co-adsorbent. This is consistent with an efficient disaggregation of the dye operated by the **GLU** co-adsorbent, by self-assembly interaction with the glucose functionality of the **PTZ-GLU**. On the other hand, the **CDCA** co-adsorbent was not able to interact with **PTZ-GLU**, likely increasing the tendency of agglomeration of the dye in segregated domains.

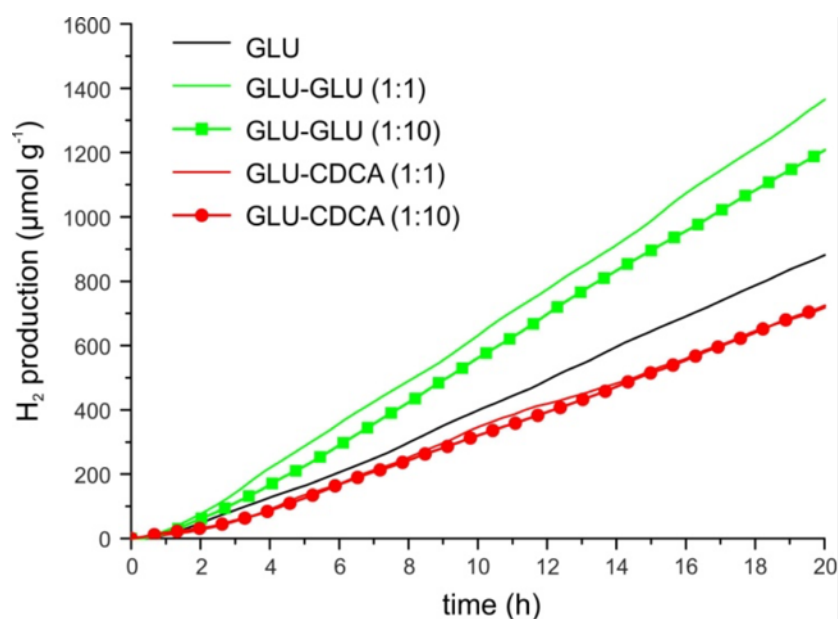


Figure 4. 20: H₂ production from TEOA 10% v/v solution at pH = 7.0 under irradiation with visible light ($\lambda > 420$ nm) over Pt/TiO₂ materials sensitized with **PTZ-GLU** in the presence of co-adsorbents **GLU** or **CDCA** 1:1 molar (lines) or 1:10 molar (lines+symbols) with respect to the dye.

In order to properly recognize the effect of the presence of the peripheral glucose functionality of **PTZ-GLU** in the process, **PTZ-ALK** was used as a control sensitizer, coupled with the same co-adsorbents (Figure 4. 21). The co-adsorbents caused an increase of H₂ photogeneration only when added in 1:10 dye:co-adsorbent molar ratio. When 1:1 co-adsorbent was added, the H₂ production was negatively affected. These results suggest that there is no specific interaction between **PTZ-ALK** and the co-adsorbents, and that the increased H₂ production is simply due to separation of the dyes molecules by a mass effect.

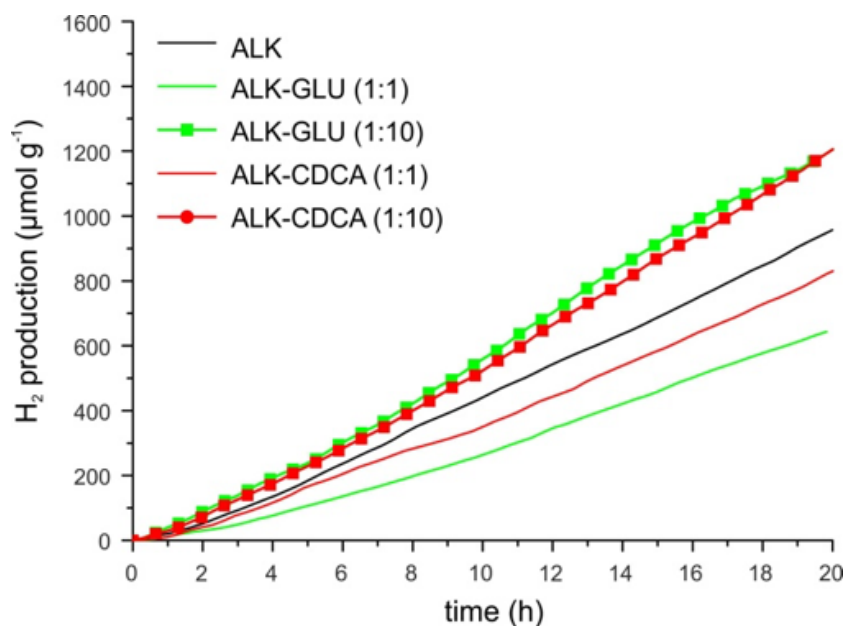


Figure 4. 21: H₂ production from TEOA 10% v/v solution at pH = 7.0 under irradiation with visible light ($\lambda > 420$ nm) over Pt/TiO₂ materials sensitized with **PTZ-ALK** in the presence of co-adsorbents **GLU** or **CDCA** 1:1 molar (lines) or 1:10 molar (lines+symbols) with respect to the dye.

TON values and Light-to-Fuel Efficiency (LFE₂₀) calculated at 20 h of irradiation for all of the sensitizer systems investigated in this work are listed in Table 4. 5. It is clear from these data that the best sensitizer system is GLU-GLU, with a 55-88% improved hydrogen generation compared to the system without co-adsorbent or in presence of the conventional CDCA co-adsorbent. Accordingly, TON and LFE₂₀ were greater for GLU-GLU sensitizer system. In contrast, the **PTZ-ALK** sensitizer did not show any hydrogen generation, TON, or LFE improvement in presence of 1:1 **GLU** or **CDCA** co-adsorbent compared to the absence of co-adsorbents.

Table 4. 5: TON values and LFE₂₀ for the studied Pt/TiO₂ sensitized catalysts.

Dye-Sensitized Solar Hydrogen Production

Sensitizing system	H ₂ amount ($\mu\text{mol g}^{-1}$ at 20h)	TON ($\mu\text{mol(H}_2\text{) } \mu\text{mol(dye)}^{-1}$ at 20h)	LFE ₂₀ (%)
GLU	880	59	0.024%
GLU-GLU (1:1)	1370	91	0.037%
GLU-GLU (1:10)	1213	81	0.033%
GLU-CDCA (1:1)	726	48	0.020%
GLU-CDCA (1:10)	728	49	0.020%
ALK	956	64	0.026%
ALK-GLU (1:1)	660	44	0.018%
ALK-GLU (1:10)	1215	81	0.033%
ALK-CDCA (1:1)	837	56	0.023%
ALK-CDCA (1:10)	1212	81	0.033%

In order to validate the overall picture, we are computing in collaboration with the group of Dr. F. De Angelis at CNR-ISTM in Perugia, by means of the DFT approach, the supramolecular arrangements on the semiconductor surface and investigated the intermolecular interactions for the different sensitizer/co-adsorbent systems (Figure 4. 22).

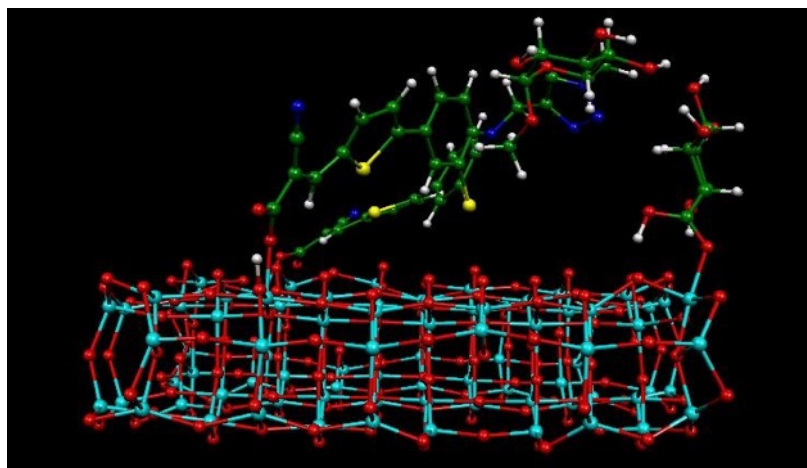


Figure 4. 22: DFT calculation of a molecule of **PTZ-GLU** and GLU adsorbed on a TiO₂ surface.

A preliminary investigation showed a possible bending of the glucose base dye to be coordinated by the glucuronic acid adsorbed on the surface of the semiconductor, validating the hypothesis of a self organization promoted by means of a judicious design of organic dyes and co-adsorbents.

Enhanced photocatalytic hydrogen generation using carbazole-based sensitizers

The photocatalytic scheme implies the use of a tandem system with two components: a redox storing catalysts (such as the benchmark Pt/TiO₂) and a sensitizer able of absorbing a broad part of solar spectrum and of transferring electron to the catalysts. The photosensitizer must also be stable in the working condition under continuous irradiation over long periods of time. Thus, a rational design of the molecular structure of the dye must be developed to improve the stability and performances of sensitized photocatalysts. Various studies on dye-sensitized hydrogen generation involves the use of more traditional organometallic dyes.⁷ Only recently, the focus is moving to metal-free sensitizers, which have the advantages of being cheaper, free of rare and toxic metals and endowed with a greater variety of structural and optical properties.^{2,13,16,28,66-68}

We have recently reported a series of branched donor-(π -acceptor)₂ phenothiazine-based sensitizers (**PTZ**) functionalized with an alkyl terminal and containing different thiophene-based spacer,³ showing lower activity but improved stability with respect to the reference system without the thiophene spacer. This fact has been related with electronic and steric effect of the thiophene spacer, favouring charge separation after light excitation of the donor group (phenothiazine) but probably inducing sulfur poisoning phenomena on surface of the Pt nanoparticles.

In this section, the effect of molecular design of the dye on the photocatalytic hydrogen generation is investigated by sequentially removing sulfur-based units from the chemical structure of the dye.

DESIGN AND SYNTHESIS

In particular, new sensitizers has been prepared by replacing the **PTZ** donor core with a sulfur-free electron-rich heteroaromatic ring and replacing the thiophene spacers with a sulfur-free heteroaromatic analog The introduction of the carbazole

(**CBZ**) moiety in the molecular structure afforded a strong enhancement of the efficiency of photocatalytic H₂ production compared to both **PTZ** and phenoxazine (**POZ**) based dyes, using Pt/TiO₂ as benchmark redox storing catalyst. The amount of produced hydrogen and turnover numbers (TON) are top-ranked amongst studies on dye-sensitized photocatalytic hydrogen production.

The **CBZ** building block has been selected as an ideal sulfur-free alternative to **PTZ**, being a strong electron-rich heteroaromatic ring thanks to the presence of the central five-membered ring containing a pyrrole-like nitrogen atom.⁶⁹ Despite **CBZ** is highly investigated for its applications in materials science,⁷⁰⁻⁷³ and in dye-sensitized solar cell (DSSCs),^{30,74-76} only very few studies on photocatalysis have been reported.^{15,77,78} Remarkably, whereas **PTZ** are associated to a typical butterfly structure,^{79,80} **CBZ** is planar, suggesting a strong effect of the charge generation and transport properties on catalytic efficiency of the tandem system. In order to separate the effects of the replacement of the S atom and of the change in the spatial arrangement, we have also investigated **POZ** donor groups. Within the scope of this work, **POZ** has the advantage of maintaining the butterfly structure as in **PTZ**, permitting to better elucidate the role of the **CBZ** unit.

To investigate the role of S in the spacer unit, we have designed new dyes by replacing the thiophene (**Th**) π -bridge with its sulfur-free five-membered analogue furan ring (**Fu**), which shares with thiophene many electronic and structural properties with the exception of the nature of the ring heteroatom.⁶⁹ The structures of new dyes are summarized in Figure 4. 23, being **PTZ-Th** the reference system.³

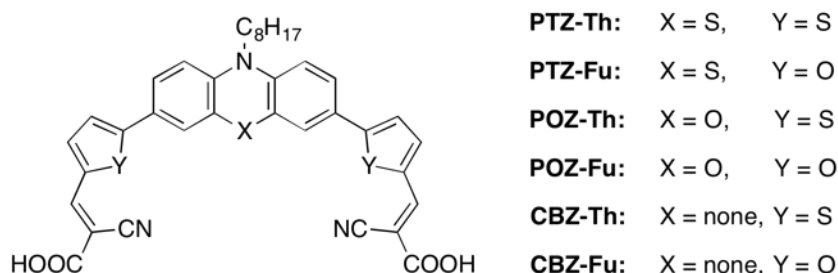
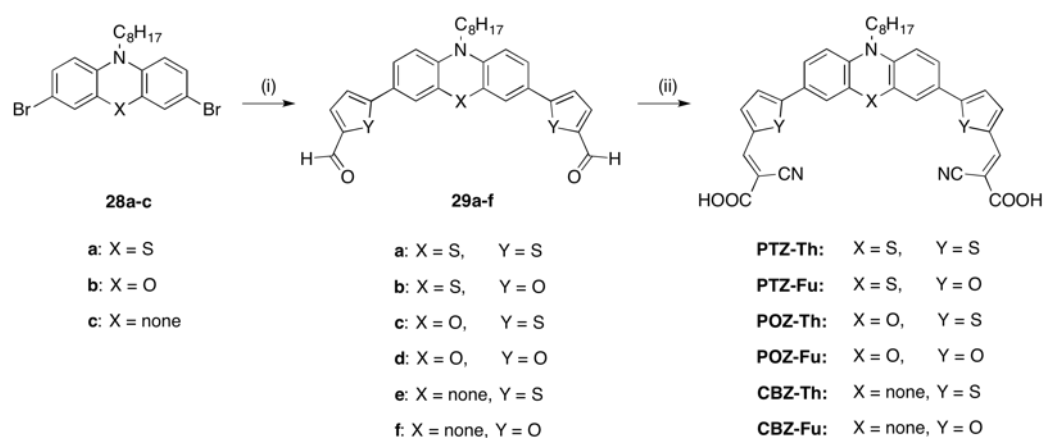


Figure 4. 23: General structure of **PTZs**, **POZs**, and **CBZs**.

PTZ-Th has been synthesized according to the literature.³ The same synthetic scheme (Scheme 4. 1) has been adopted as a simple and easily extendible procedure for synthesis of the new dyes.



Scheme 4. 1: General procedure for the synthesis of **PTZs**, **POZs**, and **CBZs**. Reagents and condition: (i) 5-Formyl-2-aryl-boronic acid, Pd(dppf)Cl₂·CH₂Cl₂ [dppf = 1,1'-bis(diphenylphosphino)ferrocene], K₂CO₃, DME/MeOH, microwave 100 °C, 90 min; (ii) cyanoacetic acid, piperidine, CHCl₃, reflux, 5 h.

The development of a general procedure is not only relevant for industrial scale-up but also to easily access an extended library of dyes. Although the synthesis of **CBZ-Th** and a molecule similar to **CBZ-Fu** (bearing a different *N*-alkyl functionalization) have been previously reported in the literature,^{75,81} the **CBZ**-based sensitizers were synthesized by the aforementioned general approach using 3,6-dibromocarbazole as a starting reagent while **POZ** derivatives were synthesized from 10-octyl-10H-phenoxazine-3,7-dibromo.⁸² **Fu** and **Th** derivatives have been prepared connecting the donor and the spacer units by Suzuki cross-coupling

reaction using the commercially available 2-furan-aldehyde-5-boronic acid and 2-thiophene-aldehyde-5-boronic acid, respectively.

OPTICAL AND ELECTROCHEMICAL CHARACTERIZATION

The absorption spectra of the dyes (10^{-5} M in DMSO) are shown in Figure 4. 24 and the detailed main optical and energetic parameters (HOMO-LUMO energies) are listed in Table 4. 6.

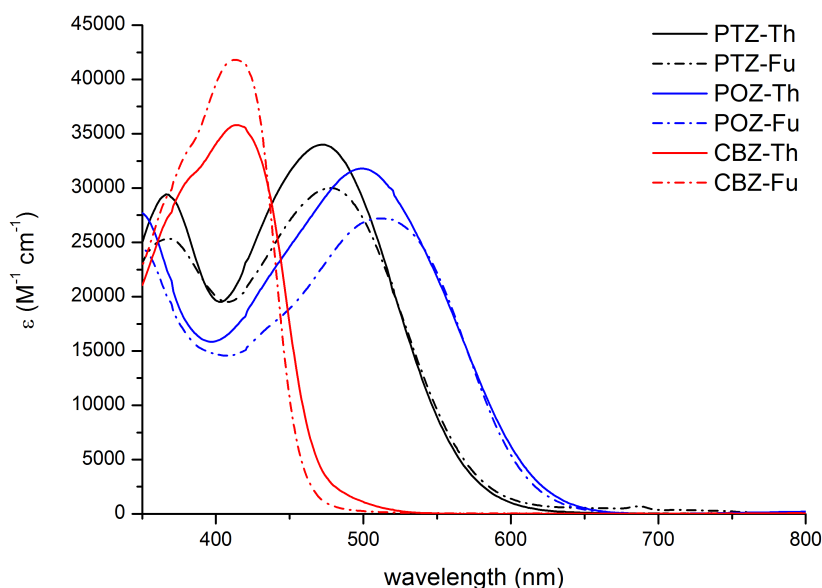


Figure 4. 24: Absorption spectra of the **PTZs**, **CBZs** and **POZs** dyes recorded in DMSO solution.

In general, the three families of **PTZ**, **POZ** and **CBZ** dyes exhibited the typical 2 bands, related to π - π^* absorption in the 300 – 450 nm range and to the intramolecular charge transfer (ICT) transition in the 400-600nm range.^{75,83} The π - π^* band shows a progressive red-shift in the order **POZ-PTZ-CBZ** as a result of increased electron delocalization in the core. On the other hand, the ICT transition is subjected to a progressive blue-shift. As a result, π - π^* and ICT transitions significantly overlap for the **CBZ** derivatives. The absorption maxima are centered around *ca.* 470 nm for **PTZ**, *ca.* 410 nm for **CBZ** and *ca.* 530 nm for the **POZ** dyes. Importantly, the maximum molar absorptivity is higher for the **CBZ** derivatives, whereas marginal differences (less than 10%) are recorded between

PTZ and **POZ** analogs. Finally, the introduction of the **Fu** spacer in place of **Th** did not significantly affect the absorption properties.

Table 4. 6: Main optical and electrochemical characterization of the PTZs, CBZs and POZs dyes.

Sample	λ_{\max}^a (nm)	ϵ (M ⁻¹ cm ⁻¹)	V_{ox} (V vs. Fc) ± 10 mV	HOMO ^b (eV) ± 0.05 eV	$E_{\text{gap}}^{\text{opt}}$ (eV)	LUMO ^b eV ± 0.05 eV
PTZ-Th ^c	470	34000 \pm 1000	0.15	-5.38	2.05	-3.33
PTZ-Fu	481	30200 \pm 700	0.36	-5.59	1.98	-3.61
POZ-Th	534	31800 \pm 1500	0.41	-5.64	1.87	-3.77
POZ-Fu	524	27200 \pm 200	0.38	-5.61	1.90	-3.71
CBZ-Th	414	35800 \pm 100	0.41	-5.64	2.26	-3.38
CBZ-Fu	409	41800 \pm 600	0.43	-5.66	2.28	-3.38

^a Dye solution 10⁻⁵ M in THF. ^b Vacuum potential = Fc/Fc⁺ + 5.23 V. ^c Values from Ref 3; CV and DPV plots are reported in Ref. 3

The electrochemical properties have been investigated for all the dyes and the main optical and electrochemical parameters are summarized in Table 4. 6. Cyclic voltammetry (CV) profiles (Figure 4. 25) showed a quasi-reversible behavior for the oxidation process in all the investigated dyes, whereas reduction was irreversible. Differential Pulsed Voltammetry (DPV) results (Figure 4. 26) was used to determine the HOMO energy levels from the current onset. The LUMO levels have been derived from electrochemical HOMO values and optical bandgaps, measured by means of Tauc plots.⁸⁴ Levels are pictorially shown in Figure 4. 27 and reported in Table 4. 6. Even though the HOMO energy levels are quite similar for most of the dyes (~ -5.60 eV), the different bandgaps significantly affect their LUMO energies and, accordingly, the electron injection capabilities to the Pt/TiO₂ system.

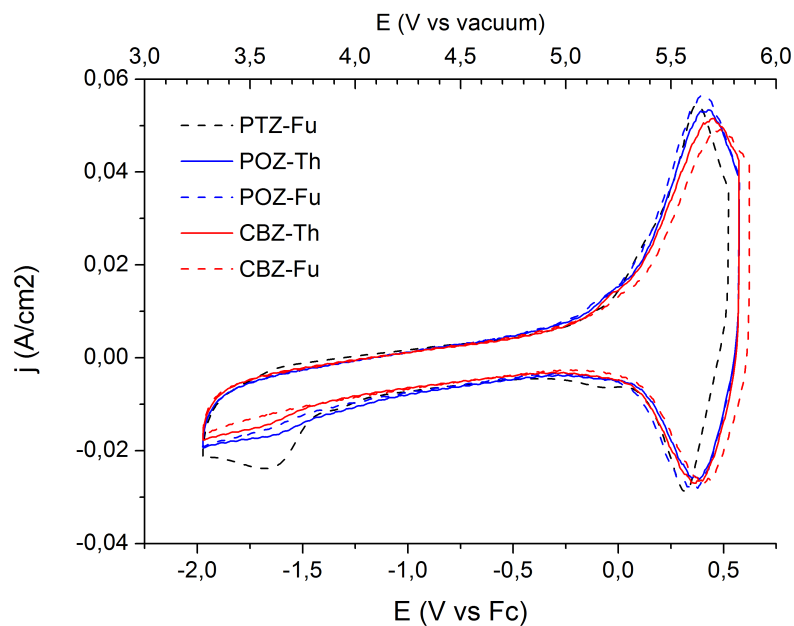


Figure 4. 25: Cyclic voltammery (CV) of the PTZs, CBZs and POZs dyes recorded in ACN:CH₂Cl₂ 3:1 TBAClO₄ 0.075M solution.

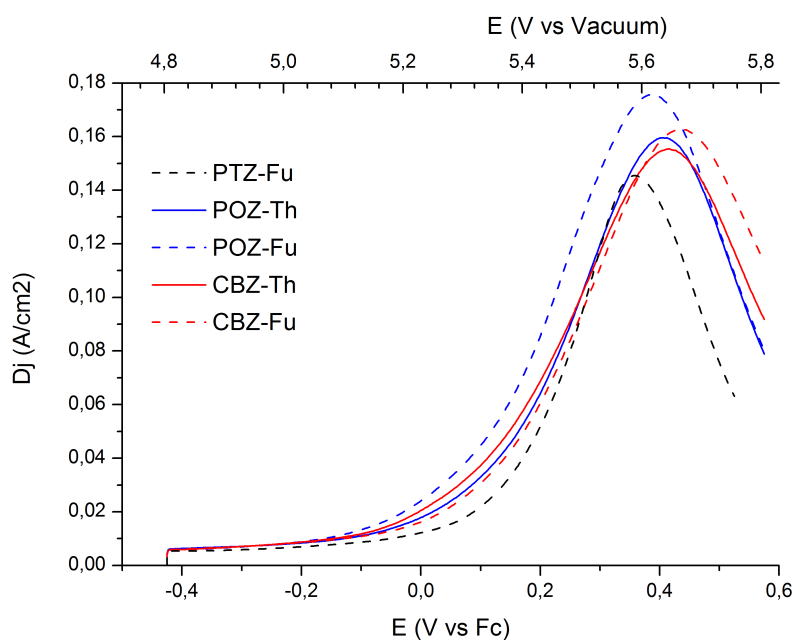


Figure 4. 26: Differential pulse voltammery (DPV) of the **PTZs**, **CBZs** and **POZs** dyes recorded in ACN:CH₂Cl₂ 3:1 TBAClO₄ 0.075M solution.

In particular, the LUMO energy of the **POZ** dyes, as well as that of **PTZ-Fu**, are very close to the conduction band (CB) of TiO₂ (-4.0eV).⁸⁵

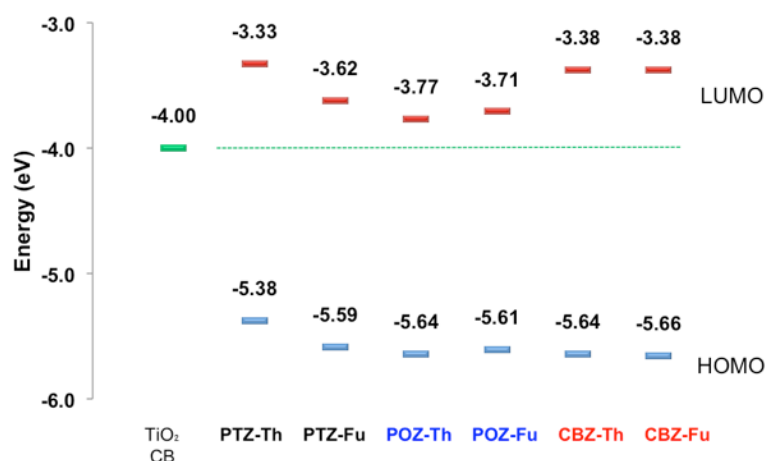


Figure 4. 27: Experimental HOMO/LUMO energy levels for the **PTZs**, **CBZs** and **POZs** dyes (CB level of TiO₂ is included as a reference for electron injection from the dye to the semiconductor).

PHOTOCATALYTIC HYDROGEN PRODUCTION

The sensitized Pt/TiO₂ photocatalysts were tested for H₂ production under Vis light irradiation ($\lambda > 420$ nm) from a triethanolamine (TEOA)/HCl aqueous buffer solution at pH = 7.0. The experiments have been performed adopting the same conditions previously optimized for **PTZ**-based photocatalysts.^{4,43} No H₂ production was observed using the bare Pt/TiO₂ under the same experimental conditions. Measured H₂ production rates and H₂ productivity vs irradiation time are presented in Figure 4. 28 and Figure 4. 29, respectively. Turnover numbers (TON) and Light-to-Fuel Efficiency (LFE₂₀) calculated after 20 h of irradiation are presented in Figure 4. 30 (obtained values are listed in Table 4. 7).

All of the investigated catalysts showed remarkable stability over a reasonable irradiation time of 20 h (Figure 4. 28). **CBZ**-sensitized photocatalysts showed by far the highest H₂ productivities, TON and LFE values.

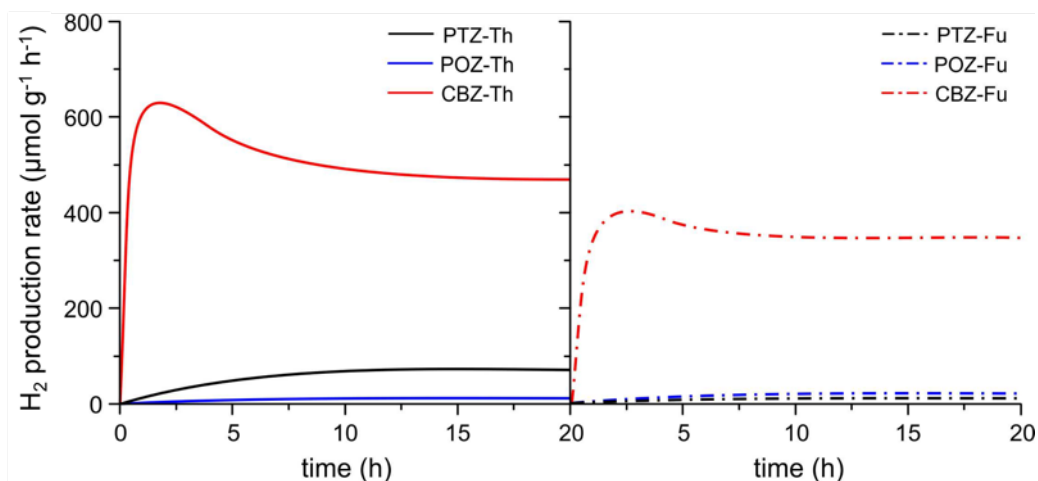


Figure 4. 28: H₂ production rate from TEOA 10% v/v solution at pH = 7.0 under irradiation with visible light ($\lambda > 420$ nm) over Pt/TiO₂ materials sensitized with PTZs, POZs and CBZs dyes.

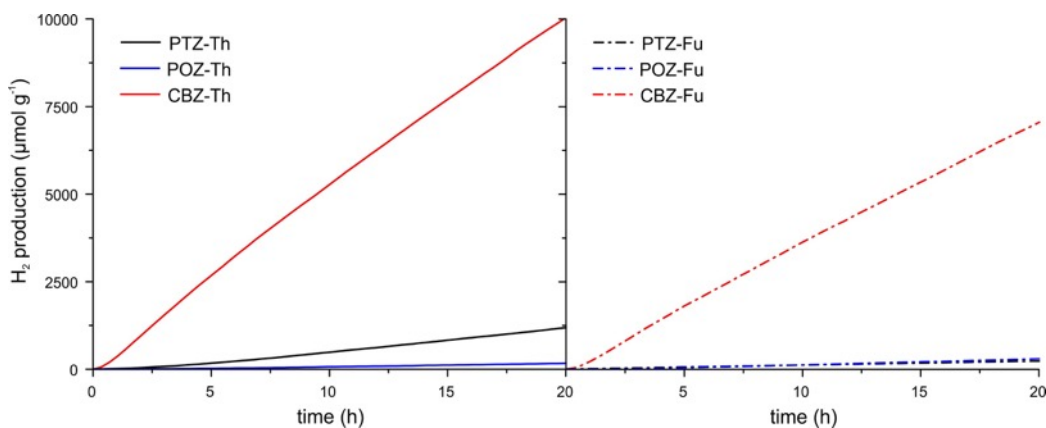


Figure 4. 29: H₂ production from TEOA 10% v/v solution at pH = 7.0 under irradiation with visible light ($\lambda > 420$ nm) over Pt/TiO₂ materials sensitized with **PTZs**, **POZs** and **CBZs** dyes.

Namely, performances were at least one order of magnitude higher than those referred to the benchmark **PTZ-Th** dye. Amongst **CBZ** based dyes, the photocatalytic activity of **CBZ-Th** was considerably higher than that of **CBZ-Fu**. The same relative trend was recorded for the **PTZ** family. Both **POZs**-sensitized photocatalysts demonstrated very small activity in H₂ production.

Table 4. 7: TON values and LFE₂₀ for PTZs, POZs, and CBZs sensitized catalysts.

Dye-Sensitized Solar Hydrogen Production

Dye sensitizer	H ₂ amount ($\mu\text{mol g}^{-1}$ at 20h)	TON ($\mu\text{mol(H}_2\text{)} \mu\text{mol(dye)}^{-1}$ at 20h)	LFE ₂₀ (%)
PTZ-Th	1178	236	0.032%
PTZ-Fu	227	45	0.006%
POZ-Th	163	33	0.004%
POZ-Fu	294	59	0.008%
CBZ-Th	10083	2017	0.272%
CBZ-Fu	7064	1413	0.190%

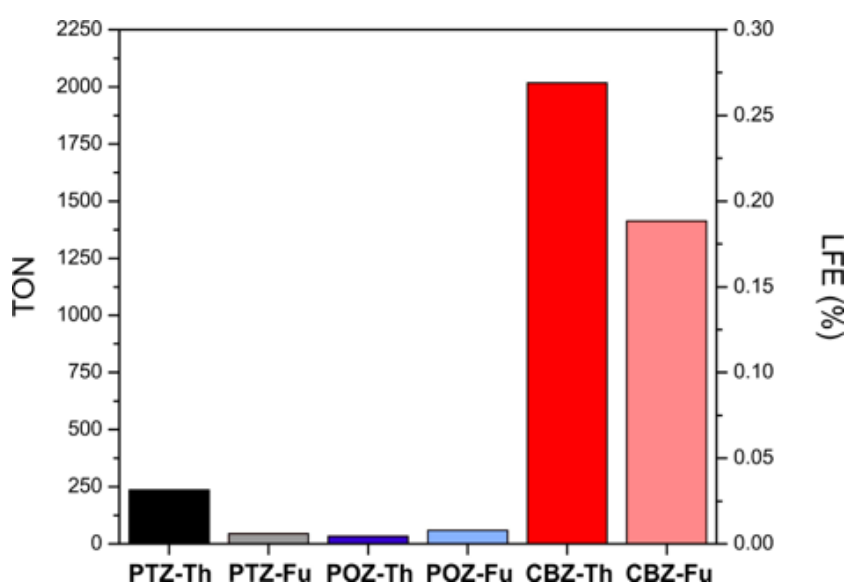


Figure 4. 30: Turnover number (TON) and Light-to-Fuel Efficiencies (LFE) calculated from H₂ production using TEOA/HCl solution at pH = 7.0 under irradiation with visible light ($\lambda > 420$ nm) over Pt/TiO₂ materials sensitized with **PTZs**, **POZs** and **CBZs** dyes.

Two main methods for achieving visible light-induced charge transfer and, consequently, photocatalytic activity of Pt/TiO₂ have been reported: dye-sensitization and ligand-to-metal charge transfer (LMCT).^{86,87} In the first case, the dye molecules located at the TiO₂/solution interface are photoexcited and subsequently inject electrons from LUMO of excited dye into the TiO₂ CB and then to Pt nanoparticles, where they are consumed for proton reduction. Dye molecules are finally restored by oxidation of the electron donor (TEOA) from the

aqueous solution. On the other hand, the LMCT mechanism is obtained when charge transfer takes place after formation of complexes between TiO_2 and the surface adsorbates. Upon coupling with TiO_2 , the relatively electron-rich compounds with linker groups (e.g., enediol, carboxylate, nitrile, and alcohol) exhibit a LMCT band in the visible region, as a result of the strong coupling between the molecular orbital (HOMO) of the adsorbate and the energy band of the semiconductor. In this case, the absorption of a photon allows the excitation of an electron directly from the ground state (HOMO level) of the adsorbate (ligand) to the semiconductor CB with mainly metal orbital characters, without involving the excited state of the adsorbate.

The photocatalytic results suggest that **PTZ**, **POZ** and **CBZ** dyes operate following different mechanism. **CBZ** derivatives (with a molecular structure very similar to that of **CBZ-Fu** and **CBZ-Th**) showed a red-shifted visible light absorption (up to 600 nm) when adsorbed on the surface of TiO_2 , typical of the sensitization by LMCT.⁷⁵ Such improved visible light absorption is not reported for **PTZ** and **POZ** molecules,²⁶ suggesting that these molecules operate mainly through the dye-sensitization pathway.

The demonstration of the importance of LMCT pathway in promoting photocatalytic activity, H_2 productivity has been checked using a cut-off filter at 515 nm (Figure 4. 31). After activation of the photocatalysts for 8 h under usual conditions, **CBZ-Th** still shows an appreciable photocatalytic activity under irradiation using photons with $\lambda > 515$ nm. This result is an indirect confirmation that LMCT is active in the **CBZ**-sensitized photocatalysts. Under the same conditions, H_2 production completely disappeared when **PTZ-Th** is used as sensitizer, despite UV-vis spectra of **PTZ** compounds show an intense light absorption up to 600 nm.

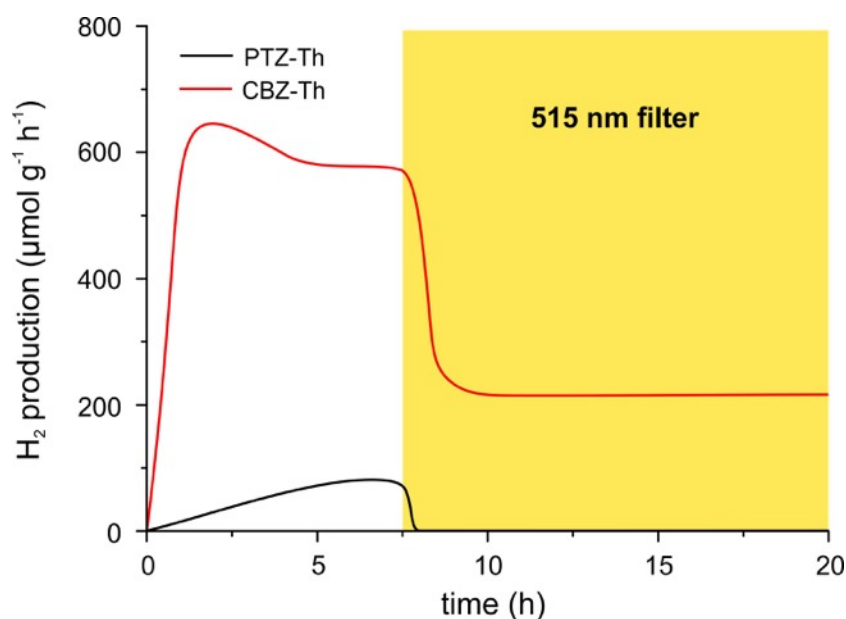


Figure 4. 31: H₂ production from TEOA 10% v/v solution at pH = 7.0 over Pt/TiO₂ materials sensitized with PTZ-Th and CBZ-Th dyes: after activation under irradiation with visible light ($\lambda > 420$ nm) for 8h, the photocatalytic activity under irradiation with photons with $\lambda > 515$ nm is presented.

This fact suggests that the ICT band, responsible for HOMO-LUMO transition and dye-sensitization of Pt/TiO₂, is very less efficient in promoting the photocatalytic H₂ production (at least in the part at higher wavelength). Taking this into account, the activity observed under irradiation with $\lambda > 420$ nm using **PTZ** and **POZ** dyes as sensitizers (Figure 4. 30) could be related to the π - π^* absorption. This latter case can also explain the very low activity observed using the **POZ** dyes, being the energy of the π - π^* band too high to be excited by visible light.

New organic p-type dyes as photocathode sensitizers for photoelectrochemical hydrogen production

From the first attempts to hydrogen production made in 1972 by Fujishima and Honda,⁵ many decades are passed and improvements have been made in the fields of artificial photosynthesis and photocatalytic hydrogen production.^{66,88} Concerning hydrogen evolution reaction (HER) the most used catalyst is so far Pt, in form of nanoparticles deposited onto the semiconductor surface or as a wire/net as passive cathode in a PEC cell.⁵ A similar efficiency can be achieved using hydrogenases decorated electrodes as HER.⁸⁹ However, owing to the large geometric size of hydrogenases, the level of loading onto the semiconductor surface is low, thus limiting the efficiency of this approach. Cobaloxime, a bio-inspired equivalent of hydrogenases, was also successfully integrated with an organic dye-sensitized-NiO or a Ru-dye-sensitized TiO₂ electrode via either non-covalent,⁹⁰ or covalent grafting.⁹¹ Another interesting approach was presented by Wu and co-workers,⁹² in which a ruthenium complex has been coordinated with an efficient cobaloxime-based catalyst (Figure 4. 32).^{93,94} This innovative design has been presented for the first time by Artero and co-workers in 2008.⁹⁴ These supramolecular compound, used for photocatalytic hydrogen production showed some interesting features. First of all, the use cobalt instead of expensive platinum, palladium, or rhodium metals in photocatalysts is a first step toward cost-effectively feasible hydrogen production. Cobaloximes appear to be good candidates for H₂-evolving catalysts, and they may provide a good basis for the design of photocatalysts that function in pure water as both the solvent and the sustainable proton source. Moreover, the use of a molecular connection between the sensitizer and the H₂-evolving catalyst appears to be advantageous in respect of photocatalytic activity. Structural modifications of this connection should allow a better tuning of the electron transfer between the light-harvesting unit and the catalytic center and leading to a higher efficiency of the system.

More recently, several examples of organic dyes have been proposed in both photocatalytic and PEC hydrogen production.^{90,95-97}

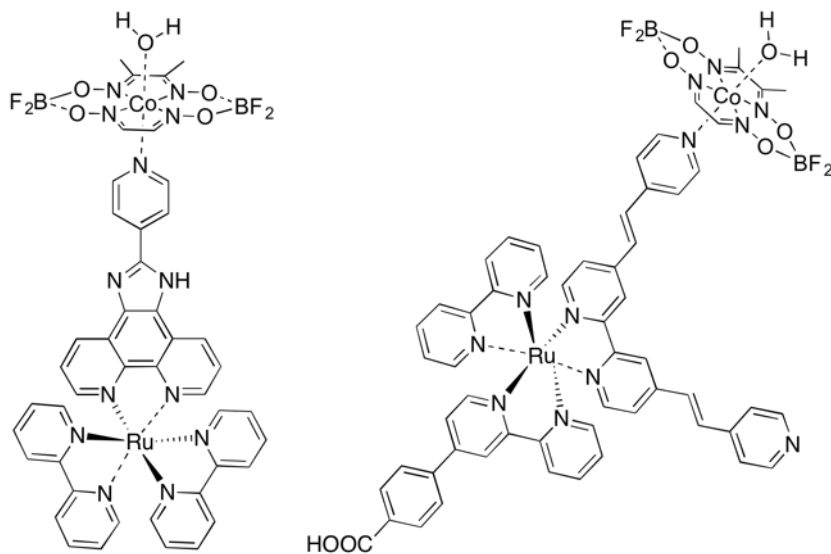


Figure 4. 32: Original supramolecular assembly proposed by Artero in 2008 (left) and Wu in 2013 (right)

In this project in collaboration with the group of Dr. Artero at CEA in Grenoble, we aim at investigating a series of p-type organic dyes to be used as Vis photosensitizers in PEC cell. These dyes are used in an active photocathode with special attention to the molecular design. The primary objective will be the study of these systems in different configurations: a) evaluation of the dye efficiency in the presence of a sacrificial electron acceptor (SEA, photocurrent measurement); b) study of the production of hydrogen in the presence of a catalyst in solution; c) study of the production of hydrogen in the presence of a catalyst bound to the sensitizer itself (Figure 4. 33).

The experiments performed in the presence of SEA are important because they allow us to assess the photocurrent generated by the system under illumination. These measures use a Co (III) complex which is reduced irreversibly to Co (II) allowing us to decouple charge photoinjection toward the electrolyte and catalysis. The experiments performed in the presence of the catalyst does not allow this sort of assessment because the charge transfer mechanism is more complicated

(foresees the transfer of two electrons to the catalyst instead of one as in SEA) and is difficult to assess the individual contributions.

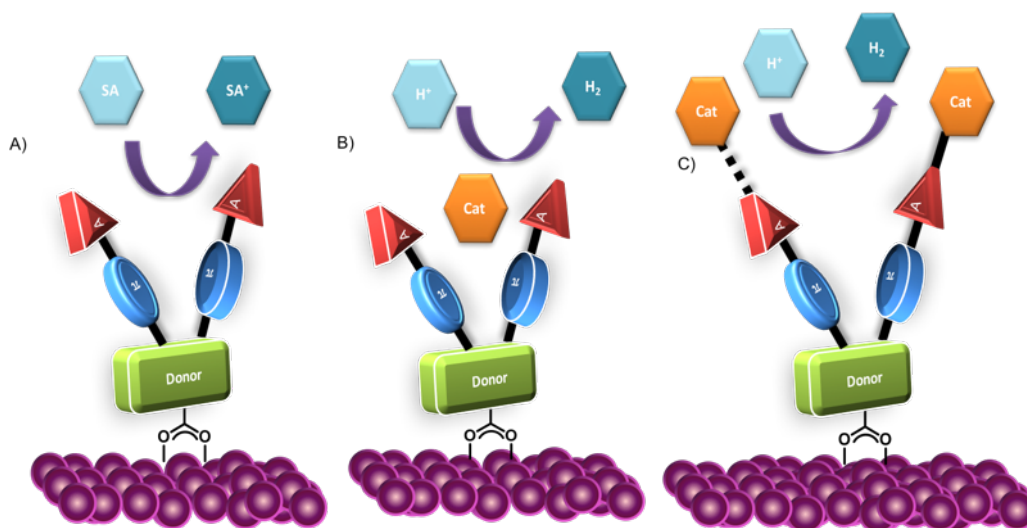


Figure 4.33: General scheme of the dye-sensitizer for PEC photocathodes; types of investigation considered in this work.

The requirements for a dye working in a p-type photocathode for a PEC are somehow similar to those for p-type DSSC. It should: a) efficiently absorb the Vis light over a broad range, b) be cheap and easy to prepare from low-cost precursors, c) own proper energy levels for charge transfer to the semiconductor and to the catalytic center, d) carry an anchoring group to bind onto the surface of the semiconductor (SC) (typically NiO). Therefore, we need for our purposes a properly designed push-pull molecule composed by an electron acceptor, a linker, and an electron donor with the binding moiety.

DESIGN AND SYNTHESIS

To design a working photocathode for hydrogen production, a favourable match of the reduction potentials between a dye and a H₂-evolving catalyst is critical. More specifically, the catalytic onset reduction potential of a H₂-evolving catalyst should be more positive than the reduction potential $E(D/D^-)$ of the dye in order to keep

the photo-induced electron transfer occurring from the dye to the catalyst. Besides, the HOMO level of the PS has to be more positive than the valence band of NiO (- 5.1 eV vs vacuum), so that the dye can inject holes into the VB of the semiconductor.

Another issue here addressed is related to the low mobility of holes within the NiO. This inherent characteristic of the semiconductor forces us to prepare thin layers onto which the dye is absorbed. For this reason, it will be crucial to synthesize a dye with a high molar extinction coefficient in order to absorb as much as possible light to maintain high efficiency of the device. Photoelectrode stability for water splitting is a further key challenge. Ideally, low pH is preferable for improving kinetics of hydrogen production on the deficient photocathode side. Thus it is crucial that the photocathode side is stable in acidic conditions. A good approach to solve this issue is strictly related to the molecular design. The basic concept is to keep proton far from the SC surface.

A possible design of a series of p-type sensitizers is depicted in Figure 4. 34, and will be compared with the **P1** dye as a reference.^{90,98} The organic push-pull dyes with a branched structure D-(π -A)₂ consist of a phenothiazine (**PTZ**) donor moiety connected to two proper acceptors such as malononitrile, or pyridineacetonitrile (A) groups. The spacer is a thiophene ring. The A groups are located above and act as the head layer whereby the aqueous electrolyte can interact. Furthermore, the pyridyl moieties can act as a coordinating agent to a proper molecular or inorganic catalyst. Upon photoexcitation, an electron can move from the donor (**PTZ**) to the acceptors (A). The peculiar feature of these dyes is the presence of a non-conjugated anchoring group on the donor moiety. This feature, in combination with appropriate HER, i.e. the cobaloxime depicted Figure 4. 34, dissolved in the electrolyte solution as hydrogen evolving catalyst, might solve the issue of charge recombination and dye desorption, thus increasing device performance and stability. The new dyes have been synthesized according to Scheme 4. 2 and the cobaloxime **[Co(dmgbF₂)₂(H₂O)₂]** has been prepared

according to literature,⁹⁹ as well as the pyridine complex **[PTZ-p-Py{Co(dmgbF₂)₂(H₂O)₂}]**.⁹⁴

Phenothiazine was brominated with Br₂ following the reported procedure,¹⁰⁰ and then followed by a Suzuki-Miyaura coupling with the 5-formyl-thiophen-2-yl-boronic acid protected as pinacol ester.¹⁰¹ After that, the anilinic nitrogen was deprotonated with NaH 60 % in DMF and added the bromoacetic acid ethyl ester to introduce the protected anchoring functionality on the donor fragment. Deprotection of the aldehyde in acidic condition by Knoevenagel condensation, allow to introduce the different accepting unit, namely malononitrile and 4-pyridylacetonitrile, enabled to afford the protected dyes with a satisfactory yield. The deprotection of the acidic functionality happen under inert condition, in pyridine as solvent in presence of LiI in harsh condition. In fact, it is necessary to run the reaction in a sealed flask under microwave irradiation at 160 °C, far above the boiling point of the solvent. This procedure allows us to get the desired product with acceptable yield.

The **[PTZ-p-Py{Co(dmgbF₂)₂(H₂O)₂}]** depicted in Figure 4. 35, has been prepared modifying a procedure reported in literature.⁹⁴ Due to the very low solubility given by the dye, the reaction has been performed in suspension instead of in solution and for longer time. Nevertheless, the product was obtained quantitatively after the removal of the solvent.

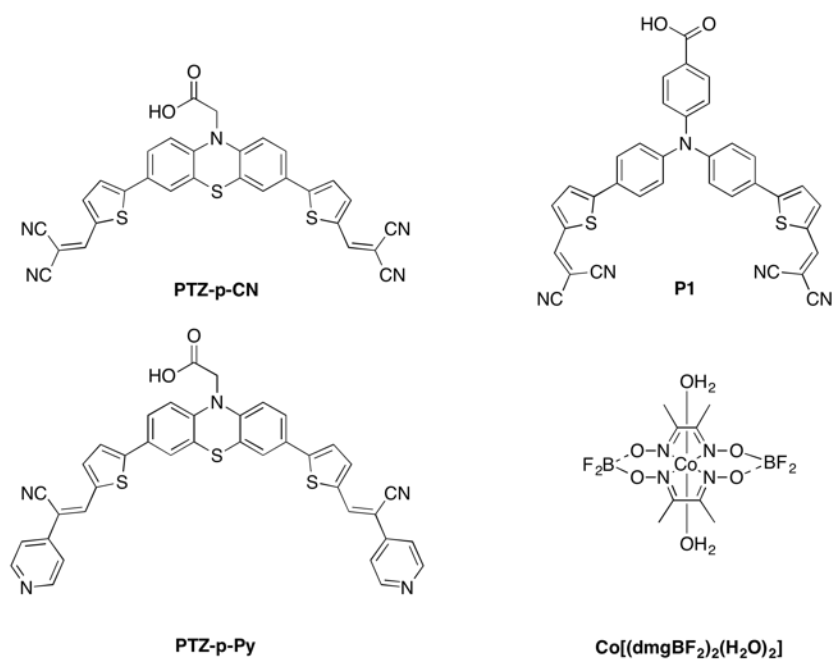


Figure 4. 34: Structure of the phthalocyanine based p-type sensitizers and cobaloxime catalysts.

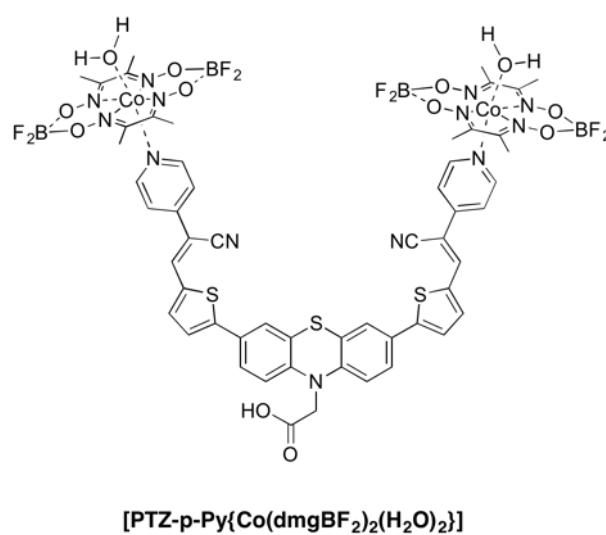
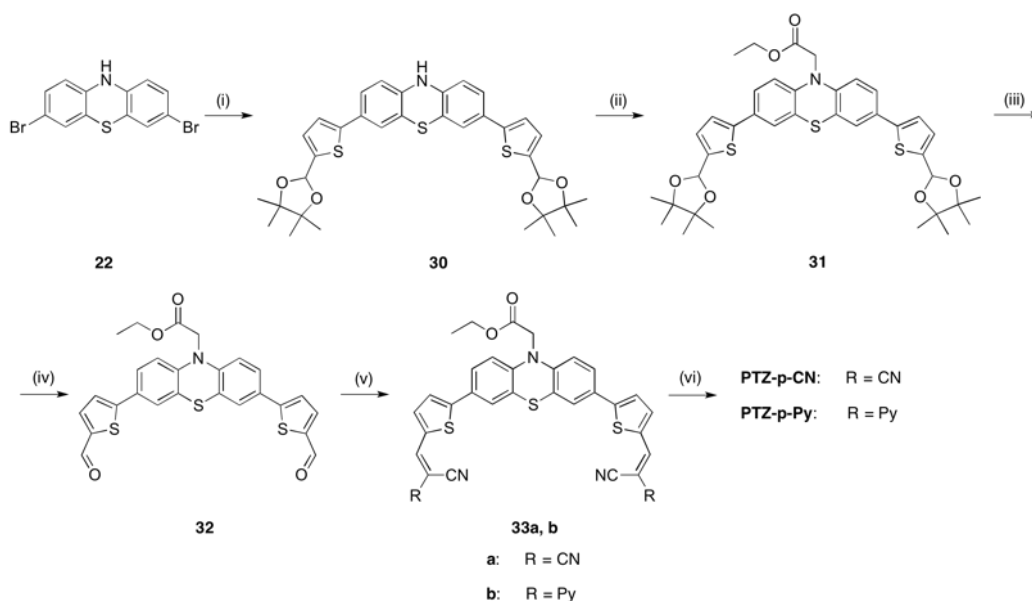


Figure 4. 35: Structure of the investigated supramolecular dyad [PTZ-p-Py{Co(dmgBF₂)₂(H₂O)₂}]



Scheme 4. 2: General procedure for the synthesis of **PTZ-p-CN** and **PTZ-p-Py**. Reagents and condition: (i) 4,4,5,5-tetramethyl-2-(5-(4,4,5,5-tetramethyl-1,3-dioxolan-2-yl)thiophen-2-yl)-1,3,2-dioxaborolane, Pd(dppf)Cl₂, K₂CO₃, DME/MeOH, N₂, microwave irradiation, 100 °C, 70 W, 1 h; (ii) bromoacetic acid ethyl ester, NaH 60% dispersion in mineral oil, N₂, THF, 0 °C to r.t.; (iii) 10% HCl H₂O/THF 1:2 v/v; reflux, 1 h; (v) a) malononitrile, piperidine, CHCl₃, reflux 4 h; b) 4-Pyridylacetonitrile hydrochloride, piperidine, CHCl₃, reflux, 4 h.

OPTICAL AND ELECTROCHEMICAL CHARACTERIZATION

The absorption spectra of the dyes (10^{-5} M in DMSO) are shown in Figure 4. 36 and the detailed main optical and energetic parameters (HOMO-LUMO energies) are listed in Table 4. 8.

The absorption spectra of the dyes show different behaviours. In the case of **P1**, **PTZ-p-Py** and the dyad ([**PTZ-p-Py**{**Co(dmgbF₂)₂(H₂O)₂**}] the typical structure for a push-pull structure has been observed, with an intense ICT band at around 490-500 nm for both dyes and the dyad, and a π - π^* absorption band at around 380 nm. Otherwise, the **PTZ-p-CN** shows an unexpected behaviour with a broad absorption band with a maximum at 391 nm with a broad tail up to 500 nm. The catalyst [**Co(dmgbF₂)₂(H₂O)₂**] shows a maximum at 471 nm with a single band absorption spectrum. The molar extinction coefficients are considerably different for all the systems, ranging from $51700 \text{ M}^{-1} \text{ cm}^{-1}$ for **P1** to $9700 \text{ M}^{-1} \text{ cm}^{-1}$

for **PTZ-p-CN**. In the case of **PTZ-p-Py** and the corresponding dyad there is a decrease in the molar absorptivity of the second. Moreover, the spectrum of the dyad shows a shoulder at low energy that can be ascribed to the MLCT band due to the coordination of the Co atom by the pyridine of the **PTZ-p-Py**.

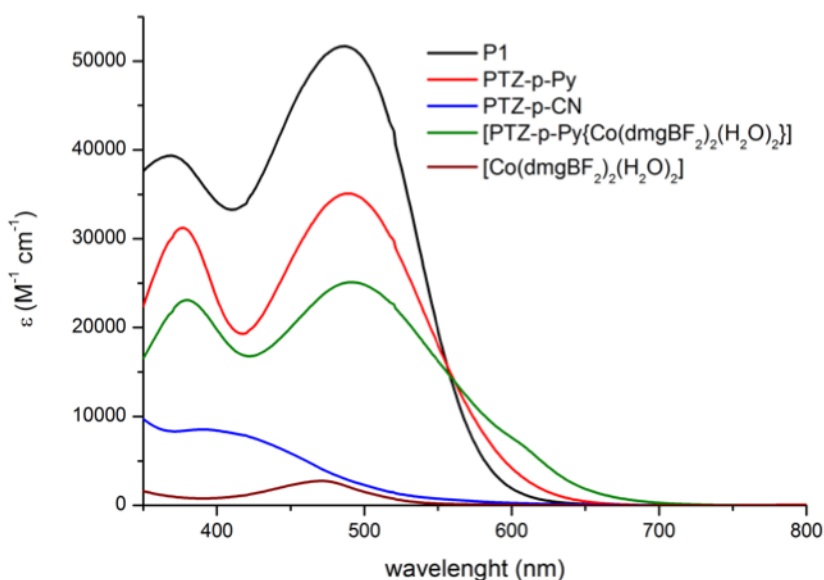


Figure 4. 36: UV-Vis spectra of the investigated dyes compared to **P1** and **Co[(dmgbF₂)₂(H₂O)₂]** catalyst.

The electrochemical properties have been investigated for all the dyes and the electrochemical parameters are summarized in Table 4. 8. Cyclic voltammetry (CV) profiles (Figure 4. 37) showed a quasi-reversible behaviour for the oxidation process in all the investigated dyes, whereas reduction was irreversible. At anodic potentials, all chromophores presented a similar oxidation behavior resulting in an oxidation wave having a peak potential at ca. 0.5 V vs. Fc/Fc⁺, which is related to the oxidation of the electron-rich group, as consequence the HOMO energy levels are quite similar for most of the dyes (~ -5.80 eV), though.

Table 4. 8: Optical and electrochemical parameters for the dyes and the catalysts.

Sample	λ_{\max}^a (nm)	ϵ ($10^3 \text{ M}^{-1}\text{cm}^{-1}$)	V_{ox} (V vs. Fc) $\pm 10 \text{ mV}$	HOMO ^b (eV) $\pm 0.05 \text{ eV}$	$E_{\text{gap}}^{\text{opt}}$ (eV)	LUMO ^b (eV) $\pm 0.05 \text{ eV}$
P1 ^c	372	39.7 ± 1.0	0.15	-6.0	2.14	-4.0
	489	51.7 ± 1.0				
PTZ-p-CN	391	9.7 ± 0.3	0.22	-5.8	2.10	-3.7
			0.52			
PTZ-p-Py	378	31.2 ± 0.5	0.25	-5.8	1.91	-3.9
	502	35.1 ± 0.5	0.54			
[Co(dmgbF ₂) ₂ (H ₂ O) ₂] ^d	471	2.74 ± 0.1	-0.03	-5.2	2.18	-4.2
[PTZ-p-Py{Co(dmgbF ₂) ₂ (H ₂ O) ₂ }]	380	23.1 ± 0.6	0.35	-5.6	1.78	-3.8
	491	25.1 ± 0.6				

^a Dye solution 10^{-5} M in THF. ^b Vacuum potential = Fc/Fc⁺ + 5.23 V. ^c Values and CV plots from Ref. 102. ^d HOMO and LUMO have been derived from electrochemical oxidation and reduction potential.

The reductive behavior is generally more complex, showing for all dyes a first, weak and irreversible wave likely originated by the reductive chemisorption of the acidic protons onto the electrode surface.¹⁰³ The following current wave corresponds to the injection of the electron into the LUMO orbital. Considering the irreversibility of the process, the LUMO levels have been derived from electrochemical HOMO values and optical bandgaps, measured by means of Tauc plots.⁸⁴ The HOMO-LUMO levels for the **[Co(dmgbF₂)₂(H₂O)₂]** have been directly calculated from the electrochemical measurements. Levels are pictorially shown in Figure 4. 38 and reported in Table 4. 8.

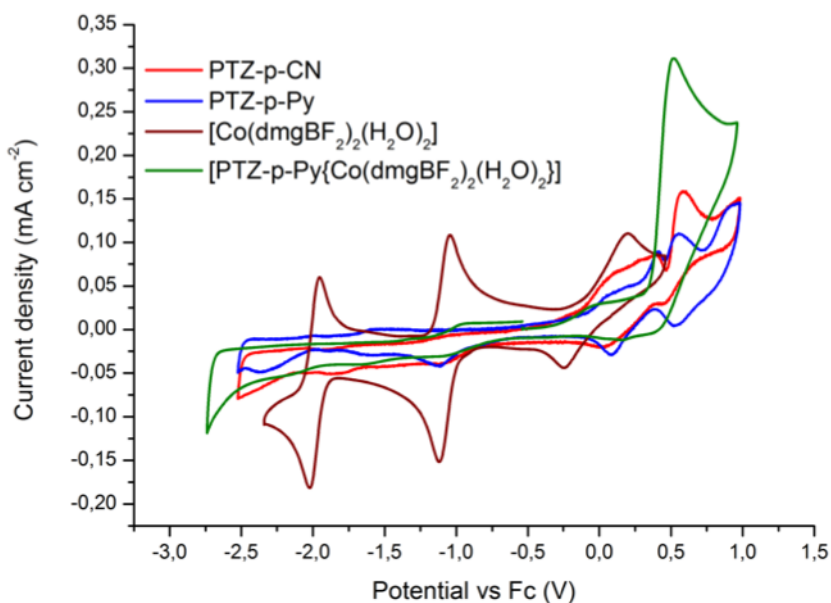


Figure 4. 37: Cyclic voltammetry (CV) of the dyes (**PTZ-p-CN**, **PTZ-p-Py**), the catalyst ($[\text{Co}(\text{dmgBF}_2)_2(\text{H}_2\text{O})_2]$) and the dyad ($[\text{PTZ-p-Py}\{\text{Co}(\text{dmgBF}_2)_2(\text{H}_2\text{O})_2\}]$), recorded in a DMF solution of TBABF₄ (0.1 M) solution in DMF on a glassy carbon electrode starting on oxidation (100 mV/s).

The reduction of **PTZ-p-Py** dye, bearing a stronger acceptor group, is comparatively more anodically shifted with a lower energy LUMO at -3.9 eV. Thus, no thermodynamic limitation to hole transfer to NiO are expected: in all cases, the HOMO energies are similar to the **P1** dye and sufficiently lower than the upper valence band edge of NiO, located at -5.1 V *vs.* Vacuum.^{104,105} Electron transfer to the catalyst ($[\text{Co}(\text{dmgBF}_2)_2(\text{H}_2\text{O})_2]$), relevant to dye regeneration, is in all cases, exergonic, with ΔG° values larger than -0.2 eV, allowing to predict favourable kinetics.

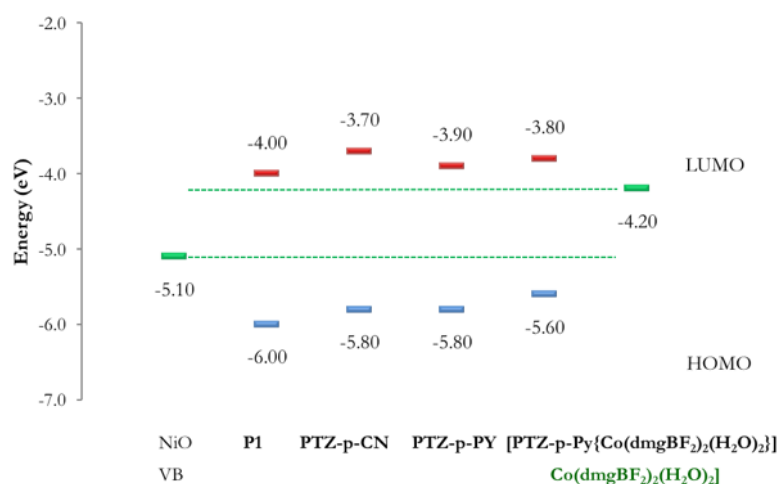


Figure 4. 38: Experimental HOMO/LUMO energy levels for the dyes (**PTZ-p-CN**, **PTZ-p-Py**), and the dyad (**[PTZ-p-Py{Co(dmgbBF₂)₂(H₂O)₂}]**), (VB level of NiO is included as a reference for hole injection from the dye to the semiconductor, and Co(II)/Co(I) reduction potential as a reference for electron injection from the dye to the catalyst (**[Co(dmgbBF₂)₂(H₂O)₂]**).

Considering that we are interested in the reductive process, and we aim to study a combined system in which the dyes and the catalyst act as a single unit, we decided to deeply investigate the reductive process of the **PTZ-p-Py** dye and the corresponding dyad. While the spectroscopic characterization of the dyad is not conclusive, and the NMR analysis is impossible due to the paramagnetic Co(II) in the complex, a powerful method to analyze the new compound could be the electrochemical analysis. The CV plot of the dye and dyad compared to the Co catalyst have been recorded and depicted in Figure 4. 39, furthermore, the CV plot of the main reductive process of the dyad have been shown in Figure 4. 40.

It is clear from the comparison of the CV traces in Figure 4. 39 that the dyad is not a mere mixture of the two molecular species, but a more complex entity. This is confirmed by the shift to more positive potential (~ 100 mV) of the Co(II)/Co(I) reversible process relative to the starting cobaloxime catalyst, in agreement with what reported in literature.⁹⁴

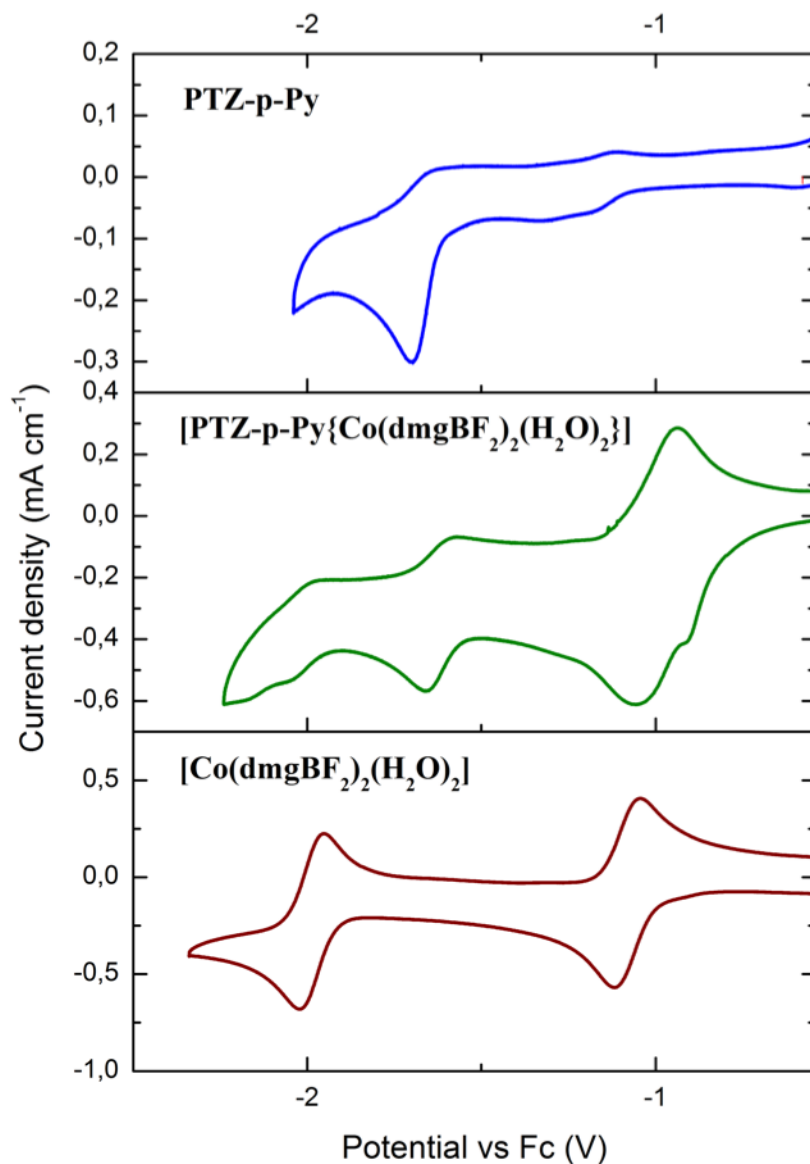


Figure 4. 39: Comparison of the CV scan of **PTZ-p-PY**, the corresponding dyad **[PTZ-p-Py{Co(dmgbF₂)₂(H₂O)₂}]** and the catalyst **Co[(dmgbF₂)₂(H₂O)₂]**, recorded in a DMF solution of TBABF₄ (0.1 M) solution in DMF on a glassy carbon electrode starting on oxidation (100 mV/s).

The different scan windows in the reduction allowed us to investigate the different reversible process. An interesting fact, not yet explained, is the formation of a shoulder peak close to the Co(II)/Co(I) transition. The nature of this peak is not yet clear but may be associated either with a mixture of molecules with mixed

coordination sphere of cobalt (with a ligand different than H_2O) or a mixture between bis and mono cobaloxime adducts.

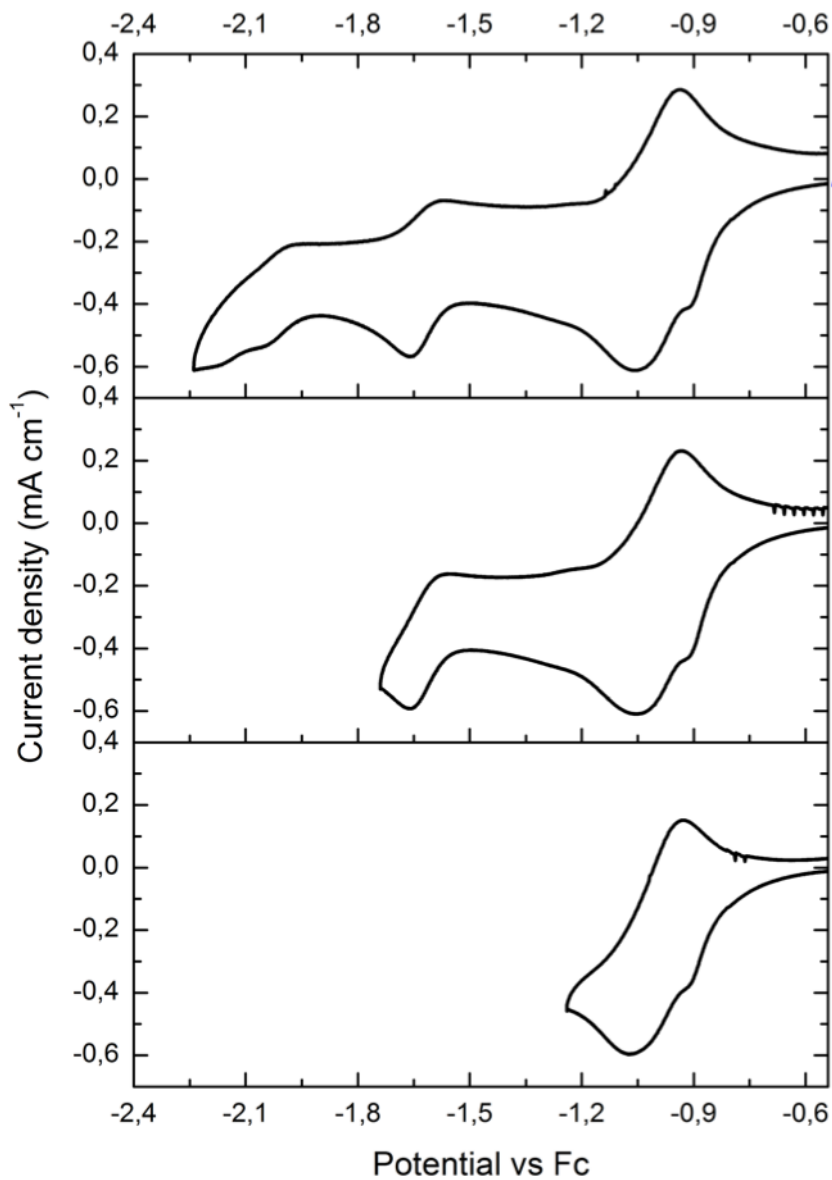


Figure 4. 40: Comparison of the CV scan of the reduction process of the dyad **[PTZ-p-Py{Co(dm gBF_2) $_2$ (H_2O) $_2$]}**, recorded in a DMF solution of TBABF $_4$ (0.1 M) solution in DMF on a glassy carbon electrode starting on oxidation (100 mV/s).

PHOTOELECTROCHEMICAL HYDROGEN PRODUCTION

The new dyes and the dyad have been tested in a PEC cell on a NiO photocathode. The NiO layer have been prepared according to literature,⁶⁸ and sensitized through soaking in a 0.2 mM solution of the dyes **PTZ-p-CN** and **PTZ-p-PY** in DMF overnight. Other electrodes have been stained using a 0.2 mM solution of the dyad **[PTZ-p-Py{Co(dmgbF₂)₂(H₂O)₂}]** in DMF. As reference, a series of electrodes previously sensitized with **PTZ-p-Py**, have been stained with a solution of cobaloxime **Co[(dmgbF₂)₂(H₂O)₂]** in acetone to evaluate the possibility to form the dyad *in situ* (we will refer to it as **[PTZ-p-Py{Co(dmgbF₂)₂(H₂O)₂}] 2 step**).

After rinsing with the same solvent, we thus measured the amount of dye loaded onto the NiO films. As previously reported, it is possible to roughly estimate the amount of dye loaded on the surface of a photoelectrode using simple spectrophotometric methods.¹⁰⁶ The absorption spectra of the sensitized NiO photocathodes are reported in Figure 4. 41, and the relative calculated dye surface concentration values in Table 4. 9.

The results of this investigation are not completely clear. In fact, while the maximum of adsorption of **P1**, as well as **PTZ-p-Py** and the dyad **[PTZ-p-Py{Co(dmgbF₂)₂(H₂O)₂}]2 step** (prepared with successive staining), are just slightly red shifted (~ 40-50 nm), the shape of the absorption spectra of the dyad **[PTZ-p-Py{Co(dmgbF₂)₂(H₂O)₂}]** (the one prepared in solution) and the **PTZ-p-CN** are different from the ones measured in solution.

It is possible to postulate that the dyad **[PTZ-p-Py{Co(dmgbF₂)₂(H₂O)₂}]** is not stable for long time in solution of coordinating solvent. It has been previously reported that solvent such as acetonitrile or DMF are able to substitute axial ligand in cobaloxime complex,¹⁰⁷ so it is possible that the long staining time could have affected the complex with the pyridine dye or even removed the cobaloxime from the dye itself.

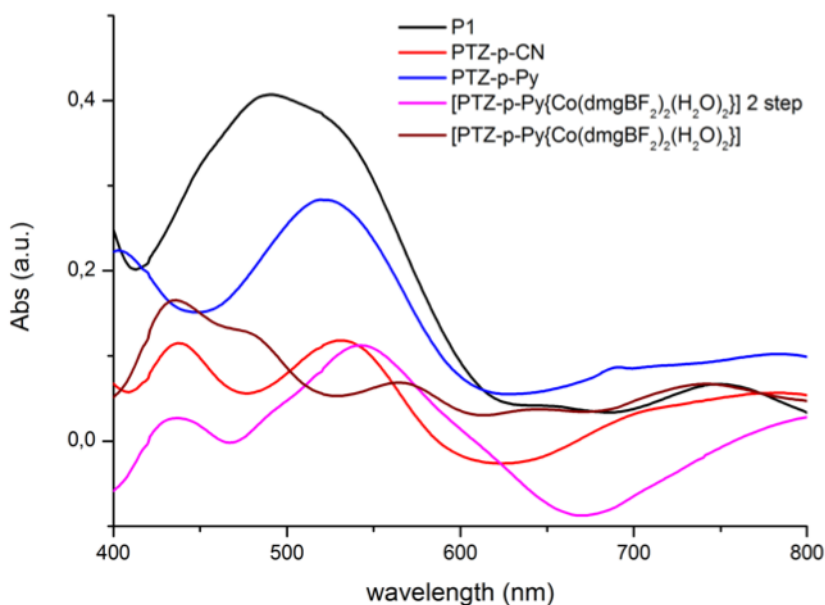


Figure 4. 41: UV-Vis spectra of sensitized NiO photocathodes with different dyes.

In the case of **PTZ-p-CN** it is possible to observe a new absorption band at ca. 550 nm that is absent in the spectrum measure in solution. The nature of this band is not clear even if it is in the expected spectral region for an ICT band such in the analogous **PTZ-p-Py.**, further experiments will be needed to settle this issue, though.

The photocathodes have been tested in a fully aqueous pH 4.5 sodium acetate 0.1 M buffer in presence of 10 mM of pentaamminechlorocobalt(III) chloride $[\text{Co}(\text{NH}_3)_5\text{Cl}]\text{Cl}_2$ as sacrificial electron acceptor, or otherwise in the presence of the cobaloxime $\text{Co}[(\text{dmgbF}_2)_2(\text{H}_2\text{O})_2]$ as catalyst.

The photocathodes have been employed as working electrode in a standard three-electrode cell, with a titanium wire as counter electrode and Ag/AgCl in 3 M KCl solution as reference. Usually, the best choice in term of working potential is -0.4 V vs Ag/AgCl (-0.2 vs NHE) to reduce recombination and enhance the photocatalytic activity, as previously reported in literature.¹⁰⁸ A series of test scans at different potential have been performed. The linear sweep voltammetry (LSV) in

presence of SEA, depicted in Figure 4. 42, was recorded under chopped light (400-800 nm filtered Xe lamp, 65 mW/cm²; 1 sun), shows the establishment of a photocurrent and a reductive process around -0.4 vs Ag/AgCl (- 0.2 V vs NHE) related to Co(III)/Co(II) irreversible reduction of the SEA. It was therefore decided to perform the experiments at 0 V vs Ag/AgCl (+ 0.2 V vs NHE), since these conditions afford the highest photocurrent values together with low dark current.

Chronoamperometry (CA) performed in the same electrolytic solution at 0 V vs Ag/AgCl (+ 0.2 V vs NHE) under chopped light is reported in Figure 4. 43. An enhancement of the photocurrent under irradiation has been observed and the variation of the current density have been estimated and reported in Table 4. 9.

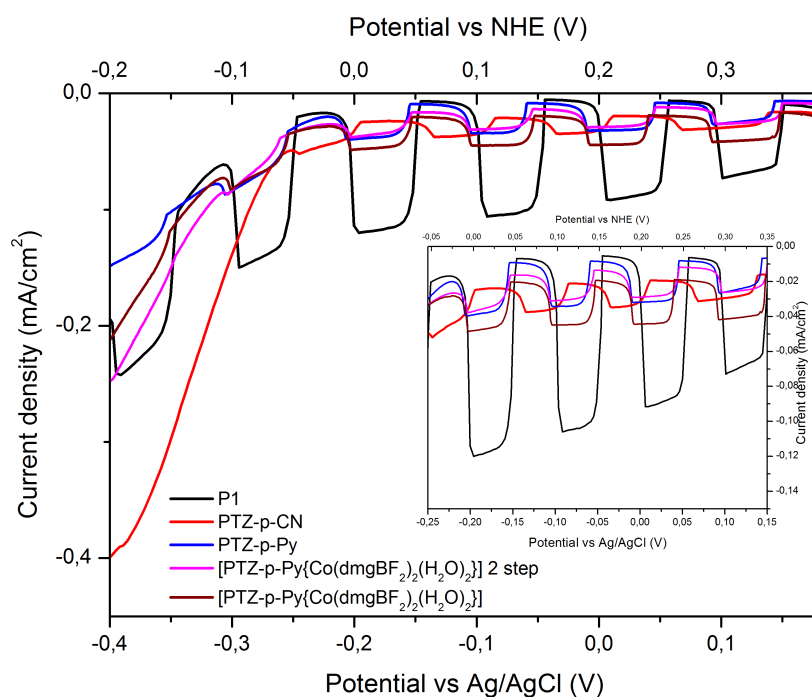


Figure 4. 42: Linear sweep voltammogram (10 mV/s) recorded under chopped light on NiO photocathodes sensitized with the investigated dyes in presence of [Co(NH₃)₅Cl]Cl₂ (10 mM)/acetate buffer (pH 4.5; 0.1 M in water).

The short CA scans showed a stable photocurrent after an initial activation time. The values of Δj_{SEA} are very similar for the new dyes (from 15 to 27 $\mu\text{A}/\text{cm}^2$), while a much higher value has been recorded for the reference P1 dye (89 $\mu\text{A}/\text{cm}^2$).

Table 4. 9: Photocurrent density obtained from chronoamperometry, charge flown during electrolysis under irradiation at 0 V vs Ag/AgCl (+ 0.2 V vs NHE), and surface dye concentration.

Dye ^a	Δj_{SEA}^b ($\Delta j_{\text{SEA}}/j_{\text{max}}$) ($\mu\text{A}/\text{cm}^2$)	Δj_{cat}^c ($\Delta j_{\text{cat}}/j_{\text{max}}$) ($\mu\text{A}/\text{cm}^2$)	Q^d (mC)	Dye surface conc. (10^{-9} mol/ cm^2)
P1	89 (0.98)	15 (0.88)	86.4	7.8
PTZ-p-CN	15 (0.50)	3 (0.50)	50.4	11.3
PTZ-p-Py	25 (0.86)	2 (0.50)	41.4	8.1
[PTZ-p-Py{Co(dm gBF_2) $_2$ (H $_2$ O) $_2$ }]	27 (0.80)	1.5 (0.50)	38.7	5.2
[PTZ-p-Py{Co(dm gBF_2) $_2$ (H $_2$ O) $_2$ }] $_2$ step	18 (0.72)	3 (0.5)	58.6	4.5

^a 1.5 μm thick, surface area 2.7 cm^2 ; ^b measured in presence of [Co(NH $_3$) $_5$ Cl]Cl $_2$ (10 mM)/acetate buffer (pH 4.5; 0.1 M in water) after 5 min with subtraction of the dark current; ^c measured in presence of [Co(dm gBF_2) $_2$ (H $_2$ O) $_2$] (1 mM)/acetate buffer (pH 4.5; 0.1 M in water) after 5 min with subtraction of the dark current; ^d measured after 3 h in presence of [Co(dm gBF_2) $_2$ (H $_2$ O) $_2$] (1 mM)/acetate buffer (pH 4.5; 0.1 M in water).

We tried to perform some tests in pure aqueous electrolyte with the dyad [PTZ-p-Py{Co(dm gBF_2) $_2$ (H $_2$ O) $_2$ }] to evaluate the possibility to directly produce H $_2$, but the recorded photocurrents were too low to be considered (less than 1.5 $\mu\text{A}/\text{cm}^2$).

In fact, the stability of the pyridine–cobalt bond in the Co(I) oxidation state has been questioned.¹⁰⁹⁻¹¹²

A weak or reversible pyridine–cobalt linkage is likely responsible, at some point, for the leaching of cobalt complexes from the dye decorated surface, resulting in limited stability as reported from Reisner and co-workers in the case of a decorated carbon nanotube electrodes.^{112,113} If the cobaloxime is released in solution at sub-

micromolar concentration, its reattachment to the electrode surface via pyridine coordination is quite unlikely, even after completion of the catalytic cycle and restoration of a higher resting oxidation state. To compensate this effect, we started the same experiments with submillimolar concentration of the selected catalyst $[\text{Co}(\text{dmgBF}_2)_2(\text{H}_2\text{O})_2]$ in solution. The LSV scans in presence of the cobaloxime are depicted in Figure 4. 44.

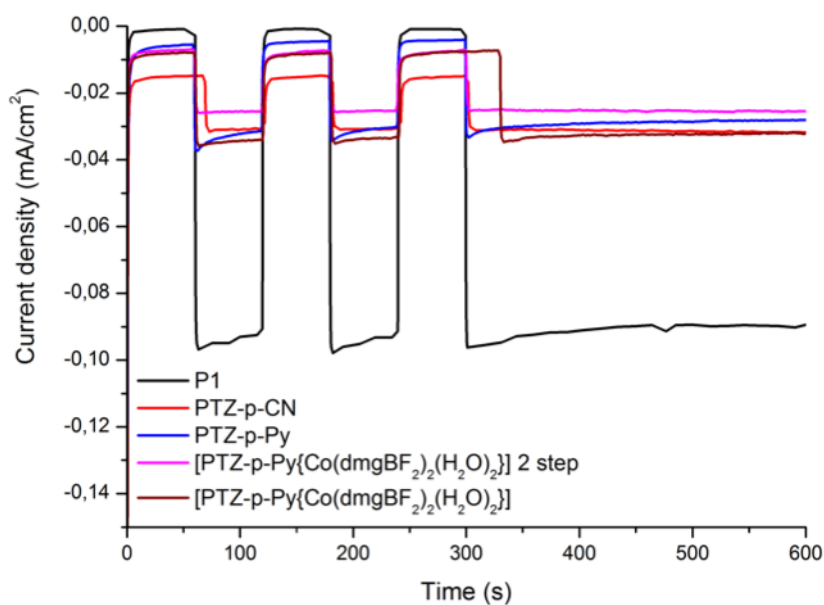


Figure 4. 43: Short chronoamperometric plot measured at 0 V vs Ag/AgCl (+ 0.2 V vs NHE) under chopped light on NiO photocathodes sensitized with the investigated dyes in presence of $[\text{Co}(\text{NH}_3)_5\text{Cl}]\text{Cl}_2$ (10 mM)/acetate buffer (pH 4.5; 0.1 M in water).

The best value recorded is for the photocathode stained with a solution of the dyad $[\text{PTZ-p-Py}\{\text{Co}(\text{dmgBF}_2)_2(\text{H}_2\text{O})_2\}]$.

The photocurrent values are considerably lower compared to the ones obtained in presence of the SEA. We still decided to perform the CA experiment at 0 V vs Ag / AgCl (+ 0.2 V vs NHE) for the same reason mentioned before.

CA scans performed in the same electrolytic solution with the cobaloxime at 0 V vs Ag/AgCl (+ 0.2 V vs NHE) under chopped light has been reported in Figure 4. 45, and the corresponding data in Table 4. 9.

A possible comparison can be made considering the relative variation of photocurrent ($\Delta j/j_{\max}$) reported in Table 4. 9.

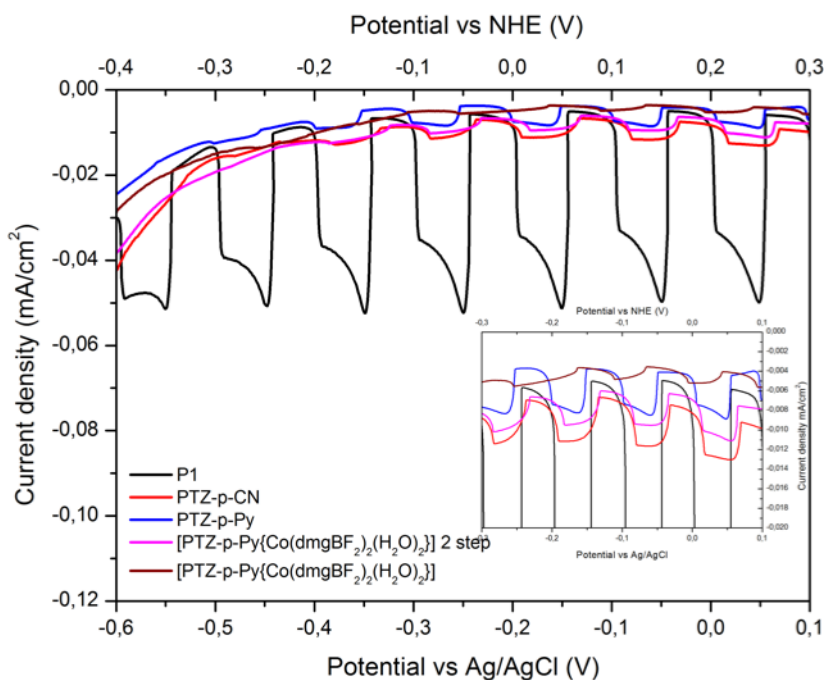


Figure 4. 44: Linear sweep voltammogram (10 mV/s) recorded under chopped light on NiO photocathodes sensitized with the investigated dyes in presence of $\text{Co}[(\text{dmgBF}_2)_2(\text{H}_2\text{O})_2]$ (1 mM)/acetate buffer (pH 4.5; 0.1 M in water).

While the **P1** dye showed a similar behavior in presence of either the SEA or the cobaloxime, the phenothiazine based dyes showed a lower photoactivity in presence of the cobaloxime. The values of the photocurrents are still stable and similar for the new dyes except **P1** (Δj_{cat} 15 $\mu\text{A}/\text{cm}^2$, with a relative variation close to 90%), ranging from 1.5 to 3 $\mu\text{A}/\text{cm}^2$, with the same relative variation of 50% compared to the maximum j value.

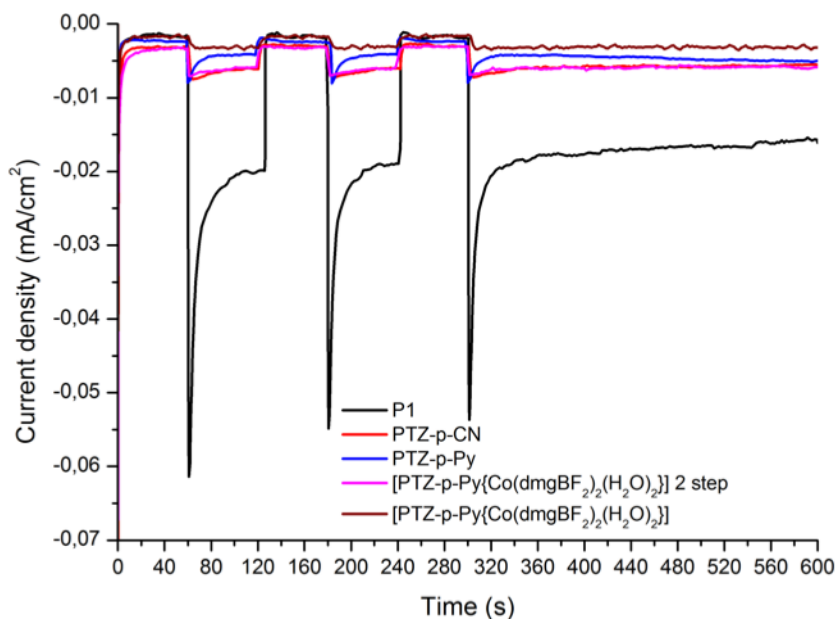


Figure 4. 45: Short chronoamperometric plot measured at 0 V vs Ag/AgCl (+ 0.2 V vs NHE) under chopped light on NiO photocathodes sensitized with the investigated dyes in presence of $\text{Co}[(\text{dmgbF}_2)_2(\text{H}_2\text{O})_2]$ (1 mM)/acetate buffer (pH 4.5; 0.1 M in water).

A possible explanation for such low photocurrents measured during electrolytic experiments could lie in the molecular design itself. In fact, the basic idea of reducing recombination between the dyes and the semiconductor introducing a not conjugated anchoring group could have negatively affected the hole transfer. It has been reported, in case of other dyes anchored with non conjugated functionalities on semiconductors, a considerable drop in photocurrent due to a poor overlap of molecular orbital with the semiconductors bands.²⁹

From these data it is difficult to understand if there is an effect of coordination in terms of photoactivity of the dyes and the corresponding dyad (both the one prepared in solution and the other prepared with subsequent staining process).

We therefore tried to perform some long photoelectrolysis experiment, in the same conditions mentioned above, to evaluate the hydrogen evolution of these systems. Unfortunately, no hydrogen has been detected after three hours of CA experiment.

Such small cathodic photocurrent could still produce hydrogen even without catalyst,¹¹⁴ although we could not detect any of it in the headspace of the cell after 3 h of continuous photoelectrolysis. In our experience with similar systems,⁶⁸ this is however very irreproducible and we always have low faradic yield, below 10% for $10 \mu\text{A}/\text{cm}^2$ photocurrent. We thus believe that a significant part of this photocurrent is due to the reduction of residual traces of O_2 present in the electrolyte or trapped within the nickel oxide films.

If we measure the amount of charge flowed in the cell during the experiments (values in Table 4. 9), and we compared it with the number of cobalt atoms in the electrolyte, it is possible to notice that the amount of charge (ranging from 2.6×10^{17} to 5.4×10^{17} electrons) is not sufficient to reduce all the cobaloxime in solution (about 2.4×10^{18} molecules of cobaloxime in 4 mL of 1 mM solution).

Experimental section

GENERAL INFORMATION

NMR spectra were recorded with a Bruker AMX-500 spectrometer operating at 500.13 MHz (^1H) and 125.77 MHz (^{13}C). Coupling constants are given in Hz. Absorption spectra were recorded with a V-570 Jasco spectrophotometer. Infrared spectra (IR) were recorded with an ATR-FTIR Perkin–Elmer Spectrum100 spectrometer. Flash chromatography was performed with Merck grade 9385 silica gel 230–400 mesh (60 Å). Reactions performed under inert atmosphere were done in oven-dried glassware and a nitrogen atmosphere was generated with Schlenk technique. Conversion was monitored by thin-layer chromatography by using UV light (254 and 365 nm) as a visualizing agent. All reagents were obtained from commercial suppliers at the highest purity grade and used without further purification. Anhydrous solvents were purchased from Sigma-Aldrich and used without further purification. Extracts were dried with Na_2SO_4 and filtered before removal of the solvent by evaporation.

ELECTROCHEMICAL AND PHOTOELECTROCHEMICAL CHARACTERIZATION

Pulsed Voltammetry (DPV) and Cyclic Voltammetry (CV) were carried out at scan rate of 20 and 50 mV/s, respectively, using a PARSTA2273 potentiostat in a two compartments, three electrode electrochemical cell in a glove box filled with N_2 ($[\text{O}_2]$ and $[\text{H}_2\text{O}] \leq 0.1$ ppm). The working, counter, and the pseudo-reference electrodes were a glassy carbon pin, a Pt flag and an Ag/AgCl wire, respectively. The working electrodes discs were well polished with alumina 0.1 μm suspension, sonicated for 15 min in deionized water, washed with 2-propanol, and cycled for 50 times in 0.5 M H_2SO_4 before use. The Ag/AgCl pseudo-reference electrode was calibrated, by adding ferrocene (10^{-3} M) to the test solution after each measurement.

Photoelectrochemical data were acquired with a *Biologic VSP 300* potentiostat. The reference electrode was made of a Ag/AgCl wire dipped into a KCl 3 M solution, separated from the supporting electrolyte by a Vycor® frit, and denoted below as Ag/AgCl. Irradiation was carried out with a 300W ozone-free Xe lamp (*Newport*) operated at 280 W and mounted with a water-filled *Spectra-Physics 6123NS* liquid filter for elimination of IR ($\lambda > 800$ nm) irradiation and a *Spectra-Physics 59472* UV cut-off filter ($\lambda < 400$ nm). The power density was calibrated using a *Newport PM1918-R* power-meter. The photocurrent measurements were carried out in a specifically designed three-electrode cell, using the NiO-sensitized film as the working electrode (2.7 cm^2), Ag/AgCl as the reference electrode and a Ti wire as the counter electrode. The counter electrode compartment was separated from the cathodic one by a Vycor® frit. The supporting electrolyte was 0.1 M acetate buffer at pH 4.5 in water. The supporting electrolyte was degassed with a flow of N_2 at least for 30 min before the measurements. In a typical experiment, the volume of supporting electrolyte was 4.0 mL and the headspace was 2.4 mL. The photocathode was illuminated with a power density of $65 \text{ mW}\cdot\text{cm}^{-2}$ (ca. one sun). The amounts of evolved hydrogen were determined by sampling aliquots of the headspace in a *Perkin Elmer Clarus 580* gas chromatograph equipped with a molecular sieve 5 Å column (30m – 0.53 mm) and a TCD detector.

PREPARATION OF Pt/TiO₂ NANOPOWDER

Platinization of TiO₂ Degussa P25 was done through a photodeposition method known in literature.^{11,14,39,40} TiO₂ Degussa P25 (2.0 g) was suspended in a solution of H₂O (200 mL) and EtOH (200 mL) containing 32.7 mg of Pt(NO₃)₂, in order to reach a final metal loading of 1.0 wt%. After stirring for 1 h in the dark, the suspension was irradiated with a 450 W medium pressure lamp for 4 h. Nanopowders were recovered through centrifugation, washed with EtOH 3 times, and dried under vacuum at 50 °C overnight.

CHARACTERIZATION OF Pt/TiO₂ NANOPOWDER

Phase composition has been analysed by Powder X-ray Diffraction (PXRD) using a Philips X'Pert diffractometer using a Cu K α ($\lambda = 0.154$ nm) X-ray source in the range $10^\circ < 2\theta < 100^\circ$ and data were analyzed by using the PowderCell 2.0 software. Mean crystallite sizes were calculated applying the Scherrer's equation to the principal reflection of each phase [(101) for anatase and (110) for rutile].

Textural properties of the catalyst has been analyzed by N₂ physisorption at the liquid nitrogen temperature using a Micromeritics ASAP 2020 automatic analyzer. The samples were previously degassed under vacuum at 200°C overnight. Specific surface area has been determined applying the BET method to the adsorption isotherm in the range $0.10 < p/p^0 < 0.35$. Pore size distribution has been evaluated applying the BJH theory to the desorption branch of the isotherm.¹¹⁵

The morphology of the composite materials and the distribution of the supported Pt nanoparticles were evaluated by High Resolution Transmission Electron Microscopy (HR-TEM) and High Angle Annular Dark Field-Scanning Transmission Electron Microscopy (HAADF-STEM) images recorded by a JEOL 2010-FEG microscope operating at the acceleration voltage of 200 kV. The microscope has 0.19 nm spatial resolution at Scherzer defocus conditions in HR-TEM mode and a probe of 0.5 nm was used in HAADF-STEM mode.

ADSORPTION OF DYES ON Pt/TiO₂

Dye staining was done by suspending 200 mg of Pt/TiO₂ nanopowders in 20 mL of dye solution (0.3 mM in ethanol) for 24 h in the dark. Then nanopowders were separated through centrifugation, washed twice with ethanol, and dried under vacuum at room temperature overnight. After adsorption, the concentration of the dyes in the solution was measured by UV-vis spectroscopy, confirming that the loading of dyes on the Pt/TiO₂ material is quantitative.

HYDROGEN PRODUCTION THROUGH WATER SPLITTING

The dye-functionalized Pt/TiO₂ nanomaterials have been tested for H₂ production following a procedure previously described.³ 50 mg of the dye-functionalized Pt/TiO₂ catalyst was suspended into 60 mL of 10 % v/v aqueous solution of triethanolamine (TEOA) previously neutralized with HCl. After purging with Ar (15 mL min⁻¹) for 30 min, the suspension was irradiated using a 150 W Xe lamp with a cut-off filter at 420 nm. Irradiance was $\sim 6 \times 10^{-3} \text{ W m}^{-2}$ in the UV-A range and $\sim 1080 \text{ W m}^{-2}$ in the visible range (400 – 1000 nm). The concentration of H₂ in gas stream coming from the reactor has been quantified using a Agilent 7890 gaschromatograph equipped with a TCD detector, connected to a Carboxen 1010 column (Supelco, 30 m x 0.53 mm ID, 30 μm film) using Ar as carrier.

DEGRADATION MEASUREMENTS OF DYE-SENSITIZED Pt/TiO₂

The degradation of the dye-sensitized catalysts has been investigated by means of optical absorption of the desorbed dye after specific irradiation times. The UV-Vis spectrum of a known amount of dye-sensitized Pt/TiO₂ catalyst, prepared as described above, has been measured for each sample by completely desorbing the dye using a known volume of a 0.1 M solution of NaOH in ethanol–H₂O (1:1). The resulting suspension has been filtered using a 0.45 μm PTFE syringe filter and the UV-Vis spectrum measured in the spectral range 320–800 nm, using a quartz cuvette with a 1-cm optical path. Spectra were collected at different irradiation times (7, 14, and 20 h) under the same experimental conditions of the hydrogen production measurements. The spectra collected before irradiation ($t = 0$ h) were used as reference data. Degradation data have been reported as relative residual absorbances $A_{\text{max}}/A_{0\text{max}}$, where A_{max} and $A_{0\text{max}}$ are the absorbances of the desorbed dyes recorded at their Vis absorption peaks after and before irradiation, respectively.

PREPARATION OF NiO PHOTOCATHODES

The precursor solution was prepared by mixing NiCl₂ (1 g), F108 triblock copolymer (1 g), Milli-Q water (3 g) and ethanol (6 g) according to the literature.^{116,117}

After overnight sonication and centrifugation, the supernatant solution was spin-coated (*SPS-Europe spin150* model) for 1 min at 5000 rpm onto FTO/glass substrates (Solems, TEC 7, sheet resistance $7\Omega/\text{sqr}$), followed by sintering (30 min temperature ramp from room temperature to 450°C and 30 min at 450°C) in the air in a flat oven. The process was repeated four times to increase the thickness up to $1\ \mu\text{m}$, as measured by cross-section scanning electron microscopy.

NiO FILMS SENSITIZATION

The NiO electrodes were soaked in a DMF solution of **PTZ-p-CN**, **PTZ-p-PY**, **Co[(dmgBF₂)₂]Py•H₂O** (0.2 mM) for 24 h at room temperature in the dark on an orbital stirring table. The electrodes stained with **Co[(dmgBF₂)₂]Py•H₂O** 2 step have been prepared staining photoelectrodes, previously stained with PTZ-p-Py, in a acetone solution of **Co[(dmgBF₂)₂]•2H₂O** (0.2 mM) for 24 h at room temperature in the dark on an orbital stirring table. The electrodes were rinsed with the same solvent used for staining and dried in air.

SYNTHETIC PROCEDURES

General Procedure for Suzuki-Miyaura Cross-Coupling: Product **1** (1 eq.) and Pd(dppf)Cl₂•CH₂Cl₂ (10 % eq.) were dissolved in dimethoxyethane (0.1 M) and stirred for 15 minutes under nitrogen atmosphere. Then boronic acid derivative (2.4 eq.) and K₂CO₃ (10 eq.) were added as suspension in methanol (0.1 M). The reaction was performed with microwave irradiation (100°C , 200 watt, 90 minutes) and then quenched by pouring into a saturated solution of NH₄Cl (50 mL). Filtration on Celite and extractions with organic solvent allowed to isolate the crude product, then purified through column chromatography on silica gel.

General Procedure for Knoevenagel Condensation: Aldehyde precursor (1 eq.), cyanoacetic acid (10 eq.) and piperidine (10 eq. + catalytic) were dissolved in CHCl₃ (0.02 M) and warmed to reflux for 5 h. After having the solvent evaporated, a solution of HCl 1 M (~50 mL) was added and the mixture was left under magnetic

stirring for 5 h at rt. The dark red solid that precipitated was filtered and washed with water (3x30 mL), PE (2x30 mL) and Et₂O (1x10 mL).

5,5'-(10-octyl-10*H*-phenothiazine-3,7-diyl)difuran-2-carbaldehyde (29b).

Product **29b** was synthesized according to general procedure for Suzuki-Miyaura cross-coupling, using product **28a** (330 mg, 0.71 mmol), Pd(dppf)Cl₂·CH₂Cl₂ (57 mg, 0.071 mmol), (5-formylfuran-2-yl)boronic acid (240 mg, 1.7 mmol), K₂CO₃ (980 mg, 7.1 mmol), DME (3 mL) and methanol (3 mL). Extractions were performed with CH₂Cl₂ (3 x 50 mL) and a mixture of PE:AcOEt – 7:3 was used as eluent for purification. The desired product was isolated as a red solid (160 mg) with a 45% of yield. ¹H NMR (500 MHz, CDCl₃) δ 9.60 (s, 2H), 7.58 (dd, *J* = 8.5, 1.9 Hz, 2H), 7.52 (d, *J* = 1.9 Hz, 2H), 7.28 (d, *J* = 3.7 Hz, 2H), 6.86 (d, *J* = 8.6 Hz, 2H), 6.71 (d, *J* = 3.7 Hz, 2H), 3.86 (t, *J* = 7.2 Hz, 2H), 1.86 – 1.74 (m, 2H), 1.50 – 1.37 (m, 2H), 1.36 – 1.18 (m, 8H), 0.86 (t, *J* = 6.9 Hz, 3H). ¹³C NMR (126 MHz, CDCl₃) δ 8.76, 158.67, 151.82, 145.39, 124.75, 124.59, 124.06, 123.78, 115.55, 106.77, 47.90, 31.65, 29.11, 29.08, 26.75, 26.71, 22.53, 13.98.

5,5'-(10-octyl-10*H*-phenoaxazine-3,7-diyl)dithiophene-2-carbaldehyde (29c).

Product **29c** was synthesized according to general procedure for Suzuki-Miyaura cross-coupling, using product **28b** (300 mg, 0.66 mmol), Pd(dppf)Cl₂·CH₂Cl₂ (54 mg, 0.066 mmol), (5-formylthiophen-2-yl)boronic acid (247 mg, 1.58 mmol), K₂CO₃ (910 mg, 6.6 mmol), DME (3 mL) and methanol (3 mL). Extractions were performed with AcOEt (3 x 50 mL) and a mixture of PE:AcOEt - 3:1 was used as eluent for purification. The desired product was isolated as a red-orange solid (50 mg) with a 15% of yield. ¹H-NMR (CDCl₃, 500 MHz): δ 9.84 (s, 2H), 7.68 (d, 2H, *J* = 4.0 Hz), 7.24 (d, 2H, *J* = 4.0 Hz), 7.14 (dd, 2H, *J* = 8.4, 2.0 Hz), 6.93 (d, 2H, *J* = 2.0 Hz), 6.49 (d, 2H, *J* = 8.4 Hz), 3.50 (t, 2H, *J* = 8.0 Hz), 1.67 (q, 2H, *J* = 8.0 Hz), 1.45-1.20 (m, 10H), 0.89 (t, 3H, *J* = 6.8 Hz). ¹³C-NMR (CDCl₃, 126 MHz): δ 182.48, 153.48, 144.78, 141.26, 137.57, 133.51, 126.37, 122.76, 122.31, 113.06, 111.80, 44.24, 31.75, 29.68, 29.31, 29.23, 26.86, 25.10, 22.60, 14.06.

5,5'-(10-octyl-10*H*-phenooxazine-3,7-diyl)furan-2-carbaldehyde (29d).

Product **29d** was synthesized according to general procedure for Suzuki-Miyaura cross-coupling, using product **28b** (300 mg, 0.66 mmol), Pd(dppf)Cl₂·CH₂Cl₂ (54 mg, 0.066 mmol), (5-formylfuran-2-yl)boronic acid (221 mg, 1.58 mmol), K₂CO₃ (910 mg, 6.6 mmol), DME (3 mL) and methanol (3 mL). Extractions were performed with AcOEt (3 x 50 mL) and a mixture of CH₂Cl₂/PE - 97:3 was used as eluent for purification. The desired product was isolated as a dark red solid (200 mg) with a 63% of yield. ¹H-NMR (CDCl₃, 500 MHz): δ 9.55 (s, 2H), 7.26 (d, 2H, *J* = 3.7 Hz), 7.24 (dd, 2H, *J* = 8.4, 2.0 Hz), 6.98 (d, 2H, *J* = 2.0 Hz), 6.62 (d, 2H, *J* = 3.7 Hz), 6.45 (d, 2H, *J* = 8.4 Hz), 3.45 (t, 2H, *J* = 7.8 Hz), 1.63 (q, 2H, *J* = 7.6 Hz), 1.45-1.20 (m, 10H), 0.89 (t, 3H, *J* = 6.7 Hz). ¹³C-NMR (CDCl₃, 126 MHz): δ 176.64, 158.85, 151.51, 144.73, 133.66, 122.24, 121.46, 112.08, 111.63, 106.46, 44.21, 31.74, 29.28, 29.22, 26.81, 25.07, 22.60, 14.06.

5,5'-(9-Octyl-9*H*-carbazole-3,6-diyl)dithiophene-2-carbaldehyde (29e).

Product **29e** was synthesized according to general procedure for Suzuki-Miyaura cross-coupling, using product **28c** (253 mg, 0.58 mmol), Pd(dppf)Cl₂·CH₂Cl₂ (48 mg, 0.059 mmol), (5-formylthiophen-2-yl)boronic acid (225 mg, 1.44 mmol), K₂CO₃ (790 mg, 5.75 mmol), DME (3 mL) and methanol (3 mL). Extractions were performed with AcOEt (3 x 50 mL) and a mixture of CH₂Cl₂/Et₂O - 95:5 was used as eluent for purification. The desired product was isolated as a red solid (210 mg) with a 72% of yield. ¹H NMR (500 MHz, CDCl₃): δ 9.89 (s, 2H), 8.40 (d, *J* = 1.7 Hz, 2H), 7.80 (dd, *J* = 8.6 Hz, 1.8 Hz, 2H), 7.77 (d, *J* = 4.0 Hz, 2H), 7.47 (d, *J* = 3.9 Hz, 2H), 7.43 (d, *J* = 8.6 Hz, 2H), 4.30 (t, *J* = 7.3 Hz, 2H), 1.88 (q, *J* = 7.3 Hz, 2H), 1.41-1.19 (m, 10H), 0.87 (t, *J* = 6.8 Hz, 3H).

5,5'-(9-Octyl-9*H*-carbazole-3,6-diyl)difuran-2-carbaldehyde (29f). Product **29f** was synthesized according to general procedure for Suzuki-Miyaura cross-coupling, using product **28c** (253 mg, 0.58 mmol), Pd(dppf)Cl₂·CH₂Cl₂ (49 mg, 0.059 mmol), (5-formylfuran-2-yl)boronic acid (193 mg, 1.38 mmol), K₂CO₃ (788 mg, 5.71 mmol), DME (3 mL) and methanol (3 mL). Extractions were performed with

CH₂Cl₂ (3 x 50 mL) and a mixture of CH₂Cl₂:AcOEt - 9:1 was used as eluent for purification. The desired product was isolated as a red solid (159 mg) with a 59% of yield. ¹H NMR (500 MHz, CDCl₃): δ 9.65 (s, 2H), 8.60 (d, *J* = 1.4 Hz, 2H), 7.94 (dd, *J* = 8.6 Hz, 1.7 Hz, 2H), 7.42 (d, *J* = 8.6 Hz, 2H), 7.37 (d, *J* = 3.8 Hz, 2H), 6.88 (d, *J* = 3.7 Hz, 2H), 4.28 (t, *J* = 7.3 Hz, 2H), 1.87 (q, *J* = 7.4 Hz, 2H), 1.42-1.18 (m, 10H), 0.86 (t, *J* = 7.0 Hz, 3H). ¹³C-NMR (CDCl₃, 126 MHz): δ 176.76, 160.76, 151.63, 141.57, 123.90, 123.14, 120.76, 118.11, 109.53, 106.39, 43.46, 31.73, 29.28, 29.12, 28.97, 27.23, 22.57, 14.04.

3,3'-(5,5'-(10-octyl-10*H*-phenothiazine-3,7-diyl)bis(furan-5,2-diyl))bis(2-cyanoacrylic acid) (PTZ-Fu). PTZ-Fu was synthesized according to general procedure for Knoevenagel condensation using product **29b** (160 mg, 0.32 mmol), cyanoacetic acid (272 mg, 3.2 mmol), piperidine (290 mg, 3.4 mmol) and CHCl₃ (10 mL). A dark red solid (185 mg) has been isolated as the product with 91 % of yield. ¹H NMR (500 MHz, DMSO-*d*₆) δ 8.03 (s, 2H), 7.75 (dd, *J* = 8.5, 2.0 Hz, 2H), 7.72 (d, *J* = 2.0 Hz, 2H), 7.52 (d, *J* = 3.8 Hz, 2H), 7.31 (d, *J* = 3.7 Hz, 2H), 7.19 (d, *J* = 8.8 Hz, 2H), 3.97 (t, *J* = 6.9 Hz, 2H), 1.70 (quint, *J* = 7.0 Hz, 2H), 1.39 (quint, *J* = 7.0 Hz, 2H), 1.31 – 1.15 (m, 8H), 0.81 (t, *J* = 6.8 Hz, 3H). ¹³C NMR (126 MHz, DMSO-*d*₆) δ 164.43, 158.54, 147.78, 145.30, 137.89, 125.28, 123.99, 123.78, 123.67, 117.20, 116.99, 31.54, 29.05, 28.89, 26.52, 26.35, 22.46, 14.35. Anal. Calcd. For : C, 68.23; H, 4.93; N, 6.63. Found: C, 68.11; H, 5.31; N, 6.69.

3,3'-(5,5'-(10-octyl-10*H*-phenoaxazine-3,7-diyl)bis(thiophene-5,2-diyl))bis(2-cyanoacrylic acid) (POZ-Th). POZ-Th was synthesized according to general procedure for Knoevenagel condensation using product **29c** (50 mg, 0.097 mmol), cyanoacetic acid (82 mg, 0.97 mmol), piperidine (103 mg, 1.16 mmol) and CHCl₃ (5 mL). A dark red solid (58 mg) has been isolated as the product with quantitative yield. ¹H-NMR (DMSO-*d*₆, 500 MHz): δ 8.35 (s, 2H), 7.87 (d, 2H, *J* = 4.2 Hz), 7.53 (d, 2H, *J* = 4.0 Hz), 7.16 (dd, 2H, *J* = 8.2, 1.8 Hz), 6.93 (d, 2H, *J* = 1.9 Hz), 6.65 (d, 2H, *J* = 8.7 Hz), 3.48 (broad s, 2H), 1.51 (broad s, 2H), 1.40-1.10 (m, 10H),

0.85 (t, 3H, $J = 6.7$ Hz). $^{13}\text{C-NMR}$ (DMSO- d_6 , 126 MHz): δ 164.21, 152.76, 146.77, 144.40, 141.81, 133.73, 133.41, 125.92, 124.27, 122.96, 117.04, 113.07, 112.61, 97.56, 31.70, 29.26, 29.22, 26.53, 25.10, 22.56, 14.40. Anal. Calcd. For : C, 66.54; H, 4.81; N, 6.47. Found: C, 66.64; H, 4.64; N 6.17.

3,3'-(5,5'-(10-octyl-10H-phenooxazine-3,7-diyl)bis(furanen-5,2-diyl))bis(2-cyanoacrylic acid) (POZ-Fu). POZ-Fu was synthesized according to general procedure for Knoevenagel condensation using product **29d** (200 mg, 0.41 mmol), cyanoacetic acid (349 mg, 4.1 mmol), piperidine (431 mg, 4.92 mmol) and CHCl_3 (5 mL). A dark red solid (190 mg) has been isolated as the product with 75 % of yield. $^1\text{H NMR}$ (500 MHz, DMSO- d_6): δ 7.89 (s, 2H), 7.38 (d, 2H, $J = 3.5$ Hz), 7.36 (d, 2H, $J = 8.9$ Hz), 7.16 (d, 2H, $J = 3.4$ Hz), 7.14 (s, 2H), 6.76 (d, 2H, $J = 8.6$ Hz), 3.56 (broad s, 2H), 1.54 (broad s, 2H), 1.45-1.15 (m, 10H), 0.85 (t, 3H, $J = 6.2$ Hz). $^{13}\text{C-NMR}$ (DMSO- d_6 , 125 MHz): δ 164.64, 158.27, 147.69, 144.46, 136.73, 133.49, 122.31, 121.99, 117.76, 113.15, 111.62, 109.13, 43.75, 31.69, 29.23, 26.45, 25.11, 22.54, 14.39. Anal. Calcd. For : C, 70.01; H, 5.06; N, 6.80. Found: C, 70.04; H, 5.39; N, 6.73.

5,5'-(9-Octyl-9H-carbazole-3,6-diyl)bis(thiophene-5,2-diyl))bis(2-cyanoacrylic acid) (CBZ-Th). CBZ-Th was synthesized according to general procedure for Knoevenagel condensation using product **29e** (210 mg, 0.42 mmol), cyanoacetic acid (370 mg, 4.35 mmol), piperidine (384 mg, 4.5 mmol) and CHCl_3 (5 mL). A dark red solid (187 mg) has been isolated as the product with 71 % of yield. $^1\text{H NMR}$ (500 MHz, DMSO- d_6): δ 8.80 (d, $J = 1.8$ Hz, 2H), 8.51 (s, 2H), 8.06 (d, $J = 4.2$ Hz, 2H), 7.93 (dd, $J = 8.6$ Hz, 1.9 Hz, 2H), 7.84 (d, $J = 4.1$ Hz, 2H), 7.74 (d, $J = 8.7$ Hz, 2H), 4.45 (t, $J = 6.7$ Hz, 2H), 1.80 (q, $J = 7.2$ Hz, 2H), 1.33-1.12 (m, 10H), 0.80 (t, $J = 6.9$ Hz, 3H). Anal. Calcd. For : C, 68.22; H, 4.93; N, 6.63. Found: C, 68.07; H, 5.09; N, 7.03.

5,5'-(9-Octyl-9H-carbazole-3,6-diyl)bis(furanen-5,2-diyl)bis(2-cyanoacrylic acid) (CBZ-Fu). CBZ-Fu was synthesized according to general procedure for Knoevenagel condensation using product **29f** (159 mg, 0.34 mmol), cyanoacetic acid (275 mg, 3.23 mmol), piperidine (300 mg, 3.5 mmol) and CHCl₃ (5 mL). A dark red solid (110 mg) has been isolated as the product with 53 % of yield. ¹H NMR (500 MHz, DMSO-*d*₆): δ 8.67 (s, 2H), 8.02 (d, *J* = 8.5 Hz, 2H), 7.94 (s, 2H), 7.74 (d, *J* = 8.5 Hz, 2H), 7.40 (d, *J* = 3.2 Hz, 2H), 7.21 (d, *J* = 3.2 Hz, 2H), 4.41 (s, 2H), 1.77 (d, *J* = 6.0 Hz, 2H), 1.31-1.10 (m, 10H), 0.80 (t, *J* = 7.0 Hz, 3H). ¹³C NMR (126 MHz, DMSO-*d*₆) δ 158.60, 148.22, 141.41, 123.68, 122.90, 121.18, 119.08, 117.55, 110.97, 43.12, 31.58, 29.12, 29.02, 28.97, 26.85, 22.43, 14.32. Anal. Calcd. For : C, 71.87; H, 5.19; N, 6.98. Found: C, 71.47; H, 5.48; N, 6.60.

3,7-bis(5-(4,4,5,5-tetramethyl-1,3-dioxolan-2-yl)thiophen-2-yl)-10H-phenothiazine (30). Product **30** was synthesized according to general procedure for Suzuki-Miyaura cross-coupling, using product **22** (156 mg, 0.43 mmol), Pd(dppf)Cl₂·CH₂Cl₂ (35 mg, 0.04 mmol), 4,4,5,5-tetramethyl-2-(5-(4,4,5,5-tetramethyl-1,3-dioxolan-2-yl)thiophen-2-yl)-1,3,2-dioxaborolane¹⁰¹ (308 mg, 0.91 mmol), K₂CO₃ (595 mg, 4.3 mmol), DME (3 mL) and methanol (3 mL). Extractions were performed with CH₂Cl₂ (3 x 50 mL) and a mixture of *n*-hexane:AcOEt – 3:1 was used as eluent for purification. The desired product was isolated as a red solid (140 mg) with a 52% of yield. ¹H NMR (benzene-*d*₆, 500 MHz): δ 7.21 (d, *J* = 1.0 Hz, 2H), 7.09 (dd, *J* = 7.2, 1.7 Hz, 2H), 6.99 (d, *J* = 3.5 Hz, 2H), 6.75 (d, *J* = 3.5 Hz, 2H), 6.24 (s, 2H), 5.76 (d, *J* = 8.2 Hz, 2H), 4.87 (s, 1H), 1.20 (s, 12H), 1.09 (s, 12H).

ethyl 2-(3,7-bis(5-(4,4,5,5-tetramethyl-1,3-dioxolan-2-yl)thiophen-2-yl)-10H-phenothiazin-10-yl)acetate (31). Compound **30** (600 mg, 1.00 mmol) was dissolved in dry DMF under N₂ atmosphere, then the solution was cooled to 0°C using an ice bath and NaH 60% (120 mg (200 mg), 5.00 mmol) was slowly added. After stirring at 0 °C for 1 h, bromoethylacetate (170 mg, 1.00 mmol) was added and the solution was stirred at rt for 4 h, when TLC revealed the complete

conversion of the starting material. The reaction mixture was quenched with iced water, then extracted with Et₂O (3 x 30 mL) and the organic phase was dried with Na₂SO₄ and concentrated. Product **31** was obtained as a dark yellow solid (700 mg) with quantitative yield. ¹H NMR (500 MHz, CDCl₃) δ 7.30 (m, 4H), 7.07 (d, *J* = 3.6 Hz, 2H), 7.04 (d, *J* = 3.6 Hz, 2H), 6.56 (dd, *J* = 7.4, 1.5 Hz, 2H), 6.16 (s, 2H), 4.51 (s, 2H), 4.33 (q, *J* = 7.1 Hz, 2H), 1.37 – 1.29 (m, 27H).

ethyl 2-(3,7-bis(5-formylthiophen-2-yl)-10H-phenothiazin-10-yl)acetate (32).

A solution of compound **31** in THF/10% HCl_{aq} (15 mL 2:1 *v/v*) has been refluxed for 1 h. The solution was allowed to cool down to room temperature and the volume has been reduced. CH₂Cl₂ (10 mL) has been added and the reaction mixture has been extracted with CH₂Cl₂ (3 x 10 mL). The collected organic phase has been washed with water till neutral pH. The organic phase was dried and evaporated. Product **32** was obtained as a orange solid (415 mg) with 85% yield. ¹H NMR (500 MHz, CDCl₃) δ 9.87 (s, 2H), 7.71 (d, *J* = 3.9 Hz, 2H), 7.41 (dd, *J* = 8.4, 2.1 Hz, 2H), 7.39 (d, *J* = 2.0 Hz, 2H), 7.30 (d, *J* = 3.9 Hz, 2H), 6.62 (d, *J* = 8.4 Hz, 2H), 4.55 (s, 2H), 4.36 (q, *J* = 7.1 Hz, 2H), 1.36 (t, *J* = 7.1 Hz, 3H).

ethyl 2-(3,7-bis(5-(2,2-dicyanovinyl)thiophen-2-yl)-10H-phenothiazin-10-yl)acetate (33a). **33a** was synthesized according to general procedure for Knoevenagel condensation using product **32** (115 mg, 0.24 mmol), malononitrile (66 mg, 1.00 mmol), piperidine (catalytic amount) and CHCl₃ (10 mL). A dark orange solid (144 mg) has been isolated as the product with quantitative of yield.

ethyl 2-(3,7-bis(5-((Z)-2-cyano-2-(pyridin-4-yl)vinyl)thiophen-2-yl)-10H-phenothiazin-10-yl)acetate (33b). **33b** was synthesized according to general procedure for Knoevenagel condensation using product **32** (300 mg, 0.60 mmol), pyridylacetonitrile hydrochloride (376 mg, 2.45 mmol), piperidine (221 mg, 2.60 mmol) and CHCl₃ (10 mL). A dark red solid (350 mg) has been isolated as the product with 83 % of yield. ¹H NMR (500 MHz, DMSO + CF₃COOD) δ 9.02 – 8.87 (m,

6H), 8.25 (d, $J = 6.5$ Hz, 4H), 7.99 (d, $J = 4.1$ Hz, 2H), 7.80 (d, $J = 3.9$ Hz, 2H), 7.66 – 7.57 (m, 3H), 6.83 (d, $J = 9.1$ Hz, 2H), 4.83 (s, 2H), 4.31 (q, $J = 6.9$ Hz, 2H), 1.37 – 1.30 (m, 3H).

2-(3,7-bis(5-(2,2-dicyanovinyl)thiophen-2-yl)-10*H*-phenothiazin-10-yl)acetic acid (PTZ-p-CN). 33a (56 mg, 0.09 mmol) was dissolved in 3 mL of dry pyridine, LiI (81 mg, 0.6 mmol) was added and the reaction mixture was bubbled with Ar for 30 min. Then, the reaction mixture was heated in a sealed vial in a microwave oven (160 °C, 85 W, 3 h). The solvent was evaporated and the solid was taken up and stirred in a citric acid saturated solution in water for 1 h. Then filtered and dried in vacuum at 40 °C overnight. The product **PTZ-p-CN** was obtained as a dark solid (22 mg) with 43 %.

2-(3,7-bis(5-((*Z*)-2-cyano-2-(pyridin-4-yl)vinyl)thiophen-2-yl)-10*H*-phenothiazin-10-yl)acetic acid (PTZ-p-Py). 33b (85 mg, 0.12 mmol) was dissolved in 4 mL of dry pyridine, LiI (106 mg, 0.78 mmol) was added and the reaction mixture was bubbled with Ar for 30 min. Then, the reaction mixture was heated in a sealed vial in a microwave oven (160 °C, 85 W, 3 h). The solvent was evaporated and the solid was taken up and stirred in a citric acid saturated solution in water for 1 h. Then filtered and dried in vacuum at 40 °C overnight. The product **PTZ-p-Py** was obtained as a dark solid (50 mg) with 50 %. ¹H NMR (500 MHz, DMSO + CF₃COOD) δ 9.02 – 8.87 (m, 6H), 8.25 (d, $J = 6.5$ Hz, 4H), 7.99 (d, $J = 4.1$ Hz, 2H), 7.80 (d, $J = 3.9$ Hz, 2H), 7.66 – 7.57 (m, 3H), 6.83 (d, $J = 9.1$ Hz, 2H), 4.93 (s, 2H).

Co[(dmgBF₂)₂]Py•H₂O. A solution of PTZ-p-Py (33 mg, 0.05 mmol) and Co[(dmgBF₂)₂]•2H₂O¹¹⁸ (42 mg, 0.1 mmol) in acetone (50 mL) was stirred overnight at room temperature. The solvent was evaporated and the solid was taken up with cold acetone (5 mL) and filtered under reduced pressure. The dark solid was dried under vacuum at 40 °C in the dark overnight. Co[(dmgBF₂)₂]Py•H₂O was obtained as a dark red solid (70 mg) with quantitative yield.

References

- (1) Arthur C. Clarke. (n.d.). BrainyQuote.com. Retrieved December 5, 2016, from BrainyQuote.com Web site: <https://www.brainyquote.com/quotes/quotes/a/arthurcl124660.html>
- (2) Cecconi, B.; Manfredi, N.; Montini, T.; Fornasiero, P.; Abboto, A. "Dye-Sensitized Solar Hydrogen Production: The Emerging Role of Metal-Free Organic Sensitizers". *Eur. J. Org. Chem.* **2016**, *2016*, 5194-5215, doi:10.1002/ejoc.201600653.
- (3) Cecconi, B.; Manfredi, N.; Ruffo, R.; Montini, T.; Romero-Ocana, I.; Fornasiero, P.; Abboto, A. "Tuning Thiophene-Based Phenothiazines for Stable Photocatalytic Hydrogen Production". *ChemSusChem* **2015**, *8*, 4216-4228, doi:10.1002/cssc.201501040.
- (4) Manfredi, N.; Cecconi, B.; Calabrese, V.; Minotti, A.; Peri, F.; Ruffo, R.; Monai, M.; Romero-Ocana, I.; Montini, T.; Fornasiero, P.; Abboto, A. "Dye-sensitized photocatalytic hydrogen production: distinct activity in a glucose derivative of a phenothiazine dye". *Chem. Commun.* **2016**, *52*, 6977-6980, doi:10.1039/c6cc00390g.
- (5) Fujishima, A.; Honda, K. "Electrochemical Photolysis of Water at a Semiconductor Electrode". *Nature* **1972**, *238*, 37-38, doi:10.1038/238037a0.
- (6) Cargnello, M.; Gasparotto, A.; Gombac, V.; Montini, T.; Barreca, D.; Fornasiero, P. "Photocatalytic H₂ and Added-Value By-Products – The Role of Metal Oxide Systems in Their Synthesis from Oxygenates". *Eur. J. Inorg. Chem.* **2011**, *2011*, 4309-4323, doi:10.1002/ejic.201100532.
- (7) Yu, Z.; Li, F.; Sun, L. "Recent advances in dye-sensitized photoelectrochemical cells for solar hydrogen production based on molecular components". *Energy Environ. Sci.* **2015**, *8*, 760-775, doi:10.1039/C4EE03565H.
- (8) Balzani, V.; Credi, A.; Venturi, M. "Photochemical conversion of solar energy". *ChemSusChem* **2008**, *1*, 26-58, doi:10.1002/cssc.200700087.
- (9) Zhang, S.; Yang, X.; Numata, Y.; Han, L. "Highly efficient dye-sensitized solar cells: progress and future challenges". *Energy Environ. Sci.* **2013**, *6*, 1443-1464, doi:10.1039/C3EE24453A.
- (10) Yen, Y.-S.; Chou, H.-H.; Chen, Y.-C.; Hsu, C.-Y.; Lin, J. T. "Recent developments in molecule-based organic materials for dye-sensitized solar cells". *J. Mater. Chem.* **2012**, *22*, 8734-8747, doi:10.1039/C2JM30362K.

- (11) Bae, E.; Choi, W.; Park, J.; Shin, H. S.; Kim, S. B.; Lee, J. S. "Effects of Surface Anchoring Groups (Carboxylate vs Phosphonate) in Ruthenium-Complex-Sensitized TiO₂ on Visible Light Reactivity in Aqueous Suspensions". *J. Phys. Chem. B* **2004**, *108*, 14093-14101, doi:10.1021/jp047777p.
- (12) Reisner, E.; Powell, D. J.; Cavazza, C.; Fontecilla-Camps, J. C.; Armstrong, F. A. "Visible Light-Driven H₂ Production by Hydrogenases Attached to Dye-Sensitized TiO₂ Nanoparticles". *J. Am. Chem. Soc.* **2009**, *131*, 18457-18466, doi:10.1021/ja907923r.
- (13) Yu, L.; Zhang, X.; Zhuang, C.; Lin, L.; Li, R.; Peng, T. "Syntheses of asymmetric zinc phthalocyanines as sensitizer of Pt-loaded graphitic carbon nitride for efficient visible/near-IR-light-driven H₂ production". *Phys. Chem. Chem. Phys.* **2014**, *16*, 4106-4114, doi:10.1039/C3CP54316A.
- (14) Lee, S. H.; Park, Y.; Wee, K. R.; Son, H. J.; Cho, D. W.; Pac, C.; Choi, W.; Kang, S. O. "Significance of hydrophilic characters of organic dyes in visible-light hydrogen generation based on TiO₂". *Org Lett* **2010**, *12*, 460-463, doi:10.1021/ol9026182.
- (15) Abe, R.; Shinmei, K.; Koumura, N.; Hara, K.; Ohtani, B. "Visible-Light-Induced Water Splitting Based on Two-Step Photoexcitation between Dye-Sensitized Layered Niobate and Tungsten Oxide Photocatalysts in the Presence of a Triiodide/Iodide Shuttle Redox Mediator". *J. Am. Chem. Soc.* **2013**, *135*, 16872-16884, doi:10.1021/ja4048637.
- (16) Li, X.; Cui, S. C.; Wang, D.; Zhou, Y.; Zhou, H.; Hu, Y.; Liu, J. G.; Long, Y. T.; Wu, W. J.; Hua, J. L.; Tian, H. "New Organic Donor-Acceptor-p-Acceptor Sensitizers for Efficient Dye-Sensitized Solar Cells and Photocatalytic Hydrogen Evolution under Visible-Light Irradiation". *ChemSuschem* **2014**, *7*, 2879-2888, doi:10.1002/Cssc.201402414.
- (17) Kakiage, K.; Aoyama, Y.; Yano, T.; Otsuka, T.; Kyomen, T.; Unno, M.; Hanaya, M. "An achievement of over 12 percent efficiency in an organic dye-sensitized solar cell". *Chem. Commun.* **2014**, *50*, 6379-6381, doi:10.1039/C4CC02192D.
- (18) Yao, Z.; Zhang, M.; Wu, H.; Yang, L.; Li, R.; Wang, P. "Donor/Acceptor Indenoperylene Dye for Highly Efficient Organic Dye-Sensitized Solar Cells". *J. Am. Chem. Soc.* **2015**, *137*, 3799-3802, doi:10.1021/jacs.5b01537.
- (19) Mishra, A.; Fischer, M. K.; Bauerle, P. "Metal-free organic dyes for dye-sensitized solar cells: from structure: property relationships to design rules". *Angew Chem Int Ed Engl* **2009**, *48*, 2474-2499, doi:10.1002/anie.200804709.

- (20) Kim, B.-G.; Chung, K.; Kim, J. "Molecular Design Principle of All-organic Dyes for Dye-Sensitized Solar Cells". *Chem. Eur. J.* **2013**, *19*, 5220-5230, doi:10.1002/chem.201204343.
- (21) Ahmad, S.; Guillen, E.; Kavan, L.; Gratzel, M.; Nazeeruddin, M. K. "Metal free sensitizer and catalyst for dye sensitized solar cells". *Energy Environ. Sci.* **2013**, *6*, 3439-3466, doi:10.1039/C3EE41888J.
- (22) Liang, M.; Chen, J. "Arylamine organic dyes for dye-sensitized solar cells". *Chem. Soc. Rev.* **2013**, *42*, 3453-3488, doi:10.1039/C3CS35372A.
- (23) Hua, Y.; Chang, S.; Huang, D.; Zhou, X.; Zhu, X.; Zhao, J.; Chen, T.; Wong, W.-Y.; Wong, W.-K. "Significant Improvement of Dye-Sensitized Solar Cell Performance Using Simple Phenothiazine-Based Dyes". *Chem. Mater.* **2013**, *25*, 2146-2153, doi:10.1021/cm400800h.
- (24) Kim, S. H.; Kim, H. W.; Sakong, C.; Namgoong, J.; Park, S. W.; Ko, M. J.; Lee, C. H.; Lee, W. I.; Kim, J. P. "Effect of Five-Membered Heteroaromatic Linkers to the Performance of Phenothiazine-Based Dye-Sensitized Solar Cells". *Organic Letters* **2011**, *13*, 5784-5787, doi:10.1021/ol2023517.
- (25) Cheng, M.; Yang, X.; Zhao, J.; Chen, C.; Tan, Q.; Zhang, F.; Sun, L. "Efficient Organic Dye-Sensitized Solar Cells: Molecular Engineering of Donor-Acceptor-Acceptor cationic dyes". *ChemSusChem* **2013**, *6*, 2322-2329, doi:10.1002/cssc.201300481.
- (26) Hung, W.-I.; Liao, Y.-Y.; Hsu, C.-Y.; Chou, H.-H.; Lee, T.-H.; Kao, W.-S.; Lin, J. T. "High-Performance Dye-Sensitized Solar Cells Based on Phenothiazine Dyes Containing Double Anchors and Thiophene Spacers". *Chem. Asian J.* **2014**, *9*, 357-366, doi:10.1002/asia.201301228.
- (27) Lee, J.; Kwak, J.; Ko, K. C.; Park, J. H.; Ko, J. H.; Park, N.; Kim, E.; Ryu, D. H.; Ahn, T. K.; Lee, J. Y.; Son, S. U. "Phenothiazine-based organic dyes with two anchoring groups on TiO₂ for highly efficient visible light-induced water splitting". *Chem. Commun.* **2012**, *48*, 11431-11433, doi:10.1039/C2CC36501D.
- (28) Watanabe, M.; Hagiwara, H.; Iribe, A.; Ogata, Y.; Shiomi, K.; Staykov, A.; Ida, S.; Tanaka, K.; Ishihara, T. "Spacer effects in metal-free organic dyes for visible-light-driven dye-sensitized photocatalytic hydrogen production". *J. Mater. Chem. A* **2014**, *2*, 12952-12961, doi:10.1039/c4ta02720e.
- (29) Abbotto, A.; Manfredi, N.; Marinzi, C.; De Angelis, F.; Mosconi, E.; Yum, J. H.; Zhang, X. X.; Nazeeruddin, M. K.; Gratzel, M. "Di-branched di-anchoring organic

dyes for dye-sensitized solar cells". *Energy Environ. Sci.* **2009**, *2*, 1094-1101, doi:10.1039/b910654e.

(30) Manfredi, N.; Cecconi, B.; Abboto, A. "Multi-Branched Multi-Anchoring Metal-Free Dyes for Dye-Sensitized Solar Cells". *Eur. J. Org. Chem.* **2014**, 7069-7086, doi:10.1002/ejoc.201402422.

(31) Lin, R. Y. Y.; Wu, F. L.; Chang, C. H.; Chou, H. H.; Chuang, T. M.; Chu, T. C.; Hsu, C. Y.; Chen, P. W.; Ho, K. C.; Lo, Y. H.; Lin, J. T. "Y-shaped metal-free D-pi-(A)(2) sensitizers for high-performance dye-sensitized solar cells". *J. Mater. Chem. A* **2014**, *2*, 3092-3101, doi:10.1039/C3ta14404f.

(32) Iqbal, Z.; Wu, W.-Q.; Zhang, H.; Han, L.; Fang, X.; Wang, L.; Kuang, D.-B.; Meier, H.; Cao, D. "Influence of spatial arrangements of π -spacer and acceptor of phenothiazine based dyes on the performance of dye-sensitized solar cells". *Org. Electron.* **2013**, *14*, 2662-2672, doi:<http://dx.doi.org/10.1016/j.orgel.2013.07.007>.

(33) Albert, I. D. L.; Marks, T. J.; Ratner, M. A. "Large Molecular Hyperpolarizabilities. Quantitative Analysis of Aromaticity and Auxiliary Donor-Acceptor Effects". *J. Am. Chem. Soc.* **1997**, *119*, 6575-6582, doi:10.1021/ja962968u.

(34) Albert, A.: *Heterocyclic Chemistry*; Oxford University Press: New York, 1968.

(35) Abboto, A.; Manfredi, N. "Electron-rich heteroaromatic conjugated polypyridine ruthenium sensitizers for dye-sensitized solar cells". *Dalton Trans* **2011**, *40*, 12421-12438, doi:10.1039/c1dt10832h.

(36) Han, W.-S.; Wee, K.-R.; Kim, H.-Y.; Pac, C.; Nabetani, Y.; Yamamoto, D.; Shimada, T.; Inoue, H.; Choi, H.; Cho, K.; Kang, S. O. "Hydrophilicity Control of Visible-Light Hydrogen Evolution and Dynamics of the Charge-Separated State in Dye/TiO₂/Pt Hybrid Systems". *Chem. Eur. J.* **2012**, *18*, 15368-15381, doi:10.1002/chem.201201500.

(37) Li, J.; E, Y.; Lian, L.; Ma, W. "Visible light induced dye-sensitized photocatalytic hydrogen production over platinized TiO₂ derived from decomposition of platinum complex precursor". *Int. J. Hydrogen Energy* **2013**, *38*, 10746-10753, doi:<http://dx.doi.org/10.1016/j.ijhydene.2013.02.121>.

(38) Sing, K. S. W.; Everett, D. H.; Haul, R. A. W.; Moscou, L.; Pierotti, R. A.; Rouquerol, J.; Siemieniewska, T. "Reporting physisorption data for gas/solid systems with special reference to the determination of surface area and porosity (Recommendations 1984)". *Pure Appl. Chem.* **1985**, *57*, 603-619, doi:10.1351/pac198557040603.

- (39) Montini, T.; Gombac, V.; Sordelli, L.; Delgado, J. J.; Chen, X.; Adami, G.; Fornasiero, P. "Nanostructured Cu/TiO₂ Photocatalysts for H₂ Production from Ethanol and Glycerol Aqueous Solutions". *ChemCatChem* **2011**, *3*, 574-577, doi:10.1002/cctc.201000289.
- (40) Romero Ocaña, I.; Beltram, A.; Delgado Jaén, J. J.; Adami, G.; Montini, T.; Fornasiero, P. "Photocatalytic H₂ production by ethanol photodehydrogenation: Effect of anatase/brookite nanocomposites composition". *Inorg. Chim. Acta* **2015**, *431*, 197-205, doi:<http://dx.doi.org/10.1016/j.ica.2015.01.033>.
- (41) Leung, D. Y. C.; Fu, X.; Wang, C.; Ni, M.; Leung, M. K. H.; Wang, X.; Fu, X. "Hydrogen Production over Titania-Based Photocatalysts". *ChemSusChem* **2010**, *3*, 681-694, doi:10.1002/cssc.201000014.
- (42) Zhang, X.; Yu, L.; Zhuang, C.; Peng, T.; Li, R.; Li, X. "Highly efficient visible/near-IR-light-driven photocatalytic H₂ production over asymmetric phthalocyanine-sensitized TiO₂". *RSC Adv.* **2013**, *3*, 14363-14370, doi:10.1039/C3RA41975D.
- (43) Kisch, H.; Bahnemann, D. "Best Practice in Photocatalysis: Comparing Rates or Apparent Quantum Yields?". *J. Phys. Chem. Lett.* **2015**, *6*, 1907-1910, doi:10.1021/acs.jpcclett.5b00521.
- (44) Lin, Y. Z.; Huang, C. H.; Chang, Y. J.; Yeh, C. W.; Chin, T. M.; Chi, K. M.; Chou, P. T.; Watanabe, M.; Chow, T. J. "Anthracene based organic dipolar compounds for sensitized solar cells". *Tetrahedron* **2014**, *70*, 262-269, doi:DOI 10.1016/j.tet.2013.11.072.
- (45) Reece, S. Y.; Hamel, J. A.; Sung, K.; Jarvi, T. D.; Esswein, A. J.; Pijpers, J. J.; Nocera, D. G. "Wireless solar water splitting using silicon-based semiconductors and earth-abundant catalysts". *Science* **2011**, *334*, 645-648, doi:10.1126/science.1209816.
- (46) Carraro, G.; Maccato, C.; Gasparotto, A.; Montini, T.; Turner, S.; Lebedev, O. I.; Gombac, V.; Adami, G.; Van Tendeloo, G.; Barreca, D.; Fornasiero, P. "Enhanced Hydrogen Production by Photoreforming of Renewable Oxygenates Through Nanostructured Fe₂O₃ Polymorphs". *Adv. Funct. Mater.* **2014**, *24*, 372-378, doi:10.1002/adfm.201302043.
- (47) Abe, R.; Shinmei, K.; Hara, K.; Ohtani, B. "Robust dye-sensitized overall water splitting system with two-step photoexcitation of coumarin dyes and metal oxide semiconductors". *Chem. Commun.* **2009**, 3577-3579, doi:10.1039/b905935k.
- (48) Kumaresan, P.; Vegiraju, S.; Ezhumalai, Y.; Yau, S.; Kim, C.; Lee, W.-H.; Chen, M.-C. "Fused-Thiophene Based Materials for Organic Photovoltaics and Dye-Sensitized Solar Cells". *Polymers* **2014**, *6*, 2645.

- (49) Zhang, G.; Bai, Y.; Li, R.; Shi, D.; Wenger, S.; Zakeeruddin, S. M.; Grätzel, M.; Wang, P. "Employ a bithienothiophene linker to construct an organic chromophore for efficient and stable dye-sensitized solar cells". *Energy Environ. Sci.* **2009**, *2*, 92-95, doi:10.1039/B817990E.
- (50) Wang, M.; Xu, M.; Shi, D.; Li, R.; Gao, F.; Zhang, G.; Yi, Z.; Humphry-Baker, R.; Wang, P.; Zakeeruddin, S. M.; Grätzel, M. "High-Performance Liquid and Solid Dye-Sensitized Solar Cells Based on a Novel Metal-Free Organic Sensitizer". *Adv. Mater.* **2008**, *20*, 4460-4463, doi:10.1002/adma.200801178.
- (51) Kim, J.; Lee, H.; Kim, D. Y.; Seo, Y. "Dye-Sensitized Solar Cells: Resonant Multiple Light Scattering for Enhanced Photon Harvesting in Dye-Sensitized Solar Cells (Adv. Mater. 30/2014)". *Adv. Mater.* **2014**, *26*, 5191-5191, doi:10.1002/adma.201470206.
- (52) Lin, R. Y.-Y.; Wu, F.-L.; Li, C.-T.; Chen, P.-Y.; Ho, K.-C.; Lin, J. T. "High-Performance Aqueous/Organic Dye-Sensitized Solar Cells Based on Sensitizers Containing Triethylene Oxide Methyl Ether". *ChemSusChem* **2015**, *8*, 2503-2513, doi:10.1002/cssc.201500589.
- (53) Leandri, V.; Ellis, H.; Gabrielsson, E.; Sun, L.; Boschloo, G.; Hagfeldt, A. "An organic hydrophilic dye for water-based dye-sensitized solar cells". *Phys. Chem. Chem. Phys.* **2014**, *16*, 19964-19971, doi:10.1039/C4cp02774d.
- (54) Berti, L.; Cucini, M.; Di Stasio, F.; Comoretto, D.; Galli, M.; Marabelli, F.; Manfredi, N.; Marinzi, C.; Abboto, A. "Spectroscopic Investigation of Artificial Opals Infiltrated with a Heteroaromatic Quadrupolar Dye". *J. Phys. Chem. C* **2010**, *114*, 2403-2413, doi:10.1021/jp906002q.
- (55) Narain, R.: *Engineered Carbohydrate-Based Materials for Biomedical Applications*; John Wiley & Sons, Inc., 2011.
- (56) Pescitelli, G.; Omar, O. H.; Operamolla, A.; Farinola, G. M.; Di Bari, L. "Chiroptical Properties of Glucose-Substituted Poly(p-phenylene-ethynylene)s in Solution and Aggregate State". *Macromolecules* **2012**, *45*, 9626-9630, doi:10.1021/ma301919u.
- (57) Alex, S.; Santhosh, U.; Das, S. "Dye sensitization of nanocrystalline TiO₂: enhanced efficiency of unsymmetrical versus symmetrical squaraine dyes". *J. Photochem. Photobiol. A: Chem.* **2005**, *172*, 63-71, doi:<http://dx.doi.org/10.1016/j.jphotochem.2004.11.005>.
- (58) Yum, J.-H.; Jang, S.-r.; Humphry-Baker, R.; Grätzel, M.; Cid, J.-J.; Torres, T.; Nazeeruddin, M. K. "Effect of Coadsorbent on the Photovoltaic Performance of Zinc

Pthalocyanine-Sensitized Solar Cells". *Langmuir* **2008**, *24*, 5636-5640, doi:10.1021/la800087q.

(59) Lee, K.-M.; Chen, C.-Y.; Wu, S.-J.; Chen, S.-C.; Wu, C.-G. "Surface passivation: The effects of CDCA co-adsorbent and dye bath solvent on the durability of dye-sensitized solar cells". *Sol. Energy Mater. Sol. Cells* **2013**, *108*, 70-77, doi:<http://dx.doi.org/10.1016/j.solmat.2012.08.008>.

(60) Melville, L. W.: In *Advances in Carbohydrate Chemistry*; Academic Press, 1954; Vol. Volume 9; pp 185-246.

(61) Jarikote, D. V.; Murphy, P. V. "Metathesis and Macrocycles with Embedded Carbohydrates". *Eur. J. Org. Chem.* **2010**, 4959-4970, doi:10.1002/ejoc.201000491.

(62) Kaur, V.; Bera, M. B.; Panesar, P. S.; Kumar, H.; Kennedy, J. F. "Welan gum: Microbial production, characterization, and applications". *Int. J. Biol. Macromol.* **2014**, *65*, 454-461, doi:10.1016/j.ijbiomac.2014.01.061.

(63) Vinnitskiy, D. Z.; Ustyuzhanina, N. E.; Nifantiev, N. E. "Natural bacterial and plant biomolecules bearing alpha-D-glucuronic acid residues". *Russ. Chem. Bull.* **2015**, *64*, 1273-1301, doi:10.1007/s11172-015-1010-7.

(64) Wadouachi, A.; Kovensky, J. "Synthesis of Glycosides of Glucuronic, Galacturonic and Mannuronic Acids: An Overview". *Molecules* **2011**, *16*, 3933-3968, doi:10.3390/molecules16053933.

(65) In *Sugar-Based Surfactants*; Ruiz, C. C., Ed.; Surfactant Science; CRC Press, 2008.

(66) Queyriaux, N.; Kaeffer, N.; Morozan, A.; Chavarot-Kerlidou, M.; Artero, V. "Molecular cathode and photocathode materials for hydrogen evolution in photoelectrochemical devices". *J. Photochem. Photobiol. C: Photochem. Rev.* **2015**, *25*, 90-105, doi:<http://dx.doi.org/10.1016/j.jphotochemrev.2015.08.001>.

(67) Ronconi, F.; Syrgiannis, Z.; Bonasera, A.; Prato, M.; Argazzi, R.; Caramori, S.; Cristino, V.; Bignozzi, C. A. "Modification of Nanocrystalline WO₃ with a Dicationic Perylene Bisimide: Applications to Molecular Level Solar Water Splitting". *J. Am. Chem. Soc.* **2015**, *137*, 4630-4633, doi:10.1021/jacs.5b01519.

(68) Kaeffer, N.; Massin, J.; Lebrun, C.; Renault, O.; Chavarot-Kerlidou, M.; Artero, V. "Covalent Design for Dye-Sensitized H₂-Evolving Photocathodes Based on a

Cobalt Diimine–Dioxime Catalyst". *J. Am. Chem. Soc.* **2016**, *138*, 12308-12311, doi:10.1021/jacs.6b05865.

(69) Katritzky, A. R.; Rees, C. W.: *Comprehensive Heterocyclic Chemistry*; Pergamon: Oxford, 1984.

(70) Schmidt, A. W.; Reddy, K. R.; Knölker, H.-J. "Occurrence, Biogenesis, and Synthesis of Biologically Active Carbazole Alkaloids". *Chem. Rev.* **2012**, *112*, 3193-3328, doi:10.1021/cr200447s.

(71) Sathiyar, G.; Sivakumar, E. K. T.; Ganesamoorthy, R.; Thangamuthu, R.; Sakthivel, P. "Review of carbazole based conjugated molecules for highly efficient organic solar cell application". *Tetrahedron Lett.* **2016**, *57*, 243-252, doi:<http://dx.doi.org/10.1016/j.tetlet.2015.12.057>.

(72) Li, J.; Grimsdale, A. C. "Carbazole-based polymers for organic photovoltaic devices". *Chem. Soc. Rev.* **2010**, *39*, 2399-2410, doi:10.1039/B915995A.

(73) Jiang, H. "Hosts for High-Performance Phosphorescent Organic Light-Emitting Diodes Based on Carbazole Derivatives". *Asian J Org Chem* **2014**, *3*, 102-112, doi:10.1002/ajoc.201300234.

(74) Chen, C.; Liao, J.-Y.; Chi, Z.; Xu, B.; Zhang, X.; Kuang, D.-B.; Zhang, Y.; Liu, S.; Xu, J. "Metal-free organic dyes derived from triphenylethylene for dye-sensitized solar cells: tuning of the performance by phenothiazine and carbazole". *J. Mater. Chem.* **2012**, *22*, 8994-9005.

(75) Gupta, K. S. V.; Suresh, T.; Singh, S. P.; Islam, A.; Han, L.; Chandrasekharam, M. "Carbazole based A- π -D- π -A dyes with double electron acceptor for dye-sensitized solar cell". *Org. Electron.* **2014**, *15*, 266-275, doi:<http://dx.doi.org/10.1016/j.orgel.2013.11.020>.

(76) Pramjit, S.; Eiamprasert, U.; Surawatanawong, P.; Lertturonchai, P.; Kiatisevi, S. "Carbazole-bridged double D–A dye for efficient dye-sensitized solar cell". *J. Photochem. Photobiol. A: Chem.* **2015**, *296*, 1-10, doi:<http://dx.doi.org/10.1016/j.jphotochem.2014.09.007>.

(77) Sprick, R. S.; Bonillo, B.; Clowes, R.; Guiglion, P.; Brownbill, N. J.; Slater, B. J.; Blanc, F.; Zwijnenburg, M. A.; Adams, D. J.; Cooper, A. I. "Visible-Light-Driven Hydrogen Evolution Using Planarized Conjugated Polymer Photocatalysts". *Angew. Chem. Int. Ed.* **2016**, *55*, 1792-1796, doi:10.1002/anie.201510542.

- (78) Su, C.; Tandiana, R.; Tian, B.; Sengupta, A.; Tang, W.; Su, J.; Loh, K. P. "Visible-Light Photocatalysis of Aerobic Oxidation Reactions Using Carbazolic Conjugated Microporous Polymers". *Acc Catal* **2016**, *6*, 3594-3599, doi:10.1021/acscatal.6b00443.
- (79) McDowell, J. "The crystal and molecular structure of phenothiazine". *Acta Crystallogr. Sect. B: Struct. Sci.* **1976**, *32*, 5-10, doi:doi:10.1107/S0567740876002215.
- (80) Park, S. S.; Won, Y. S.; Choi, Y. C.; Kim, J. H. "Molecular Design of Organic Dyes with Double Electron Acceptor for Dye-Sensitized Solar Cell". *Energy & Fuels* **2009**, *23*, 3732-3736.
- (81) Grisorio, R.; De Marco, L.; Allegretta, G.; Giannuzzi, R.; Suranna, G. P.; Manca, M.; Mastrolilli, P.; Gigli, G. "Anchoring stability and photovoltaic properties of new D(- π -A)² dyes for dye-sensitized solar cell applications". *Dyes Pigm.* **2013**, *98*, 221-231, doi:<http://dx.doi.org/10.1016/j.dyepig.2013.02.012>.
- (82) Soloducho, J.; Doskocz, J.; Nowakowska, A.; Cabaj, J.; Lapkowski, M.; Golba, S. "The Facile Synthesis, Theoretical Study and Electrochemical Characterization of Poly (Arylene) Derivatives". *Pol. J. Chem.* **2007**, *81*, 2001 - 2012.
- (83) Liu, X.; Long, J.; Wang, G.; Pei, Y.; Zhao, B.; Tan, S. "Effect of structural modification on the performances of phenothiazine-dye sensitized solar cells". *Dyes Pigm.* **2015**, *121*, 118-127, doi:<http://dx.doi.org/10.1016/j.dyepig.2015.05.012>.
- (84) Tauc, J. "Optical properties and electronic structure of amorphous Ge and Si". *Mater. Res. Bull.* **1968**, *3*, 37-46, doi:[http://dx.doi.org/10.1016/0025-5408\(68\)90023-8](http://dx.doi.org/10.1016/0025-5408(68)90023-8).
- (85) *Dye Sensitized Solar Cells*; K.Kalyanasundaram ed.; CRC Press: Boca Raton, FL, USA, 2010. pp. 320.
- (86) Park, H.; Kim, H.-i.; Moon, G.-h.; Choi, W. "Photoinduced charge transfer processes in solar photocatalysis based on modified TiO₂". *Energy Environ. Sci.* **2016**, *9*, 411-433, doi:10.1039/c5ee02575c.
- (87) Zhang, G.; Kim, G.; Choi, W. "Visible light driven photocatalysis mediated via ligand-to-metal charge transfer (LMCT): an alternative approach to solar activation of titania". *Energy Environ. Sci.* **2014**, *7*, 954-966, doi:10.1039/C3EE43147A.
- (88) Barber, J.; Tran, P. D. "From natural to artificial photosynthesis". *J R Soc Interface* **2013**, *10*, 20120984, doi:10.1098/rsif.2012.0984.

- (89) Hambourger, M.; Gervaldo, M.; Svedruzic, D.; King, P. W.; Gust, D.; Ghirardi, M.; Moore, A. L.; Moore, T. A. "[FeFe]-hydrogenase-catalyzed H₂ production in a photoelectrochemical biofuel cell". *J Am Chem Soc* **2008**, *130*, 2015-2022, doi:10.1021/ja077691k.
- (90) Li, L.; Duan, L.; Wen, F.; Li, C.; Wang, M.; Hagfeldt, A.; Sun, L. "Visible light driven hydrogen production from a photo-active cathode based on a molecular catalyst and organic dye-sensitized p-type nanostructured NiO". *Chem. Commun.* **2012**, *48*, 988-990, doi:10.1039/c2cc16101j.
- (91) Lakadamyali, F.; Reisner, E. "Photocatalytic H₂ evolution from neutral water with a molecular cobalt catalyst on a dye-sensitized TiO₂ nanoparticle". *Chem. Commun.* **2011**, *47*, 1695-1697, doi:10.1039/c0cc04658b.
- (92) Ji, Z.; He, M.; Huang, Z.; Ozkan, U.; Wu, Y. "Photostable p-Type Dye-Sensitized Photoelectrochemical Cells for Water Reduction". *J. Am. Chem. Soc.* **2013**, *135*, 11696-11699, doi:10.1021/ja404525e.
- (93) Fihri, A.; Artero, V.; Pereira, A.; Fontecave, M. "Efficient H₂-producing photocatalytic systems based on cyclometalated iridium- and tricarbonylrhenium-diimine photosensitizers and cobaloxime catalysts". *Dalton Transactions* **2008**, 5567-5569, doi:10.1039/B812605B.
- (94) Fihri, A.; Artero, V.; Razavet, M.; Baffert, C.; Leibl, W.; Fontecave, M. "Cobaloxime-Based Photocatalytic Devices for Hydrogen Production". *Angew. Chem. Int. Ed.* **2008**, *47*, 564-567, doi:10.1002/anie.200702953.
- (95) Click, K. A.; Beauchamp, D. R.; Huang, Z.; Chen, W.; Wu, Y. "Membrane-Inspired Acidically Stable Dye-Sensitized Photocathode for Solar Fuel Production". *J. Am. Chem. Soc.* **2016**, *138*, 1174-1179, doi:10.1021/jacs.5b07723.
- (96) Fan, K.; Li, F.; Wang, L.; Daniel, Q.; Gabrielsson, E.; Sun, L. "Pt-free tandem molecular photoelectrochemical cells for water splitting driven by visible light". *Phys. Chem. Chem. Phys.* **2014**, *16*, 25234-25240, doi:10.1039/C4CP04489D.
- (97) Li, F.; Fan, K.; Xu, B.; Gabrielsson, E.; Daniel, Q.; Li, L.; Sun, L. "Organic Dye-Sensitized Tandem Photoelectrochemical Cell for Light Driven Total Water Splitting". *J. Am. Chem. Soc.* **2015**, *137*, 9153-9159, doi:10.1021/jacs.5b04856.
- (98) Qin, P.; Zhu, H.; Edvinsson, T.; Boschloo, G.; Hagfeldt, A.; Sun, L. "Design of an organic chromophore for p-type dye-sensitized solar cells". *J Am Chem Soc* **2008**, *130*, 8570-8571, doi:10.1021/ja8001474.

(99) Yasuomi, N.; Kohsuke, H. "The Effects of the BF₂- and B(C₂H₅)₂-substitution for Bridging Hydrogen Atoms in the Cobalt(II), Nickel(II), and Copper(II) Complexes with Some Oximate Ligands". *Bull. Chem. Soc. Jpn.* **1981**, *54*, 3185-3190, doi:doi:10.1246/bcsj.54.3185.

(100) Sailer, M.; Franz, A. W.; Müller, T. J. J. "Synthesis and Electronic Properties of Monodisperse Oligophenothiazines". *Chem. Eur. J.* **2008**, *14*, 2602-2614, doi:10.1002/chem.200701341.

(101) Leandri, V.; Ruffo, R.; Trifiletti, V.; Abboto, A. "Asymmetric Tribranched Dyes: An Intramolecular Cosensitization Approach for Dye-Sensitized Solar Cells". *Eur. J. Org. Chem.* **2013**, *2013*, 6793-6801, doi:10.1002/ejoc.201300962.

(102) Karamshuk, S.; Caramori, S.; Manfredi, N.; Salamone, M.; Ruffo, R.; Carli, S.; Bignozzi, C. A.; Abboto, A. "Molecular Level Factors Affecting the Efficiency of Organic Chromophores for p-Type Dye Sensitized Solar Cells". *Energies* **2016**, *9*, 33, doi:ARTN 33

10.3390/en9010033.

(103) Barolo, C.; Nazeeruddin, M. K.; Fantacci, S.; Di Censo, D.; Comte, P.; Liska, P.; Viscardi, G.; Quagliotto, P.; De Angelis, F.; Ito, S.; Grätzel, M. "Synthesis, Characterization, and DFT-TDDFT Computational Study of a Ruthenium Complex Containing a Functionalized Tetradentate Ligand". *Inorg. Chem.* **2006**, *45*, 4642-4653, doi:10.1021/ic051970w.

(104) Nattestad, A.; Mozer, A. J.; Fischer, M. K. R.; Cheng, Y. B.; Mishra, A.; Bauerle, P.; Bach, U. "Highly efficient photocathodes for dye-sensitized tandem solar cells". *Nat Mater* **2010**, *9*, 31-35, doi:http://www.nature.com/nmat/journal/v9/n1/supinfo/nmat2588_S1.html.

(105) Qin, P.; Wiberg, J.; Gibson, E. A.; Linder, M.; Li, L.; Brinck, T.; Hagfeldt, A.; Albinsson, B.; Sun, L. C. "Synthesis and Mechanistic Studies of Organic Chromophores with Different Energy Levels for p-Type Dye-Sensitized Solar Cells". *J. Phys. Chem. C* **2010**, *114*, 4738-4748, doi:Doi 10.1021/Jp911091n.

(106) Massin, J.; Bräutigam, M.; Kaeffer, N.; Queyriaux, N.; Field, M. J.; Schacher, F. H.; Popp, J.; Chavarot-Kerlidou, M.; Dietzek, B.; Artero, V. "Dye-sensitized PS-b-P2VP-templated nickel oxide films for photoelectrochemical applications". *Interface Focus* **2015**, *5*, doi:10.1098/rsfs.2014.0083.

(107) Baffert, C.; Artero, V.; Fontecave, M. "Cobaloximes as Functional Models for Hydrogenases. 2. Proton Electroreduction Catalyzed by Difluoroborylbis(dimethylglyoximate)cobalt(II) Complexes in Organic Media". *Inorg. Chem.* **2007**, *46*, 1817-1824, doi:10.1021/ic061625m.

(108) D'Amario, L.; Antila, L. J.; Pettersson Rimgard, B.; Boschloo, G.; Hammarström, L. "Kinetic Evidence of Two Pathways for Charge Recombination in NiO-Based Dye-Sensitized Solar Cells". *J. Phys. Chem. Lett.* **2015**, *6*, 779-783, doi:10.1021/acs.jpcclett.5b00048.

(109) Panagiotopoulos, A.; Ladomenou, K.; Sun, D.; Artero, V.; Coutsolelos, A. G. "Photochemical hydrogen production and cobaloximes: the influence of the cobalt axial N-ligand on the system stability". *Dalton Transactions* **2016**, *45*, 6732-6738, doi:10.1039/C5DT04502A.

(110) Veldkamp, B. S.; Han, W.-S.; Dyar, S. M.; Eaton, S. W.; Ratner, M. A.; Wasielewski, M. R. "Photoinitiated multi-step charge separation and ultrafast charge transfer induced dissociation in a pyridyl-linked photosensitizer-cobaloxime assembly". *Energy Environ. Sci.* **2013**, *6*, 1917-1928, doi:10.1039/C3EE40378E.

(111) Lawrence, M. A. W.; Celestine, M. J.; Artis, E. T.; Joseph, L. S.; Esquivel, D. L.; Ledbetter, A. J.; Cropek, D. M.; Jarrett, W. L.; Bayse, C. A.; Brewer, M. I.; Holder, A. A. "Computational, electrochemical, and spectroscopic studies of two mononuclear cobaloximes: the influence of an axial pyridine and solvent on the redox behaviour and evidence for pyridine coordination to cobalt(i) and cobalt(ii) metal centres". *Dalton Transactions* **2016**, *45*, 10326-10342, doi:10.1039/C6DT01583B.

(112) Willkomm, J.; Muresan, N. M.; Reisner, E. "Enhancing H₂ evolution performance of an immobilised cobalt catalyst by rational ligand design". *Chem Sci* **2015**, *6*, 2727-2736, doi:10.1039/C4SC03946G.

(113) Reuillard, B.; Warnan, J.; Leung, J. J.; Wakerley, D. W.; Reisner, E. "Δ Poly(cobaloxime)/Carbon Nanotube Electrode: Freestanding Buckypaper with Polymer-Enhanced H₂-Evolution Performance". *Angewandte Chemie (International Ed. in English)* **2016**, *55*, 3952-3957, doi:10.1002/anie.201511378.

(114) Tong, L.; Iwase, A.; Nattestad, A.; Bach, U.; Weidelener, M.; Gotz, G.; Mishra, A.; Bauerle, P.; Amal, R.; Wallace, G. G.; Mozer, A. J. "Sustained solar hydrogen generation using a dye-sensitised NiO photocathode/BiVO₄ tandem photo-electrochemical device". *Energy Environ. Sci.* **2012**, *5*, 9472-9475, doi:10.1039/C2EE22866A.

(115) Sing, K. S. W.; Everett, D. H.; Haul, R. A. W.; Moscou, L.; Pierotti, R. A.; Rouquerol, J.; Siemieniowska, T.

Pure Appl. Chem. 1985, *57*, 603.

(116) Li, L.; Gibson, E. A.; Qin, P.; Boschloo, G.; Gorlov, M.; Hagfeldt, A.; Sun, L. "Double-Layered NiO Photocathodes for p-Type DSSCs with Record IPCE". *Adv. Mater.* **2010**, *22*, 1759-1762, doi:10.1002/adma.200903151.

(117) Sumikura, S.; Mori, S.; Shimizu, S.; Usami, H.; Suzuki, E. "Syntheses of NiO nanoporous films using nonionic triblock co-polymer templates and their application to photo-cathodes of p-type dye-sensitized solar cells". *J. Photochem. Photobiol. A: Chem.* **2008**, *199*, 1-7, doi:<http://dx.doi.org/10.1016/j.jphotochem.2008.04.007>.

(118) Bakac, A.; Espenson, J. H. "Unimolecular and bimolecular homolytic reactions of organochromium and organocobalt complexes. Kinetics and equilibria". *J. Am. Chem. Soc.* **1984**, *106*, 5197-5202, doi:10.1021/ja00330a027.

Chapter 5

Shallow men believe in luck.

Strong men believe in cause and effect.

Ralph Waldo Emerson, Poet, 1803-1882

Conclusions

In this PhD project, we have studied several new molecules and materials to be used in the conversion of solar energy in electricity and fuels.

Concerning the synthesized molecules used in the field of photovoltaics and the photocatalytic hydrogen production, we have studied a series of triarylamine push-pull dyes, prepared in by the group of Prof. Baldoli at the University of Milano, containing the benzo[1,2-b:4,5-b]dithiophene spacer in which bulky alkyl chains were inserted on the triarylamine moiety or on the conjugated spacer. The effect of the alkyl chain position on the dye properties and photovoltaic performances were investigated. The new dyes were used as sensitizers in liquid DSSC. The best PCE was recorded for dye **1** (6.6% at 0.5 sun, 8.4% without mask on top of the cell), the molecule with the simplest donor core, to be compared with a value of 8.1% for N719-based devices under the same fabrication conditions. Therefore, the photovoltaic performance of the sensitizer **1** was only ~20% less than the benchmark dye N719. The best LHE profile, in agreement with optical properties,

and the APCE values, greater than 80%, suggested that the efficiency of **1** originates from high light harvesting and charge formation and collection efficiency. Photovoltaic performances were dramatically dependent on the choice of the solvent used for the dye-sensitizing bath. The results were correlated, through extensive optical studies in different solvents and acid/base additives, with protonation equilibria of COOH/COO group of dyes. These data clearly show that when an unsuitable, though very common, solvent as EtOH is used for dye solutions, misleading PCEs even close to 0% may be obtained, although in the presence of performing sensitizers, as ascertained when proper conditions are alternatively selected, thus showing the strategic importance of selecting appropriate solvents for DSSC fabrication conditions.

We have designed and investigated a series of phenothiazine-based donor-acceptor dyes for dye-sensitized photocatalytic hydrogen production from water and dye-sensitized solar cells. The series is characterized by having different thiophene-based π -spacers, from the simple thiophene ring to the alkoxy-substituted thiophene derivatives. The introduction of the thiophene-based π -spacers afforded significantly enhanced optical properties both in terms of longer wavelength absorption and molar absorptivities, with up to a four-fold increase compared to the reference dye **PTZ1**. Pt/TiO₂ photocatalysts sensitized by dyes **PTZ1-6** showed a remarkable H₂ productivity from TEOA aqueous solution at pH = 7.0 under irradiation with visible light for long irradiation times (20 h). The preferred longer irradiation times are in contrast with previously reported experimental conditions, which typically use much shorter irradiation periods (2-5 h). Although the photocatalyst sensitized by the dye **PTZ1** without the thiophene spacers demonstrated the highest initial H₂ production rate, it undergoes a progressive deactivation with irradiation time, a behaviour commonly reported, but so far not clearly rationalized, for this class of dyes. Such characteristic is critical for practical long-term applications. On the contrary, photocatalysts sensitized with the new substituted **PTZ2-6** dyes revealed improved stability after longer irradiation

times and enhanced performances after an initial activation period. An unprecedented degradation study has revealed for the first time that the anomalous photocatalytic activity of the catalyst sensitized by the reference dye **PTZ1** is the clear consequence of the strong degradation of the dye with irradiation times. Notably, the new dye **PTZ5** is a promising candidate for efficient dye-sensitized photocatalytic H₂ production, with stable H₂ production rate and an overall productivity comparable to that of the reference compound **PTZ1**. The degradation investigation has evidenced that this finding is the direct consequence of the remarkable stability of **PTZ5** under irradiation, though the intrinsic photocatalytic efficiency was lower than that of the reference dye.

Moreover, a sugar derivative of a multibranched organic sensitizer (**PTZ-GLU**) has been efficiently used in the dye-sensitized photocatalytic production of hydrogen through careful catalyst design. The insertion of the glucose unit yielded a higher affinity towards the aqueous medium compared to the commonly used hydrophilic TEG functionality, while maintaining the high activity recorded for the alkyl derivative. By comparing contact angle measurements, photocatalytic data, and by considering the structural peculiar features of the side substituents, we have thus concluded that the distinct behaviour of **PTZ-GLU** is associated to the unique rigid, bulky, hydrophilic geometry of the glucose ring, where lower degrees of freedom and extra-wettability, favouring the interaction with reactants in aqueous solution and suppressing intermolecular quenching, cooperate in producing the final findings. The general and scalable synthetic approach and the large variety of sugar derivatives will allow the access to a library of photosensitizers with finely tuned properties and abilities to improve the efficiency of the production of solar fuels.

We have investigated the photocatalytic hydrogen generation of the previously presented glucose-functionalized phenothiazine dye (**PTZ-GLU**) in presence of properly designed glucose-based co-adsorbents (**GLU**) in order to promote beneficial directional interactions on the semiconductor catalytic surface and,

eventually, access enhanced catalytic activity. Indeed, we have demonstrated that the combined use of the glucose-based dye and co-adsorbent afforded enhanced photocatalytic hydrogen generation, in terms of hydrogen generation, TON, and LFE, compared to the absence of co-adsorbents or to the presence of a conventional co-adsorbent (**CDCA**) not capable of establishing specific strong intermolecular bonds with the glucose dye. Furthermore, the experiment with a conventional dye with an alkyl chain in place of the glucose end-group showed that no enhancement could be observed in this case by adding any of the two co-adsorbents compared to the bare dye. In this case the enhancement was only observed, for both co-adsorbents, only in presence of higher co-adsorbent/dye ratios (mass effect). The check experiment thus validated the rationale for the enhanced activity of the GLU-GLU system. Preliminary DFT computations, performed in the group of Dr. De Angelis at CNR in Perugia, on the investigated dye/co-adsorbents systems on the TiO_2 surface further confirmed the overall picture. This is the first example where properly devised self-assembling arrangements on the catalyst surface by means of a judicious design of organic dyes and co-adsorbents is used to greatly enhance the photocatalytic hydrogen generation, paving the way to a completely novel supramolecular strategy to access important hydrogen production from water and sunlight

A series of sulfur free sensitizers have been synthesized and used in photocatalytic hydrogen production. The presence of heteroatoms in the core and spacer moieties of the investigated sensitizers dramatically affects the photocatalytic hydrogen generation in the visible range over Pt/TiO_2 . In particular, the judicious combination of sulfur-free planar donor cores (**CBZ**) with sulfur-free five-membered heterocyclic spacers (**Fu**) afforded top efficiencies compared to state-of-the-art dye-sensitized hydrogen generation.

The position of the LUMO energy levels represents a strategic factor driving the photocatalytic activity, since the electron injection to TiO_2 CB depends on the LUMO/CB energy gap. Replacing **Th** with **Fu** moieties in the spacers of **POZs**

and **CBZs** sensitizers, for which similar electrochemical and optical properties were observed, yielded increased hydrogen production. This proves that sulfur sites have a detrimental effect on activity, which is probably associated to its poisoning effect on the Pt active phase. A rational design of the sensitizers was shown to be the key to obtain greatly enhanced performances in H₂ photogeneration under visible light irradiation.

A preliminary investigation has been done on a new series of phenothiazine based p-type dyes to be used as sensitizers in PEC cells, in collaboration with Dr. Artero at CEA in Grenoble, FR. The peculiar design of the target molecule was intended to be anchored on the semiconductor with a not-conjugated functionality to reduce the recombination between the dye and the semiconductor itself. On the other side, the sensitizer has been functionalized with a pyridine terminal to allow coordination as axial ligand in a cobaloxime used as reduction catalyst in photoelectrochemical hydrogen production. These dyes have been compared with the analogous functionalized with a malononitrile functionality in presence of the catalyst, and with the benchmark dye **P1**. The dyes and the dyad have been characterized with their optical and electrochemical properties, both in solution and adsorbed on the semiconductor. The photoelectrochemical properties in presence of a SEA and a cobaloxime as reduction catalyst have been investigated showing a lower photocurrent generated by the new dyes compared to the reference P1. Nonetheless, the design seems to be interesting and deserves to be deeply investigated in the future.

Concerning the devices fabrication, we have studied a series of C-doped TiO₂ prepared in collaboration with the group of Prof Brusatin at the University of Padova. The innovative and cheap doping procedure allows to tune the amount of carbon doping to finely tune the properties of the material. The devices prepared using these new pastes have been tested with the benchmark dye N719, in single layer devices, or in combination with commercial scattering paste to boost the efficiency and compared to devices prepared with different commercial pastes. The

new titania pastes showed photovoltaic efficiency comparable or equal to the reference devices. These results have been achieved with a reduced amount, namely half, of sensitizer adsorbed on the surface of the C-doped titania. These results suggest that the synthesized C-doped titania nanoparticles could be a potential candidate to replace the commercial formulation due to their low cost and the high efficiency achieved in DSSCs devices. New experiments will be performed to clarify the role of doping on the electronic properties of the material.

In the field of PSC, after a comprehensive study of literature, a reliable procedure for the fabrication of the PSCs devices has been developed and applied to the study of two different configurations of the devices themselves. We have noticed that the most reproducible results have been achieved using the planar configuration which also appears the easier to be produced due to the lack of the second mesoporous layer of titania. Furthermore, we have improved the design of the final device in order to meet the conditions imposed by the deposition method. This new geometry positions the four cells of a single device at the centre of the same, exploiting the most homogeneous part of the deposited material by improving the efficiency and reproducibility of results. Transparent counter electrodes, in combination with this new geometry, have been employed in the study of feasibility of the fabrication of a multijunction cell in combination with a mc-Si solar cell proving the validity of this approach.

New candidates as HTM, based on hydrazone functionalized electron rich heteroaromatic cores, have been synthesized and their optical and electrochemical properties have been studied showing interesting reversible electrochemistry. A study on the deposition method has been done to tune and improve the quality of the deposited film. OFET have been prepared and studied to measure the carrier mobility in the synthesized material. This investigation showed that the only one HTH capable of conducting charges should be the pyrrole based one. The three 3,4-bisalkoxythienyl derivatives appeared to be insulating materials instead of

semiconductors. The new HTMs have been used in PSC confirming the mobility measurements. Novel pyrrole based derivatives are now under investigation.